

**Development of Noble Gas Techniques to Fingerprint Shale Gas and to Trace  
Sources of Hydrocarbons in Groundwater**

**by**

**Tao Wen**

**A dissertation submitted in partial fulfillment  
of the requirements for the degree of  
Doctor of Philosophy  
(Geology)  
in the University of Michigan  
2017**

**Doctoral Committee:**

**Professor Maria Clara Cruz Da Silva Castro, Chair  
Professor Avery H. Demond  
Assistant Professor Brian R. Ellis  
Associate Research Scientist Chris M. Hall  
Professor Kyger C Lohmann  
Professor Daniele L. Pinti, Université du Québec à Montréal**

Tao Wen

[jaywen@umich.edu](mailto:jaywen@umich.edu)

ORCID iD: [0000-0002-6113-7532](https://orcid.org/0000-0002-6113-7532)

© Tao Wen 2017

To Wenqing and our families

## **ACKNOWLEDGEMENTS**

I would like to express deep appreciation and gratitude to my advisor, Dr. Clara Castro, who introduced me to noble gas geochemistry, guided me with endless patience, and continually encouraged me to think critically in addressing challenging scientific questions, through to the completion of this degree. Without her generous support, this dissertation would not have been possible.

I would also like to thank my committee members Drs. Avery Demond, Brian Ellis, Chris Hall, Kacey Lohmann, and Daniele Pinti for their friendly guidance and insightful suggestions on the work presented in this dissertation. Special thanks go to Dr. Avery Demond for her helpful, informative hydrology class, to Dr. Brian Ellis for making the first project in this dissertation possible by sharing his network and arranging the sampling campaign, to Dr. Chris Hall for teaching me instrumental analysis techniques in the noble gas lab, to Dr. Kacey Lohmann for his advice on stable isotopes and the geology in the Michigan Basin, and to Dr. Daniele Pinti for sharing invaluable and constructive thoughts on this dissertation from Montreal.

I would also like to extend my thanks to Dr. Jean-Philippe Nicot from the Bureau of Economic Geology, University of Texas at Austin for educating me on environmental sciences and petroleum geology and for guiding me in our Barnett Shale gas project in Texas. Without the generous and enormous help from Dr. Jean-Philippe Nicot, the completion of the Barnett Shale

project will be impossible. I would also like to thank Dr. Jean-Philippe Nicot for his constructive suggestions on noble gas papers we co-authored in the Barnett Shale gas project.

The help from departmental staff, especially Ms. Anne Hudon and Nancy Kingsbury, is greatly appreciated. I also learned a lot from past and current members of our noble gas research group: Lin Ma, Jessica Malone, Rohit Warriar, Yi Niu, Julien Amalberti. This dissertation benefits from them in many ways. All of them have definitely made my PhD study easier and more enjoyable.

Surrounded by so many supportive friends, I have had a great time here at University of Michigan. To name a few: Peng Ni, Xiaojian Liu, Yi Niu, Haolu Feng, Xiaofei Pu, Yi Yu, Chenghuan Guo, Ke Yuan, and many more.

Thanks to my parents for their constant encouragement and support along this journey. Lastly, thanks to my wife, Wenqing and our catdog little Fanfan for joining me on this adventure. Thanks to Wenqing for shouldering far more than her fair share of the parenting and household burdens while I pursued this degree.

# TABLE OF CONTENTS

|  |             |
|--|-------------|
| <b>DEDICATION .....</b>  | <b>ii</b>   |
| <b>ACKNOWLEDGEMENTS .....</b>  | <b>iii</b>  |
| <b>LIST OF TABLES .....</b>  | <b>vii</b>  |
| <b>LIST OF FIGURES .....</b>   | <b>viii</b> |
| <b>LIST OF APPENDICES .....</b>  | <b>xii</b>  |
| <b>ABSTRACT.....</b>   | <b>xiii</b> |
| <b>CHAPTER 1 INTRODUCTION.....</b>   | <b>1</b>    |
| 1.1 NOBLE GASES AS NATURAL TRACERS IN GROUNDWATER AND HYDROCARBON FLUIDS .....   | 2           |
| 1.2 APPLICATION OF NOBLE GAS GEOCHEMISTRY IN SHALE GAS STUDIES .....   | 5           |
| 1.3 DISSERTATION STRUCTURE.....  | 8           |
| 1.4 REFERENCES .....   | 11          |
| <b>CHAPTER 2 ASSESSING COMPOSITIONAL VARIABILITY AND MIGRATION OF<br/>NATURAL GAS IN THE ANTRIM SHALE IN THE MICHIGAN BASIN USING NOBLE<br/>GAS GEOCHEMISTRY .....</b> | <b>19</b>   |
| 2.1 ABSTRACT .....   | 19          |
| 2.2 INTRODUCTION .....   | 20          |
| 2.3 GEOLOGIC SETTING .....   | 25          |
| 2.4 SAMPLING AND ANALYTICAL METHODS.....   | 27          |
| 2.5 RESULTS .....  | 29          |
| 2.5.1 Major Gas Components in the Antrim Shale Gas .....   | 29          |
| 2.5.2 Noble Gas Signatures in the Antrim Shale Gas .....   | 30          |
| 2.6 DISCUSSION .....   | 41          |
| 2.6.1 Mixing of Deep Brine and Freshwater Recharge in the Antrim .....   | 41          |
| 2.6.2 <sup>4</sup> He Groundwater Ages.....  | 48          |
| 2.6.3 Differentiated Xe Signatures Relative to He, Ne and Ar .....   | 55          |
| 2.6.4 Origin of Produced Gases in the Antrim Shale: Thermogenic versus Biogenic Origin .....   | 56          |
| 2.7 CONCLUSIONS.....   | 61          |
| 2.8 ACKNOWLEDGEMENTS.....  | 62          |
| 2.9 REFERENCES .....   | 64          |

|   |            |
|---|------------|
| <b>CHAPTER 3 METHANE SOURCES AND MIGRATION MECHANISMS IN SHALLOW GROUNDWATERS IN PARKER AND HOOD COUNTIES, TEXAS – A HEAVY NOBLE GAS ANALYSIS.....</b>  | <b>72</b>  |
| 3.1 ABSTRACT .....  | 72         |
| 3.2 INTRODUCTION .....  | 73         |
| 3.3 GEOLOGIC SETTING .....  | 76         |
| 3.4 SAMPLING AND ANALYTICAL METHODS.....  | 78         |
| 3.5 RESULTS AND DISCUSSION.....   | 79         |
| 3.5.1 Spatial Distribution of Dissolved Methane .....   | 79         |
| 3.5.2 Noble Gas Signatures versus Methane Content .....   | 80         |
| 3.5.3 Stray Gas Source and Migration Mechanisms – Production Wells versus Water Wells .....   | 85         |
| 3.6 ACKNOWLEDGEMENTS.....   | 94         |
| 3.7 REFERENCES .....  | 96         |
| <br>  |            |
| <b>CHAPTER 4 CHARACTERIZING THE NOBLE GAS ISOTOPIC COMPOSITION OF THE BARNETT SHALE AND STRAWN GROUP AND CONSTRAINING THE SOURCE OF STRAY GAS IN THE TRINITY AQUIFER, NORTH-CENTRAL TEXAS</b> | <b>102</b> |
| 4.1 ABSTRACT .....  | 102        |
| 4.2 INTRODUCTION .....  | 103        |
| 4.3 GEOLOGIC SETTING .....  | 105        |
| 4.4 SAMPLING AND ANALYTICAL METHODS.....  | 107        |
| 4.5 RESULTS AND DISCUSSION.....   | 110        |
| 4.5.1 Noble Gas Signatures versus Methane Content .....   | 110        |
| 4.5.2 Barnett Shale versus Strawn Group and Stray Natural Gas - Crustal and Atmospheric Noble Gas Signatures .....  | 115        |
| 4.6 ACKNOWLEDGEMENTS.....   | 124        |
| 4.7 REFERENCES .....  | 125        |
| <br>  |            |
| <b>CHAPTER 5 SUMMARY AND CONCLUSIONS.....</b>   | <b>131</b> |
| 5.1 SUMMARY OF MAJOR RESULTS.....   | 131        |
| 5.2 OVERALL CONCLUSIONS.....  | 136        |
| 5.3 REFERENCES .....  | 138        |
| <br>  |            |
| <b>APPENDICES .....</b>   | <b>140</b> |

# LIST OF TABLES

## CHAPTER 2

|                  |   |    |
|------------------|---|----|
| <b>Table 2.1</b> | Well location and major gas components (shown in volume %) for Antrim Shale gas samples ..... | 33 |
| <b>Table 2.2</b> | Noble gas isotopic ratios for Antrim Shale gas samples .....                                  | 34 |
| <b>Table 2.3</b> | Noble Gas Signatures versus Methane Content.....  | 40 |
| <b>Table 2.4</b> | Noble Gas Signatures versus Methane Content.....  | 51 |

## APPENDIX A

|                 |  |     |
|-----------------|--|-----|
| <b>Table A1</b> | Well location and methane concentrations for Trinity Aquifer groundwater samples.....  | 150 |
| <b>Table A2</b> | Total and crustal (*) noble gas isotopic concentrations ( $\text{cm}^3\text{STP/g}_{\text{H}_2\text{O}}$ ) for Trinity Aquifer groundwater samples ..... | 151 |
| <b>Table A3</b> | Noble gas isotopic ratios in the Trinity Aquifer .....   | 153 |
| <b>Table A4</b> | He component separation results for Trinity groundwater samples .....  | 163 |
| <b>Table A5</b> | Isotopic ratios of atmospheric noble gases and chloride concentrations in groundwater samples .....  | 165 |

## APPENDIX B

|                 |   |     |
|-----------------|---|-----|
| <b>Table B1</b> | Sampling date, methane content and depth for groundwater stray gas samples and production gas samples from the Strawn Group and Barnett Shale .....   | 179 |
| <b>Table B2</b> | Noble gas volume fractions ( $\text{cm}^3/\text{cm}^3$ ) and corresponding isotopic ratios for groundwater stray gas samples and production gas samples from the Strawn Group and Barnett Shale ..... | 181 |
| <b>Table B3</b> | Noble gas isotopic ratios for groundwater stray gas samples and production gas samples from the Strawn Group and Barnett Shale .....  | 182 |
| <b>Table B4</b> | Isotopic ratios of atmospheric noble gases in stray gas as well as production gas from the Strawn Group and Barnett Shale .....   | 197 |
| <b>Table B5</b> | Parameter used in single-stage and two-stage fractionation models.....  | 198 |

# LIST OF FIGURES

## CHAPTER 2

- Figure 2.1** (a) Central portion of the Michigan Basin (lower peninsula of Michigan). The subcrop of the Antrim Shale is shown in dark brown; the Northern Producing Trend (NPT) of the Antrim Shale gas play is indicated by the rectangular area [adapted from *Martini et al.*, 1998]; (b) General schematic geological representation along cross section A–A' in (a); Rock salts are present in the Michigan Basin as represented by the black layer; (c) Schematic of the Michigan Basin stratigraphy; major formations and lithologies in the basin are identified .....22
- Figure 2.2** (a) Location map of all sampled Antrim wells, with Antrim Shale subcrop (stripped area) and Mid-Continent Rift System in the Michigan Basin (black shadow) also indicated; (b) Contour map of perforation depths for sampled Antrim Shale gas wells in this study .....23
- Figure 2.3** Depth profiles of (a) radiogenic  $^4\text{He}$  volume fractions, (b)  $R/R_a$  ratios, (c)  $^{20}\text{Ne}/^{22}\text{Ne}$  ratios, (d)  $^{21}\text{Ne}/^{22}\text{Ne}$  ratios, (e)  $^{40}\text{Ar}/^{36}\text{Ar}$  ratios and (f)  $^{136}\text{Xe}/^{130}\text{Xe}$  ratios for collected Antrim gas samples revealing high spatial variability of noble gas signatures within the Antrim Shale. Corresponding atmospheric noble gas values are indicated (dashed lines) .....31
- Figure 2.4** Contour maps of (a) total  $^4\text{He}$  volume fractions, (b) radiogenic  $^4\text{He}$  volume fractions, (c) total  $^{40}\text{Ar}$  volume fractions and (d) radiogenic  $^{40}\text{Ar}$  volume fractions for Antrim Shale gas wells in this study .....39
- Figure 2.5** Depth profile of (a) Measured  $^{20}\text{Ne}/^{36}\text{Ar}$  and (b)  $^{36}\text{Ar}/^{84}\text{Kr}$  ratios of collected Antrim gas samples versus predicted  $^{20}\text{Ne}/^{36}\text{Ar}$  and  $^{36}\text{Ar}/^{84}\text{Kr}$  ratios for a gas phase in equilibrium with seawater (i.e., gas/liquid volume ratio approaches 0 or  $+\infty$ ) under reservoir conditions .....45
- Figure 2.6** (a)  $^{40}\text{Ar}/^{36}\text{Ar}$  versus  $1/^{36}\text{Ar}$ ; and (b) radiogenic  $^4\text{He}$  volume fraction versus Cl. These reveal variable impact of deep brines on  $^4\text{He}$  and Ar composition in the Antrim Shale .....47
- Figure 2.7** Groundwater  $^4\text{He}$  ages are shown for sampled Antrim wells in this study assuming: (a) only in-situ production (blue squares), and; (b) both in-situ production & external He flux (red triangles), and compared with previously reported groundwater  $^{14}\text{C}$  ages (*Martini et al.*, 1998) as well as timing of three major glacial periods (Wisconsin, Illinoian and Kansan) in the Michigan Basin .....54
- Figure 2.8** Depth profiles versus (a) measured  $^{40}\text{Ar}/^{36}\text{Ar}$  (red open triangles); and (b) predicted  $^{40}\text{Ar}/^{36}\text{Ar}$  ratios (open blue square) for Antrim gas samples in this study. The atmospheric  $^{40}\text{Ar}/^{36}\text{Ar}$  ratio is also indicated (dashed line) .....60

## CHAPTER 3

- Figure 3.1** Spatial distribution maps of dissolved methane and total  $^4\text{He}$  concentrations for sampled Trinity Aquifer wells. The South Cluster is located close to the Brazos River between the City of Granbury to the south and the City of Weatherford to the north whereas the North Cluster is located

north of the City of Weatherford. Small red dots represent wellhead locations of horizontal wells producing from the Barnett Shale.....77

**Figure 3.2** (a) Total He concentrations, (b)  $^4\text{He}^*$  concentrations, (c) R/Ra ratios, (d)  $^{21}\text{Ne}/^{22}\text{Ne}$  ratios, (e)  $^{40}\text{Ar}/^{36}\text{Ar}$  ratios, and (f)  $^{136}\text{Xe}/^{130}\text{Xe}$  as a function of measured dissolved methane concentrations in collected groundwater samples. Corresponding atmospheric noble gas values are indicated (dashed lines). Samples with undetected methane concentrations are plotted at the methane detection limit (0.001 mg/L) .....83

**Figure 3.3** (a)  $^{20}\text{Ne}$ , (b)  $^{84}\text{Kr}$  and (c)  $^{132}\text{Xe}$  concentrations as a function of  $^{36}\text{Ar}$  concentrations for all collected Trinity groundwater samples. Predicted  $^{20}\text{Ne}$ ,  $^{36}\text{Ar}$ ,  $^{84}\text{Kr}$  and  $^{132}\text{Xe}$  concentrations in air saturated water (ASW) are shown for temperatures varying from 0 °C to 25 °C (red solid line). Predicted  $^{20}\text{Ne}$ ,  $^{36}\text{Ar}$ ,  $^{84}\text{Kr}$  and  $^{132}\text{Xe}$  concentrations in the water phase are also calculated for two scenarios: 1) addition of excess air (EA) (green solid lines) and; 2) residual water phase following water-gas interaction in a closed-system (red dashed lines) at 18 °C and 25 °C .....89

**Figure 3.4** Comparison of fractionation F levels of atmospheric noble gas isotopic ratios  $^{132}\text{Xe}/^{36}\text{Ar}$  versus  $^{84}\text{Kr}/^{36}\text{Ar}$  for all Trinity Aquifer groundwater samples.  $^{132}\text{Xe}/^{36}\text{Ar}$  and  $^{84}\text{Kr}/^{36}\text{Ar}$  ratios are normalized to the ASW value at 18°C (Table A5; cf. Appendix A). The air value is indicated by a red diamond. Calculated closed-system fractionation curve [red dashed line; cf. *Ballentine et al.* 2002] for a residual water phase that has an initial ASW composition at 18°C is also indicated.....92

## CHAPTER 4

**Figure 4.1** Approximate location of all collected stray gases from water wells and production gases from Barnett and Strawn gas wells.....109

**Figure 4.2** (a) total  $^4\text{He}$  volume fractions, (b)  $^4\text{He}^*$  volume fractions, (c) R/Ra ratios, (d)  $^{21}\text{Ne}/^{22}\text{Ne}$  ratios, (e)  $^{40}\text{Ar}/^{36}\text{Ar}$  ratios and (f)  $^{136}\text{Xe}/^{130}\text{Xe}$  ratios as a function of methane volume fractions for all gas samples. Corresponding atmospheric and crustal noble gas values are indicated by dashed lines and shadow area, respectively .....112

**Figure 4.3** (a)  $^{40}\text{Ar}/^{36}\text{Ar}$  versus  $1/^{36}\text{Ar}$  and (b)  $^{21}\text{Ne}/^{22}\text{Ne}$  versus  $1/^{22}\text{Ne}$  for all gas samples in this study as well as Barnett and Strawn gas samples from *Darrah et al.* [2014]. Linear regression lines are also shown for certain groups of gas samples (see text). Air values are shown for comparison .....117

**Figure 4.4**  $F(^{22}\text{Ne})$ ,  $F(^{84}\text{Kr})$ , and  $F(^{132}\text{Xe})$  are plotted for gas samples.  $F(^{22}\text{Ne})$ ,  $F(^{84}\text{Kr})$ , and  $F(^{132}\text{Xe})$  are measured  $^{22}\text{Ne}/^{36}\text{Ar}$ ,  $^{84}\text{Kr}/^{36}\text{Ar}$ ,  $^{132}\text{Xe}/^{36}\text{Ar}$  ratios normalized to corresponding air values. F values of ASW at the temperature of 18 °C (light blue line) and air (black line) are shown. F values for groundwater samples with high methane content in the study area [*Wen et al.*, 2016] are also shown 122

**Figure 4.5** (a)  $^{84}\text{Kr}/^{36}\text{Ar}$  versus  $^{22}\text{Ne}/^{36}\text{Ar}$  and (b)  $^{132}\text{Xe}/^{36}\text{Ar}$  versus  $^{22}\text{Ne}/^{36}\text{Ar}$  are shown for gas samples. Predicted values in the gas phase following a single-stage groundwater degassing model for closed-system (black curve) and open-system (black dashed curve) are shown in (a) and (b). Calculated values in the gas phase following oil-modified groundwater exsolution (OMGE) model with varying amount of sedimentary noble gas are also shown (blue and red dotted curves; see also Appendix B Text B5).....123

## CHAPTER 5

**Figure 5.1** Schematic cross-section of the Trinity Aquifer and Strawn Group in the study area [adapted from Kornacki and McCaffrey 2014] .....134

## APPENDIX A

**Figure A1** Map showing extent of the Fort Worth Basin, its major structural features, extent of Mississippian Barnett Shale, and relation to early historical production (so-called “core area”). Contours are drawn on top of the Ordovician Ellenburger Group; contour intervals equal 1,000 feet [adapted from Bruner and Smosna, 2011]. Green circle shows the area of study. ....144

**Figure A2** Generalized local stratigraphic column within the study area in the vicinity of the Parker-Hood county line [data from Herkommer and Denke, 1982 and CLI (Core Laboratories Inc.), 1972]145

**Figure A3** EW generalized cross-sections through the Fort Worth Basin from Nicot et al. [2013] 146

**Figure A4** Excerpts of Dallas GAT Sheet (1:250,000). Red circle encloses the Parker-Hood south cluster. Continuous and dotted red lines represent major roads. The figure is from <http://www.twdb.texas.gov/groundwater/aquifer/GAT/> (Geological Atlas of Texas) .....147

**Figure A5**  $R_{exc}/R_a$  values versus  $^4He_{exc}$  concentrations for the Trinity groundwater samples within the Barnett Shale footprint. Shaded areas indicate typical crustal R/Ra values (0.02–0.05) .....161

**Figure A6**  $R_{noea}/R_a$  versus  $^4He_{eq}/^4He_{noea}$  for Trinity groundwater samples within the Barnett Shale footprint. R/Ra values for the crust and the mantle are assumed to be 0.02 and 8, respectively [O’Nions and Oxburgh, 1983; Oxburgh et al., 1986; Castro et al., 2000; Graham, 2002; Starkey et al., 2009]. The pre-bomb background tritium concentration in this area of 5 TU is also indicated [Castro et al., 2000]. Lines corresponding to 0%, 1% and 2% mantle helium and 0 TU, 5 TU, and 200 TU tritogenic He are shown .....162

**Figure A7** (a) Comparison of fractionation F levels of atmospheric noble gas isotopic ratios  $^{132}Xe/^{36}Ar$  versus  $^{84}Kr/^{36}Ar$  for all Trinity Aquifer groundwater samples, and (b) a close-up of (a).  $^{132}Xe/^{36}Ar$  and  $^{84}Kr/^{36}Ar$  ratios are normalized to the air saturated water value at 18°C (Table A5). The air value is indicated by a red diamond in (a). Circle sizes are proportional to methane concentrations in water .....167

**Figure A8** (a)  $F(^{132}Xe/^{36}Ar)$  and (b)  $^4He/^{20}Ne$  ratios versus distances to nearest Barnett gas well, (c)  $F(^{132}Xe/^{36}Ar)$  and (d)  $^4He/^{20}Ne$  ratios versus distances to nearest non-Barnett gas well, and (e)  $F(^{132}Xe/^{36}Ar)$  and (f)  $^4He/^{20}Ne$  ratios versus distances to nearest production gas well which can be either Barnett or non-Barnett gas wells.  $^4He/^{20}Ne$  values for typical Strawn gas [Darrah et al., 2014] and ASW at 18°C are also indicated (gray domain and dashed line) .....169

**Figure A9**  $CH_4/^{36}Ar$  ratios versus  $Cl^-$  concentrations are plotted for all collected water samples with methane concentrations above 0.001 mg/L in this study.  $CH_4/^{36}Ar$  value in  $CH_4$  saturated ASW at 18 °C is also indicated (black solid line) .....171

## APPENDIX B

**Figure B1** Map showing extent of the Fort Worth Basin, its major structural features, extent of Mississippian Barnett Shale, and relation to early historical production (so-called “core area”). Contours are drawn on top of the Ordovician Ellenburger Group; contour intervals equal 1,000 feet [adapted from Bruner and Smosna, 2011]. Green circle shows the area of study .....175

**Figure B2** Generalized local stratigraphic column within the study area in the vicinity of the Parker-Hood county line [data from Herkommer and Denke, 1982 and CLI (Core Laboratories Inc.), 1972]176

**Figure B3**  $^{20}Ne/^{22}Ne$  as a function of (a)  $^{21}Ne/^{22}Ne$ , (b)  $^{38}Ar/^{36}Ar$ , (c)  $^{40}Ar/^{36}Ar$ , and (d)  $^{22}Ne/^{36}Ar$  for all gas samples. Calculated ratios in the escaped gas phase following mass-dependent fractionation [Matsumoto et al., 2004] are shown for two scenarios: (1) ASW at 18 °C (light blue dashed line) and (2) air (blue dashed line). In (a), mixing lines (Air-Solar, Air-MORB [mid-ocean ridge basalt], Air-OIBs [ocean island basalt], and Air-Crust) are indicated for previously reported values as summarized in Castro et al. [2009] .....186

**Figure B4**  $^{132}\text{Xe}/^{36}\text{Ar}$  versus  $^{84}\text{Kr}/^{36}\text{Ar}$  are shown for gas samples. Predicted values in the gas phase following a single-stage groundwater degassing model for closed-system (black curve) and open-system (black dashed curve) are shown. Previously reported  $^{84}\text{Kr}/^{36}\text{Ar}$  and  $^{132}\text{Xe}/^{36}\text{Ar}$  values in kerogen [gray square in the upper-right corner; *Frick and Chang, 1977*] and oil field gases [black crosses; *Torgersen and Kennedy, 1999*] are also shown for reference .....199

## LIST OF APPENDICES

### APPENDIX A

|           |   |     |
|-----------|---|-----|
| <b>A1</b> | Local Geology and Hydrostratigraphy .....                       | 141 |
| <b>A2</b> | Noble Gas Measurement Procedures.....                           | 148 |
| <b>A3</b> | He Systematics and Individual Helium Component Separation ..... | 155 |
| <b>A4</b> | Natural Gas Accumulations in the Strawn. ....                   | 168 |

### APPENDIX B

|           |  |     |
|-----------|--|-----|
| <b>B1</b> | Noble Gas Measurement Procedures.....  | 177 |
| <b>B2</b> | Calculation of Crustal Noble Gas Components ( $^4\text{He}^*$ , $^{21}\text{Ne}^*$ , $^{40}\text{Ar}^*$ )..... | 180 |
| <b>B3</b> | Mass-Dependent Fractionation (MDF) in Barnett Gas Samples .....  | 183 |
| <b>B4</b> | Neon (Ne) Systematics .....  | 188 |
| <b>B5</b> | Solubility-Controlled Noble Gas Fractionation .....  | 189 |

## ABSTRACT

The combined use of hydraulic fracturing (HF) and horizontal drilling has greatly increased the natural gas recovery from shales, so called “shale gas”. This steep increase in shale gas production has caused public concern for fear that enhanced permeability through HF may facilitate migration of natural gas, thereby threatening drinking-water supplies.

My dissertation presents a pioneer study of the entire set of noble gases (He, Ne, Ar, Kr, Xe) in natural shale gas and associated groundwater. Noble gases are used to fingerprint unconventional shale gas, to characterize natural gas generation, to trace the source of crustal fluids (i.e., natural gas and groundwater), and to assess the mixing and migration of various crustal fluids.

Noble gas signatures of Antrim Shale gas in the Michigan Basin are investigated to assess mixing of deep brine and freshwater recharge. High horizontal and vertical variability in crustal noble gas signatures in the Antrim Shale are observed, which are due to variable noble gas input with brine migration from deeper formations. Noble gas ratios suggest also dominance of thermogenic over biogenic natural gas in this shale formation.

I also place constraints on the source and transport mechanisms of methane found in the shallow Trinity Aquifer within the Barnett Shale footprint in Parker and Hood counties, Texas, using the entire set of noble gases with an emphasis on  $^{84}\text{Kr}$  and  $^{132}\text{Xe}$ . Dissolved methane concentrations are positively correlated with crustal noble gases and suggest that noble gases and

methane originate from a common source, likely the Strawn Group as opposed to the Barnett Shale. Overall, noble gas signatures in the Trinity Aquifer do not support the notion that methane present in these groundwaters migrated from nearby production wells either conventional or using HF techniques. Instead, this study suggests that methane in the Trinity Aquifer originates from noncommercial small gas accumulations in the underlying Strawn Group, which these groundwater wells have reached.

Atmospheric and crustal noble gas signatures for natural gas samples from the deep Barnett Shale and shallow Strawn Group in Texas are presented and compared with those of stray gas (methane) in the Trinity Aquifer. It is apparent that Barnett Shale and Strawn Group natural gas display highly distinct noble gas signatures and point to different evolution histories. Comparison of these production shale gas samples with stray gas in the Trinity aquifer reinforces the notion that stray gas in the Trinity originates in the Strawn Group as opposed to the Barnett Shale. At this stage, our findings do not point specifically to anthropogenic causes (e.g., poor-quality cementing of natural gas production wells either conventional or using HF technology) that would be responsible for the presence of methane in the Trinity Aquifer.

# CHAPTER 1

## INTRODUCTION

Lower natural gas prices and recent changes in laws and regulations, including the U.S. Environmental Protection Agency's (EPA) Clean Power Plan (CPP) to reduce drastically CO<sub>2</sub> emissions, have been two critical contributing factors for the increase of U.S. natural gas production [US EIA, 2016]. Total natural gas production in the U.S. is predicted to increase from 27.2 Tcf (trillion cubic feet) in 2015 to 42.1 Tcf in 2040 [US EIA, 2016]. The projected natural gas production from unconventional shale gas and tight oil plays account for 50% of total U.S. natural gas production in 2015 and it will reach 69% of total U.S. natural gas production in 2040 [US EIA, 2016]. The explosive growth of unconventional shale gas production in the U.S., benefiting from technology improvements (e.g., hydraulic fracturing (HF) and horizontal drilling) and abundant domestic resources, has also generated intense public concerns about its potential impact on groundwater quality [Osborn *et al.*, 2011; Nicot and Scanlon, 2012; Jackson *et al.*, 2013; Nicot *et al.*, 2014]. To guide the exploration and production of unconventional natural gas resources and to respond to the associated increasing environmental concern among the public, characterization of natural gas reservoirs and evaluation of hydrocarbon generation, migration, and interaction with other crustal fluids (e.g., fresh recharge water, deep brines) are very critical [Pinti and Marty, 2000; Hunt *et al.*, 2012; Prinzhofer, 2013].

Stable noble gases (Helium – He, Neon – Ne, Argon – Ar, Krypton – Kr, Xenon - Xe) are chemically inert and stable and are thus mostly sensitive to physical processes (e.g., migration of crustal fluids and multi-phase interaction), making them ideal fluid source tracers [Ozima and Podosek, 2002]. The application of noble gas geochemistry has gained greater importance for natural gas characterization, especially in the last three decades [Prinzhofer, 2013]. In this introductory chapter, a brief overview of noble gases systematics in crustal fluids (i.e., groundwater, natural gas, and oil) is followed by the review of application of noble gases as natural tracers of subsurface fluids migration in oil and gas fields specifically. A detailed structure of this dissertation is provided in the last section.

### **1.1 Noble Gases as Natural Tracers in Groundwater and Hydrocarbon Fluids**

Because of their stable orbital configuration with the outer shell filled with electrons [Ozima and Podosek, 2002], noble gases are excellent nonreactive natural tracers to constrain the physical conditions affecting geologic systems [Andrews and Lee, 1979; Ballentine and O'nions, 1994; Ballentine et al., 1994; Castro et al., 1998a; 1998b; Ozima and Podosek, 2002]. Therefore, the study of noble gases in groundwater and hydrocarbon in sedimentary basins has been recognized as an important tool to trace the source of crustal fluids [Zartman et al., 1961; Mazor and Bosch, 1987; Bosch and Mazor, 1988; Ballentine and Burnard, 2002; Zhou et al., 2005; Hunt et al., 2012], to provide insights into subsurface fluid migration pattern at the basin scale and their associated mechanisms [Kennedy et al., 1990; Torgersen et al., 1992; Elliot et al., 1993; Pinti and Marty, 1995; Battani et al., 2000; Ballentine and Sherwood Lollar, 2002; Castro et al., 2005; Ma et al., 2005, 2009; Prinzhofer et al., 2010], and to delineate the degree of mixing between various crustal fluids enhancing our understanding of crustal fluid dynamics [Andrews

*et al.*, 1982; *Hiyagon and Kennedy*, 1992; *Castro et al.*, 2000; *Schlegel et al.*, 2011]. Furthermore, noble gases in crustal fluids are derived from the atmosphere, crust, and mantle, all of which show distinct isotopic and elemental signatures [*Pinti and Marty*, 2000; *Ozima and Podosek*, 2002; *Porcelli et al.*, 2002; *Castro et al.*, 2009; *Prinzhofer*, 2013]. While all of these three origins of noble gases in crustal fluids are discussed in this dissertation, particular emphasis is placed on the atmospheric and the crustal noble gas components.

Atmospheric noble gases in aquifer systems are incorporated into the subsurface through rainwater infiltration, i.e., during recharge. Freshwater recharge is commonly referred to as air-saturated water (ASW) and it is generally assumed to be in solubility equilibrium with the atmosphere in sedimentary systems. Because the solubility of noble gases in water is primarily temperature-dependent [*Weiss*, 1970; 1971; *Weiss and Kyser*, 1978; *Ozima and Podosek*, 2002], noble gases have been widely used to reconstruct the evolution of past climate [*Mazor*, 1972; *Stute et al.*, 1992b; 1995; *Aeschbach-Hertig et al.*, 2000; 2002; *Kipfer et al.*, 2002; *Castro and Goblet*, 2003; *Castro et al.*, 2012]. Previous studies have also shown that atmospheric noble gases in hydrocarbons originate from groundwater (the ASW phase), and subsequently preferentially partitioned into the hydrocarbon phase [*Zartman et al.*, 1961; *Bosch and Mazor*, 1988]. Because noble gas solubility is 10 to 100 times higher in oil than in groundwater [*Kharaka and Specht*, 1988], groundwater which has interacted with a natural gas or oil phase will be strongly depleted in atmospheric noble gases. Consequently, the studies of noble gas depletion in hydrocarbon-associated groundwater allowed the identification and quantification of the oil, gas, and water phase interactions in the subsurface [*Zartman et al.*, 1961; *Bosch and Mazor*, 1988; *Pinti and Marty*, 1995; *Zhou et al.*, 2005; *Darrah et al.*, 2014; *Wen et al.*, 2016]. The occurrence of past thermal events has also been suggested as an alternative explanation of

observed depletion in atmospheric noble gases in hydrothermal systems [Mazor and Truesdell, 1984; Kennedy, 1988; Winckler et al., 2000; Ma et al., 2009; Pinti et al., 2012; Warriar et al., 2013]. The delineation of atmospheric noble gas components allows the characterization of oil and gas fields as well as associated aquifers, thereby rendering possible the distinction between various crustal fluids in a diversity of geologic settings.

In addition to atmospheric noble gases, noble gases of crustal origin are also present in geological fluids and can be dominant for certain noble gas isotopes (e.g.,  $^4\text{He}^*$ ,  $^{21}\text{Ne}^*$ ,  $^{40}\text{Ar}^*$ ), where crustal noble gases are indicated with a “\*” notation. While  $^4\text{He}^*$  and  $^{40}\text{Ar}^*$  (radiogenic) are produced from radioactive decay of U-Th, and K, respectively [Ozima and Podosek, 2002],  $^{21}\text{Ne}^*$  is mainly from reactions between  $\alpha$  particles (derived from U-Th decay) and O and Mg atoms in crustal rocks [Wetherill, 1954]. The concentration of crustal noble gases in groundwater is a function of water residence times and noble gas production rates [Torgersen and Ivey, 1985; Torgersen and Clarke, 1985; Stute et al., 1992a; Castro et al., 2000; Phillips and Castro, 2003]. Crustal noble gases can have either an in-situ origin, i.e., be produced within the aquifer or hydrocarbon reservoir rock itself, or be external to the reservoirs being studied and result from deeper sedimentary formations or deeper levels within the crystalline crust. Water-hydrocarbon phase interaction controls the transfer of crustal noble gases from the water phase into the hydrocarbon phase. The combination of noble gases in the hydrocarbon phase can be used to reconstruct  $^4\text{He}^*$  concentrations in the associated water phase, leading to water residence ages characterization [Zhou et al., 2005; Zhou and Ballentine, 2006; Schlegel et al., 2011]. Crustal noble gases are produced within the rock and are subsequently released into the water, gas or oil phases. The variability in their concentrations and elemental ratios (e.g.,  $^4\text{He}^*/^{40}\text{Ar}^*$  and  $^{21}\text{Ne}^*/^{40}\text{Ar}^*$ ) have been attributed to multiple processes: (1) differences in the abundance of U,

Th, and K in the source and/or host rocks; (2) preferential release of the light noble gases (He, Ne) over Ar (because of their respective diffusion properties); (3) the thermal regime (controlling the diffusion of noble gases from rock to fluids); and (4) the degree of mixing and interaction between various crustal fluids [Zartman *et al.*, 1961; Torgersen *et al.*, 1989; Ballentine *et al.*, 1994; Ballentine and O'Nions, 1994; Pinti and Marty, 1995; Solomon *et al.*, 1996; Castro *et al.*, 1998a; 1998b; Pinti and Marty, 2000; Kennedy *et al.*, 2002].

The mantle represents also an important reservoir of noble gases (primordial origin), which were trapped during the early accretion of the Earth [Ozima and Podosek, 2002]. Mantle noble gases in aquifers, oil and gas fields can be characterized by their distinct isotopic signatures (e.g., high  $^3\text{He}/^4\text{He}$  and  $^{20}\text{Ne}/^{22}\text{Ne}$  ratios). Mantle noble gases have been observed in sedimentary basins in both tectonically active regions [Oxburgh *et al.*, 1986; O'Nions *et al.*, 1993] and currently tectonically stable areas [Hiyagon and Kennedy, 1992; Ma *et al.*, 2005; Castro *et al.*, 2009].

## 1.2 Application of Noble Gas Geochemistry to Shale Gas

Early pioneering studies of noble gases in natural gas in the last century [Rogers, 1921; Zartman *et al.*, 1961; Nagao *et al.*, 1981; Sano *et al.*, 1982; Oxburgh *et al.*, 1986; Bosch and Mazor, 1988], have been followed up in more recent times by the widespread use of noble gases to characterize natural gas. [Poreda *et al.*, 1988; Ballentine, 1991; Elliot *et al.*, 1993; O'Nions *et al.*, 1993; Sherwood-Lollar *et al.*, 1994; Pinti and Marty, 1995; Torgersen and Kennedy, 1999; Battani *et al.*, 2000; Pinti and Marty, 2000; Zhou *et al.*, 2005; Zhou and Ballentine, 2006; Kotarba and Nagao, 2008; Hunt *et al.*, 2012; Darrah *et al.*, 2014; 2015; Wen *et al.*, 2015]. Indeed, the combined studies of atmospheric and crustal noble gases are particularly useful to

constrain subsurface mixing and migration patterns of crustal fluids in conventional natural gas fields throughout the world (e.g., Po Basin in Italy, Songliao Basin in China, San Juan and Anadarko Basins in the U.S.) [Elliot *et al.*, 1993; Xu *et al.*, 1995; Ballentine and Sherwood-Lollar, 2002; Zhou *et al.*, 2005].

Unlike conventional natural gas reservoirs (e.g., sandstone or carbonate), shale is an unconventional reservoir with very low permeability (often less than 5%), which corresponds to the source rocks where natural gas was produced over geological times [Boyer *et al.*, 2006]. The recent increasing interest in unconventional gas production has further advanced both commercial and scientific applications of noble gas geochemistry in the petroleum and natural gas industry [Hunt *et al.*, 2012; Darrah *et al.*, 2014; 2015; Heath *et al.*, 2015; Wen *et al.*, 2015, 2016]. Moreover, the presence of elevated concentrations of light hydrocarbon (i.e., stray gas) in shallow drinking groundwater in the vicinity of unconventional gas production wells in some areas (e.g., the Marcellus Shale and Barnett Shale) [Osborn *et al.*, 2011; Jackson *et al.*, 2013; Darrah *et al.*, 2014; Moritz *et al.*, 2015; Siegel *et al.*, 2015; Sherwood *et al.*, 2016; Siegel *et al.*, 2016; Wen *et al.*, 2016] has lead the scientific community to place effort in identifying the sources and migration mechanisms of stray gas. Here, “stray gas” refers to natural gas present in shallow aquifers of an undetermined origin. These environmental forensic studies require novel geochemical tools since traditional geochemical tracers (e.g., hydrocarbon molar -  $[C_2H_6+]/[CH_4]$  and stable isotopic ratios -  $\delta^{13}C_{CH_4}$ ), unlike unreactive noble gas tracers, might be altered by microbial activity and oxidation [Lollar and Ballentine, 2009; Molofsky *et al.*, 2013].

Thus, one of the goals of this dissertation is to extend the use of noble gases to fingerprint unconventional shale gases. A thorough understanding of shale gas characteristics is critical for delineating the migration pattern of crustal fluids (i.e., groundwater, natural gas, and oil) within

the shale formations and shallow aquifers. *Hunt et al.* [2012] investigated the usefulness of noble gases to determine the genetic fingerprint and post-genetic processes of natural gases in shale in the eastern US Appalachian Basin. Integrated with hydrocarbon and water chemistry, light noble gases (i.e., He, Ne, and Ar) were used to distinguish between produced gases from Upper Devonian formations and the Marcellus Shale and thus, to reveal the source of dissolved stray gas in shallow aquifers within the Marcellus Shale footprint [*Darrah et al.*, 2014; 2015]. *Darrah et al.* [2014] also compared light crustal and atmospheric noble gas signatures (i.e.,  $^4\text{He}/^{40}\text{Ar}^*$  and  $^4\text{He}/^{20}\text{Ne}$ ) of production gases from the Strawn Group and the Barnett Shale, aiming at discriminating production gases from these two formations. They concluded that the source of dissolved stray gas in the shallow Trinity Aquifer within the Barnett Shale footprint is likely the Strawn Group as opposed to the Barnett Shale. The migration of Strawn gas into the shallow aquifers was hypothesized to be due to gas leakage through the well annulus, probably as a result of poor cementation [*Darrah et al.*, 2014]. However, to this day, few noble gas studies have been conducted on shale gas and associated groundwater due in part to the difficulty in analyzing these samples. Unlike He content, volume fractions of all other noble gases in shale gas are orders of magnitude lower than those found in groundwater, rendering the achievement of high precision measurements challenging. On the other hand, the excess air component has a greater impact on the light noble gas composition compared to the heavy ones in groundwater [*Ballentine and Hall*, 1999; *Ozima and Podosek*, 2002]. Moreover, the contribution of sedimentary Kr and Xe in hydrocarbon-associated crustal fluids (e.g., groundwater and natural gas) has been suggested by previous studies [*Fanale and Cannon*, 1971; *Frick and Chang*, 1977; *Frick et al.*, 1979; *Podosek et al.*, 1981; *Torgersen and Kennedy*, 1999; *Pitre and Pinti*, 2010]. Here, sedimentary Kr and Xe refer to heavy noble gases adsorbed on fine sediments (clays)

and/or organic matter (kerogen). Thus, the study of heavy noble gases is important to fully understand the phase interactions and flow dynamics of shale gas and other related crustal fluids in unconventional gas reservoirs.

### 1.3 Dissertation Structure

This section introduces the structure of this dissertation with a brief outline of how the above goals are investigated as well as the aims and scope of each of the following chapters. The two first chapters that follow have been published (Chapters 2 and 3) [Wen *et al.*, 2015; 2016]. The third chapter is in review in the journal of Environmental Science & Technology (Chapter 4) [Wen *et al.*, in review].

Based on the combined study of crustal (i.e.,  $^4\text{He}^*$ ,  $^{21}\text{Ne}^*$ , and  $^{40}\text{Ar}^*$ ) and atmospheric (i.e.,  $^{20}\text{Ne}$ ,  $^{36}\text{Ar}$ , and  $^{84}\text{Kr}$ ) noble gases, Chapter 2 assesses the compositional variability and transport processes of subsurface fluids (i.e., shale gas and brine) in the Antrim Shale in the Michigan Basin. High horizontal and vertical variability of noble gas isotopic signatures in the Antrim Shale are observed. Noble gas data (e.g., atmospheric  $^{36}\text{Ar}$ , crustal  $^4\text{He}^*$  and  $^{40}\text{Ar}^*$ ) as well as water chemistry data are used to assess the impact of deep brine over freshwater recharge, suggesting that the observed variability in noble gas content is due to variable noble gas input with brine migration from deeper formations. The timing of freshwater recharge is also estimated based on  $^4\text{He}$  ages of co-produced formation water. Of particular relevance is the consistency between measured  $^{40}\text{Ar}/^{36}\text{Ar}$  ratios of Antrim Shale gas and calculated values assuming total crustal Ar released from its source rock into the gas phase. Such great consistency suggests that thermogenic natural gas might constitute the majority for the Antrim Shale gas. These findings confirm that noble gases are excellent tracers capable of fingerprinting shale gas and tracing its

migration in groundwater reservoirs. These results were published in *Chemical Geology* [Wen et al., 2015].

This novel application of noble gases can be used to track the source of methane in shallow aquifers in areas where shale gas exploitation through high-volume hydraulic fracturing is prevalent, and where high levels of dissolved methane have been identified (e.g., the Barnett Shale footprint in Texas). Chapters 3 and 4 therefore systematically investigate the atmospheric and crustal noble gas components in water or production gas samples from the Barnett Shale, Strawn Group and Trinity Aquifer, in an attempt to identify the source of dissolved stray gas in the shallow Trinity Aquifer with the Barnett Shale footprint in north-central Texas. Specifically, Chapter 3 focuses on groundwater samples with a particular emphasis on their atmospheric heavy noble gas compositions (i.e.,  $^{84}\text{Kr}$  and  $^{132}\text{Xe}$ ). Concentrations of crustal noble gases correlate with dissolved methane contents in groundwater confirming that these two components have a common source. Atmospheric noble gases in collected groundwater samples display significant depletion compared to corresponding values in the freshwater recharge, in agreement with predicted values in a water phase following groundwater degassing. Combined with water well logs and distances between water wells and nearest gas production wells, these noble gas signatures suggest that stray gas in the Trinity Aquifer is likely related to noncommercial small gas accumulations in the Strawn Group as opposed to the Barnett Shale. These water wells might also allow the migration of Strawn gas into the Trinity Aquifer. This work has been published in *Environmental Science & Technology* [Wen et al., 2016].

In Chapter 4, we examine the evolution of  $^{21}\text{Ne}/^{22}\text{Ne}$  and  $^{40}\text{Ar}/^{36}\text{Ar}$  isotopic ratios in order to further track the source of stray gas in water wells and to distinguish between Barnett and Strawn production gas. The combined noble gas analyses of stray gas, Barnett Shale and Strawn

Group production gas show that stray gas represents a mixing of two end-members: (1) the atmosphere and (2) a crustal component defined by pristine Strawn gas. Noble gas composition of Barnett Shale gas samples cannot explain the observed noble gas signatures in stray gas samples. This reinforces the hypothesis that the Strawn Group is likely the source of stray gas in the Trinity Aquifer. Moreover, an in-depth comparison of atmospheric noble gas components (i.e.,  $^{22}\text{Ne}$ ,  $^{36}\text{Ar}$ ,  $^{84}\text{Kr}$ , and  $^{132}\text{Xe}$ ) of Barnett and Strawn gases show elevated  $^{22}\text{Ne}/^{36}\text{Ar}$ ,  $^{84}\text{Kr}/^{36}\text{Ar}$ , and  $^{132}\text{Xe}/^{36}\text{Ar}$  ratios compared to ASW and air values. A two-stage Rayleigh-type fractionation model considering the oil phase is suggested to be the most viable option to explain observed high  $^{22}\text{Ne}/^{36}\text{Ar}$  ratios in the Barnett Shale gas, while sedimentary Kr and Xe input is required to account for the relative enrichment in  $^{84}\text{Kr}$  and  $^{132}\text{Xe}$  in Barnett and Strawn gases. This study highlights the use of both atmospheric and crustal noble gases to distinguish between natural gas from various sources, and to trace the migration of subsurface fluids. This work is in review in the journal of Environmental Science & Technology [Wen *et al.*, in review].

A summary of major results and conclusions of this dissertation is provided in Chapter 5. This dissertation is of great societal relevance with respect to conventional and unconventional oil and gas as well as environmental impact assessment. Indeed, there is concern by local communities, the industry and scientists that unconventional gas production in particular might negatively affect groundwater quality in production areas. This dissertation shows that noble gas-based environmental studies can greatly contribute to the identification of natural gas sources in groundwater as well as the migration mechanisms of dissolved methane in drinking groundwater. These findings will positively impact future groundwater management plans in these regions.

## 1.4 References

- Aeschbach-Hertig, W., F. Peeters, U. Beyerle, and R. Kipfer (2000), Palaeotemperature reconstruction from noble gases in ground water taking into account equilibration with entrapped air, *Nature*, 405(6790), 1040–1044, doi:10.1038/35016542.
- Aeschbach-Hertig, W., M. Stute, J. F. Clark, R. F. Reuter, and P. Schlosser (2002), A paleotemperature record derived from dissolved noble gases in groundwater of the Aquia Aquifer (Maryland, USA), *Geochimica et Cosmochimica Acta*, 66(5), 797–817.
- Andrews, J. N., and D. J. Lee (1979), Inert gases in groundwater from the Bunter Sandstone of England as indicators of age and palaeoclimatic trends, *Journal of Hydrology*, 41(3–4), 233–252, doi:10.1016/0022-1694(79)90064-7.
- Andrews, J. N., I. S. Giles, R. L. F. Kay, D. J. Lee, J. K. Osmond, J. B. Cowart, P. Fritz, J. F. Barker, and J. Gale (1982), Radioelements, radiogenic helium and age relationships for groundwaters from the granites at Stripa, Sweden, *Geochimica et Cosmochimica Acta*, 46(9), 1533–1543, doi:10.1016/0016-7037(82)90312-X.
- Ballentine, C. J. (1991), He, Ne, and Ar Isotopes as Tracers in Crustal Fluids, Cambridge University Press.
- Ballentine, C. J., and B. Sherwood Lollar (2002), Regional groundwater focusing of nitrogen and noble gases into the Hugoton-Panhandle giant gas field, USA, *Geochimica et Cosmochimica Acta*, 66(14), 2483–2497, doi:10.1016/S0016-7037(02)00850-5.
- Ballentine, C. J., and C. M. Hall (1999), Determining paleotemperature and other variables by using an error-weighted, nonlinear inversion of noble gas concentrations in water, *Geochimica et Cosmochimica Acta*, 63(16), 2315–2336, doi:10.1016/S0016-7037(99)00131-3.
- Ballentine, C. J., and P. G. Burnard (2002), Production, Release and Transport of Noble Gases in the Continental Crust, *Reviews in Mineralogy and Geochemistry*, 47(1), 481–538, doi:10.2138/rmg.2002.47.12.
- Ballentine, C. J., and R. K. O'Nions (1994), The use of natural He, Ne and Ar isotopes to study hydrocarbon-related fluid provenance, migration and mass balance in sedimentary basins, *Geological Society, London, Special Publications*, 78(1), 347–361, doi:10.1144/GSL.SP.1994.078.01.23.
- Ballentine, C. J., M. Mazurek, and A. Gautschi (1994), Thermal constraints on crustal rare gas release and migration: Evidence from Alpine fluid inclusions, *Geochimica et Cosmochimica Acta*, 58(20), 4333–4348.
- Battani, A., P. Sarda, and A. Prinzhofer (2000), Basin scale natural gas source, migration and trapping traced by noble gases and major elements: the Pakistan Indus basin, *Earth and Planetary Science Letters*, 181(1–2), 229–249.

- Bosch, A., and E. Mazor (1988), Natural gas association with water and oil as depicted by atmospheric noble gases: case studies from the southeastern Mediterranean Coastal Plain, *Earth and Planetary Science Letters*, 87(3), 338–346, doi:10.1016/0012-821X(88)90021-0.
- Boyer, C., J. Kieschnick, R. Suarez-Rivera, and R. E. Lewis (2006), Producing gas from its source, *Oilfield Review*.
- Castro, M. C., A. Jambon, G. de Marsily, and P. Schlosser (1998a), Noble gases as natural tracers of water circulation in the Paris Basin: 1. Measurements and discussion of their origin and mechanisms of vertical transport in the basin, *Water Resources Research*, 34(10), 2443–2466, doi:10.1029/98WR01956.
- Castro, M. C., and P. Goblet (2003), Noble gas thermometry and hydrologic ages: evidence for late Holocene warming in Southwest Texas, *Geophysical research letters*, 30(24), 2251, doi:10.1029/2003GL018875.
- Castro, M. C., D. Patriarche, and P. Goblet (2005), 2-D numerical simulations of groundwater flow, heat transfer and 4 He transport—implications for the He terrestrial budget and the mantle helium–heat imbalance, *Earth and Planetary Science Letters*, 237(3), 893–910, doi:10.1016/j.epsl.2005.06.037.
- Castro, M. C., L. Ma, and C. M. Hall (2009), A primordial, solar He–Ne signature in crustal fluids of a stable continental region, *Earth and Planetary Science Letters*, 279(3–4), 174–184, doi:10.1016/j.epsl.2008.12.042.
- Castro, M. C., M. Stute, and P. Schlosser (2000), Comparison of 4He ages and 14C ages in simple aquifer systems: implications for groundwater flow and chronologies, *Applied Geochemistry*, 15(8), 1137–1167, doi:10.1016/S0883-2927(99)00113-4.
- Castro, M. C., P. Goblet, E. Ledoux, S. Violette, and G. de Marsily (1998b), Noble gases as natural tracers of water circulation in the Paris Basin: 2. Calibration of a groundwater flow model using noble gas isotope data, *Water Resources Research*, 34(10), 2467–2483, doi:10.1029/98WR01957.
- Castro, M. C., R. B. Warrier, C. M. Hall, and K. C. Lohmann (2012), A Late Pleistocene-Mid-Holocene Noble Gas and Stable Isotope Climate and Subglacial Record in Southern Michigan, *Geophysical research letters*, 39(19), n–a–n–a, doi:10.1029/2012GL053098.
- Crovetto, R., R. Fernandez-Prini, and M. L. Japas (1982), Solubilities of inert gases and methane in H<sub>2</sub>O and in D<sub>2</sub>O in the temperature range of 300 to 600 K, *J. Chem. Phys.*, 76(2), 1077–1086, doi:10.1063/1.443074.
- Darrah, T. H., A. Vengosh, R. B. Jackson, N. R. Warner, and R. J. Poreda (2014), Noble gases identify the mechanisms of fugitive gas contamination in drinking-water wells overlying the Marcellus and Barnett Shales, *Proceedings of the National Academy of Sciences*, 111(39), 14076–14081, doi:10.1073/pnas.1322107111.

- Darrah, T. H., R. B. Jackson, A. Vengosh, N. R. Warner, C. J. Whyte, T. B. Walsh, A. J. Kondash, and R. J. Poreda (2015), The evolution of Devonian hydrocarbon gases in shallow aquifers of the northern Appalachian Basin: Insights from integrating noble gas and hydrocarbon geochemistry, *Geochimica et Cosmochimica Acta*, 170 IS -, 321–355, doi:10.1016/j.gca.2015.09.006.
- Elliot, T., C. J. Ballentine, R. K. O'Nions, and T. Ricchiuto (1993), Carbon, helium, neon and argon isotopes in a Po basin (northern Italy) natural gas field, *Chemical Geology*, 106(3-4), 429–440, doi:10.1016/0009-2541(93)90042-H.
- Fanale, F. P., and W. A. Cannon (1971), Physical adsorption of rare gas on terrigenous sediments, *Earth and Planetary Science Letters*, 11(1-5), 362–368, doi:10.1016/0012-821X(71)90195-6.
- Frick, U., and S. Chang (1977), Ancient carbon and noble gas fractionation, *Lunar and Planetary Science Conference ....*
- Frick, U., R. Mack, and S. Chang (1979), Noble gas trapping and fractionation during synthesis of carbonaceous matter, *Lunar and Planetary Science ....*
- Heath, J. E., K. L. Kuhlman, D. G. Robinson, and S. J. Bauer (2015), *Appraisal of Transport and Deformation in Shale Reservoirs using Natural Noble Gas Tracers.*, Sandia National Laboratories.
- Hiyagon, H., and B. M. Kennedy (1992), Noble gases in CH<sub>4</sub>-rich gas fields, Alberta, Canada, *Geochimica et Cosmochimica Acta*, 56(4), 1569–1589, doi:10.1016/0016-7037(92)90226-9.
- Hunt, A. G., T. H. Darrah, and R. J. Poreda (2012), Determining the source and genetic fingerprint of natural gases using noble gas geochemistry: A northern Appalachian Basin case study, *AAPG Bulletin*, 96(10), 1785–1811, doi:10.1306/03161211093.
- Jackson, R. B., A. Vengosh, T. H. Darrah, N. R. Warner, A. Down, R. J. Poreda, S. G. Osborn, K. Zhao, and J. D. Karr (2013), Increased stray gas abundance in a subset of drinking water wells near Marcellus shale gas extraction, *Proceedings of the National Academy of Sciences of the USA*, 110(28), 11250–11255, doi:10.1073/pnas.1221635110/-/DCSupplemental/pnas.201221635SI.pdf.
- Kennedy, B. M. (1988), Noble gases in vent water from the Juan de Fuca Ridge, *Geochimica et Cosmochimica Acta*, 52(7), 1929–1935, doi:10.1016/0016-7037(88)90016-6.
- Kennedy, B. M., H. Hiyagon, and J. H. Reynolds (1990), Crustal neon: a striking uniformity, *Earth and Planetary Science Letters*, 98(3-4), 277–286, doi:10.1016/0012-821X(90)90030-2.
- Kennedy, B. M., T. Torgersen, and M. C. van Soest (2002), Multiple atmospheric noble gas components in hydrocarbon reservoirs, *Geochimica et Cosmochimica Acta*, 66(16), 2807–2822, doi:10.1016/S0016-7037(02)00883-9.

- Kharaka, Y. K., and D. J. Specht (1988), The solubility of noble gases in crude oil at 25–100°C, *Applied Geochemistry*, 3(2), 137–144, doi:10.1016/0883-2927(88)90001-7.
- Kipfer, R., W. Aeschbach-Hertig, F. Peeters, and M. Stute (2002), Noble Gases in Lakes and Ground Waters, *Reviews in Mineralogy and Geochemistry*, 47(1), 615–700.
- Kotarba, M. J., and K. Nagao (2008), Composition and origin of natural gases accumulated in the Polish and Ukrainian parts of the Carpathian region: Gaseous hydrocarbons, noble gases, carbon dioxide and nitrogen, *Chemical Geology*, 255(3-4), 426–438, doi:10.1016/j.chemgeo.2008.07.011.
- Lollar, B. S., and C. J. Ballentine (2009), Insights into deep carbon derived from noble gases,, 2(8), 543–547, doi:10.1038/ngeo588.
- Lollar, B. S., S. M. Weise, S. K. Frape, and J. F. Barker (1994), *Isotopic Constraints on the Migration of Hydrocarbon and Helium Gases of Southwestern Ontario*, *Bulletin of Canadian Petroleum Geology*, 42(3), 283–295.
- Ma, L., M. C. Castro, and C. M. Hall (2009), Atmospheric noble gas signatures in deep Michigan Basin brines as indicators of a past thermal event, *Earth and Planetary Science Letters*, 277(1–2), 137–147, doi:10.1016/j.epsl.2008.10.015.
- Ma, L., M. C. Castro, C. M. Hall, and L. M. Walter (2005), Cross-formational flow and salinity sources inferred from a combined study of helium concentrations, isotopic ratios, and major elements in the Marshall aquifer, southern Michigan, *Geochemistry Geophysics Geosystems*, 6(10), Q10004, doi:10.1029/2005GC001010.
- Mazor, E. (1972), Paleotemperatures and other hydrological parameters deduced from noble gases dissolved in groundwaters; Jordan Rift Valley, Israel, *Geochimica et Cosmochimica Acta*, 36(12), 1321–1336, doi:10.1016/0016-7037(72)90065-8.
- Mazor, E. (2003), *Chemical and Isotopic Groundwater Hydrology*, CRC Press.
- Mazor, E., and A. Bosch (1987), Noble gases in formation fluids from deep sedimentary basins: a review, *Applied Geochemistry*, 2(5-6), 621–627, doi:10.1016/0883-2927(87)90014-X.
- Mazor, E., and A. H. Truesdell (1984), Dynamics of a geothermal field traced by noble gases: Cerro Prieto, Mexico, *Geothermics*, 13(1–2), 91–102, doi:10.1016/0375-6505(84)90009-9.
- Molofsky, L. J., J. A. Connor, A. S. Wylie, T. Wagner, and S. K. Farhat (2013), Evaluation of Methane Sources in Groundwater in Northeastern Pennsylvania, *Ground Water*, 51(3), 333–349.
- Moritz, A., J.-F. Helie, D. L. Pinti, M. Larocque, D. Barnetche, S. Retailleau, R. Lefebvre, and Y. Gelinat (2015), Methane Baseline Concentrations and Sources in Shallow Aquifers from the Shale Gas-Prone Region of the St. Lawrence Lowlands (Quebec, Canada), *Environ. Sci. Technol.*, 49(7), 4765–4771, doi:10.1021/acs.est.5b00443.

- Nagao, K., N. Takaoka, and O. Matsubayashi (1981), Rare gas isotopic compositions in natural gases of Japan, *Earth and Planetary Science Letters*, 53(2), 175–188, doi:10.1016/0012-821X(81)90152-7.
- Nicot, J.-P., and B. R. Scanlon (2012), Water Use for Shale-Gas Production in Texas, U.S, *Environ. Sci. Technol.*, 46(6), 3580–3586, doi:10.1021/es204602t.
- Nicot, J.-P., B. R. Scanlon, R. C. Reedy, and R. A. Costley (2014), Source and Fate of Hydraulic Fracturing Water in the Barnett Shale: A Historical Perspective, *Environ. Sci. Technol.*, 48(4), 2464–2471, doi:10.1021/es404050r.
- O'Nions, R. K., C. J. Ballentine, A. Halliday, D. P. McKenzie, and M. L. Coleman (1993), Rare Gas Studies of Basin Scale Fluid Movement [and Discussion], *Philosophical Transactions: Physical Sciences and Engineering*, 344(1670), 141–156.
- Osborn, S. G., A. Vengosh, N. R. Warner, and R. B. Jackson (2011), Methane contamination of drinking water accompanying gas-well drilling and hydraulic fracturing, *Proceedings of the National Academy of Sciences*, 108(20), 8172–8176, doi:10.1073/pnas.1100682108.
- Oxburgh, E. R., R. K. O'Nions, and R. I. Hill (1986), Helium isotopes in sedimentary basins, *Nature*, 324(6098), 632–635, doi:10.1038/324632a0.
- Ozima, M., and F. A. Podosek (2002), *Noble Gas Geochemistry*, Cambridge University Press, New York.
- Phillips, F. M., and M. C. Castro (2003), 5.15 - Groundwater Dating and Residence-time Measurements, in *Treatise on Geochemistry*, edited by H. D. Holland and K. K. Turekian, pp. 451–497, Pergamon, Oxford.
- Pinti, D. L., and B. Marty (1995), Noble gases in crude oils from the Paris Basin, France: Implications for the origin of fluids and constraints on oil-water-gas interactions, *Geochimica et Cosmochimica Acta*, 59(16), 3389–3404, doi:10.1016/0016-7037(95)00213-J.
- Pinti, D. L., and B. Marty (2000), Chapter 7. NOBLE GASES IN OIL AND GAS FIELDS: ORIGINS AND PROCESSES, vol. 28, pp. 160–196, Fluids and Basin Evolution. Mineral Soc Can Short Course.
- Pinti, D. L., M. C. Castro, O. Shouakar-Stash, A. Tremblay, V. H. Garduño, C. M. Hall, J. F. Hélie, and B. Ghaleb (2012), Evolution of the geothermal fluids at Los Azufres, Mexico, as traced by noble gas isotopes,  $\delta^{18}\text{O}$ ,  $\delta\text{D}$ ,  $\delta^{13}\text{C}$  and  $^{87}\text{Sr}/^{86}\text{Sr}$ , *Journal of Volcanology and Geothermal Research*, 249(0), 1–11, doi:10.1016/j.jvolgeores.2012.09.006.
- Pitre, F., and D. L. Pinti (2010), Noble gas enrichments in porewater of estuarine sediments and their effect on the estimation of net denitrification rates, *Geochimica et Cosmochimica Acta*, 74(2), 531–539, doi:10.1016/j.gca.2009.10.004.
- Podosek, F. A., T. J. Bernatowicz, and F. E. Kramer (1981), Adsorption of xenon and krypton on

- shales, *Geochimica et Cosmochimica Acta*, 45(12), 2401–2415, doi:10.1016/0016-7037(81)90094-6.
- Porcelli, D., C. J. Ballentine, and R. Wieler (2002), An Overview of Noble Gas Geochemistry and Cosmochemistry, *Reviews in Mineralogy and Geochemistry*, 47(1), 1–19, doi:10.2138/rmg.2002.47.1.
- Poreda, R. J., A. Jeffrey, I. R. Kaplan, and H. Craig (1988), Magmatic helium in subduction-zone natural gases, *Chemical Geology*, 71(1), 199–210.
- Prinzhofer, A. (2013), Noble Gases in Oil and Gas Accumulations., 225–247, doi:10.1007/978-3-642-28836-4\_9.
- Prinzhofer, A., E. V. Dos Santos Neto, and A. Battani (2010), Coupled use of carbon isotopes and noble gas isotopes in the Potiguar basin (Brazil): Fluids migration and mantle influence, *Marine and Petroleum Geology*, 27(6), 1273–1284, doi:10.1016/j.marpetgeo.2010.03.004.
- Rogers, G. S. (1921), *Helium-bearing natural gas*, United States Geological Survey, Washington D. C.
- Sano, Y., T. Tominaga, and H. Wakita (1982), Elemental and isotopic abundances of rare gases in natural gases obtained by a quadrupole mass spectrometer, *Geochem. J.*, 16(6), 279–286, doi:10.2343/geochemj.16.279.
- Schlegel, M. E., Z. Zhou, J. C. McIntosh, C. J. Ballentine, and M. A. Person (2011), Constraining the timing of microbial methane generation in an organic-rich shale using noble gases, Illinois Basin, USA, *Chemical Geology*, 287(1–2), 27–40, doi:10.1016/j.chemgeo.2011.04.019.
- Sherwood, O. A., J. D. Rogers, G. Lackey, T. L. Burke, S. G. Osborn, and J. N. Ryan (2016), Groundwater methane in relation to oil and gas development and shallow coal seams in the Denver-Julesburg Basin of Colorado, *Proceedings of the National Academy of Sciences*, 113(30), 8391–8396.
- Siegel, D. I., N. A. Azzolina, B. J. Smith, A. E. Perry, and R. L. Bothun (2015), Methane Concentrations in Water Wells Unrelated to Proximity to Existing Oil and Gas Wells in Northeastern Pennsylvania, *Environ. Sci. Technol.*, 49(7), 4106–4112, doi:10.1021/es505775c.
- Siegel, D., B. Smith, E. Perry, R. Bothun, and M. Hollingsworth (2016), Dissolved methane in shallow groundwater of the Appalachian Basin: Results from the Chesapeake Energy predrilling geochemical database, *Environ. Geosci.*, 23(1), 1–47, doi:10.1306/eg.01051615015.
- Smith, S. P. (1985), *Noble gas solubility in water at high temperature*, Eos.
- Solomon, D. K., A. Hunt, and R. J. Poreda (1996), Source of radiogenic helium 4 in shallow

- aquifers: Implications for dating young groundwater, *Water Resources Research*, 32(6), 1805–1813, doi:10.1029/96WR00600.
- Stute, M., C. Sonntag, J. Deak, and P. Schlosser (1992a), Helium in deep circulating groundwater in the Great Hungarian Plain: Flow dynamics and crustal and mantle helium fluxes, *Geochimica et Cosmochimica Acta*, 56(5), 2051–2067, doi:10.1016/0016-7037(92)90329-H.
- Stute, M., J. F. Clark, P. Schlosser, W. S. Broecker, and G. Bonani (1995), A 30,000 yr Continental Paleotemperature Record Derived from Noble Gases Dissolved in Groundwater from the San Juan Basin, New Mexico, *Quaternary Research*, 43(2), 209–220, doi:10.1006/qres.1995.1021.
- Stute, M., P. Schlosser, J. F. Clark, and W. S. Broecker (1992b), Paleotemperatures in the Southwestern United States Derived from Noble Gases in Ground Water, *Science*, 256(5059), 1000–1003, doi:10.1126/science.256.5059.1000.
- Torgersen, T., and B. M. Kennedy (1999), Air-Xe enrichments in Elk Hills oil field gases: role of water in migration and storage, *Earth and Planetary Science Letters*, 167(3–4), 239–253, doi:10.1016/S0012-821X(99)00021-7.
- Torgersen, T., and G. N. Ivey (1985), Helium accumulation in groundwater. II: A model for the accumulation of the crustal  $4\text{He}$  degassing flux, *Geochimica et Cosmochimica Acta*, 49(11), 2445–2452, doi:10.1016/0016-7037(85)90244-3.
- Torgersen, T., and W. B. Clarke (1985), Helium accumulation in groundwater, I: An evaluation of sources and the continental flux of crustal  $4\text{He}$  in the Great Artesian Basin, Australia, *Geochimica et Cosmochimica Acta*, 49(5), 1211–1218, doi:10.1016/0016-7037(85)90011-0.
- Torgersen, T., B. M. Kennedy, H. Hiyagon, K. Y. Chiou, J. H. Reynolds, and W. B. Clarke (1989), Argon accumulation and the crustal degassing flux of  $40\text{Ar}$  in the Great Artesian Basin, Australia, *Earth and Planetary Science Letters*, 92(1), 43–56.
- Torgersen, T., M. A. Habermehl, and W. B. Clarke (1992), Crustal helium fluxes and heat flow in the Great Artesian Basin, Australia, *Chemical Geology*, 102(1-4), 139–152, doi:10.1016/0009-2541(92)90152-U.
- US EIA (2016), *Annual Energy outlook 2016*, US Energy Information Administration.
- Warrier, R. B., M. C. Castro, C. M. Hall, and K. C. Lohmann (2013), Large atmospheric noble gas excesses in a shallow aquifer in the Michigan Basin as indicators of a past mantle thermal event, *Earth and Planetary Science Letters*, 375(0), 372–382, doi:10.1016/j.epsl.2013.06.001.
- Weiss, R. F. (1970), The solubility of nitrogen, oxygen and argon in water and seawater, *Deep Sea Research and Oceanographic Abstracts*, 17(4), 721–735, doi:10.1016/0011-7471(70)90037-9.

- Weiss, R. F. (1971), Solubility of helium and neon in water and seawater, *J. Chem. Eng. Data*, 16(2), 235–241, doi:doi: 10.1021/je60049a019.
- Weiss, R. F., and T. K. Kyser (1978), Solubility of krypton in water and sea water, *J. Chem. Eng. Data*, 23(1), 69–72.
- Wen, T., M. C. Castro, B. R. Ellis, C. M. Hall, and K. C. Lohmann (2015), Assessing compositional variability and migration of natural gas in the Antrim Shale in the Michigan Basin using noble gas geochemistry, *Chemical Geology*, 417, 356–370, doi:10.1016/j.chemgeo.2015.10.029.
- Wen, T., M. C. Castro, J.-P. Nicot, C. M. Hall, T. Larson, P. Mickler, and R. Darvari (2016), Methane Sources and Migration Mechanisms in Shallow Groundwaters in Parker and Hood Counties, Texas—A Heavy Noble Gas Analysis, *Environ. Sci. Technol.*, doi:10.1021/acs.est.6b01494.
- Wen, T., M. C. Castro, J.-P. Nicot, C. M. Hall, D. L. Pinti, P. Mickler, R. Darvari, and T. Larson, Characterizing the Noble Gas Isotopic Composition of the Barnett Shale and Strawn Group and Constraining the Source of Stray Gas in the Trinity Aquifer, North-Central Texas, submitted to *Environ. Sci. Technol.*
- Wetherill, G. (1954), Variations in the Isotopic Abundances of Neon and Argon Extracted from Radioactive Minerals, *Physical Review*, 96(3), 679–683, doi:10.1103/PhysRev.96.679.
- Winckler, G., R. Kipfer, W. Aeschbach-Hertig, R. Botz, M. Schmidt, S. Schuler, and R. Bayer (2000), Sub sea floor boiling of Red Sea brines: new indication from noble gas data, *Geochimica et Cosmochimica Acta*, 64(9), 1567–1575, doi:10.1016/S0016-7037(99)00441-X.
- Xu, S., S. Nakai, H. Wakita, and X. Wang (1995), Mantle-derived noble gases in natural gases from Songliao Basin, China, *Geochimica et Cosmochimica Acta*, 59(22), 4675–4683, doi:10.1016/0016-7037(95)00301-0.
- Zartman, R. E., G. J. Wasserburg, and J. H. Reynolds (1961), Helium, argon, and carbon in some natural gases, *J. Geophys. Res.*, 66(1), 277–306, doi:10.1029/JZ066i001p00277.
- Zhou, Z., and C. J. Ballentine (2006), 4He dating of groundwater associated with hydrocarbon reservoirs, *Chemical Geology*, 226(3–4), 309–327.
- Zhou, Z., C. J. Ballentine, R. Kipfer, M. Schoell, and S. Thibodeaux (2005), Noble gas tracing of groundwater/coalbed methane interaction in the San Juan Basin, USA, *Geochimica et Cosmochimica Acta*, 69(23), 5413–5428, doi:10.1016/j.gca.2005.06.027.

# CHAPTER 2

## ASSESSING COMPOSITIONAL VARIABILITY AND MIGRATION OF NATURAL GAS IN THE ANTRIM SHALE IN THE MICHIGAN BASIN USING NOBLE GAS GEOCHEMISTRY <sup>1</sup>

### 2.1 Abstract

This study uses stable noble gases' (He, Ne, Ar, Kr, Xe) volume fractions and isotopic ratios from Antrim Shale natural gas to assess compositional variability and vertical fluid migration within this reservoir, in addition to distinguishing between the presence of thermogenic versus biogenic methane. R/Ra values, where R is the measured  $^3\text{He}/^4\text{He}$  ratio and Ra is the atmospheric value of  $1.384 \pm 0.013 \times 10^{-6}$ , vary from 0.01 to 0.34 suggesting a largely dominant crustal  $^4\text{He}$  component with minor atmospheric and mantle contributions. Crustal  $^{21}\text{Ne}$ ,  $^{40}\text{Ar}$  and  $^{136}\text{Xe}$  contributions are also present but the atmospheric component is largely dominant for these gases. Crustal contributions for  $^{21}\text{Ne}$ ,  $^{40}\text{Ar}$  and  $^{136}\text{Xe}$  vary between 1.1% and 12.5%, between 0.7% and 19% and between 0.1% and 2.7%, respectively. A few samples present higher than atmospheric  $^{20}\text{Ne}/^{22}\text{Ne}$  ratios pointing to the presence of a small mantle Ne component. High

---

<sup>1</sup> Citation: Wen, T., Castro, M.C., Ellis, B.R., Hall, C.M., Lohmann, K.C., 2015. Assessing compositional variability and migration of natural gas in the Antrim Shale in the Michigan Basin using noble gas geochemistry. *Chemical Geology* 417, 356–370. doi:10.1016/j.chemgeo.2015.10.029

horizontal and vertical variability of noble gas signatures in the Antrim Shale are observed. These are mainly due to variable noble gas input from deep brines and, to a smaller extent, variable in-situ production within different layers of the Antrim Shale, in particular, the Lachine and Norwood Members. Estimated  $^4\text{He}$  ages, considering external  $^4\text{He}$  input for Antrim Shale water, vary between 0.9 ka and 238.2 ka and match well for most samples with the timing of the major Wisconsin glaciation, suggesting that Antrim Shale water was influenced by glaciation-induced recharge. Consistency between measured and predicted  $^{40}\text{Ar}/^{36}\text{Ar}$  ratios assuming Ar release temperatures  $\geq 250^\circ\text{C}$  supports a thermogenic origin for most of the methane in these samples. This thermogenic methane is likely to originate at greater depths, either from the deeper portion of the Antrim Shale in the central portion of the Michigan Basin or from deeper formations given that the thermal maturity of the Antrim Shale in the study area is rather low.

## **2.2 Introduction**

With rising demands for cleaner domestic energy resources, unconventional hydrocarbon production has been extensively developed since 1979 [Hill and Nelson, 2000; Curtis, 2002; Nicot *et al.*, 2014]. As a result, unconventional reservoirs (*e.g.*, black shales) accounted for more than one third of the total natural gas production in the United States in 2013 [US EIA, 2015].

The Antrim Shale in the Michigan Basin has been one of the most actively developed shale gas plays in the USA with its major expansion taking place in the late 1980s [Walter *et al.*, 1996; Curtis, 2002; Harrison, 2007]. Unlike most shale gas plays in the USA (*e.g.*, Barnett and Marcellus Shales) [Nicot and Scanlon, 2012], the Antrim Shale is naturally highly fractured [Aprotia *et al.*, 1994; Ryder, 1996]. It has been suggested that ice sheet advances and retreats enhanced the dilation of preexisting fractures and induced freshwater recharge into the Antrim

Shale [McIntosh *et al.*, 2011]. This, in turn, supported microbial methanogenesis [Clark, 1982; Martini *et al.*, 1998; 2003; McIntosh and Walter, 2005]. Previous natural gas exploitation in the Antrim Shale indicates that natural gas production rates could vary over an order of magnitude suggesting possibly highly localized heterogeneities within the Antrim Shale, particularly within the Lachine and Norwood Members [Manger *et al.*, 1991]. However, little is known about the relationship between variable natural gas production rates and geochemical composition variability in the Antrim Shale.

Previous studies, located mostly in the northern lower peninsula of Michigan (NPT: Northern Producing Trend) (Figures 2.1 and 2.2a), investigated the origin of the main dissolved solids as well as timing ( $^{14}\text{C}$  ages) of meteoric recharge into the Antrim Shale [Farrand and Eschman, 1974; Martini *et al.*, 1996; Walter *et al.*, 1996; Martini *et al.*, 1998]. Based on methane and co-produced formation waters, a biogenic origin for the majority of the methane was suggested, with thermogenic gas making up < 20% of the total produced gas [Martini *et al.*, 1996]. However, recent studies have suggested that the contribution of thermogenic methane should be comparable to that of biogenic methane, based on measurement of multiple substituted methane isotopologues ( $^{13}\text{CH}_3\text{D}$ ,  $^{12}\text{CH}_2\text{D}_2$ ) [Stolper *et al.*, 2014; 2015]. Although identifying the timing of freshwater recharge into the Antrim Shale and the relative contribution of thermogenic vs. biogenic methane in Antrim Shale gas can be challenging due to the migration and mixing of waters and gases in the subsurface [Price and Schoell, 1995; Hunt, 1996; Martini *et al.*, 1998; Stolper *et al.*, 2015; Wen *et al.*, 2015], this knowledge is essential to understand the origin, migration and mixing of methane within and beyond the Antrim Shale. Filling these knowledge gaps is important to guide natural gas exploration and to identify the source of methane in the Antrim Shale.

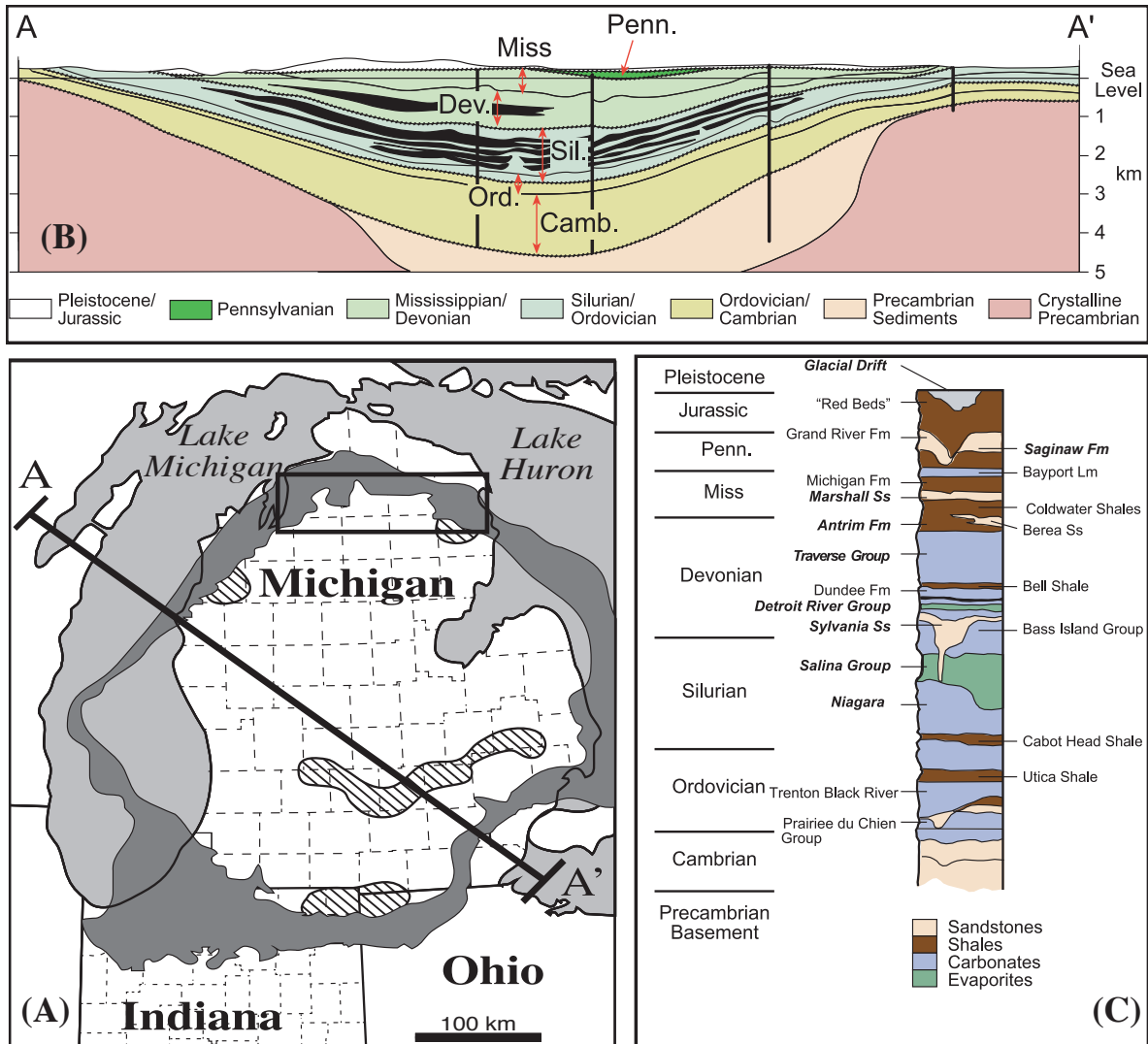
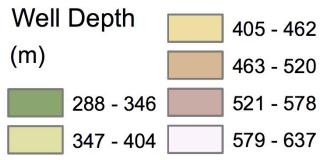
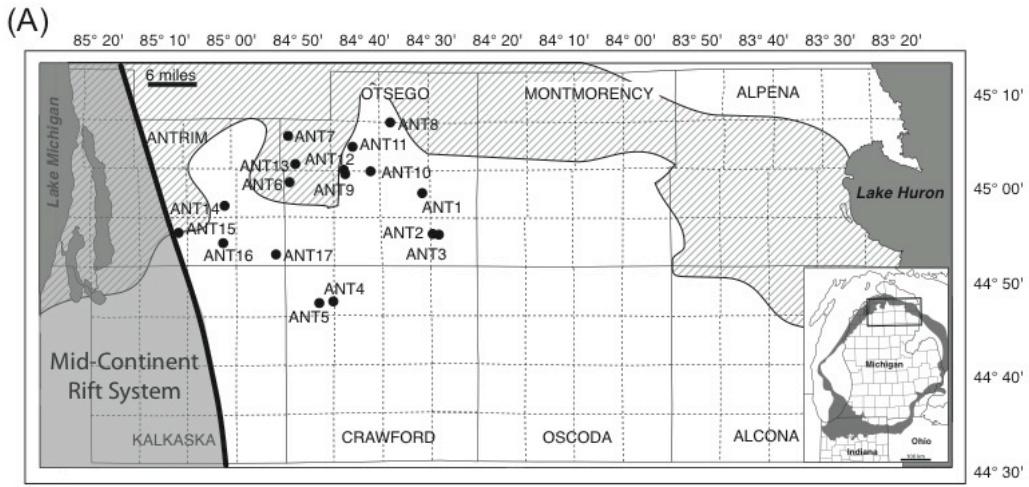


**Figure 2.1** (a) Central portion of the Michigan Basin (lower peninsula of Michigan). The subcrop of the Antrim Shale is shown in dark brown; the Northern Producing Trend (NPT) of the Antrim Shale gas play is indicated by the rectangular area [adapted from *Martini et al.*, 1998]; (b) General schematic geological representation along cross section A–A' in (a); Rock salts are present in the Michigan Basin as represented by the black layer; (c) Schematic of the Michigan Basin stratigraphy; major formations and lithologies in the basin are identified.



(B)

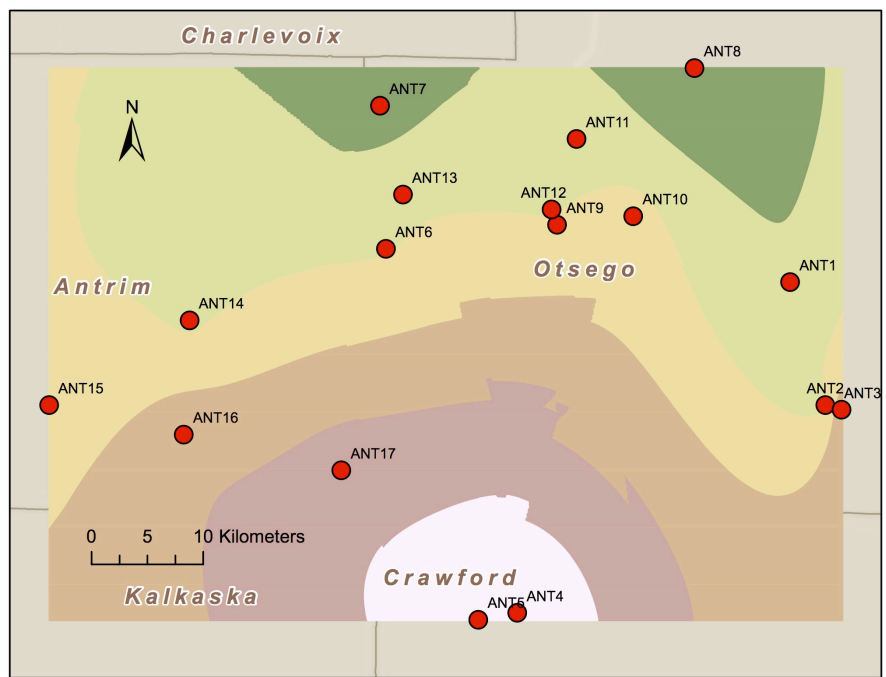


**Figure 2.2** (a) Location map of all sampled Antrim wells, with Antrim Shale subcrop (stripped area) and Mid-Continent Rift System in the Michigan Basin (black shadow) also indicated; (b) Contour map of perforation depths for sampled Antrim Shale gas wells in this study.

Stable noble gases (Helium – He, Neon – Ne, Argon – Ar, Krypton – Kr, Xenon - Xe) are chemically inert and are thus transported without being affected by chemical reactions or microbial activity [Ballentine, 1991; Ozima and Podosek, 2002; Hilton and Porcelli, 2003a]. Moreover, noble gases in subsurface fluids (e.g., freshwater, natural gas) are derived from the atmosphere, crust and mantle, all of which show distinct isotopic and elemental signatures [Ozima and Podosek, 2002; Porcelli et al., 2002; Hilton and Porcelli, 2003b; Pinti et al., 2012]. This fact makes noble gases ideal natural tracers for studying the origin and evolution of crustal fluids in sedimentary basins [Oxburgh et al., 1986; Ballentine, 1991; Pinti and Marty, 1995; Castro et al., 1998a; 1998b; Hilton and Porcelli, 2003b; Kulongoski et al., 2005; Warriar et al., 2013]. In most subsurface fluids in sedimentary systems, noble gases are dominated by an atmospheric origin (Air Saturated Water or ASW, containing Ne, Ar, Kr and Xe in solubility equilibrium with the atmosphere) and/or crustal components (e.g.,  $^4\text{He}^*$ ,  $^{21}\text{Ne}^*$ ,  $^{40}\text{Ar}^*$ ,  $^{136}\text{Xe}^*$ ) where crustal He, Ne, Ar, Kr, and Xe are indicated with the a “\*” notation. These result from radioactive decay of U/Th and  $^{40}\text{K}$  [Ozima and Podosek, 2002]. Mantle contributions are generally minor but not negligible [Pinti and Marty, 2000; Ma et al., 2005; Castro et al., 2009; Ma et al., 2009b; Darrah et al., 2014; Wen et al., 2015].

Previous studies of noble gas isotopic ratios and crustally-produced noble gas components in the shallower Glacial Drift, Saginaw and Marshall aquifers suggest the presence of vertical cross-formational flow (i.e., upward leakage) into these aquifers from deeper formations [Ma et al., 2005; Warriar et al., 2013; Wen et al., 2015]. Deep (0.5–3.6 km) brine samples were also collected and analyzed for noble gas concentrations and isotopic ratios in the Michigan Basin and point to the presence of cross-formational flow [Castro et al., 2009; Ma et al., 2009b]. Depletion of atmospheric noble gases in these brines is also observed, indicating the

occurrence of a past thermal event in this system [Castro *et al.*, 2009; Ma *et al.*, 2009a; 2009b; Warriar *et al.*, 2013]. Such a depletion can be used to identify the contribution of deeper saline formation waters into the Antrim Shale.

In this study, we use noble gas isotopic ratios and volume fractions of natural gas samples from the Antrim Shale to assess the compositional variability of crustally produced noble gases, which would point to variable in-situ production from their parent elements (*i.e.*, U, Th,  $^{40}\text{K}$ ) and/or the variable contribution of external brines from deeper formations into the Antrim Shale. In addition,  $^4\text{He}$  ages for Antrim brines are calculated and compared with previously reported  $^{14}\text{C}$  ages of Antrim water samples [Martini *et al.*, 1998]. We also use  $^{40}\text{Ar}/^{36}\text{Ar}$  ratios to distinguish between the presence of thermogenic versus biogenic methane in the Northern Producing Trend (NPT) of the Antrim Shale. The Northern Producing Trend, centered near Otsego County, extends to its neighboring counties to the east and west. It is in this area that most of the natural gas producing wells in the Antrim Shale are located in.

### **2.3 Geologic Setting**

Located in the northeastern United States, the Michigan Basin is a concentric intracratonic depression floored by crystalline Precambrian basement (Figure 2.1), and consists of a succession of sedimentary rocks from Precambrian to Jurassic that reaches depths of over 5 km [Dorr and Eschman, 1970; Catacosinos and Daniels, 1991]. The entire sedimentary strata are covered by thick Pleistocene Glacial Drift sediments and are composed mainly of evaporites (*e.g.*, Salina Group), carbonates (*e.g.*, Traverse Formation), shales (*e.g.*, Antrim and Coldwater Formations), and sandstones (*e.g.*, Marshall Formation) (Figure 2.1c). Depending on their nature, these sedimentary rocks constitute either aquitards (*e.g.*, shale, evaporites) or aquifers (mostly

sandstones and reefal and dolomitized limestones), giving origin to a multi-layered aquifer system [Vugrinovich, 1986; Westjohn and Weaver, 1996]. Major tectonic structures such as the Albion-Scipio Fault, the Lucas Fault, and the Howell Anticline are present in southern Michigan and penetrate the Precambrian crystalline basement [Fisher *et al.*, 1988]. The Howell Anticline belongs to the Eastern Granite and Rhyolite Province (EGRP), and displays an age of  $\sim 1.5$  Ga [Hinze *et al.*, 1975; Van Schmus, 1992; Menuge *et al.*, 2002].

The Antrim Shale is a later Devonian formation and consists mainly of black carbonaceous shale. It underlies all of the Mississippian formations and is underlain by the middle Devonian Traverse Group [Gutschick and Sandberg, 1991; Apotria *et al.*, 1994]. The circular subcrop of the Antrim Shale is close to the basin margin and underlies the Pleistocene glacial sediments (Figure 2.1). From Figure 2.2b, which displays contours of perforation depth of the sampled wells, it is apparent that the Antrim Shale deepens from the north to the south. Overall, the Antrim Shale is significantly shallower than other shale gas plays (*e.g.*, Barnett Shale) in the USA, with a perforation depth ranging from 317 to 637 m in the sampling area. The Antrim Shale is divided into four members based on total organic carbon (TOC) content. These members include the Norwood, Paxton, Lachine, and Upper Antrim [Gutschick and Sandberg, 1991], of which the Norwood and Lachine Members have the highest organic content (0.5-24 wt% TOC) and are the main targets of gas exploitation [Walter *et al.*, 1996; Martini *et al.*, 1998]. The thermal maturity of the Antrim Shale in the NPT of the Michigan Basin was determined by vitrinite reflectance ( $R_o$ ) and ranges from 0.4 to 0.6% [Rullkötter *et al.*, 1992], indicating a low level of thermal maturation (preoil generation) [Waples, 1985].

Fractures in the Antrim Shale are regional and were formed during deeper burial [Martini *et al.*, 2003]. Two sets of fractures are dominant in the Antrim Shale: (1) NW-striking fractures

formed by natural hydraulic fracturing as hydrocarbons were generated near the end of the Alleghenian orogeny, and; (2) NE-striking fractures formed as a result of cooling and unloading during the 1-1.5 km of basin uplift since the Permian [*Cercone and Pollack, 1991; Apotria et al., 1994; Wang et al., 1994; Ryder, 1996*]. The fracture network present in the NPT of the Antrim Shale acts as a reservoir and conduit allowing the migration and mixing of meteoric water from the above Glacial Drift aquifer, and brine from the underlying permeable Traverse limestone [*Walter et al., 1996*].

The Antrim Shale is somewhat unique among shale gas reservoirs since it produces significant volumes of water and its gas production occurs at relatively shallow depths (~300-600 m below the surface) [*Dolton and Quinn, 1996; Boyer et al., 2006*]; Total average porosity in the Antrim is 9%, and it is assumed that natural gas fills roughly half of this porosity [*Curtis, 2002*].

## **2.4 Sampling and Analytical Methods**

A total of 17 Antrim Shale gas samples were collected at the wellhead of production wells in the NPT area (Figures 2.2a, b) in standard refrigeration grade 3/8" Cu tubes which were then sealed by steel pinch-off clamps [*Weiss, 1968*]. Atmospheric contamination during sampling was minimized by allowing the gas to flush through the system for approximately 5 min. The complete measurement procedure, carried out in the Noble Gas Lab at the University of Michigan, comprises estimation of He, Ne, Ar, Kr, and Xe volume fractions and their respective isotopic ratios, with standard errors for volume estimates of 1.5, 1.3, 1.3, 1.5 and 2.2%, respectively. When replicate analyses are available, an error-weighted average is reported. Analysis procedures are described briefly below.

Shale gas samples in Cu tubes were attached to a vacuum extraction and purification system. The copper tube is connected to a vacuum system at a pressure of  $\sim 2 \times 10^{-5}$  Torr. Once this pressure is achieved and the system isolated from its turbo-molecular vacuum pump, the lower clamp is released to allow gas samples to flow into the extraction and purification section. Dry gas samples are then inlet to a getter with Ti sponge at 600°C for 5 minutes to remove all actives gases. Noble gases are then quantitatively extracted and sequentially allowed to enter a Thermo Scientific® Helix SFT mass spectrometer using a cryo-separator. Subsequently, noble gases are trapped onto the cryo-separator at a temperature of  $\sim 10$  K. The cryo-temperature is subsequently increased sequentially to release temperatures for He, Ne, Ar, Kr, and Xe, at 42 K, 80 K, 205 K, 215K, and 280 K, respectively. Specifically, at the He release temperature, He is introduced into the mass spectrometer and the signal intensity of  $^4\text{He}$  is determined for the He concentration estimate. This estimate is then used by the automated system to optimize the amount of He that should be introduced for measurement of the  $^3\text{He}/^4\text{He}$  ratio.

Complete measurement procedures involve estimating the concentration of each noble gas component, measuring the isotopic ratios for Ne, Ar, Kr, and Xe, as well as the  $^3\text{He}/^4\text{He}$  ratio. First, a portion of a known volume of air is introduced into the molecular sieve section of the extraction system, and all noble gases are measured in turn with the Helix SFT mass spectrometer. This calibrates the mass spectrometer signal size for each noble gas. Subsequent to the air calibration run, the same measurement procedure is performed on a portion of the unknown sample. All noble gas isotopes are measured using a Faraday detector, except for  $^3\text{He}$  which is measured using an electron multiplier in ion counting mode.

A total of 17 co-produced formation water samples were also collected at the same time for analysis of chloride concentrations ( $\text{Cl}^-$ ). Water samples were filtered with a 0.45  $\mu\text{m}$  Gelman

Laboratory AquaPrep filter, and kept in high-density polyethylene bottles with no headspace prior to analysis. Chloride concentrations were determined in the HydroGeochemistry Laboratory at the University of Michigan and were analyzed by ion chromatograph (Dionex DX) with a AS4A column (precision,  $\pm 2\%$ ). Abundances of major gas components ( $\text{CH}_4$ ,  $\text{CO}_2$ ,  $\text{N}_2$ ) in the produced natural gas samples were collected at the wellheads in stainless steel cylinders and analyzed by Southern Petroleum Laboratories Inc. and Fibertec Environmental Services. Routine methods of gas chromatography were applied to determine the concentrations of  $\text{CH}_4$ ,  $\text{CO}_2$  and  $\text{N}_2$ .

## **2.5 Results**

### ***2.5.1 Major Gas Components in the Antrim Shale Gas***

Sample names and ID, location, well depth and abundances of major gas components ( $\text{CH}_4$ ,  $\text{CO}_2$ ,  $\text{N}_2$ ) for collected Antrim Shale gas samples are given in Table 2.1. Locations of all sampled Antrim gas wells are close to the southern boundary of the Antrim subcrop within the NPT region where we may identify the contribution of thermogenic methane in addition to microbial methane (Figure 2.2a). This sampling area overlaps also with that of *Martini et al.* [1998], thus allowing us to compare previous findings by these authors with those of the current study.

Among the major gas components  $\text{CH}_4$  ( $\text{C}_1$ ) is largely dominant, ranging from 79.72% to 92.40% by volume and displaying no obvious correlation with depth.  $\text{CO}_2$  and  $\text{N}_2$  contents are variable and range from 6.97% to 20.18% and from 0.04% to 0.15%, respectively. Similar to  $\text{CH}_4$ , no obvious correlations are observed between  $\text{CO}_2$  and  $\text{N}_2$  versus depth (Table 2.1). However, an inverse correlation is present between  $\text{CH}_4$  and  $\text{CO}_2$  contents regardless of whether

C<sub>1</sub> and CO<sub>2</sub> contents are variable over the sampling area. Because CO<sub>2</sub> is more strongly sorbed initially in the Antrim Shale as pressures continually drop with gas production, a greater percentage of CO<sub>2</sub> is desorbed compared to CH<sub>4</sub> [Martini *et al.*, 2003]. This likely explains the observed CH<sub>4</sub> and CO<sub>2</sub> content inverse correlation in this study.

Volume fractions of heavier hydrocarbons (C<sub>2+</sub>) as well as the carbon isotopic composition of hydrocarbon species are not available for the Antrim gas samples. However, previous geochemical studies in the Antrim Shale have determined the range of C<sub>1</sub>/(C<sub>2</sub>+C<sub>3</sub>) to vary from 1 to 10000, strongly suggesting mixing between thermogenic and biogenic gas components within the NPT [Martini *et al.*, 1996; 1998]. Methane from the Antrim Shale gas has δ<sup>13</sup>C values ranging from -45 to -55‰, straddling typical values of these two gases: thermogenic versus biogenic [Martini *et al.*, 1996]. Unusually high δ<sup>13</sup>C values of CO<sub>2</sub> co-produced with methane (~+22‰) and dissolved inorganic carbon in formation waters (~+28‰) require a bacterial mechanism [Martini *et al.*, 1996].

### ***2.5.2 Noble Gas Signatures in the Antrim Shale Gas***

Noble gas isotopic ratios (He, Ne, Ar, Kr, Xe) are listed in Table 2.2. Atmospheric isotopic ratios are also reported for reference.

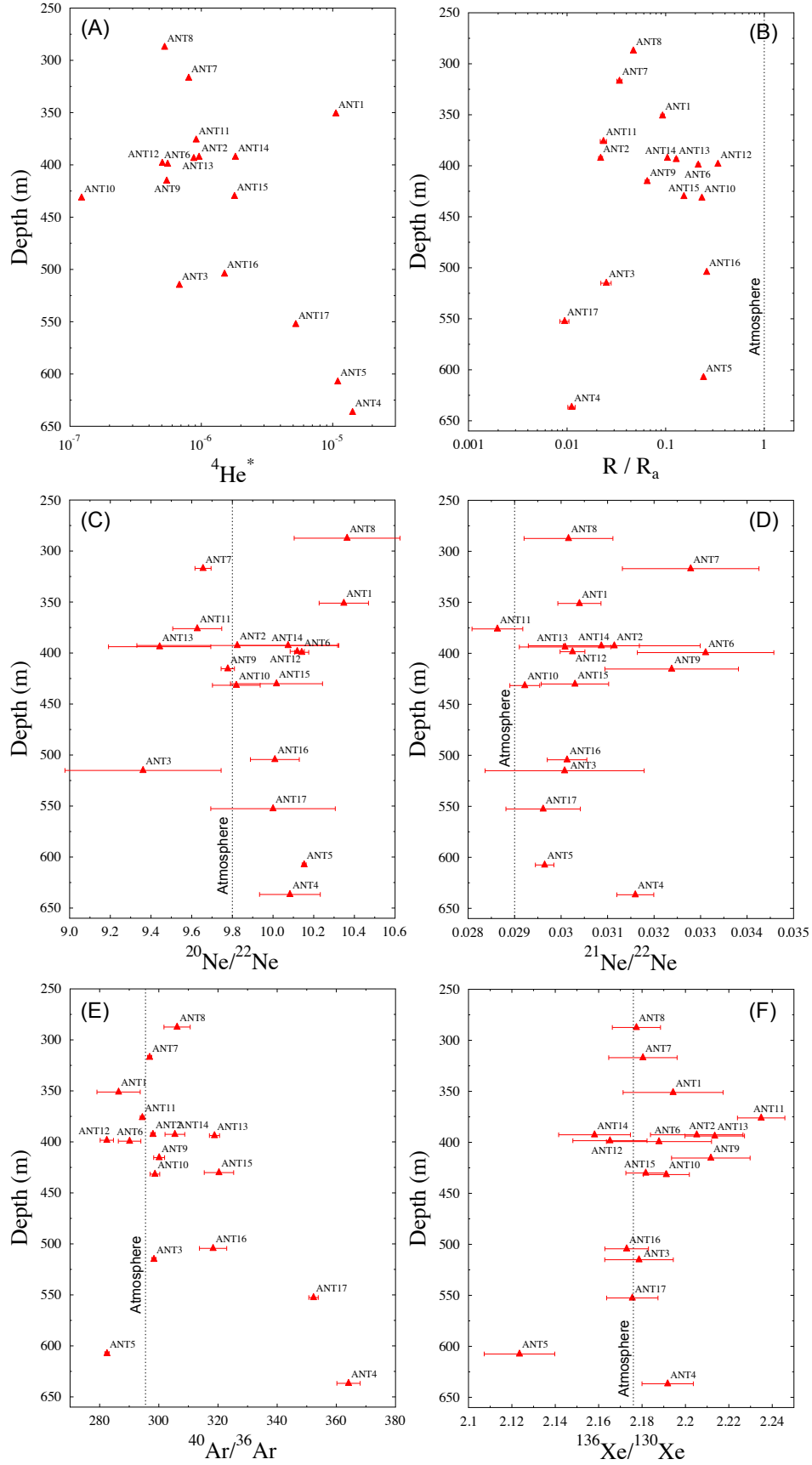


**Figure 2.3** Depth profiles of (a) radiogenic  $^4\text{He}$  volume fractions, (b)  $R/R_a$  ratios, (c)  $^{20}\text{Ne}/^{22}\text{Ne}$  ratios, (d)  $^{21}\text{Ne}/^{22}\text{Ne}$  ratios, (e)  $^{40}\text{Ar}/^{36}\text{Ar}$  ratios and (f)  $^{136}\text{Xe}/^{130}\text{Xe}$  ratios for collected Antrim gas samples revealing high spatial variability of noble gas signatures within the Antrim Shale. Corresponding atmospheric noble gas values are indicated (dashed lines).

**Table 2.1** Well location and major gas components (shown in volume %) for Antrim Shale gas samples.

| Sample ID | Well Name               | County   | State | Date     | Latitude | Longitude | Depth (m) | CH <sub>4</sub> (%) | CO <sub>2</sub> (%) | N <sub>2</sub> (%) |
|-----------|-------------------------|----------|-------|----------|----------|-----------|-----------|---------------------|---------------------|--------------------|
| ANT1      | Chester East D3-14      | Otsego   | MI    | 12/19/13 | 44.9881  | -84.5135  | 351       | 79.73               | 20.06               | 0.13               |
| ANT2      | State Charlton 4-7      | Otsego   | MI    | 12/19/13 | 44.9180  | -84.4851  | 393       | 92.40               | 6.97                | 0.12               |
| ANT3      | Allen Park 9-8          | Otsego   | MI    | 12/19/13 | 44.9154  | -84.4721  | 515       | 88.09               | 11.01               | 0.14               |
| ANT4      | St. Frederic X A3-25    | Crawford | MI    | 12/19/13 | 44.7995  | -84.7331  | 637       | -                   | 12.60               | -                  |
| ANT5      | St. Frederic IX B1-26   | Crawford | MI    | 12/19/13 | 44.7956  | -84.7646  | 607       | -                   | 13.16               | -                  |
| ANT6      | Hayes 7 C2-7            | Otsego   | MI    | 12/19/13 | 45.0071  | -84.8388  | 399       | 80.76               | 19.18               | 0.06               |
| ANT7      | State Elmira D3-7       | Otsego   | MI    | 12/19/13 | 45.0885  | -84.8436  | 317       | 91.46               | 7.68                | 0.86               |
| ANT8      | Dover Ridge A1-5 HDL    | Otsego   | MI    | 12/19/13 | 45.1098  | -84.5904  | 287       | 92.01               | 7.20                | 0.80               |
| ANT9      | Bagley 5 D2-5           | Otsego   | MI    | 12/19/13 | 45.0208  | -84.7011  | 415       | 84.27               | 15.63               | 0.10               |
| ANT10     | Bagley -Livingston B2-2 | Otsego   | MI    | 10/2/14  | 45.0256  | -84.6398  | 432       | 79.72               | 20.18               | 0.04               |
| ANT11     | Livingston A2-21        | Otsego   | MI    | 10/2/14  | 45.0696  | -84.6854  | 376       | 84.21               | 15.69               | 0.10               |
| ANT12     | St. Livingston D2-32    | Otsego   | MI    | 10/2/14  | 45.0295  | -84.7055  | 398       | 84.27               | 15.63               | 0.10               |
| ANT13     | Camp Ten B3-32          | Otsego   | MI    | 10/2/14  | 45.0379  | -84.8252  | 394       | 84.07               | 15.79               | 0.15               |
| ANT14     | Green River C3-26       | Antrim   | MI    | 10/2/14  | 44.9663  | -84.9969  | 393       | 85.23               | 13.08               | 0.11               |
| ANT15     | State Custer D1-12      | Antrim   | MI    | 10/2/14  | 44.9180  | -85.1100  | 430       | 86.51               | 9.60                | 0.07               |
| ANT16     | Mancelona East A2-23    | Antrim   | MI    | 10/2/14  | 44.9012  | -85.0016  | 504       | 82.20               | 11.19               | 0.14               |
| ANT17     | State Mancelona 3-26    | Antrim   | MI    | 10/2/14  | 44.8809  | -84.8748  | 553       | 79.78               | 13.80               | 0.12               |

**Table 2.2** Noble gas isotopic ratios for Antrim Shale gas samples.

| Sample ID        | R/R <sub>a</sub> | <sup>20</sup> Ne/ <sup>22</sup> Ne | <sup>21</sup> Ne/ <sup>22</sup> Ne | <sup>40</sup> Ar/ <sup>36</sup> Ar | <sup>136</sup> Xe/ <sup>130</sup> Xe | <sup>4</sup> He/ <sup>20</sup> Ne | <sup>20</sup> Ne/ <sup>36</sup> Ar | <sup>36</sup> Ar/ <sup>84</sup> Kr | $\frac{(^{40}\text{Ar}/^{36}\text{Ar})_{\text{predicted}}}{(^{40}\text{Ar}/^{36}\text{Ar})_{\text{measured}}}$ |
|------------------|------------------|------------------------------------|------------------------------------|------------------------------------|--------------------------------------|-----------------------------------|------------------------------------|------------------------------------|--|
| ANT1             | 0.093±0.004      | 10.35±0.12                         | 0.0304±0.0005                      | 286.4±7.3                          | 2.194±0.023                          | 74±2.4                            | 1.428±0.028                        | 44.6±1                             | 1.11   |
| ANT2             | 0.022±0.001      | 9.82±0.49                          | 0.0311±0.0013                      | 298±0.8                            | 2.205±0.021                          | 321±2                             | 0.018±0.001                        | 17±0.3                             | 1  |
| ANT3             | 0.025±0.003      | 9.36±0.38                          | 0.0301±0.0011                      | 298.3±0.7                          | 2.179±0.016                          | 230±2                             | 0.013±0.001                        | 22.8±0.5                           | 0.99   |
| ANT4             | 0.011±0.001      | 10.08±0.15                         | 0.0316±0.0004                      | 364.1±3.9                          | 2.192±0.012                          | 3099±2                            | 0.205±0.004                        | 11±0.2                             | 1.17   |
| ANT5             | 0.242±0.006      | 10.15±0.01                         | 0.0296±0.0002                      | 282.5±0.7                          | 2.123±0.016                          | 3±2                               | 0.773±0.014                        | 71.8±1.4                           | 1.05   |
| ANT6             | 0.214±0.008      | 10.14±0.03                         | 0.0331±0.0004                      | 290.1±3.8                          | 2.188±0.024                          | 6±2                               | 0.563±0.011                        | 30.9±0.6                           | 1.02   |
| ANT7             | 0.034±0.002      | 9.66±0.04                          | 0.0328±0.0004                      | 296.9±0.7                          | 2.18±0.016                           | 29±2                              | 0.084±0.002                        | 22.3±0.4                           | 1  |
| ANT8             | 0.047±0.001      | 10.36±0.26                         | 0.0302±0.001                       | 306.2±4.4                          | 2.177±0.011                          | 93±2                              | 0.199±0.004                        | 9.8±0.2                            | 0.98   |
| ANT9             | 0.065±0.003      | 9.78±0.03                          | 0.0324±0.0004                      | 300.1±1.8                          | 2.212±0.018                          | 39±2                              | 0.291±0.005                        | 23.8±0.5                           | 0.99   |
| ANT10            | 0.233±0.005      | 9.82±0.12                          | 0.0292±0.0003                      | 298.7±1.6                          | 2.191±0.011                          | 65±2                              | 0.129±0.002                        | 7.1±0.1                            | 0.99   |
| ANT11            | 0.023±0.002      | 9.63±0.12                          | 0.0286±0.0005                      | 294.4±0.7                          | 2.235±0.011                          | 84±2                              | 0.038±0.001                        | 35±0.7                             | 1.01   |
| ANT12            | 0.339±0.006      | 10.12±0.03                         | 0.0302±0.0003                      | 282.4±2.2                          | 2.165±0.017                          | 3±2                               | 0.728±0.013                        | 50.9±1                             | 1.05   |
| ANT13            | 0.128±0.004      | 9.44±0.25                          | 0.0301±0.001                       | 318.8±1.7                          | 2.213±0.014                          | 64±2                              | 0.308±0.009                        | 10.9±0.3                           | 0.94   |
| ANT14            | 0.104±0.003      | 10.07±0.25                         | 0.0309±0.0008                      | 305.4±3.3                          | 2.158±0.017                          | 192±2                             | 0.095±0.002                        | 22.1±0.4                           | 0.98   |
| ANT15            | 0.153±0.003      | 10.02±0.23                         | 0.0303±0.0007                      | 320.3±5                            | 2.182±0.009                          | 152±2                             | 0.29±0.006                         | 9.8±0.2                            | 0.95   |
| ANT16            | 0.261±0.005      | 10.01±0.12                         | 0.0301±0.0004                      | 318.3±4.6                          | 2.173±0.01                           | 64±2                              | 0.514±0.01                         | 10.9±0.2                           | 0.95   |
| ANT17            | 0.009±0.001      | 10±0.31                            | 0.0296±0.0008                      | 352.3±1.6                          | 2.175±0.012                          | 846±2                             | 0.256±0.009                        | 8.4±0.3                            | 0.96   |
| Air <sup>a</sup> | 1                | 9.8                                | 0.029                              | 295.5                              | 2.176                                | 0.288                             | -                                  | -                                  | -  |

<sup>a</sup> After Ozima and Podosek [2002].

R/Ra ratios in Antrim Shale gas, where R is the measured  $^3\text{He}/^4\text{He}$  and Ra is the atmospheric ratio value of  $1.384 \pm 0.013 \times 10^{-6}$ , vary from an almost pure radiogenic (crustal) value of  $0.009 \pm 0.001$  [typical crustal production values are  $\sim 0.01$ - $0.05$ ; *Oxburgh et al.*, 1986], to  $0.339 \pm 0.006$  (Figure 2.3b). Higher values of measured R/Ra ratios likely indicate the impact of mixing with an atmospheric component (R/Ra=1) introduced during meteoric recharge. A minor mantle He component is also likely present which may contribute, to a lesser extent, to increased R/Ra ratios. R/Ra values in Mid Ocean Ridge Basalts (MORB) and Ocean Island Basalts (OIB) are  $\sim 8$  and  $50$ , respectively [*Graham*, 2002; *Starkey et al.*, 2009]. R/Ra values of samples ANT5, ANT6, ANT10, ANT12 and ANT16 are greater than typical crustal values (Table 2.2 and Figure 2.3b). However, irrespective of an atmospheric or mantle origin leading to slightly higher R/Ra values, the radiogenic  $^4\text{He}$  component is largely dominant. For example, if He is treated as a two component mixture, a mantle and a crustal component, using a mantle R/Ra value of 8 and a crustal production value of 0.01 [*Ballentine et al.*, 1991], crustal  $^4\text{He}$  contributions in these samples vary between 96.8% and 100% of total measured  $^4\text{He}$ , which strongly indicates the dominance of crustal He in Antrim gas samples. No obvious correlation is observed between R/Ra and depth (Figure 2.3b). Typically, one would expect the R/Ra ratio to increase toward the surface due to incorporation of atmospheric He being carried by recharge water, leading to dilution of crustally produced He.

Some samples (*e.g.*, ANT1, ANT8, ANT4, ANT5) also display  $^{20}\text{Ne}/^{22}\text{Ne}$  ratios greater than the atmospheric value (9.8) which suggests the presence of some mantle Ne in these samples (Figure 2.3c).  $^{21}\text{Ne}/^{22}\text{Ne}$  ratios vary from  $0.0286 \pm 0.0005$  to  $0.0331 \pm 0.0004$  (Figure 2.3d) reflecting the addition of crustally produced  $^{21}\text{Ne}$  for samples with values greater than the atmospheric one (0.029) through the nuclear reactions of  $^{18}\text{O}(\alpha, n)^{21}\text{Ne}$  and  $^{24}\text{Mg}(n, \alpha)^{21}\text{Ne}$

[Wetherill, 1954]. Ne isotopic ratios in the Antrim gas samples point to a largely dominant atmospheric  $^{21}\text{Ne}$  contribution varying from 87.5% to 98.9% of total measured  $^{21}\text{Ne}$  and a much smaller amount of crustal  $^{21}\text{Ne}$  ( $^{21}\text{Ne}^*$ ) contribution ranging from 1.1% to 12.5%. No clear correlation between  $^{21}\text{Ne}/^{22}\text{Ne}$  with depth is observed (see also section 2.5.2).

Most Antrim Shale gas samples display  $^{40}\text{Ar}/^{36}\text{Ar}$  ratios above the atmospheric value (295.5), reflecting the addition of radiogenic  $^{40}\text{Ar}$  ( $^{40}\text{Ar}^*$ , Figure 2.3e). In contrast to R/Ra and Ne isotopic ratios where no apparent correlation is found with depth,  $^{40}\text{Ar}/^{36}\text{Ar}$  ratios display an overall increase with depth. Similar to  $^4\text{He}$ , excesses of  $^{40}\text{Ar}$  are commonly observed in old crustal fluids due to natural decay of  $^{40}\text{K}$  in the rock [Ballentine *et al.*, 1991; Elliot *et al.*, 1993; Ballentine *et al.*, 1994]. Atmospheric  $^{40}\text{Ar}$  is also largely dominant varying from 81% to 99.3% of total measured  $^{40}\text{Ar}$ . The presence of crustally produced  $^{40}\text{Ar}$  ( $^{40}\text{Ar}^*$ ) is further discussed below. Some samples also display  $^{136}\text{Xe}/^{130}\text{Xe}$  ratios above the atmospheric value (2.176), up to  $2.235 \pm 0.011$ , clearly showing the presence of excess crustally produced  $^{136}\text{Xe}$  (Figure 2.3f and Table 2.2). This excess  $^{136}\text{Xe}$  was suggested to originate mainly from crustally produced  $^{136}\text{Xe}$  from the spontaneous fission of  $^{238}\text{U}$  in the Michigan Basin [Ma *et al.*, 2009a]. Unlike  $^{40}\text{Ar}/^{36}\text{Ar}$  ratios, the highest ratios of  $^{136}\text{Xe}/^{130}\text{Xe}$  are found at much shallower depths. From these observations it is apparent that noble gas isotopic ratios are highly variable with depth (Figure 2.3).

Volume fractions of noble gas isotopes ( $^4\text{He}$ ,  $^{21}\text{Ne}$  and  $^{40}\text{Ar}$ ) and their crustally produced components in the Antrim Shale gas samples are reported in Table 2.3. Crustal He volume fractions ( $^4\text{He}^*$ ) in these Antrim gases are estimated by using the He isotopic ratios as discussed above (Figure 2.3a). He is assumed to be essentially of crustal origin, while Ne, Ar and Xe are treated as a two-component mixture, with an atmospheric and a crustal end-member. Crustal  $^{21}\text{Ne}$ ,  $^{40}\text{Ar}$  and  $^{136}\text{Xe}$  contributions ( $^{21}\text{Ne}^*$ ,  $^{40}\text{Ar}^*$ ,  $^{136}\text{Xe}^*$ ) are estimated as follow [Ballentine, 1991]:

$${}^{21}\text{Ne}^* = {}^{21}\text{Ne}_{\text{measured}} \times \left( 1 - \left( \frac{{}^{21}\text{Ne}}{{}^{22}\text{Ne}} \right)_{\text{air}} / \left( \frac{{}^{21}\text{Ne}}{{}^{22}\text{Ne}} \right)_{\text{measured}} \right) \quad (2.1)$$

$${}^{40}\text{Ar}^* = {}^{40}\text{Ar}_{\text{measured}} \times \left( 1 - \left( \frac{{}^{40}\text{Ar}}{{}^{36}\text{Ar}} \right)_{\text{air}} / \left( \frac{{}^{40}\text{Ar}}{{}^{36}\text{Ar}} \right)_{\text{measured}} \right) \quad (2.2)$$

$${}^{136}\text{Xe}^* = {}^{136}\text{Xe}_{\text{measured}} \times \left( 1 - \left( \frac{{}^{136}\text{Xe}}{{}^{130}\text{Xe}} \right)_{\text{air}} / \left( \frac{{}^{136}\text{Xe}}{{}^{130}\text{Xe}} \right)_{\text{measured}} \right) \quad (2.3)$$

where  $({}^{21}\text{Ne}/{}^{22}\text{Ne})_{\text{air}} = 0.029$ ,  $({}^{40}\text{Ar}/{}^{36}\text{Ar})_{\text{air}} = 295.5$  and  $({}^{136}\text{Xe}/{}^{130}\text{Xe})_{\text{air}} = 2.176$  [Ozima and Podosek, 2002]. Calculated  ${}^{21}\text{Ne}^*$ ,  ${}^{40}\text{Ar}^*$  and  ${}^{136}\text{Xe}^*$  are reported in volume fractions (Table 2.3). Neglecting the presence of a potentially minor mantle Ne, Ar and Xe contributions would not affect the discussion and conclusions that follow [Ma et al., 2009a].

${}^4\text{He}^*$  volume fractions vary over two orders of magnitude, from  $1.23 \times 10^{-7}$  to  $1.42 \times 10^{-5}$  (Table 2.3). A plot of  ${}^4\text{He}^*$  versus depth (Figure 2.3a) points to the presence of two groups, one at depths shallower than 450 m where no obvious correlation with depth is observed, the other at greater depths, displaying an correlation between  ${}^4\text{He}^*$  and depth (samples ANT3, ANT4, ANT5, ANT16 and ANT17). Overall, the high variability of  ${}^4\text{He}^*$  volume fractions with depth suggests variable in-situ radiogenic  ${}^4\text{He}^*$  production rates and/or variable external  ${}^4\text{He}$  inputs. Figures 2.4a, b display the spatial distribution of volume fractions of total  ${}^4\text{He}$  and  ${}^4\text{He}^*$  within the sampling area. Volume fractions of both total  ${}^4\text{He}$  and  ${}^4\text{He}^*$  are identical with an overall increase from NW towards SE (samples ANT4 and ANT5). These identical distribution patterns and volume fractions suggest that  ${}^4\text{He}^*$  is the dominant component. Unlike total  ${}^4\text{He}$  and  ${}^4\text{He}^*$ , spatial distributions of  ${}^{21}\text{Ne}^*$  (not shown) and  ${}^{40}\text{Ar}^*$  (Figure 2.4d) differ greatly from that of total  ${}^{21}\text{Ne}$  (not shown) and  ${}^{40}\text{Ar}$ , respectively (Figure 2.4c). This is expected since, as mentioned earlier, atmospheric  ${}^{21}\text{Ne}$  and  ${}^{40}\text{Ar}$  contents dominate total  ${}^{21}\text{Ne}$  and  ${}^{40}\text{Ar}$  volume fractions.  ${}^{136}\text{Xe}^*$

volume fractions vary from  $1.60 \times 10^{-13}$  to  $3.83 \times 10^{-12}$  (Table 2.3). No correlation is observed between  $^{136}\text{Xe}^*$  and depth. This is discussed below.

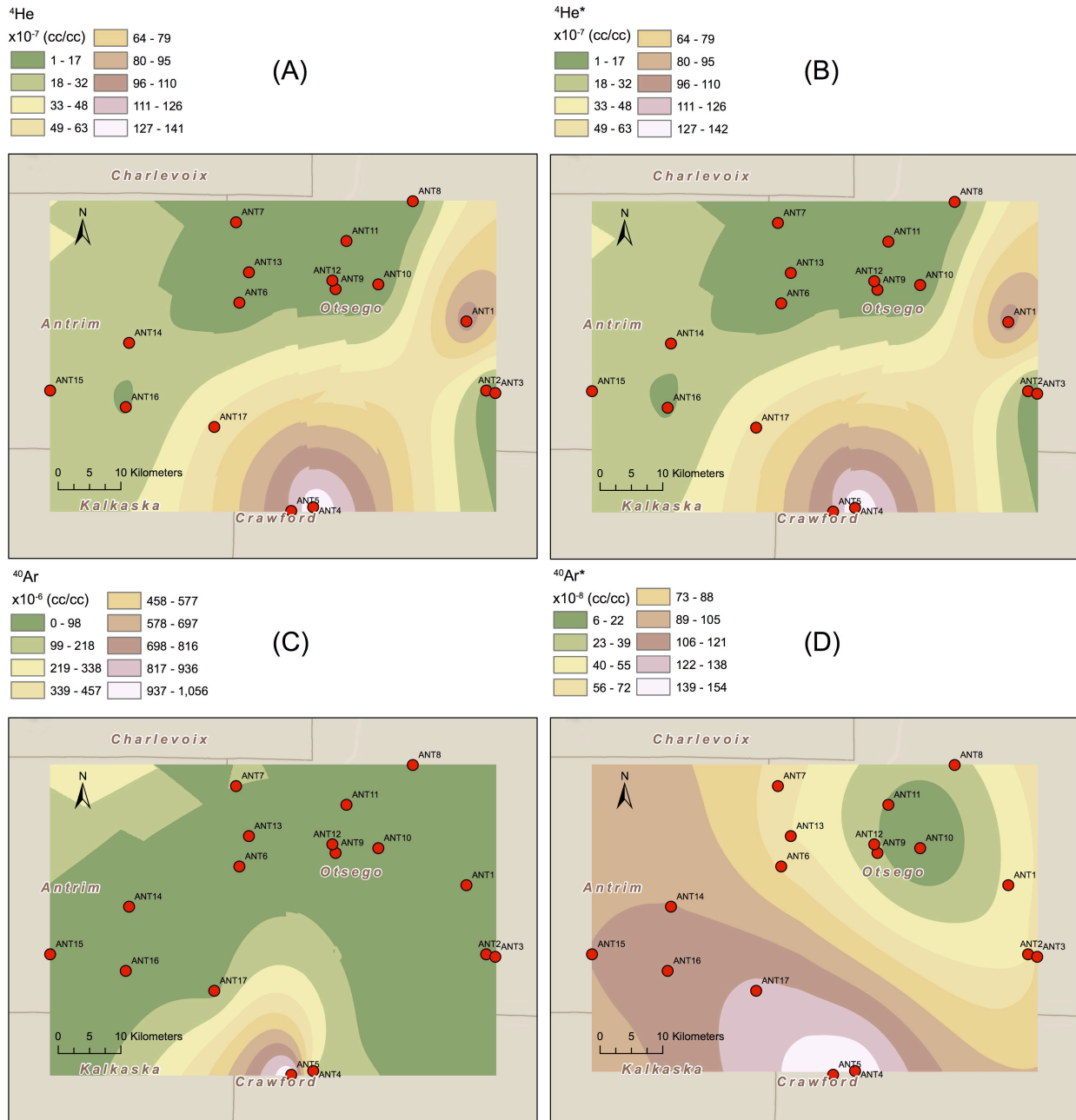


**Figure 2.4** Contour maps of (a) total  $^4\text{He}$  volume fractions, (b) radiogenic  $^4\text{He}$  volume fractions, (c) total  $^{40}\text{Ar}$  volume fractions and (d) radiogenic  $^{40}\text{Ar}$  volume fractions for Antrim Shale gas wells in this study.

**Table 2.3** Noble gas isotopic volume fractions and calculated  $^4\text{He}$  ages using representative values for only in-situ production, as well as both in-situ production and external He flux for Antrim Shale gas samples.

| Sample ID | $^4\text{He}$<br>( $\times 10^{-7}$ ) | $^{21}\text{Ne}$<br>( $\times 10^{-12}$ ) | $^{40}\text{Ar}$<br>( $\times 10^{-6}$ ) | $^4\text{He}^*$<br>( $\times 10^{-7}$ ) | $^{21}\text{Ne}^*$<br>( $\times 10^{-13}$ ) | $^{40}\text{Ar}^*$<br>( $\times 10^{-8}$ ) | $^{136}\text{Xe}^*$<br>( $\times 10^{-12}$ ) | $^4\text{He}$ ages<br>without<br>external flux<br>( $\times 10^5$ yr) | $^4\text{He}$ ages<br>with<br>external flux<br>( $\times 10^3$ yr) |
|-----------|---------------------------------------|---|--|---|---|--|--|---|--|
| ANT1      | 106.71±2.18                           | 423.63±5.51                               | 28.23±0.37                               | 105.78±2.16                             | 199.23±76.07                                | -  | 0.54±2                                       | 18.22±0.46  | 39.65±1  |
| ANT2      | 9.61±0.14                             | 9.55±0.3                                  | 48.69±0.63                               | 9.61±0.14                               | 6.69±3.83                                   | 50.56±89.05                                | 1.89±4.4                                     | 1.02±0.02   | 2.21±0.04  |
| ANT3      | 6.81±0.1                              | 9.38±0.28                                 | 68.54±0.89                               | 6.8±0.1                                 | 3.47±3.48                                   | 78.65±125.29                               | 0.24±5.9                                     | 0.51±0.01   | 1.11±0.02  |
| ANT4      | 141.46±2.12                           | 13.98±0.18                                | 8.12±0.11                                | 141.62±2.12                             | 8.56±2.69                                   | 154.38±13.59                               | 0.72±3.06                                    | 109.43±2.17   | 238.19±4.73  |
| ANT5      | 111.31±1.67                           | 10721.98±139.39                           | 1338.63±17.4                             | 109.32±1.64                             | 2841.08±1945.27                             | -  | -  | 0.41±0.01   | 0.88±0.02  |
| ANT6      | 5.65±0.08                             | 328.05±4.26                               | 51.84±0.67                               | 5.54±0.08                               | 410.61±56.66                                | -  | 0.91±5.19                                    | 0.55±0.01   | 1.19±0.02  |
| ANT7      | 8.02±0.12                             | 93.89±1.22                                | 98.15±1.28                               | 8.02±0.12                               | 109.46±16.29                                | 65.09±179.85                               | 0.48±7.1                                     | 0.42±0.01   | 0.91±0.02  |
| ANT8      | 5.27±0.08                             | 16.65±0.53                                | 8.73±0.11                                | 5.26±0.08                               | 7.8±6.59                                    | 32.06±17.24                                | 0.16±6.93                                    | 3.19±0.07   | 6.94±0.15  |
| ANT9      | 5.48±0.08                             | 46.76±0.61                                | 14.54±0.19                               | 5.45±0.08                               | 49.3±8.16                                   | 25.13±26.5                                 | 1.69±3.22                                    | 1.95±0.04   | 4.25±0.08  |
| ANT10     | 1.26±0.02                             | 5.61±0.07                                 | 4.49±0.06                                | 1.23±0.02                               | -   | 5.65±8.21                                  | 1.34±5.95                                    | 1.45±0.03   | 3.15±0.06  |
| ANT11     | 9.14±0.14                             | 31.04±0.59                                | 84.25±1.1                                | 9.14±0.14                               | -   | -  | 3.83±4.45                                    | 0.55±0.01   | 1.2±0.02   |
| ANT12     | 5.22±0.08                             | 456.11±5.93                               | 59.42±0.77                               | 5.05±0.08                               | 181.24±82.21                                | -  | -  | 0.43±0.01   | 0.93±0.02  |
| ANT13     | 8.88±0.13                             | 41.25±1.34                                | 13.78±0.18                               | 8.76±0.13                               | -   | 55.42±39.89                                | 3.47±6.3                                     | 3.42±0.11   | 7.44±0.23  |
| ANT14     | 18.36±0.28                            | 28.39±0.75                                | 30.62±0.4                                | 18.17±0.27                              | 9.08±10.13                                  | 105.34±55.34                               | -  | 3.16±0.06   | 6.88±0.14  |
| ANT15     | 18.19±0.27                            | 35.52±0.84                                | 13.29±0.17                               | 17.89±0.27                              | 8.07±11.57                                  | 105.36±26.18                               | 0.36±4.12                                    | 7.57±0.17   | 16.48±0.36   |
| ANT16     | 15.49±0.23                            | 66.77±0.89                                | 14.94±0.19                               | 15.03±0.23                              | -   | 109.88±28.34                               | -  | 5.7±0.12  | 12.4±0.26  |
| ANT17     | 52.27±0.78                            | 18.1±0.48                                 | 8.38±0.11                                | 52.34±0.79                              | 1.91±7.3                                    | 125.74±25.23                               | -  | 37.34±1.32  | 81.27±2.87   |

## 2.6 Discussion

Overall, multiple sources of noble gases (*i.e.*, atmospheric, crustal, mantle) are present in the Antrim Shale. The contribution of each source varies significantly for different noble gases, *e.g.*, total  $^4\text{He}$  is dominated by crustally produced  $^4\text{He}^*$  while  $^{21}\text{Ne}^*$  and  $^{40}\text{Ar}^*$  are relatively minor compared to corresponding atmospheric components. To assess whether or not such high variability in the noble gas signatures is caused by variable in-situ noble gas production from their parent elements (*i.e.*, U, Th,  $^{40}\text{K}$ ) or instead due to variable contributions of the external flux into the Antrim Shale from deeper formations (brine migration) [Walter *et al.*, 1996; Ma *et al.*, 2005; 2009b], we evaluate below the extent of brine migration into the Antrim Shale.

### 2.6.1 Mixing of Deep Brine and Freshwater Recharge in the Antrim

Previous geochemical studies suggest that recharge (meteoric) water into the Antrim Shale accounts for 40%-80% of the co-produced water, with 20%-60% of co-produced water originating from deep brines, within the sampling area [McIntosh and Walter, 2005]. In order to assess the impact of deep brines in each sampled Antrim well, we look at the measured  $^{20}\text{Ne}/^{36}\text{Ar}$  ratios of the Antrim Shale gas samples.

$^{36}\text{Ar}$  in sedimentary systems is almost entirely of atmospheric origin [Elliot *et al.*, 1993; Ozima and Podosek, 2002]. Similarly, Ne isotopes are predominantly of atmospheric origin with negligible  $^{20}\text{Ne}$  mantle contributions in some of the samples (ANT1, ANT5, ANT6, ANT12, ANT16). In the analysis that follows, it is assumed that all  $^{20}\text{Ne}$  and  $^{36}\text{Ar}$  in the samples are of atmospheric origin. Atmospheric  $^{20}\text{Ne}$  and  $^{36}\text{Ar}$  components in the Antrim shale gases are assumed to originally derive from seawater with a salinity of 0.623 M in equilibrium with the atmosphere at 25 °C [Gutschick and Sandberg, 1991; Harrell *et al.*, 1991], with  $^{20}\text{Ne}/^{36}\text{Ar} =$

0.175 [Elliot *et al.*, 1993; Ozima and Podosek, 2002]. When a gas phase (*e.g.*, CH<sub>4</sub>) is present in contact with the water phase, <sup>20</sup>Ne/<sup>36</sup>Ar ratios in the gas phase may be calculated if Henry's coefficients are known and a single-stage gas-liquid partitioning model is assumed [Smith and Kennedy, 1983; Elliot *et al.*, 1993]. Under current reservoir temperature of 24°C and a water salinity of 5 M [Martini *et al.*, 1998; Hill and Nelson, 2000; Curtis, 2002; Ma *et al.*, 2009a], Ne and Ar Henry's coefficients are 458314 and 197872 atm, respectively [Crovetto *et al.*, 1982; Smith and Kennedy, 1983]. For a gas/liquid volume ratio ( $V_g/V_l$ ) approaching 0, which is the maximum increase of <sup>20</sup>Ne volume fraction in the gas phase relative to the <sup>36</sup>Ar volume fraction under the single-stage gas-liquid equilibrium assumption, the predicted <sup>20</sup>Ne/<sup>36</sup>Ar ratio in the gas phase is 0.405.

<sup>20</sup>Ne/<sup>36</sup>Ar ratios (Table 2.2) of sampled Antrim gases are plotted in Figure 2.5a and compared with <sup>20</sup>Ne/<sup>36</sup>Ar ratios in the two extreme scenarios mentioned above, *i.e.*, in which  $V_g/V_l \rightarrow +\infty$  and 0. The first scenario represents the <sup>20</sup>Ne/<sup>36</sup>Ar ratio (0.175) in the gas phase (left dashed line in Figure 2.5a) assuming present-day reservoir conditions and  $V_g/V_l$  approaching  $+\infty$ , with all noble gases being transferred into the gas phase. The second scenario represents the <sup>20</sup>Ne/<sup>36</sup>Ar ratio (0.405) in the gas phase (right dashed line in Figure 2.5a) under current reservoir conditions assuming  $V_g/V_l$  approaching 0. In a closed system where the gas phase escapes from the liquid phase under variable gas/liquid volume ratios, all <sup>20</sup>Ne/<sup>36</sup>Ar ratios in the gas phase (*e.g.*, ANT8, ANT9, ANT13, etc.) should fall within the range of 0.175-0.405 as shown by the gray domain region in Figure 2.5a. However, two groups of Antrim gas samples are found outside of this gray domain. One group, comprising samples ANT1, ANT5, ANT6, ANT12 and ANT16 displays <sup>20</sup>Ne/<sup>36</sup>Ar ratios higher than the predicted upper limit of 0.405 suggesting addition of mantle <sup>20</sup>Ne in the Antrim Shale other than the re-distribution of noble gases between the water

and oil phases. It should be mentioned that the oil phase is scarce within the NPT area. In contrast, the second group, which includes samples ANT2, ANT3, ANT7, ANT10, ANT11 and ANT14, displays  $^{20}\text{Ne}/^{36}\text{Ar}$  ratios which are lower than the  $^{20}\text{Ne}/^{36}\text{Ar}$  ratio for  $V_g/V_l \rightarrow +\infty$ . These unusually low  $^{20}\text{Ne}/^{36}\text{Ar}$  ratios in some of the Antrim Shale gas samples point to  $^{20}\text{Ne}$  that is depleted relative to  $^{36}\text{Ar}$ .

Similarly,  $^{84}\text{Kr}$  is also almost entirely of atmospheric origin.  $^{36}\text{Ar}/^{84}\text{Kr}$  ratios (Table 2.2) of sampled Antrim Shale gases are also plotted and compared with calculated  $^{36}\text{Ar}/^{84}\text{Kr}$  ratios in the gas phase for the same two extreme scenarios (Figure 2.5b). From Figure 2.5b, it is apparent that  $^{36}\text{Ar}/^{84}\text{Kr}$  ratios of most Antrim Shale gas samples are lower than the predicted minimum  $^{36}\text{Ar}/^{84}\text{Kr}$  ratio in the gas phase ( $V_g/V_l \rightarrow +\infty$ ), strongly indicating depletion of  $^{36}\text{Ar}$  relative to  $^{84}\text{Kr}$ . From Figures 2.5a, b it is apparent that noble gas volume fractions of Antrim Shale gases display a mass-dependent depletion pattern with lighter noble gases being more heavily depleted compared to the heavier ones. A boiling model was suggested by *Ma et al.* [2009a] to explain such a mass-dependent depletion pattern in noble gas abundances from other formations in the Michigan Basin. This boiling model, proposed by *Mazor and Truesdell* [1984], describes the partitioning of noble gases between the water and steam phases according to Henry's Law. Atmospheric noble gas (e.g.,  $^{36}\text{Ar}$ ) concentrations from the original seawater composition for both closed and open systems will leave the residual brine phase to the gas phase as boiling proceeds. Due to the higher solubility of the heavier noble gases (e.g.,  $^{84}\text{Kr}$ ) compared to the lighter ones (e.g.,  $^{36}\text{Ar}$ ) in brine, lighter noble gases will escape preferentially from the residual brine phase and will lead to mass-dependent depletion of noble gas in the brine. With the migration of deeper residual brines strongly depleted in noble gases into the Antrim Shale, noble gas from the residual brine will be transferred into the Antrim natural gas. Therefore, this mass-

dependent depletion pattern will be observed in the Antrim gas samples we collected. This boiling model points strongly to the occurrence of past thermal events, which have been previously suggested to have occurred in the Michigan Basin [*Sanford et al.*, 1985; *Fisher et al.*, 1988; *Coniglio et al.*, 1994; *Wang et al.*, 1994; *Girard and Barnes*, 1995; *Castro et al.*, 2009; *Ma et al.*, 2009a; 2009b]. Major thermal events in the Michigan Basin took place during the late Devonian-Mississippian (370-323 Ma), Triassic (~224 Ma) and Cretaceous (~111-159 Ma) related to the reactivation of the Precambrian basement structures. These are likely the cause of high paleo-temperatures (170-400 °C) in the Michigan Basin, which are thought to have ultimately led to the observed extreme depletion of atmospheric noble gases in the deep brines of the Michigan Basin. Occurrence of meteoric recharge water in the Antrim Shale is relatively recent and thought to have occurred during the Pleistocene and thus, far more recent than the occurrence of the past thermal events. Therefore, depletion of atmospheric noble gases would be expected to be found in old brines but not in the relatively young recharge water in the Antrim Shale. Volume fractions of atmospheric noble gases (*e.g.*,  $^{36}\text{Ar}$ ) can be used to indicate the contribution of deep brines over the meteoric recharge water in the Antrim Shale gas.

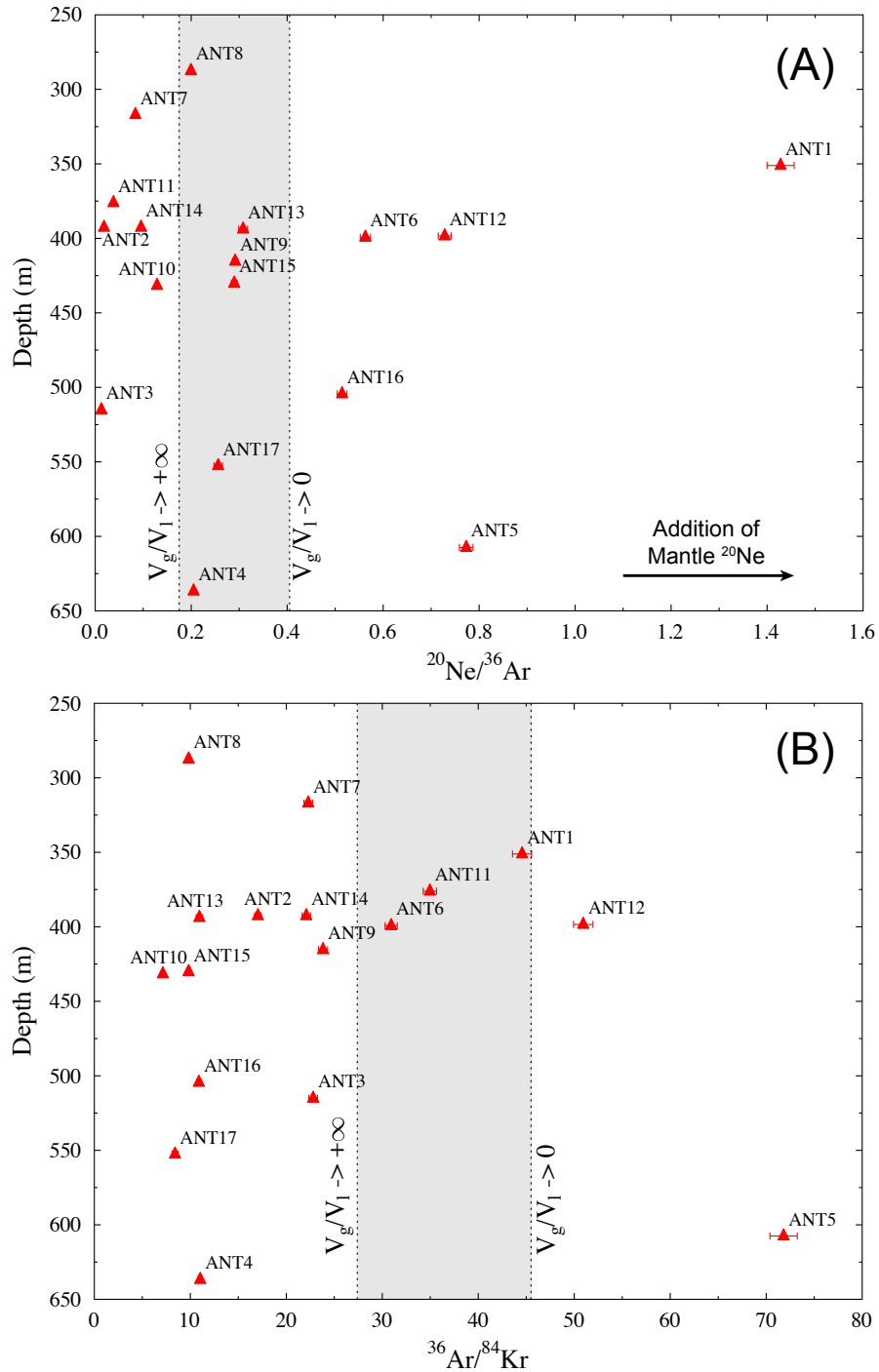


**Figure 2.5** Depth profile of (a) Measured  $^{20}\text{Ne}/^{36}\text{Ar}$  and (b)  $^{36}\text{Ar}/^{84}\text{Kr}$  ratios of collected Antrim gas samples versus predicted  $^{20}\text{Ne}/^{36}\text{Ar}$  and  $^{36}\text{Ar}/^{84}\text{Kr}$  ratios for a gas phase in equilibrium with seawater (i.e., gas/liquid volume ratio approaches 0 or  $+\infty$ ) under reservoir conditions.

Figure 2.6a plots  $^{40}\text{Ar}/^{36}\text{Ar}$  ratios of the Antrim Shale gas as a function of  $1/^{36}\text{Ar}$  ratios. Both  $^{40}\text{Ar}/^{36}\text{Ar}$  and  $1/^{36}\text{Ar}$  ratios of the Antrim gas samples are highly variable, ranging from 282.4 to 364.1 and from  $2.11 \times 10^5$  to  $6.66 \times 10^7$  for  $^{40}\text{Ar}/^{36}\text{Ar}$  and  $1/^{36}\text{Ar}$  ratios, respectively. Such high variability is the result of variable contributions of old brine from deeper formations into the Antrim Shale mixing with recharge water. Unlike recharge water, deep brines come with high  $^{40}\text{Ar}/^{36}\text{Ar}$  ratios due to crustally produced  $^{40}\text{Ar}$  and higher  $1/^{36}\text{Ar}$  ratios resulting from depletion of atmospheric noble gases which occurred during past thermal events [Ma *et al.*, 2009a]. Variable impact of the deep brines over recharge water can also be observed in the relationship displayed between  $^4\text{He}^*$  and chloride concentrations in the co-produced water of the sampled wells (Figure 2.6b). The chloride concentration of sampled co-produced formation water ranges from 16 to 3637 mM and the volume fractions of crustally produced  $^4\text{He}^*$  vary over two orders of magnitude for the samples. Deep brines have higher salinity values [up to 5.7 M salinity, Wilson and Long 1993a; 1993b] and more  $^4\text{He}^*$  compared to meteoric water, although we cannot quantitatively evaluate brine and meteoric water end-members in our case due to the difficulty in comparing water and gas samples with respect to noble gas volume fractions. Samples ANT4 and ANT5 represent values close to the deep brine end members while ANT7, ANT10 and ANT11 are much closer to the recharge water end-member (He concentration and salinity are  $5.1 \times 10^{-8} \text{ cm}^3\text{STP/g}$  and 0 M Cl<sup>-</sup> at 0 °C, respectively).

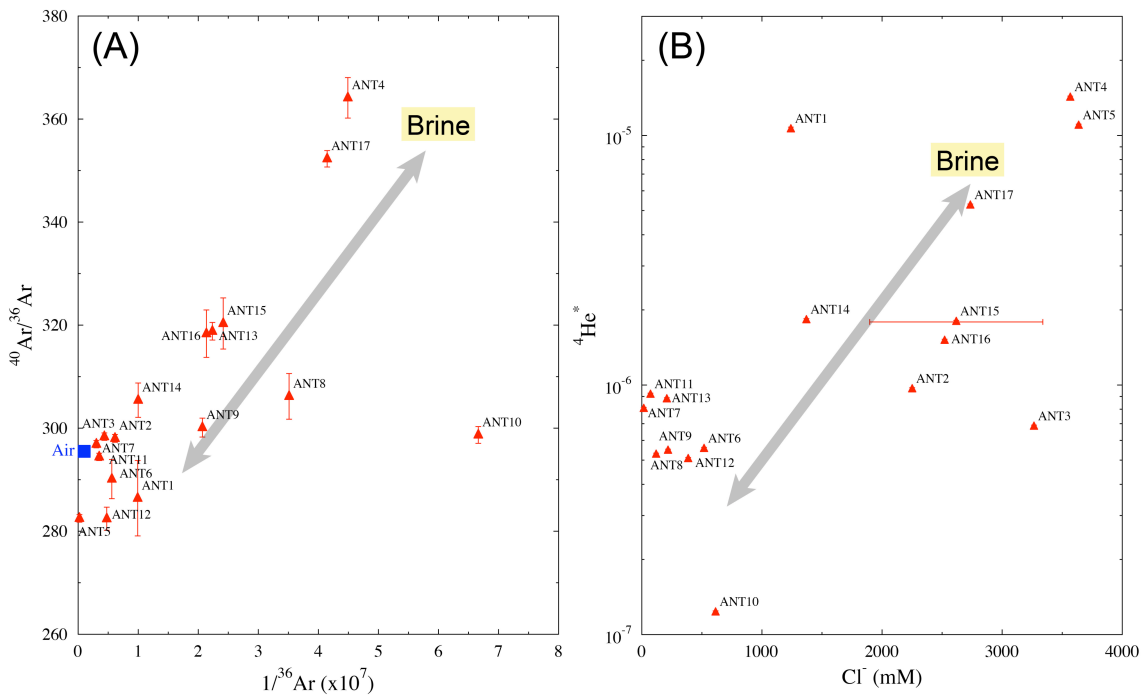


**Figure 2.6 (a)**  $^{40}\text{Ar}/^{36}\text{Ar}$  versus  $1/^{36}\text{Ar}$ ; and **(b)** radiogenic  $^4\text{He}^*$  volume fraction versus  $\text{Cl}^-$ . These reveal variable impact of deep brines on  $^4\text{He}$  and Ar composition in the Antrim Shale.

It is apparent from the gas samples that large amounts of meteoric water recharged the Antrim Shale and mixed with variable amounts of old brines, which are derived from deep formations beneath the Antrim Shale and depleted in atmospheric noble gases (e.g.,  $^{36}\text{Ar}$ ). Recharge of diluted meteoric waters likely stimulated microbial activity and the formation of biogenic methane in the Antrim Shale [Martini *et al.*, 1996; Walter *et al.*, 1996]. It is thus critical to constrain both the origin of this recharge water as well as the timing of recharge.

### **2.6.2 $^4\text{He}$ Groundwater Ages**

The accumulation of radiogenic  $^4\text{He}$  ( $^4\text{He}^*$ ) has been widely used as a dating tool to constrain the age of groundwater beyond the ~50 ka limit of  $^{14}\text{C}$  [Torgersen and Ivey, 1985; Torgersen and Clarke, 1985; Castro *et al.*, 2000; Castro and Goblet, 2003; Ma *et al.*, 2005; Schlegel *et al.*, 2011; Wen *et al.*, 2015]. Water-gas interactions also result in the transfer of accumulated  $^4\text{He}^*$ , together with other dissolved atmospheric noble gases (e.g.,  $^{36}\text{Ar}$ ), from the water to the gas phase [Ballentine, 1991; Zhou and Ballentine, 2006]. The combined analyses of  $^4\text{He}^*$  and other noble gases allow us to estimate the accumulated  $^4\text{He}^*$  concentration in the water prior to the phase separation and thus, to acquire  $^4\text{He}$  ages for the associated water phase [Zhou *et al.*, 2005; Zhou and Ballentine, 2006; Schlegel *et al.*, 2011].

As discussed above, crustal  $^4\text{He}$  dominates the total  $^4\text{He}$  concentrations in the Antrim Shale gases, with minor amounts of mantle-derived and atmosphere-derived  $^4\text{He}$ . The Antrim Shale samples display  $^4\text{He}/^{20}\text{Ne}$  ratios ranging from 3 to 3099 (Table 2.2), which are much higher than the corresponding atmospheric ratio of 0.288 [Kipfer *et al.*, 2002]. High  $^4\text{He}/^{20}\text{Ne}$  ratios also suggest minimal contamination of atmospheric He. Atmospheric noble gases are significantly depleted in deep brines which migrated into the Antrim Shale from deeper formations [Ma *et al.*,

2009a]. Past thermal events led to the decrease of atmospheric noble gas contents (*e.g.*,  $^{36}\text{Ar}$ ) by a factor of  $\sim 100$  [Ma *et al.*, 2009a]. Thus, most atmospheric noble gases (*e.g.*,  $^{36}\text{Ar}$ ) in the Antrim are likely derived from relatively recent recharge water considering that contributions of meteoric water and brine are fairly equitable in the sampling area [McIntosh and Walter, 2005].  $^{20}\text{Ne}/^{36}\text{Ar}$  and  $^{36}\text{Ar}/^{84}\text{Kr}$  ratios of some Antrim Shale gases are out of the predicted ratio ranges for ASW (Figure 2.5). However, considering the mixing of depleted deep brine and meteoric water, it is reasonable to assume that there has been minimal fractionation of the noble gases after the mixing of deep brine and meteoric water, with near complete transfer of noble gases from the water into the gas phase [Schlegel *et al.*, 2011]. Thus, all 17 Antrim Shale gas samples are used to calculate  $^4\text{He}$  ages of associated formation water as a first-order estimation of the recharge timing in the Antrim Shale following Zhou and Ballentine [2006].

In the Antrim Shale, the major fraction of total  $^4\text{He}$  is, by far, of radiogenic origin ( $^4\text{He}^*$ ), resulting from radioactive decay of U and Th both, within the Antrim Shale (in-situ production), and from  $^4\text{He}$  produced at greater depths and migrating upwards with brine into the Antrim Shale. Thus, crustally produced  $^4\text{He}^*$  is given by Schlegel *et al.* [2011]:

$$^4\text{He}^* = ^4\text{He}_{\text{in-situ}} + ^4\text{He}_{\text{external}} \quad (2.4)$$

where  $^4\text{He}_{\text{in-situ}}$  and  $^4\text{He}_{\text{external}}$  represent the in-situ and externally produced  $^4\text{He}$ , respectively.

Assuming that noble gases have been completely transferred from the associated water phase into the gas phase,  $^4\text{He}$  concentrations in the water phase can be calculated based on  $^4\text{He}$  and  $^{36}\text{Ar}$  volume fractions in the gas phase as follows:

$$^4\text{He}_{\text{water}} = \left( \frac{^4\text{He}_{\text{measured}}}{^{36}\text{Ar}_{\text{measured}}}_{\text{air}} \right) \times ^{36}\text{Ar}_{\text{ASW}} \quad (2.5)$$

where  $^{36}\text{Ar}_{\text{ASW}}$  represents the concentration of dissolved atmospheric  $^{36}\text{Ar}$  in the water which is dependent on elevation, temperature and salinity of the recharge water. An average Ar concentration of  $3.77 \times 10^{-4} \text{ cm}^3 \text{STPg}^{-1}_{\text{H}_2\text{O}}$  in the freshwater (0‰ salinity) at the temperature range of 0-25 °C and an elevation of 300 m [Gutschick and Sandberg, 1991; Harrell et al., 1991; Ma et al., 2004; 2005; Wen et al., 2015] is taken as the representative value of  $^{36}\text{Ar}$  to calculate the  $^4\text{He}$  concentrations in the water for each Antrim gas sample.

The in-situ production of  $^4\text{He}$  is given by *Torgersen* [1980]:

$$^4\text{He}_{\text{in-situ}} = P(^4\text{He}) \times \rho_r \times \Lambda \times \left( \frac{1-\omega}{\omega} \right) \times t \quad \text{cm}^3 \text{STPg}^{-1}_{\text{H}_2\text{O}} \quad (2.6)$$

where  $\rho_r$  is the density of the rock in  $\text{g cm}^{-3}$ ,  $t$  is the accumulation time ( $^4\text{He}$  age),  $\omega$  is the porosity of the reservoir rock,  $\Lambda$  is the transfer efficiency of He from the rock matrix to the water, assumed to be 1 [Torgersen, 1980; Torgersen and Clarke, 1985], and  $P(^4\text{He})$  is the in-situ production rate of  $^4\text{He}$  within the Antrim Shale calculated by:

$$P(^4\text{He}) = 1.207 \times 10^{-13} [\text{U}] + 2.867 \times 10^{-14} [\text{Th}] \quad \text{cm}^3 \text{STPg}^{-1}_{\text{rock yr}^{-1}} \quad (2.7)$$

where [U] and [Th] represent the U and Th concentrations (in ppm), respectively (Table 2.4).

The external  $^4\text{He}$  flux can be subsequently calculated by:

$$^4\text{He}_{\text{external}} = P(^4\text{He}) \times \rho_{\text{crust}} \times H \times \left( \frac{1}{\omega h} \right) \times t \quad \text{cm}^3 \text{STPg}^{-1}_{\text{H}_2\text{O}} \quad (2.8)$$

where  $\rho_{\text{crust}}$  represents the density of the crust,  $H$  is the thickness of the crust in meters and  $h$  is the thickness of the Antrim Shale also in meters (Table 2.4).

**Table 2.4** Calculated  $^4\text{He}$  production rates in the Antrim Shale and the crust using representative values for estimated parameters.

| Lithology                 | Thickness (m) | Porosity (%) | Th (ppm) | U (ppm) | Density (g/cm <sup>3</sup> ) | P( $^4\text{He}$ ) <sup>c</sup> (cm <sup>3</sup> STP g <sub>rock</sub> <sup>-1</sup> yr <sup>-1</sup> ) |
|---------------------------|---------------|--------------|----------|---------|------------------------------|---|
| Antrim Shale <sup>a</sup> | 95            | 9            | 1        | 20      | 2.7                          | 2.71E-12  |
| Upper Crust <sup>b</sup>  | 12300         | -            | 10.7     | 2.8     | 2.6                          | 6.45E-13  |
| Lower Crust <sup>b</sup>  | 36900         | -            | 1.06     | 0.28    | 3.3                          | 6.42E-14  |

<sup>a</sup> U and Th contents derived from *Leventhal* [1980] and *Swanson* [1960]; thickness, porosity and density values after well logs (this study), *Curtis* [2002] and *Clark* [1966].

<sup>b</sup> U and Th contents derived from *Taylor and McLennan* [1985]; thickness and density values after *Ruff et al.* [1994], *Taylor and McLennan* [1985] and *Zhou and Ballentine* [2006].

<sup>c</sup> Production rate of  $^4\text{He}$  in the Antrim Shale, upper crust and lower crust. Please refer to the main text for detailed description.

$^4\text{He}$  ages are calculated for two scenarios. In the first scenario, it is assumed that the Antrim Shale is a closed system and only in-situ  $^4\text{He}$  has accumulated over geological times. The second scenario assumes that the Antrim Shale is an open system in which an average external  $^4\text{He}$  flux migrated into the Antrim Shale and accumulated, in addition to the in-situ  $^4\text{He}$  production. This external  $^4\text{He}$  flux is partly supplied by underlying formations within the sedimentary sequence, partly from the crystalline basement in the Michigan Basin [Ma *et al.*, 2005; Wen *et al.*, 2015]. In this contribution, we assume the upper crust and lower crust to be the source of this external  $^4\text{He}$  flux (Table 2.4). Calculated  $^4\text{He}$  ages using representative values (Table 2.4) for estimated parameters are listed in Table 2.3 and plotted in Figure 2.7 for both scenarios. Considering only in-situ  $^4\text{He}$  production, calculated  $^4\text{He}$  ages range from 0.04 to 10.9 Ma (average 1.15 Ma), ages that are much younger than the formation age of the host rock (late Devonian is about 370 Ma). However, it has been shown that in most sedimentary basins, an external  $^4\text{He}$  flux is present and must be accounted for in the calculation of groundwater ages [Torgersen and Clarke, 1985; Castro and Goblet, 2003; Ma *et al.*, 2005; Zhou and Ballentine, 2006; Wen *et al.*, 2015]. More specifically, it was shown that a significant upward  $^4\text{He}$  flux is present both at depth and in the shallow (shallower than the Antrim Shale) subsurface of the Michigan Basin [Ma *et al.*, 2005; Castro *et al.*, 2009; Ma *et al.*, 2009a; 2009b; Wen *et al.*, 2015]. This external  $^4\text{He}$  flux, from the upper and lower crust, is estimated at  $3.33 \times 10^{-9} \text{ cm}^3 \text{ STPg}^{-1}_{\text{H}_2\text{O}}$  in the Antrim Shale (Table 2.4). Accounting for the upward  $^4\text{He}$  flux in the calculation of  $^4\text{He}$  water ages in the Antrim Shale leads to water residence times ranging from 0.9 to 238.2 ka (average 25 ka), values which are on average younger by about two orders of magnitude than water ages considering a closed system (Figure 2.7). Such large differences in these two sets of  $^4\text{He}$  ages strongly suggest that in-situ  $^4\text{He}$  production is minor compared to the external  $^4\text{He}$  flux input in

the Antrim Shale, which is present in shallower formations in the Michigan Basin [Ma *et al.*, 2005; Wen *et al.*, 2015]. Comparing the  $^4\text{He}$  ages with previously reported  $^{14}\text{C}$  ages [Martini *et al.*, 1998] for the Antrim Shale formation water [Figure 2.7; Martini *et al.*, 1998], we find that the latter, which vary from 2150 to 21630 yrs, overlap with  $^4\text{He}$  ages considering external  $^4\text{He}$  input and further reinforce the notion that the Antrim Shale is an open system and that an external  $^4\text{He}$  flux is present. Figure 2.7 displays the timing of three major glaciation periods, *i.e.*, Wisconsin (10 to 79 ka), Illinoian (132 to 202 ka) and Kansan (450 to 600 ka) glaciations in the Michigan Basin [Dorr and Eschman, 1970; Schaetzl *et al.*, 2008; Bergquist, 2009]. Except for samples ANT15 and ANT17, open system calculated  $^4\text{He}$  ages are within or younger than the Wisconsin glaciation period in the Michigan Basin. Samples ANT15 and ANT17 overlap with the Illinoian and Kansan glaciations (Figure 2.7). These comparisons strongly suggest that Antrim Shale formation water in the study area was influenced to some extent by glaciation-associated meteoric recharge, the brines in the Antrim Shale may form from evaporated concentrated seawater which was subsequently modified by rock-water interactions at greater depths over geological time [Wilson and Long, 1993a; 1993b]. Recharge of glacial meltwaters has been previously suggested based on geochemical evidence and numerical modeling studies [McIntosh and Walter, 2005; McIntosh and Martini, 2008; McIntosh *et al.*, 2012] and shown to have close ties with the formation of biogenic methane in the Antrim Shale [Martini *et al.*, 1996; 1998; 2003]. As expected, calculated  $^4\text{He}$  ages considering an external  $^4\text{He}$  flux increase from NW to SE, following the observed  $^4\text{He}^*$  increase (Figure 2.4b).

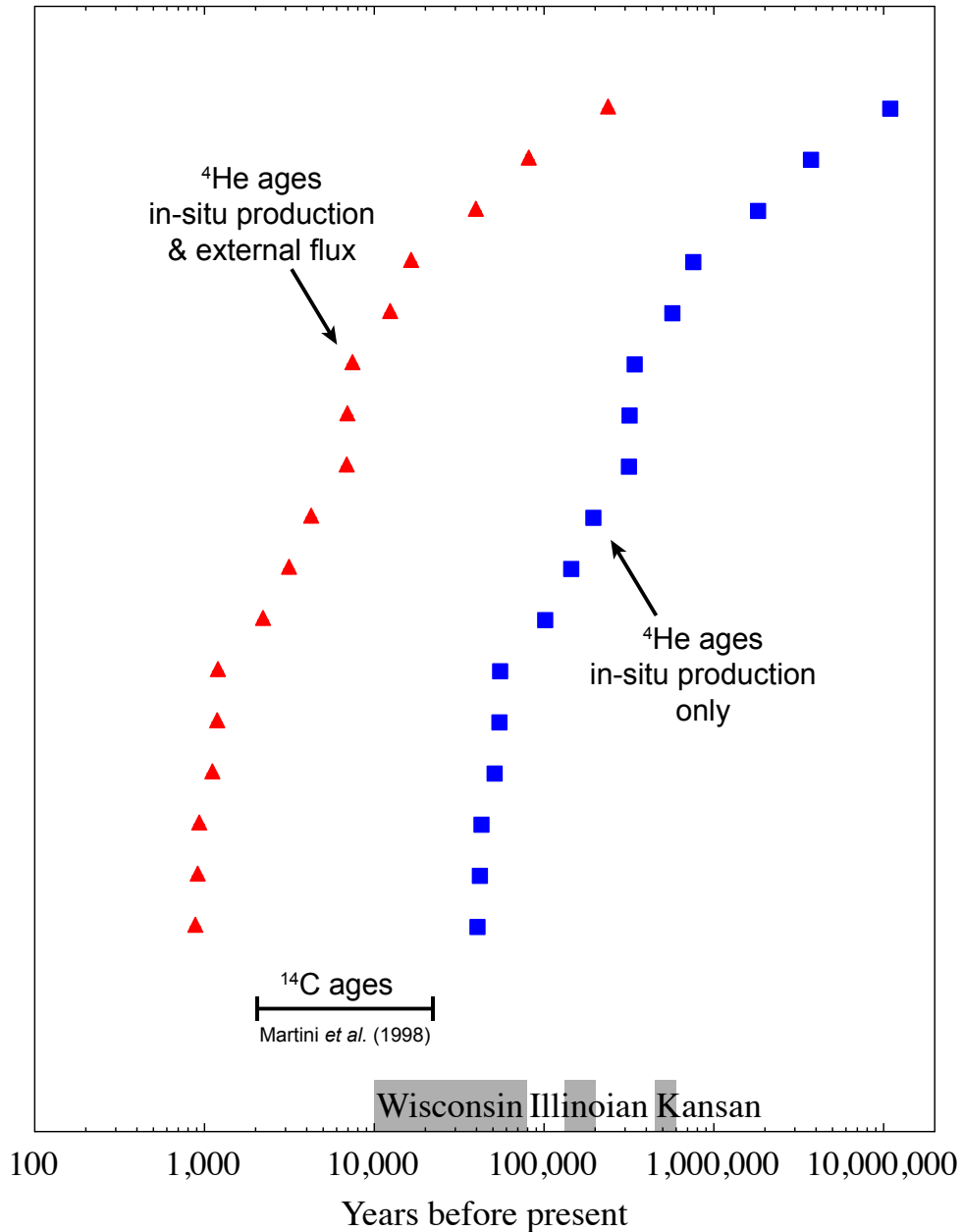


**Figure 2.7** Groundwater  $^4\text{He}$  ages are shown for sampled Antrim wells in this study assuming: (a) only in-situ production (blue squares), and; (b) both in-situ production & external He flux (red triangles), and compared with previously reported groundwater  $^{14}\text{C}$  ages (Martini *et al.*, 1998) as well as timing of three major glacial periods (Wisconsin, Illinoian and Kansan) in the Michigan Basin.

### 2.6.3 Differentiated Xe Signatures Relative to He, Ne and Ar

$^4\text{He}$  formation water ages were obtained by accounting for the external  $^4\text{He}$  flux entering the Antrim Shale (see section 2.6.2). This external  $^4\text{He}$  flux accounts for most radiogenic  $^4\text{He}$  in the Antrim Shale relative to the negligible in-situ  $^4\text{He}$  production. Similar findings are reported in shallower and deeper formations in the Michigan Basin (e.g., Saginaw Formation, Marshall Sandstone, Berea Sandstone, Traverse Group; cf. Figure 2.1) [Ma *et al.*, 2005; 2009b; Wen *et al.*, 2015]. In addition to  $^4\text{He}$  flux, Ma *et al.* [2009b] called upon an external  $^{136}\text{Xe}$  flux to account for most of the measured crustally produced  $^{136}\text{Xe}$  in the basin (e.g., Berea Sandstone and Traverse Group; Figure 2.1). Ma *et al.* [2009b] also concluded that only the Precambrian crystalline basement can account for most of the measured crustally produced  $^4\text{He}^*$  and  $^{136}\text{Xe}^*$  in the Michigan Basin. Therefore, a good correlation is expected between excess  $^4\text{He}$  and excess  $^{136}\text{Xe}$ . However, while  $^4\text{He}^*$  volume fractions show an overall correlation with depth, the same does not hold true for  $^{136}\text{Xe}^*$  (Figure 2.3a, Table 2.3). This inconsistency between excess He and excess Xe can be explained by upward transport of crustal noble gases and associated elemental fractionation processes controlled by both diffusion- and solubility-related mechanisms [Ma *et al.*, 2009b]. High diffusivities and preferential volume fractions in the gas phase of He with respect to Xe lead to an enrichment of  $^4\text{He}$  relative to  $^{136}\text{Xe}$  in shallower formations (i.e., the Antrim Shale) during upward transport. Relatively lower external  $^{136}\text{Xe}$  abundance combined with the in-situ  $^{136}\text{Xe}^*$  production from the  $^{238}\text{U}$  spontaneous fission [Eikenberg *et al.*, 1993] in the Antrim Shale may blur the correlation between  $^{136}\text{Xe}^*$  and depth. On the other hand,  $^{136}\text{Xe}^*$  volume fractions may reflect compositional variability within the Antrim Shale with respect to the radioactive parent (i.e.,  $^{238}\text{U}$ ). According to Ma *et al.* [2009b],  $^{40}\text{Ar}^*$  volume fractions should also be relatively depleted as compared to  $^4\text{He}^*$  in the relatively shallow formation (i.e., the

Antrim Shale) in the Michigan Basin. Thus no correlation should be observed between the  $^{40}\text{Ar}^*$  volume fraction and depth. However, unlike  $^{136}\text{Xe}^*$ ,  $^{40}\text{Ar}^*$  has significant correlation with  $^4\text{He}^*$  (not shown), which strongly points to the same external source, the Precambrian crystalline basement in the Michigan Basin, for both  $^4\text{He}^*$  and  $^{40}\text{Ar}^*$  components in the Antrim Shale. In addition to the in-situ crustally produced  $^{136}\text{Xe}^*$  in the Antrim Shale, release of sedimentary Xe from the organic-rich black shale may also contribute to the total Xe composition in the Antrim Shale as previously suggested by *Ma et al.* [2009a], *Podosek et al.* [1980], *Torgersen and Kennedy* [1999] and *Zhou et al.* [2005]. This contribution from sedimentary Xe may also dilute the  $^{136}\text{Xe}^*$  and thus, may weaken the correlation between  $^{136}\text{Xe}/^{130}\text{Xe}$  and depth (Figure 2.3f). We note that the level that is most enriched in  $^{136}\text{Xe}^*$  within the Antrim Shale is one of the shallowest, which might point to some local processes taking place. It is, however, premature at this stage to know with certainty the cause of this particular enriched layer in  $^{136}\text{Xe}^*$ . Additional samples with a wider spatial variability and depth need to be analyzed.

#### **2.6.4 Origin of Produced Gases in the Antrim Shale: Thermogenic versus Biogenic Origin**

Produced hydrocarbon gases in the Antrim Shale consist of biogenic gases, which are associated with microbial activity stimulated by meteoric recharge through the well-developed fracture network in the Antrim Shale, as well as thermogenic gases, which were generated from cracking of oil or refractory kerogen [*Martini et al.*, 1996; *Stolper et al.*, 2014; 2015]. However, the contribution of thermogenic methane with respect to the total produced methane in the study area is still under debate. Some early studies suggest that the thermogenic gas component contributes less than 20% of the total produced methane [*Martini et al.*, 1996; 1998] while others argue for a more equal contribution of thermogenic and biogenic gases if not a dominating

thermogenic component [Dolton and Quinn, 1996; Stolper et al., 2015]. Below, we use noble gases as a tool to distinguish between thermogenic and biogenic methane and to assess their respective contributions in the study area.

We have shown that an external crustal  $^4\text{He}$  flux is required to estimate the ages of Antrim Shale formation water. Similar to  $^4\text{He}$ ,  $^{40}\text{Ar}$  also has external sources to the Antrim Shale [e.g., Ma et al., 2009b]. If the radioelement composition in  $^4\text{He}^*$  and  $^{40}\text{Ar}^*$  source rock is assumed to be that of an average crustal composition with Th/U and K/U ratios of 3.8 and  $1.2 \times 10^4$ , respectively [Taylor and McLennan, 1985; Elliot et al., 1993], the radiogenic  $^4\text{He}/^{40}\text{Ar}$  production ratio in the source formation will be 4.92 [Ballentine et al., 1991]. The  $^4\text{He}/^{40}\text{Ar}$  ratio of the external flux into the Antrim Shale will also be 4.92 assuming both that the subsurface temperature in the source rock is high enough to release all the Ar, i.e.,  $\geq 250\text{ }^\circ\text{C}$  [Lippolt and Weigel, 1988; Pinti et al., 2011] and that no other processes have led to fractionation of the  $^4\text{He}/^{40}\text{Ar}$  ratio [e.g., Castro et al., 1998a; 1998b]. Given measured atmospheric-derived  $^{36}\text{Ar}$  volume fractions and the atmospheric  $^{40}\text{Ar}/^{36}\text{Ar}$  ratio of 295.5 [Ozima and Podosek, 2002], predicted  $^{40}\text{Ar}/^{36}\text{Ar}$  ratios can be calculated assuming that Ar is fully released from the source formation ( $T > 250\text{ }^\circ\text{C}$ ) [Elliot et al., 1993]:

$$\left(\frac{^{40}\text{Ar}}{^{36}\text{Ar}}\right)_{\text{predicted}} = \frac{^{36}\text{Ar}_{\text{measured}} \times 295.5 + ^4\text{He}^*/4.92}{^{36}\text{Ar}_{\text{measured}}} \quad (2.9)$$

Predicted  $^{40}\text{Ar}/^{36}\text{Ar}$  ratios are plotted in Figure 2.8 together with measured  $^{40}\text{Ar}/^{36}\text{Ar}$  ratios for all sampled Antrim Shale gases. The predicted  $^{40}\text{Ar}/^{36}\text{Ar}$  over measured  $^{40}\text{Ar}/^{36}\text{Ar}$  ratios are also listed in Table 2.2. The formation of thermogenic gases require reservoir temperatures between 157 and 221°C, whereas biogenic gases yield formation temperatures consistent with their comparatively low-temperature formation environments ( $< 50^\circ\text{C}$ ) [Stolper et al., 2015],

However this is lower than the Ar release temperature (250 °C) [Lippolt and Weigel, 1988]. Given that predicted and measured  $^{40}\text{Ar}/^{36}\text{Ar}$  ratios match well with each other, paleo subsurface temperatures in the source rock should be higher than the Ar release temperature and thus high enough for thermogenic methane formation. From the ratios of predicted over measured  $^{40}\text{Ar}/^{36}\text{Ar}$ , it is apparent that, with the exception of samples ANT1 and ANT4, all other Antrim gas samples have consistent measured and predicted  $^{40}\text{Ar}/^{36}\text{Ar}$  ratio values, which tend to support that the contribution of thermogenic methane is greater than expected (< 20%) in these samples. Stolper *et al.* [2015] established a mixing model of biogenic vs. thermogenic gases for Antrim Shale gases based on assumed formation temperatures of 18°C and 144°C for biogenic and thermogenic components, respectively. Their findings point to a larger proportion (~50%) of thermogenic gas in the Antrim Shale than previously thought. It is important to note that higher formation temperature of the thermogenic component in the mixing model will result in lower required amounts of the thermogenic gases. In our study, a greater formation temperature for thermogenic gas (> 250 °C) is suggested. Even with this very high assumed temperature, their mixing model still suggests > 25% thermogenic gases in the Antrim Shale. Thermal maturity of the Antrim Shale in the study area is relatively low and does not support in-situ production of thermogenic methane [Rullkötter *et al.*, 1992], although the TOC content of the Antrim Shale is up to 24% [Martini *et al.*, 1998]. Therefore, thermogenic methane, as the major component of the total produced methane in the Antrim within the study area (NPT), must have an external origin. This external origin for the thermogenic methane might be either the portion of the Antrim Shale located in the deeper, central portion of the Michigan Basin or more deeply buried Silurian and older strata underlying the Antrim Shale [Stolper *et al.*, 2015]. Further work is

required to distinguish these two external sources of thermogenic methane for Antrim Shale gas samples.

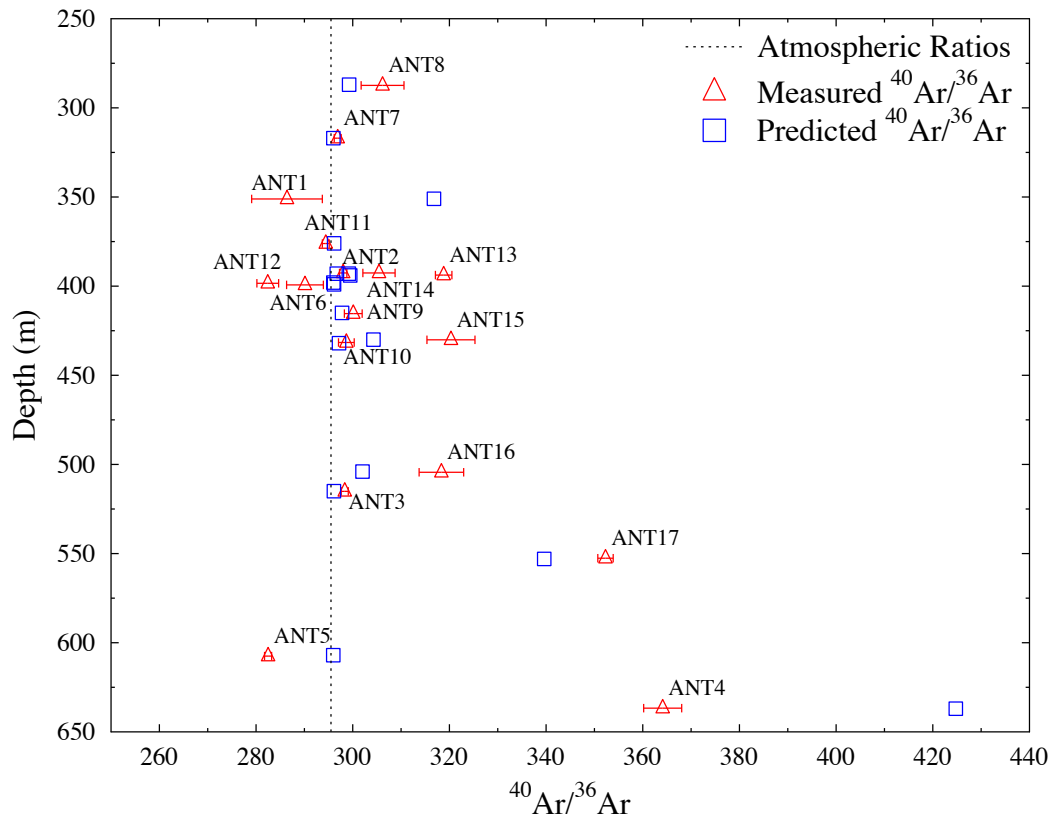


**Figure 2.8** Depth profiles versus (a) measured  $^{40}\text{Ar}/^{36}\text{Ar}$  (red open triangles); and (b) predicted  $^{40}\text{Ar}/^{36}\text{Ar}$  ratios (open blue square) for Antrim gas samples in this study. The atmospheric  $^{40}\text{Ar}/^{36}\text{Ar}$  ratio is also indicated (dashed line).

## 2.7 Conclusions

This study uses stable noble gases' (He, Ne, Ar, Kr, Xe) volume fractions and isotopic ratios from Antrim Shale gas samples to clarify vertical fluid migration, the occurrence of a past thermal event previously identified [Sanford *et al.*, 1985; Fisher *et al.*, 1988; Coniglio *et al.*, 1994; Wang *et al.*, 1994; Girard and Barnes, 1995; Castro *et al.*, 2009; Ma *et al.*, 2009a; 2009b], ages of formation water associated with natural gas, and to distinguish between thermogenic and biogenic methane in the Antrim Shale.

R/Ra ratios in Antrim Shale gas, where R is the measured  $^3\text{He}/^4\text{He}$  ratio and Ra is the atmospheric ratio value of  $1.384 \pm 0.013 \times 10^{-6}$ , vary from an almost pure radiogenic (crustal) value of  $0.009 \pm 0.001$  [typical crustal production values are  $\sim 0.01$ - $0.05$ ; Oxburgh *et al.*, 1986], to  $0.339 \pm 0.006$ . Higher values of measured R/Ra ratios likely indicate the impact of mixing with an atmospheric component (R/Ra=1) introduced during freshwater recharge. Crustal  $^{21}\text{Ne}^*$ ,  $^{40}\text{Ar}^*$  and  $^{136}\text{Xe}^*$  contributions are also present but the atmospheric component is largely dominant for these gases. Crustal contributions for  $^{21}\text{Ne}$ ,  $^{40}\text{Ar}$  and  $^{136}\text{Xe}$  vary between 1.1% and 12.5%, between 0.7% and 19% and between 0.1% and 2.7%, respectively. Elevated  $^{20}\text{Ne}/^{22}\text{Ne}$  ratios (up to 10.4) point to a minor mantle Ne component. High horizontal and vertical variability of noble gas signatures in the Antrim Shale are observed, which are due to variable noble gas input with brine migration from deeper formations and, to a smaller extent, are also due to variable in-situ production, in particular, the Lachine and Norwood Members.

$^4\text{He}$  ages are calculated for two scenarios: 1) the Antrim Shale is a closed system and only in-situ  $^4\text{He}$  has accumulated over geological times; 2) the Antrim Shale is an open system and external  $^4\text{He}$  flux migrated into the Antrim Shale and accumulated, in addition to the in-situ  $^4\text{He}$  production. Considering only in-situ  $^4\text{He}$  production, calculated  $^4\text{He}$  ages range from 0.04 to

10.9 Ma (average 1.15 Ma), which are much older than  $^4\text{He}$  ages of 0.9 to 238.2 ka (average 25 ka) considering both the upward external  $^4\text{He}$  flux and in-situ  $^4\text{He}$  production. Estimated  $^4\text{He}$  ages considering external  $^4\text{He}$  input for Antrim Shale water match well for most samples with the timing of the major Wisconsin glaciation (10 to 79 ka) in the Michigan Basin [Dorr and Eschman, 1970; Schaetzl et al., 2008; Bergquist, 2009], suggesting that Antrim Shale water was influenced by glaciation-induced recharge.

Given measured atmospheric-derived  $^{36}\text{Ar}$  volume fractions and the atmospheric  $^{40}\text{Ar}/^{36}\text{Ar}$  ratio of 295.5 [Ozima and Podosek, 2002], predicted  $^{40}\text{Ar}/^{36}\text{Ar}$  ratios can be calculated assuming that Ar is fully released from the source formation ( $T > 250\text{ }^\circ\text{C}$ ) [Elliot et al., 1993]. Measured and predicted  $^{40}\text{Ar}/^{36}\text{Ar}$  ratios match well with each other for most Antrim Shale gases, indicating that paleo subsurface temperatures in the source rock should be higher than the Ar release temperature ( $250\text{ }^\circ\text{C}$ ) and thus high enough for thermogenic methane formation ( $157$  and  $221\text{ }^\circ\text{C}$ ) [Stolper et al., 2015]. Thermal maturity of the Antrim Shale in the study area is relatively low and does not support in-situ production of thermogenic methane [Rullkötter et al., 1992], although the TOC content of the Antrim Shale is up to 24% [Martini et al., 1998]. Therefore, thermogenic methane, which contributes most of the total produced methane in the Antrim within the study area, must originate from an external source. That might be either the deeper portion of the Antrim Shale located in the central Michigan Basin or more deeply buried Silurian and older strata underlying the Antrim Shale [Stolper et al., 2015].

## 2.8 Acknowledgements

We thank Prof. David Hilton for the editorial handling of this manuscript as well as Dr. Greg Holland and an anonymous reviewer for their insightful and thorough reviews. Financial

support by the University of Michigan M-Cubed initiative and NSF awards 1049822 and CBET-1214416 is greatly appreciated. We also thank BreitBurn Energy Partners L.P. for access to their Antrim Shale gas wells as well as Phillip Brenz and Laura Bouvier for their assistance in the field.

## 2.9 References

- Apotria, T., C. J. Kaiser, and B. A. Cain (1994), Fracturing and stress history of the Devonian Antrim Shale, Michigan basin, *SPE REPRINT SERIES*, 9–9.
- Ballentine, C. J. (1991), He, Ne, and Ar Isotopes as Tracers in Crustal Fluids, Cambridge University Press.
- Ballentine, C. J., M. Mazurek, and A. Gautschi (1994), Thermal constraints on crustal rare gas release and migration: Evidence from Alpine fluid inclusions, *Geochimica et Cosmochimica Acta*, 58(20), 4333–4348.
- Ballentine, C. J., R. K. O'Nions, E. R. Oxburgh, F. Horvath, and J. Deak (1991), Rare gas constraints on hydrocarbon accumulation, crustal degassing and groundwater flow in the Pannonian Basin, *Earth and Planetary Science Letters*, 105(1–3), 229–246, doi:10.1016/0012-821X(91)90133-3.
- Bergquist, S. G. (2009), The glacial history and development of Michigan, *Michigan State University*, 1–12.
- Boyer, C., J. Kieschnick, R. Suarez-Rivera, and R. E. Lewis (2006), Producing gas from its source, *Oilfield Review*.
- Castro, M. C., A. Jambon, G. de Marsily, and P. Schlosser (1998a), Noble gases as natural tracers of water circulation in the Paris Basin: 1. Measurements and discussion of their origin and mechanisms of vertical transport in the basin, *Water Resources Research*, 34(10), 2443–2466, doi:10.1029/98WR01956.
- Castro, M. C., and P. Goblet (2003), Calibration of regional groundwater flow models: Working toward a better understanding of site-specific systems, *Water Resources Research*, 39(6), 1172–n/a, doi:10.1029/2002WR001653.
- Castro, M. C., L. Ma, and C. M. Hall (2009), A primordial, solar He–Ne signature in crustal fluids of a stable continental region, *Earth and Planetary Science Letters*, 279(3–4), 174–184, doi:10.1016/j.epsl.2008.12.042.
- Castro, M. C., M. Stute, and P. Schlosser (2000), Comparison of <sup>4</sup>He ages and <sup>14</sup>C ages in simple aquifer systems: implications for groundwater flow and chronologies, *Applied Geochemistry*, 15(8), 1137–1167, doi:10.1016/S0883-2927(99)00113-4.
- Castro, M. C., P. Goblet, E. Ledoux, S. Violette, and G. de Marsily (1998b), Noble gases as natural tracers of water circulation in the Paris Basin: 2. Calibration of a groundwater flow model using noble gas isotope data, *Water Resources Research*, 34(10), 2467–2483, doi:10.1029/98WR01957.
- Catacosinos, A. P., and P. A. J. Daniels (1991), Stratigraphy of Middle Proterozoic to Middle Ordovician formations of the Michigan Basin, *Spec. Pap. Geol. Soc. Am.*, (256), 53–71.

- Cercone, K. R., and H. N. Pollack (1991), Thermal maturity of the Michigan Basin, *Geological Society of America Special Papers*, 256, 1–12.
- Clark, S.P. (1966), Handbook of Physical Constants, Geological Society of America, New York.
- Clark, J. A. (1982), Glacial Loading: A Cause of Natural Fracturing and a Control of the Present Stress State in Regions of High Devonian Shale Gas Production, *SPE-10798-MS*, doi:10.2118/10798-MS.
- Coniglio, M., R. Sherlock, A. E. Williams-Jones, K. Middleton, and S. K. Frape (1994), Burial and Hydrothermal Diagenesis of Ordovician Carbonates from the Michigan Basin, Ontario, Canada, in *onlinelibrary.wiley.com*, pp. 231–254, Blackwell Publishing Ltd., Oxford, UK.
- Crovetto, R., R. Fernandez-Prini, and M. L. Japas (1982), Solubilities of inert gases and methane in H<sub>2</sub>O and in D<sub>2</sub>O in the temperature range of 300 to 600 K, *J. Chem. Phys.*, 76(2), 1077–1086, doi:10.1063/1.443074.
- Curtis, J. B. (2002), Fractured shale-gas systems, *AAPG Bulletin*, 86(11), 1921–1938.
- Darrah, T. H., A. Vengosh, R. B. Jackson, N. R. Warner, and R. J. Poreda (2014), Noble gases identify the mechanisms of fugitive gas contamination in drinking-water wells overlying the Marcellus and Barnett Shales, *Proceedings of the National Academy of Sciences*, 111(39), 14076–14081, doi:10.1073/pnas.1322107111.
- Dolton, G. L., and J. C. Quinn (1996), *An Initial Resource Assessment of the Upper Devonian Antrim Shale in the Michigan Basin*, U S Geological Survey.
- Dorr, J. A. J., and D. F. Eschman (1970), *Geology of Michigan*, University of Michigan, Ann Arbor.
- Eikenberg, J., P. Signer, R. Wieler (1993), U–Xe, U–Kr, and U–Pb systematics for dating uranium minerals and investigations of the production of nucleogenic neon and argon, *Geochim. Cosmochim. Acta* 57, 1053–1069.
- Elliot, T., C. J. Ballentine, R. K. O'Nions, and T. Ricchiuto (1993), Carbon, helium, neon and argon isotopes in a Po basin (northern Italy) natural gas field, *Chemical Geology*, 106(3–4), 429–440, doi:10.1016/0009-2541(93)90042-H.
- Farrand, W. R., and D. F. Eschman (1974), Glaciation of the southern peninsula of Michigan: a review, *Michigan Academician*, 7(1), 31–56.
- Fisher, J. H., M. W. Barratt, J. B. Droste, and R. H. Shaver (1988), Michigan Basin, in *Sedimentary Cover-North American Craton*, edited by L. L. Sloss, *Geol. Soc. of Am.*, 361–382.
- Girard, J.-P., and D. A. Barnes (1995), Illitization and Paleothermal Regimes in the Middle Ordovician St. Peter Sandstone, Central Michigan Basin: K-Ar, Oxygen Isotope, and

- Fluid Inclusion Data, *AAPG Bulletin*, 79(1), 49–69.
- Graham, D. W. (2002), Noble Gas Isotope Geochemistry of Mid-Ocean Ridge and Ocean Island Basalts: Characterization of Mantle Source Reservoirs, *Reviews in Mineralogy and Geochemistry*, 47(1), 247–317, doi:10.2138/rmg.2002.47.8.
- Gutschick, R. C., and C. A. Sandberg (1991), Late Devonian history of Michigan basin, *Geological Society of America Special Papers*, 256, 181–202.
- Harrell, J. A., C. B. Hatfield, and G. R. Gunn (1991), Mississippian System of the Michigan Basin; Stratigraphy, sedimentology, and economic geology, *Geological Society of America Special Papers*, 256, 203–220.
- Harrison, W. B. (2007), Production History and Reservoir Characteristics of the Antrim Shale Gas Play, Michigan Basin, *AAPG Eastern Section Meeting 2007*, 1–1.
- Hill, D. G., and C. R. Nelson (2000), *Gas productive fractured shales - An overview and update: Gas Tips*, edited by D. G. Hill and C. R. Nelson.
- Hilton, D. R., and D. Porcelli (2003a), 2.06 - Noble Gases as Mantle Tracers, in *Treatise on Geochemistry*, edited by H. D. H. K. Turekian, pp. 277–318, Pergamon, Oxford.
- Hilton, D. R., and D. Porcelli (2003b), Noble gases as mantle tracers, in the Mantle and Core, in *Treatise on Geochemistry*, edited by H. D. Holland and K. K. Turekian, Elsevier, New York.
- Hinze, W. J., R. L. Kellogg, and N. W. O'Hara (1975), Geophysical Studies of Basement Geology of Southern Peninsula of Michigan, *AAPG Bulletin*, 59(9), 1562–1584.
- Hunt, J. M. (1996), *Petroleum Geochemistry and Geology*, W H Freeman & Company.
- Kipfer, R., W. Aeschbach-Hertig, F. Peeters, and M. Stute (2002), Noble Gases in Lakes and Ground Waters, *Reviews in Mineralogy and Geochemistry*, 47(1), 615–700.
- Kulongoski, J. T., D. R. Hilton, and J. A. Izbicki (2005), Source and movement of helium in the eastern Morongo groundwater Basin: The influence of regional tectonics on crustal and mantle helium fluxes, *Geochimica et Cosmochimica Acta*, 69(15), 3857–3872, doi:10.1016/j.gca.2005.03.001.
- Leventhal, J.S. (1980), Comparative Geochemistry of Devonian Shale Cores from the Appalachian Basin, Mason, Monongalia, and Upshur Counties, West Virginia; Illinois Basin, Tazwell County, Illinois; Clark County, Indiana; and Michigan Basin, Sanilac County, Michigan, United States Geological Survey.
- Lippolt, H. J., and E. Weigel (1988),  $^4\text{He}$  diffusion in  $^{40}\text{Ar}$ -retentive minerals, *Geochimica et Cosmochimica Acta*, 52(6), 1449–1458, doi:10.1016/0016-7037(88)90215-3.
- Ma, L., M. C. Castro, and C. M. Hall (2009a), Atmospheric noble gas signatures in deep

- Michigan Basin brines as indicators of a past thermal event, *Earth and Planetary Science Letters*, 277(1–2), 137–147, doi:10.1016/j.epsl.2008.10.015.
- Ma, L., M. C. Castro, and C. M. Hall (2009b), Crustal noble gases in deep brines as natural tracers of vertical transport processes in the Michigan Basin, *Geochemistry Geophysics Geosystems*, 10(6), Q06001, doi:10.1029/2009GC002475.
- Ma, L., M. C. Castro, and C. M. Hall (2004), A late Pleistocene–Holocene noble gas paleotemperature record in southern Michigan, *Geophysical research letters*, 31(23), L23204, doi:10.1029/2004GL021766.
- Ma, L., M. C. Castro, C. M. Hall, and L. M. Walter (2005), Cross-formational flow and salinity sources inferred from a combined study of helium concentrations, isotopic ratios, and major elements in the Marshall aquifer, southern Michigan, *Geochemistry Geophysics Geosystems*, 6(10), Q10004, doi:10.1029/2005GC001010.
- Manger, K. C., S. J. P. Oliver, J. B. Curtis, and R. J. Scheper (1991), Geologic Influences on the Location and Production of Antrim Shale Gas, Michigan Basin, *SPE-21854-MS*, 1–10.
- Martini, A. M., J. M. Budai, L. M. Walter, and M. Schoell (1996), Microbial generation of economic accumulations of methane within a shallow organic-rich shale, *Nature*, 383(6596), 155–158, doi:10.1038/383155a0.
- Martini, A. M., L. M. Walter, J. M. Budai, T. C. W. Ku, C. J. Kaiser, and M. Schoell (1998), Genetic and temporal relations between formation waters and biogenic methane: Upper Devonian Antrim Shale, Michigan Basin, USA, *Geochimica et Cosmochimica Acta*, 62(10), 1699–1720, doi:10.1016/S0016-7037(98)00090-8.
- Martini, A. M., L. M. Walter, T. C. W. Ku, J. M. Budai, J. C. McIntosh, and M. Schoell (2003), Microbial production and modification of gases in sedimentary basins: A geochemical case study from a Devonian shale gas play, Michigan basin, *AAPG Bulletin*, 87(8), 1355–1375, doi:10.1306/031903200184.
- Mazor, E., and A. H. Truesdell (1984), Dynamics of a geothermal field traced by noble gases: Cerro Prieto, Mexico, *Geothermics*, 13, 91–102. [http://dx.doi.org/10.1016/0375-6505\(84\)90009-9](http://dx.doi.org/10.1016/0375-6505(84)90009-9).
- McIntosh, J. C., and A. M. Martini (2008), Chapter Five: Hydrogeochemical Indicators for Microbial Methane in Fractured Organic-Rich Shales: Case Studies of the Antrim, New Albany, and Ohio Shales, *archives.datapages.com.proxy.lib.umich.edu*, 162–174.
- McIntosh, J. C., and L. M. Walter (2005), Volumetrically significant recharge of Pleistocene glacial meltwaters into epicratonic basins: Constraints imposed by solute mass balances, *Chemical Geology*, 222(3–4), 292–309.
- McIntosh, J. C., G. Garven, and J. S. Hanor (2011), Impacts of Pleistocene glaciation on large-scale groundwater flow and salinity in the Michigan Basin, *Geofluids*, 11(1), 18–33.

- McIntosh, J. C., M. E. SCHLEGEL, and M. PERSON (2012), Glacial impacts on hydrologic processes in sedimentary basins: evidence from natural tracer studies, *Geofluids*, 12(1), 7–21, doi:10.1111/j.1468-8123.2011.00344.x.
- Menuge, J. F., S. T. Brewer, and C. M. Seeger (2002), Petrogenesis of metaluminous A-type rhyolites from the St. Francois Mountains, Missouri and the Mesoproterozoic evolution of the southern Laurentian margin, *Precambrian Res.*, (113), 269–291.
- Nicot, J.-P., and B. R. Scanlon (2012), Water Use for Shale-Gas Production in Texas, U.S, *Environ. Sci. Technol.*, 46(6), 3580–3586, doi:10.1021/es204602t.
- Nicot, J.-P., B. R. Scanlon, R. C. Reedy, and R. A. Costley (2014), Source and Fate of Hydraulic Fracturing Water in the Barnett Shale: A Historical Perspective, *Environ. Sci. Technol.*, 48(4), 2464–2471, doi:10.1021/es404050r.
- Oxburgh, E. R., R. K. O'Nions, and R. I. Hill (1986), Helium isotopes in sedimentary basins, *Nature*, 324(6098), 632–635, doi:10.1038/324632a0.
- Ozima, M., and F. A. Podosek (2002), *Noble Gas Geochemistry*, Cambridge University Press, New York.
- Pinti, D. L., and B. Marty (1995), Noble gases in crude oils from the Paris Basin, France: Implications for the origin of fluids and constraints on oil-water-gas interactions, *Geochimica et Cosmochimica Acta*, 59(16), 3389–3404, doi:10.1016/0016-7037(95)00213-J.
- Pinti, D. L., and B. Marty (2000), Chapter 7. NOBLE GASES IN OIL AND GAS FIELDS: ORIGINS AND PROCESSES, vol. 28, pp. 160–196, Fluids and Basin Evolution. Mineral Soc Can Short Course.
- Pinti, D. L., C. Béland-Otis, A. Tremblay, M. C. Castro, C. M. Hall, J.-S. Marcil, J.-Y. Lavoie, and R. Lapointe (2011), Fossil brines preserved in the St-Lawrence Lowlands, Québec, Canada as revealed by their chemistry and noble gas isotopes, *Geochimica et Cosmochimica Acta*, 75(15), 4228–4243, doi:10.1016/j.gca.2011.05.006.
- Pinti, D. L., M. C. Castro, O. Shouakar-Stash, A. Tremblay, V. H. Garduño, C. M. Hall, J. F. Hélie, and B. Ghaleb (2012), Evolution of the geothermal fluids at Los Azufres, Mexico, as traced by noble gas isotopes,  $\delta^{18}\text{O}$ ,  $\delta\text{D}$ ,  $\delta^{13}\text{C}$  and  $^{87}\text{Sr}/^{86}\text{Sr}$ , *Journal of Volcanology and Geothermal Research*, 249(0), 1–11, doi:10.1016/j.jvolgeores.2012.09.006.
- Podosek, F.A., M. Honda, M. Ozima (1980), Sedimentary noble gases, *Geochim. Cosmochim. Acta*, 44, 1875–1884. [http://dx.doi.org/10.1016/0016-7037\(80\)90236-7](http://dx.doi.org/10.1016/0016-7037(80)90236-7).
- Porcelli, D., C. J. Ballentine, and R. Wieler (2002), An Overview of Noble Gas Geochemistry and Cosmochemistry, *Reviews in Mineralogy and Geochemistry*, 47(1), 1–19, doi:10.2138/rmg.2002.47.1.
- Price, L. C., and M. Schoell (1995), Constraints on the origins of hydrocarbon gas from

- compositions of gases at their site of origin, *Nature*, 378(6555), 368–371, doi:10.1038/378368a0.
- Ruff, L., R. LaForge, R. Thorson, T. Wagner, and F. Goudaen (1994), Geophysical Investigation of the Western Ohio–Indiana Region, Final Report 1986–1992, U.S. Nuclear Regulatory Commission: NUREG/CR-3145 10 p. 73.
- Rullkötter, J., R. Marzi, and P. Meyers (1992), Biological Markers in Paleozoic Sedimentary Rocks and Crude Oils from the Michigan Basin: Reassessment of Sources and Thermal History of Organic Matter, in *Early Organic Evolution*, edited by M. Schidlowski, S. Golubic, M. Kimberley, D. McKirdy Sr, and P. Trudinger, pp. 324–335–335, Springer Berlin Heidelberg, Berlin, Heidelberg.
- Ryder, R. T. (1996), *Fracture Patterns and Their Origin in the Upper Devonian Antrim Shale Gas Reservoir of the Michigan Basin*.
- Sanford, B. V., F. J. Thompson, and G. H. McFall (1985), Plate Tectonics -- A Possible Controlling Mechanism in the Development of Hydrocarbon Traps in Southwestern Ontario, *Bulletin of Canadian Petroleum Geology*, 33(1), 52–71.
- Schaetzl, R. J., J. T. Darden, and D. S. Brandt (2008), *Michigan geography and geology*, Pearson Custom Pub.
- Schlegel, M. E., Z. Zhou, J. C. McIntosh, C. J. Ballentine, and M. A. Person (2011), Constraining the timing of microbial methane generation in an organic-rich shale using noble gases, Illinois Basin, USA, *Chemical Geology*, 287(1–2), 27–40, doi:10.1016/j.chemgeo.2011.04.019.
- Smith, S. P., and B. M. Kennedy (1983), The solubility of noble gases in water and in NaCl brine, *Geochimica et Cosmochimica Acta*, 47(3), 503–515, doi:10.1016/0016-7037(83)90273-9.
- Starkey, N. A., F. M. Stuart, R. M. Ellam, J. G. Fitton, S. Basu, and L. M. Larsen (2009), Helium isotopes in early Iceland plume picrites: Constraints on the composition of high <sup>3</sup>He/<sup>4</sup>He mantle, *Earth and Planetary Science Letters*, 277(1–2), 91–100.
- Stolper, D. A. et al. (2014), Formation temperatures of thermogenic and biogenic methane, *Science*, 344(6191), 1500–1503, doi:10.1126/science.1254509.
- Stolper, D. A., A. M. Martini, M. Clog, P. M. Douglas, S. S. Shusta, D. L. Valentine, A. L. Sessions, and J. M. Eiler (2015), Distinguishing and understanding thermogenic and biogenic sources of methane using multiply substituted isotopologues, *Geochimica et Cosmochimica Acta*, doi:10.1016/j.gca.2015.04.015.
- Swanson, V.E. (1960), Oil Yield and Uranium Content of Black Shales, United States Geological Survey.
- Taylor, S. R., and S. M. McLennan (1985), *The Continental Crust: Its Composition and Evolution*, Wiley-Blackwell, Oxford.

- Torgersen, T. (1980), Controls on pore-fluid concentration of  $^4\text{He}$  and  $^{222}\text{Rn}$  and the calculation of  $^4\text{He}/^{222}\text{Rn}$  ages, *Journal of Geochemical Exploration*, 13(1), 57–75, doi:10.1016/0375-6742(80)90021-7.
- Torgersen, T., and G. N. Ivey (1985), Helium accumulation in groundwater. II: A model for the accumulation of the crustal  $^4\text{He}$  degassing flux, *Geochimica et Cosmochimica Acta*, 49(11), 2445–2452, doi:10.1016/0016-7037(85)90244-3.
- Torgersen, T., and W. B. Clarke (1985), Helium accumulation in groundwater, I: An evaluation of sources and the continental flux of crustal  $^4\text{He}$  in the Great Artesian Basin, Australia, *Geochimica et Cosmochimica Acta*, 49(5), 1211–1218, doi:10.1016/0016-7037(85)90011-0.
- Torgersen, T., B. M. Kennedy (1999), Air-Xe enrichments in Elk Hills oil field gases: role of water in migration and storage, *Earth Planet. Sci. Lett.*, 167, 239–253. [http://dx.doi.org/10.1016/S0012-821X\(99\)00021-7](http://dx.doi.org/10.1016/S0012-821X(99)00021-7).
- US EIA (2015), *Annual Energy Outlook 2015*, US Energy Information Administration, Washington, DC.
- Van Schmus, W. R. (1992), Tectonic setting of the Midcontinent Rift system, *Tectonophysics*, (215), 1–15.
- Vugrinovich, R. (1986), *Patterns of Regional Subsurface Fluid Movement in the Michigan Basin*, United States Geological Survey, Lansing.
- Walter, L. M., J. M. Budai, L. M. Abriola, C. H. Stearns, and A. M. Martini (1996), Hydrogeochemistry of the antrim shale northern michigan basin. Annual report, September 1, 1993-May 1, 1995,
- Wang, H. F., K. D. Crowley, and G. C. Nadon (1994), Thermal history of the Michigan Basin from apatite fission-track analysis and vitrinite reflectance,
- Waples, D. W. (1985), *Geochemistry in petroleum exploration*,
- Warrier, R. B., M. C. Castro, C. M. Hall, and K. C. Lohmann (2013), Large atmospheric noble gas excesses in a shallow aquifer in the Michigan Basin as indicators of a past mantle thermal event, *Earth and Planetary Science Letters*, 375(0), 372–382, doi:10.1016/j.epsl.2013.06.001.
- Weiss, R. F. (1968), Piggyback sampler for dissolved gas studies on sealed water samples, *Deep Sea Research and Oceanographic Abstracts*, 15(6), 695–699.
- Wen, T., M. C. Castro, C. M. Hall, D. L. Pinti, and K. C. Lohmann (2015), Constraining groundwater flow in the glacial drift and saginaw aquifers in the Michigan Basin through helium concentrations and isotopic ratios, *Geofluids*, 16, 3–25, doi:10.1111/gfl.12133.
- Westjohn, D. B., and T. L. Weaver (1996), *Hydrogeologic framework of Mississippian rocks in*

*the central Lower Peninsula of Michigan*, United States Geological Survey.

- Wetherill, G. (1954), Variations in the Isotopic Abundances of Neon and Argon Extracted from Radioactive Minerals, *Physical Review*, 96(3), 679–683, doi:10.1103/PhysRev.96.679.
- Wilson, T. P., and D. T. Long (1993a), Geochemistry and isotope chemistry of CaNaCl brines in Silurian strata, Michigan Basin, U.S.A, *Applied Geochemistry*, 8(5), 507–524, doi:10.1016/0883-2927(93)90079-V.
- Wilson, T. P., and D. T. Long (1993b), Geochemistry and isotope chemistry of Michigan Basin brines: Devonian formations, *Applied Geochemistry*, 8(1), 81–100, doi:10.1016/0883-2927(93)90058-O.
- Zhou, Z., and C. J. Ballentine (2006), 4He dating of groundwater associated with hydrocarbon reservoirs, *Chemical Geology*, 226(3–4), 309–327.
- Zhou, Z., C. J. Ballentine, R. Kipfer, M. Schoell, and S. Thibodeaux (2005), Noble gas tracing of groundwater/coalbed methane interaction in the San Juan Basin, USA, *Geochimica et Cosmochimica Acta*, 69(23), 5413–5428, doi:10.1016/j.gca.2005.06.027.

# CHAPTER 3

## METHANE SOURCES AND MIGRATION MECHANISMS IN SHALLOW GROUNDWATERS IN PARKER AND HOOD COUNTIES, TEXAS – A HEAVY NOBLE GAS ANALYSIS <sup>2</sup>

### 3.1 Abstract

This study places constraints on the source and transport mechanisms of methane found in groundwater within the Barnett Shale footprint in Texas using dissolved noble gases, with particular emphasis on <sup>84</sup>Kr and <sup>132</sup>Xe. Dissolved methane concentrations are positively correlated with crustal <sup>4</sup>He, <sup>21</sup>Ne and <sup>40</sup>Ar and suggest that noble gases and methane originate from common sedimentary strata, likely the Strawn Group. In contrast to most samples, four water wells with the highest dissolved methane concentrations unequivocally show strong depletion of all atmospheric noble gases (<sup>20</sup>Ne, <sup>36</sup>Ar, <sup>84</sup>Kr, <sup>132</sup>Xe) with respect to air-saturated water (ASW). This is consistent with predicted noble gas concentrations in a water phase in contact with a gas phase with initial ASW composition at 18°C-25°C and it suggests an in-situ, highly localized gas source. All of these four water wells tap into the Strawn Group and it is likely that small gas accumulations known to be present in the shallow subsurface were reached. Additionally, lack of correlation of <sup>84</sup>Kr/<sup>36</sup>Ar and <sup>132</sup>Xe/<sup>36</sup>Ar fractionation levels along with

---

<sup>2</sup> Citation: Wen, T., Castro, M.C., Nicot, J.-P., Hall, C.M., Larson, T., Mickler, P., Darvari, R., 2016. Methane Sources and Migration Mechanisms in Shallow Groundwaters in Parker and Hood Counties, Texas—A Heavy Noble Gas Analysis. *Environ. Sci. Technol.* doi:10.1021/acs.est.6b01494

$^4\text{He}/^{20}\text{Ne}$  with distance to the nearest gas production wells does not support the notion that methane present in these groundwaters migrated from nearby production wells either conventional or using hydraulic fracturing techniques.

### 3.2 Introduction

With rising demands for domestic energy resources, unconventional hydrocarbon production has been extensively developed since the early 2000's [Nicot *et al.*, 2014]. The combined use of hydraulic fracturing (HF) and horizontal drilling has greatly increased the hydrocarbon recovery from shales, tight formations and other unconventional reservoirs [Nicot and Scanlon, 2012; Nicot *et al.*, 2014]. As a result, unconventional gas resources (*e.g.*, so-called shale gas) accounted for more than one third of the total natural gas production in the United States in 2013 [Nicot *et al.*, 2014; US EIA, 2015]. However, the occasional presence of elevated concentrations of light hydrocarbons in nearby shallow drinking groundwater has caused public concern. For example, enhanced permeability in targeted formations such as the Marcellus or Barnett Shales (at depths of 1800 m to >2000 m) may facilitate migration of natural gas, formation brines and other contaminants into shallow aquifers (<500 m), thereby threatening drinking-water supplies [Osborn *et al.*, 2011; Nicot and Scanlon, 2012; Thompson, 2012; Jackson *et al.*, 2013; Molofsky *et al.*, 2013]. Previous work has focused on identifying sources of methane in shallow groundwaters *e.g.*, the Trinity Aquifer in the Barnett Shale footprint, which can be either from thermogenic or microbial sources [Osborn *et al.*, 2011; Jackson *et al.*, 2013; Molofsky *et al.*, 2013; Darrah *et al.*, 2014; Kornacki and McCaffrey, 2014; Li and Carlson, 2014; Moritz *et al.*, 2015]. It should be noted, however, that the occurrence of both thermogenic and microbial gas in shallow groundwater could be due to either natural or anthropogenic causes

[Darrah *et al.*, 2014; Kornacki and McCaffrey, 2014; Siegel *et al.*, 2015; 2016].

The Barnett Shale in the Fort Worth Basin is the oldest shale gas play in which HF became a major stimulation technique [Nicot *et al.*, 2014]. Large sections of the basin have also undergone conventional production for decades, including the study area where most of the produced gas originated from the Strawn Group. Within the Barnett Shale footprint, the presence of localized stray gas in the shallow Trinity Aquifer has been investigated with respect to its migration mechanisms and origin in several studies [Darrah *et al.*, 2014; Kornacki and McCaffrey, 2014]. Here, “stray gas” refers to natural gas present in shallow aquifers of an undetermined origin. In addition, the descriptor “Trinity Aquifer” is understood as water-bearing rocks mostly of the Trinity Group of Cretaceous age but that can also include the occasional sandstones of the Paleozoic Strawn Group in hydrogeologic continuity with them. Based on well headspace observations of hydrocarbon molar ( $[C_2H_6+]/[CH_4]$ ), stable isotopic (e.g.,  $\delta^{13}C-CH_4$ ) ratios and other information, Kornacki and McCaffrey [2014] tentatively concluded that stray gas in shallow water wells in the Trinity Aquifer within Parker county is of thermogenic origin and originates from the Strawn Group as opposed to the deep Barnett Shale. However, microbial activity and oxidation can alter the original geochemical signature and thus, obscure the original sources and/or mechanisms of fluid migration [Lollar and Ballentine, 2009; Molofsky *et al.*, 2013; Darrah *et al.*, 2014].

In contrast, stable noble gases (Helium – He, Neon – Ne, Argon – Ar, Krypton – Kr, Xenon - Xe) are chemically inert and are thus transported without being affected by chemical reactions [Ozima and Podosek, 2002; Hilton and Porcelli, 2003]. Noble gases in subsurface fluids (e.g., freshwater, natural gas) are derived from the atmosphere, crust and mantle, all of which show distinct isotopic and elemental signatures [Ozima and Podosek, 2002; Porcelli *et al.*,

2002; Hilton and Porcelli, 2003; Castro et al., 2009; Pinti et al., 2012]. This makes noble gases ideal natural tracers for studying the origin and evolution of crustal fluids in sedimentary basins [Oxburgh et al., 1986; Ballentine et al., 1991; Pinti and Marty, 1995; Castro et al., 1998a; 1998b; Hilton and Porcelli, 2003; Kulongoski et al., 2005; Holland and Gilfillan, 2013; Warriier et al., 2013; Wen et al., 2015a; 2015b]. In most subsurface fluids in sedimentary systems, noble gases are dominated by an atmospheric origin (Air Saturated Water or ASW) and/or a crustal component deriving primarily from radioactive decay of U, Th and  $^{40}\text{K}$  [Ozima and Podosek, 2002]. In this study, the crustal component is identified with the “\*” notation.

Previous noble gas work on natural gas from the Barnett and Strawn formations and from the shallow Trinity Aquifer in the Barnett Shale footprint in Parker county suggested that dissolved methane in groundwater is likely derived from the Strawn Group [Darrah et al., 2014]. Some of this stray gas would presumably have migrated along the annulus of a producing well due to poor cementation [Darrah et al., 2014].

Here, we present noble gas concentrations and isotopic ratios from groundwater samples collected in the Trinity Aquifer within the Barnett Shale footprint in Parker and Hood counties in north-central Texas (Figure 3.1). This data, together with information provided by well logs of the sampled water wells is used in an attempt to clarify both the origin of stray gas in the Trinity Aquifer, as well as potential mechanisms responsible for its migration from its source into the Trinity Aquifer water wells. Based on collected data, at this stage, our findings do not point specifically to anthropogenic causes (e.g., poor-quality cementing of natural gas production wells either conventional or using HF technology) that would be responsible for the presence of methane in the Trinity Aquifer in Parker County.

### 3.3 Geologic Setting

The Fort Worth Basin, where the Barnett Shale and Strawn Group are located, is a north-south elongated trough covering roughly 38,100 km<sup>2</sup> in north-central Texas in the southern United States (Figure A1; Appendix A) [Pollastro *et al.*, 2007; Nicot *et al.*, 2014]. It is floored by a Precambrian basement. The Barnett Shale of Late Mississippian age (~331-323 Ma) is the primary petroleum source rock in the Fort Worth Basin and found at a depth of ~1800 m in the study area (Figure A2; Appendix A) [Montgomery *et al.*, 2005; Hill *et al.*, 2007; Pollastro *et al.*, 2007; Bruner and Smosna, 2011; Nicot and Scanlon, 2012; Nicot *et al.*, 2013]. Overlying the Barnett Shale are, from oldest to youngest, the ~150-200 m thick Marble Falls (mostly carbonates) and ~600-700 m thick mostly siliciclastic Bend/Atoka Formations, of Late Mississippian and Lower Pennsylvanian age (~323-299 Ma) [Herkommer and Denke, 1982; Nicot *et al.*, 2015; US EIA, 2015]. The 650-750 m thick Lower Strawn (Kickapoo Creek Formation) unconformably overlain by Cretaceous rocks in the study area consists of alternating sandstone and dominant shale layers with episodic carbonates [Herkommer and Denke, 1982]. Both the Strawn Group and the overlying Cretaceous formations include also minor coal seams [Hackley *et al.*, 2009; Kornacki and McCaffrey, 2014; Kreitler, 2014]. Montgomery *et al.* [2005] and Pollastro *et al.* [2007] suggested that significant migration of hydrocarbons occurred from the Barnett Shale into the Strawn Group over geologic times charging commercially-produced reservoirs. The timing of migration, however, is poorly constrained.

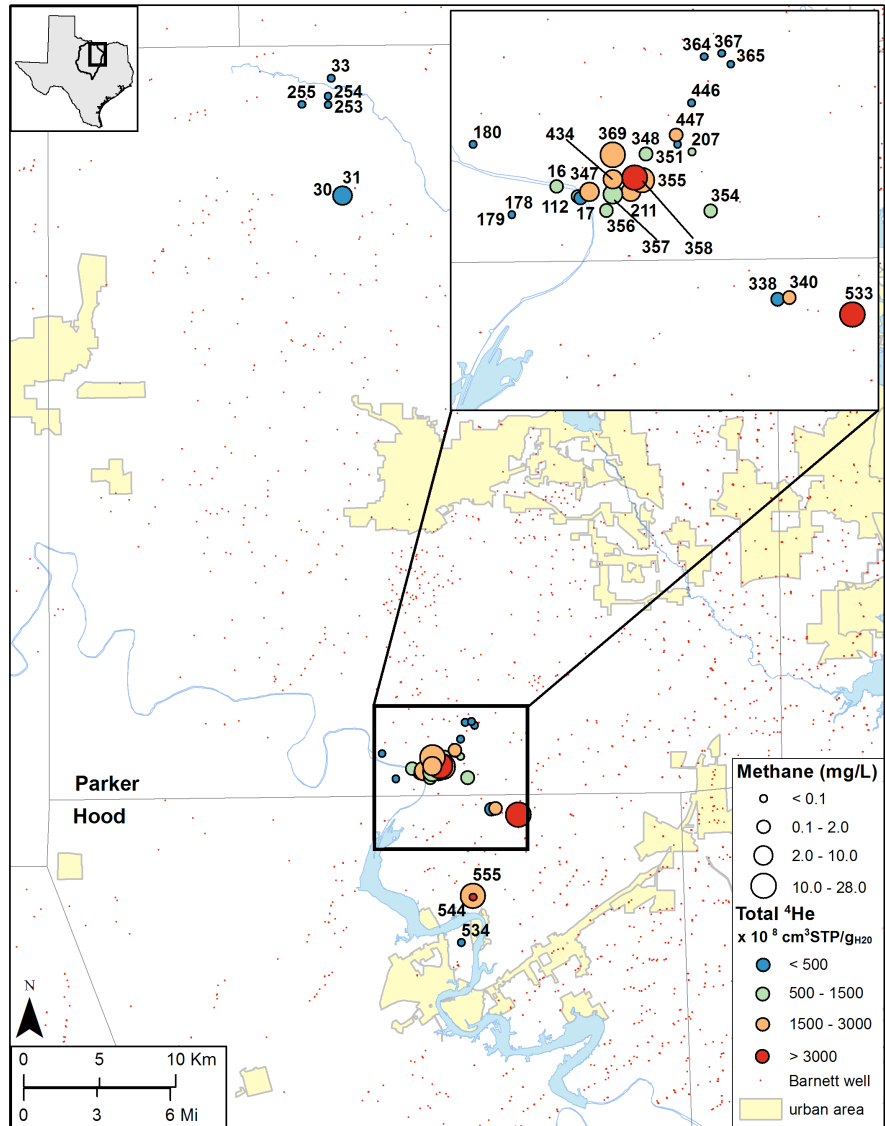


**Figure 3.1** Spatial distribution maps of dissolved methane and total <sup>4</sup>He concentrations for sampled Trinity Aquifer wells. The South Cluster is located close to the Brazos River between the City of Granbury to the south and the City of Weatherford to the north whereas the North Cluster is located north of the City of Weatherford. Small red dots represent wellhead locations of horizontal wells producing from the Barnett Shale.

The Trinity Group hosting the Trinity Aquifer is the main source of drinking water in Parker and Hood counties, where it crops out [Henry, 1982; Darrah *et al.*, 2014; Kornacki and McCaffrey, 2014]. The Trinity Aquifer locally consists of sandstones, silts and conglomerates overlaid by the carbonate Glenrose Formation that acts as a confining unit. In the study area, the Cretaceous sedimentary cover is very thin (< 200m; cf. Appendix A Text A1). Basal sands of the Trinity Group overlie the Strawn Group in an angular unconformity (Figure A2; cf. Appendix A) [Kornacki and McCaffrey, 2014; Kelley *et al.*, 2014]. Predevelopment hydraulic heads in the Trinity Aquifer indicate that the general direction of flow in the study area is along dip from the outcrop to the East [Kelley *et al.*, 2014].

There are no mapped faults at the surface in Parker and Hood counties but several exist at depth, impacting at least some of the Paleozoic section. In addition to the Ouachita thrust belt on the eastern edge of the Barnett, a major fault, “the Mineral Wells fault”, trending SW-NE is present in southern Denton and northern Parker counties (Figure A1; Appendix A) [Ewing, 1991; Pollastro *et al.*, 2007]. This fault, which was active throughout the Paleozoic, appears to be rooted in the Precambrian basement [Montgomery *et al.*, 2005; Pollastro *et al.*, 2007]. Several minor normal faults parallel to it are present in the Fort Worth Basin, including in southern Parker county [Pollastro *et al.*, 2007].

### **3.4 Sampling and Analytical Methods**

Forty-five groundwater samples were collected from 35 wells for measurement of He, Ne, Ar, Kr, and Xe concentrations and their respective isotopic ratios (Table A1; Figure 3.1; cf. Appendix A) in November 2014. Duplicates were collected from 10 well sites (Table A1). Groundwater samples were collected in standard refrigeration grade 3/8” Cu tubing after

temperature, pH and electrical conductivity reached equilibrium. Cu tubes were sealed by steel pinch-off clamps [Weiss, 1968] after water was allowed to flush through the system for approximately 10 min.

The complete measurement procedure for groundwater samples was carried out in the Noble Gas Laboratory at the University of Michigan. Additional sampling, extraction and purification procedures can be found in the literature [Castro *et al.*, 2009; Wen *et al.*, 2015b]. He and Ne were analyzed in a Thermo Scientific® Helix SFT mass spectrometer while Ar, Kr and Xe were sequentially inlet into an ARGUS VI mass spectrometer using a computer-controlled double-head cryo-separator. Analysis procedures are described in the Appendix A Text A2.

Groundwater samples were also collected in glass serum vials with thick rubber septa for CH<sub>4</sub> concentrations following *Kampbell and Vandegrift* [1998] as described in *Nicot et al.* [2015] and were analyzed at The University of Texas at Austin (UT) [Nicot *et al.*, 2015] The detection limit was 0.001 mg/L for dissolved methane [Kampbell and Vandegrift, 1998]. It should be noted, however, that this sampling approach could underestimate oversaturated CH<sub>4</sub> concentrations in water. Collected water samples for Cl concentrations (Table A5; cf. Appendix A) were also analyzed at the UT Bureau of Economic Geology (BEG) [Nicot *et al.*, 2015].

## **3.5 Results and Discussion**

### ***3.5.1 Spatial Distribution of Dissolved Methane***

Groundwater samples in the Trinity Aquifer are grouped into two clusters based on their location (Figure 3.1; Table A1): 1) the “south cluster”, for samples located in Hood and Parker counties, proximal to the boundary between the counties, where high dissolved methane concentrations were previously documented [Darrah *et al.*, 2014; Kornacki and McCaffrey,

2014], and; 2) the “north cluster”, for samples located in the northern portion of Parker county, that was chosen to be away from the south cluster where high methane concentrations are known to be present. With the exception of one sample (i.e., sample 31) noted in the discussion, all the dissolved methane carries the signature of a thermogenic origin, relatively heavy  $\delta^{13}\text{C}$  (-54.1‰ to -26.2‰) and is accompanied by ethane and propane [Nicot *et al.*, 2015].

Following the classification of methane concentrations dissolved in groundwater by *Eltzschlager et al.* [2001], only five groundwater samples all from the “south cluster” (samples 355, 358, 369, 533 and 555) display dissolved methane concentrations of concern, i.e., >10 mg/L (Table A1; cf. Appendix A). In addition, five samples show methane concentrations between 2 and 10 mg/L, whereas twenty-five out of thirty-five wells display dissolved methane concentrations of 0.1-2 mg/L. Many of these wells are located in the proximity of natural gas wells currently being exploited both in the Barnett (using HF techniques) and the Strawn (conventional exploitation) formations, but no strong and definite spatial correlation has been observed between these production wells and water wells displaying high dissolved methane concentrations [Nicot *et al.*, 2015]. In addition, water wells with concentrations >2 mg/L are located in close proximity to wells with low and trace methane concentrations (Figure 3.1). These spatial observations suggest, a priori, a lack of correlation between high dissolved methane concentrations and the locations of natural gas production wells from either the Barnett Shale or the Strawn Group.

### ***3.5.2 Noble Gas Signatures versus Methane Content***

Total dissolved  $^4\text{He}$ ,  $^{20}\text{Ne}$ ,  $^{36}\text{Ar}$ ,  $^{84}\text{Kr}$  and  $^{132}\text{Xe}$  concentrations and isotopic ratios are listed in Tables A2 and A3, respectively.  $^3\text{He}/^4\text{He}$  ratios (R) are normalized to the atmospheric ratio  $R_a$ ,

where  $R_a = (1.384 \pm 0.013) \times 10^{-6}$  [Clarke *et al.*, 1976]. Atmospheric concentrations and isotopic ratios are also reported for reference.

All groundwater samples, without exception, display  $^4\text{He}$  concentrations in excess of ASW values, reaching over three orders of magnitude above that of ASW for temperatures ranging between  $0^\circ\text{C}$  and  $25^\circ\text{C}$  (Figure 3.1). Similar to the spatial distribution of dissolved methane concentrations, highest total  $^4\text{He}$  concentrations are found in some of the south cluster wells (samples 355, 358, 369, 533 and 555; Table A2, Figure 3.1). Overall, a direct correlation is observed between dissolved methane and total  $^4\text{He}$  concentrations, suggesting a common source for both the stray gas and  $^4\text{He}$  present in these groundwaters (Figure 3.2a). Main outliers to this general trend are samples 31 and 253, both located in the north cluster. Higher methane concentrations in sample 31 are due to the presence of microbial methane [2 mg/L methane, no measured ethane,  $\delta^{13}\text{C} = -66\text{‰}$ ; cf. Nicot *et al.*, 2015], whereas mantle He present in sample 253 can explain the deviation of this sample from the observed correlation between methane and total He concentrations (Figure 3.2a; cf. Appendix A Text A3). Crustal  $^4\text{He}$  concentrations ( $^4\text{He}^*$ ) are estimated following Castro and colleagues [Castro *et al.*, 2000; Castro, 2004] and vary by over three orders of magnitude, from  $1.47 \times 10^{-8}$  to  $1.40 \times 10^{-4}$   $\text{cm}^3\text{STP/g}_{\text{H}_2\text{O}}$ . Similar to observations for total  $^4\text{He}$  concentrations,  $^4\text{He}^*$  concentrations display a good correlation with dissolved methane concentrations (Figure 3.2b). Overall, the south cluster exhibits highly contrasting dissolved methane and  $^4\text{He}^*$  concentrations within a very limited area, an observation that is consistent with previous findings [Darrah *et al.*, 2014]. In addition to being well correlated with dissolved methane in groundwater, concentrations of both total  $^4\text{He}$  and  $^4\text{He}^*$  are very similar and point to a dominantly crustal  $^4\text{He}$  component in most samples, as opposed to atmospheric and mantle-derived components (cf. Appendix A Text A3).

Measured R/Ra values vary from an almost pure crustal value of  $0.030 \pm 0.001$  (typical crustal production values are  $\sim 0.02-0.05$ ) [Oxburgh *et al.*, 1986] for most samples to  $0.889 \pm 0.008$  in a few samples, a value very close to that of the atmosphere. Most of the measured higher R/Ra ratios reflect the impact of mixing between older groundwater and recharge water carrying a pure atmospheric component (R/Ra=1) [Castro *et al.*, 1998a; Castro, 2004]. Our helium component analysis (cf. Appendix A Text A3) also points to the likely presence of a minor but non-negligible mantle He component of up to 2% in some samples (e.g., samples 253 and 364), which contributes, to a lesser extent, to increased R/Ra values. Irrespective of the presence of an atmospheric or mantle origin for He leading to slightly higher R/Ra values, a  $^4\text{He}^*$  component is largely dominant for most samples. As expected, R/Ra values display an inverse correlation with methane concentrations. This points to increased amounts of  $^4\text{He}^*$  (lower R/Ra values) with increasing methane concentrations thus, strongly suggesting a common source for both methane and  $^4\text{He}^*$  (Figures 3.2b, c).

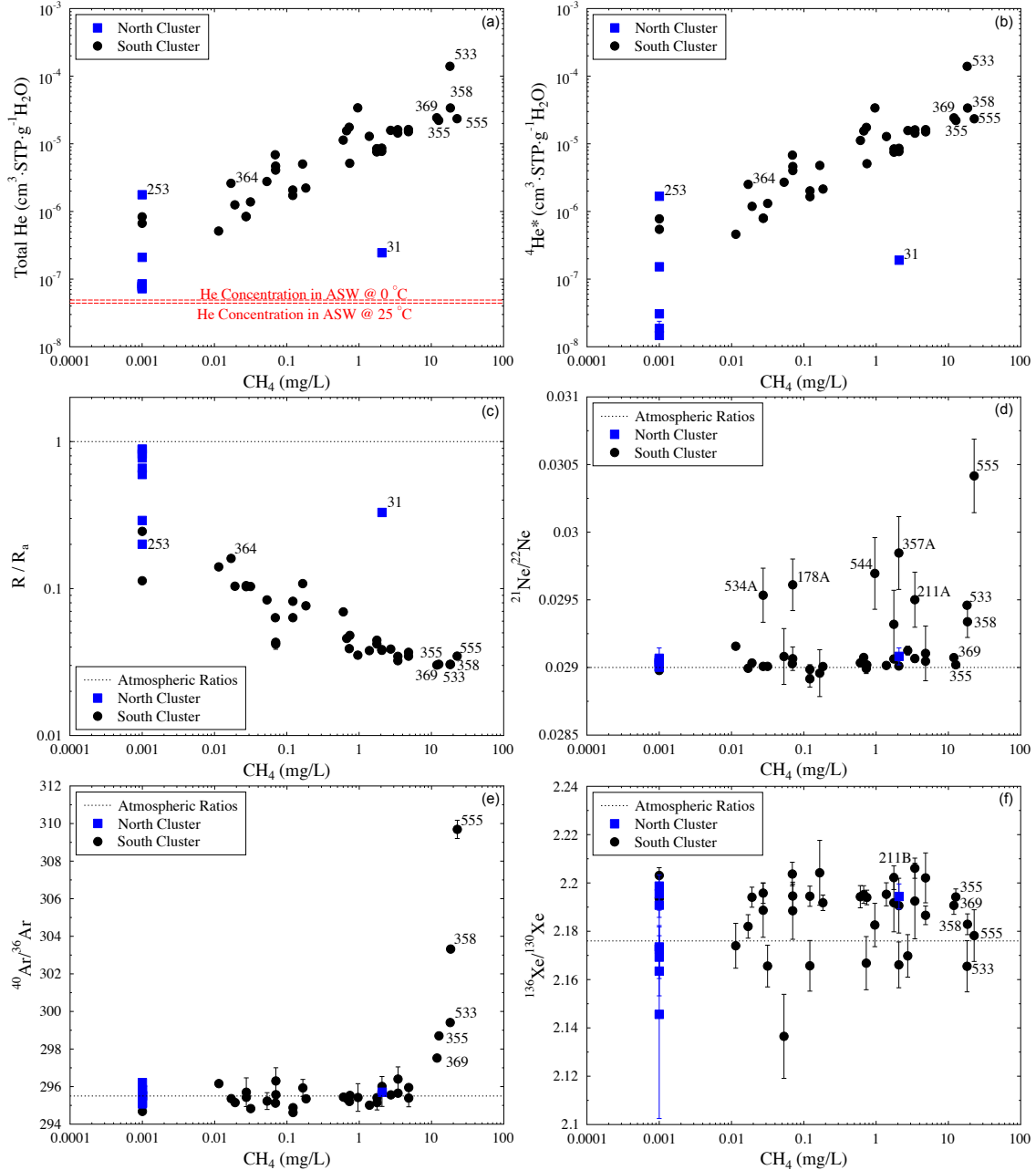


**Figure 3.2** (a) Total He concentrations, (b)  $^4\text{He}^*$  concentrations, (c)  $R/R_a$  ratios, (d)  $^{21}\text{Ne}/^{22}\text{Ne}$  ratios, (e)  $^{40}\text{Ar}/^{36}\text{Ar}$  ratios, and (f)  $^{136}\text{Xe}/^{130}\text{Xe}$  as a function of measured dissolved methane concentrations in collected groundwater samples. Corresponding atmospheric noble gas values are indicated (dashed lines). Samples with undetected methane concentrations are plotted at the methane detection limit (0.001 mg/L).

Most measured  $^{20}\text{Ne}/^{22}\text{Ne}$  ratios are close to the atmospheric value of 9.80 (Table A3; cf. Appendix A).  $^{21}\text{Ne}/^{22}\text{Ne}$  ratios range from  $0.0289 \pm 0.0001$  to  $0.0304 \pm 0.0003$  reflecting the addition of minor but non-negligible crustally produced  $^{21}\text{Ne}^*$  through the nuclear reactions  $^{18}\text{O}(\alpha, n)^{21}\text{Ne}$  and  $^{24}\text{Mg}(n, \alpha)^{21}\text{Ne}$  [Wetherill, 1954].  $^{21}\text{Ne}^*$  values are estimated following Ballentine *et al.* [1991] and vary between 0% and 4.8% of total measured  $^{21}\text{Ne}$  with an atmospheric  $^{21}\text{Ne}$  contribution varying between 95.2% and 100%. It is apparent that, for all samples displaying  $^{21}\text{Ne}/^{22}\text{Ne}$  ratios higher than ASW values, a direct correlation between  $^{21}\text{Ne}^*$  and dissolved methane in groundwater is also observed, pointing again to a common origin between crustally produced  $^{21}\text{Ne}^*$  and stray gas present in the Trinity Aquifer (Figure 3.2d).

All  $^{38}\text{Ar}/^{36}\text{Ar}$  ratios are close to the atmospheric value of 0.188 (Table A3; cf. Appendix A). In contrast, some groundwater samples display  $^{40}\text{Ar}/^{36}\text{Ar}$  ratios (samples 355, 358, 369, 533 and 555) above the atmospheric value of 295.5, reflecting the addition of crustally produced  $^{40}\text{Ar}^*$  (Table A3; Figure 3.2e). Similar to excess  $^4\text{He}$  from U and Th, excesses of  $^{40}\text{Ar}$  are commonly observed in old crustal fluids due to the natural decay of  $^{40}\text{K}$  in rock formations [Ballentine *et al.*, 1991; 1994; Ma *et al.*, 2009b]. Contribution of crustally produced  $^{40}\text{Ar}^*$  is estimated following Ballentine *et al.* [1991]  $^{40}\text{Ar}^*$  varies from 0% to 4.6%, with atmospheric  $^{40}\text{Ar}$  varying between 95.4% and 100%. Similar to  $^4\text{He}^*$  and  $^{21}\text{Ne}^*$ ,  $^{40}\text{Ar}^*$  correlates well with dissolved methane concentrations (Figure 3.2e), pointing once again to an origin similar to that of dissolved methane.

In contrast, all Kr isotopic ratios (e.g.,  $^{86}\text{Kr}/^{84}\text{Kr}$ ) are indistinguishable from the atmospheric values (Table A3). Unlike Kr, some groundwater samples display  $^{136}\text{Xe}/^{130}\text{Xe}$  ratios above the atmospheric ratio of 2.176, up to  $2.206 \pm 0.004$ , and point to the presence of excess  $^{136}\text{Xe}$  in these samples (e.g., sample 211B; Table A3; Figure 3.2f). These elevated Xe isotopic

ratios suggest the presence of crustal and/or mantle Xe components derived from  $^{238}\text{U}$  spontaneous fission [Eikenberg *et al.*, 1993], in addition to the atmospheric component. Unlike R/Ra,  $^{21}\text{Ne}/^{22}\text{Ne}$  and  $^{40}\text{Ar}/^{36}\text{Ar}$  ratios though,  $^{136}\text{Xe}/^{130}\text{Xe}$  ratios display no correlation with dissolved methane concentrations. In contrast to total  $^4\text{He}$ ,  $^{21}\text{Ne}$  and  $^{40}\text{Ar}$ , sedimentary Xe can be released from organic matter that has accumulated Xe due to a diffusion-controlled fractionation process and this may contribute to the total  $^{136}\text{Xe}$ . This contribution may dilute excess  $^{136}\text{Xe}$  and thus weaken the correlation between  $^{136}\text{Xe}/^{130}\text{Xe}$  and methane contents. This hypothesis was previously suggested in the literature [Podosek *et al.*, 1980; Torgersen and Kennedy, 1999; Zhou *et al.*, 2005; Ma *et al.*, 2009a; Wen *et al.*, 2015a].

### ***3.5.3 Stray Gas Source and Migration Mechanisms – Production Wells versus Water Wells***

As shown above, dissolved methane concentrations display positive correlations with multiple crustal noble gas isotopes, in particular,  $^4\text{He}^*$ ,  $^{21}\text{Ne}^*$  and  $^{40}\text{Ar}^*$  suggesting that noble gases and methane in the Trinity Aquifer originate from a common source. Here, through a combined analysis of atmospheric-derived  $^{20}\text{Ne}$ ,  $^{36}\text{Ar}$ ,  $^{84}\text{Kr}$  and  $^{132}\text{Xe}$  together with information provided by well logs, we place constraints on the specific stray gas source and, in particular, whether the presence of methane in the Trinity Aquifer might originate from production wells or not have a connection with gas production.

To determine whether this external origin is the Strawn Group or the Barnett Shale and, more importantly, to assess whether or not the presence of stray gas results from a conventional or HF production well, we examine measured  $^{20}\text{Ne}$ ,  $^{36}\text{Ar}$ ,  $^{84}\text{Kr}$ , and  $^{132}\text{Xe}$  concentrations of Trinity Aquifer samples (Figure 3.3). All four isotopes in these groundwater samples are almost entirely of atmospheric origin and are introduced by freshwater recharge previously equilibrated

with the atmosphere (ASW). Predicted ASW  $^{20}\text{Ne}$ ,  $^{36}\text{Ar}$ ,  $^{84}\text{Kr}$  and  $^{132}\text{Xe}$  concentrations for temperatures varying between 0 °C and 25 °C are shown (Figures 3.3a, b, c; bold red line). All groundwater samples from both the south (closed black circles) and north (closed blue squares) clusters are shown. Figure 3.3a shows that  $^{20}\text{Ne}$  concentrations in most groundwater samples are above the predicted ASW composition. These include all north cluster and most south cluster samples. Because  $^{20}\text{Ne}/^{22}\text{Ne}$  ratios for most samples display atmospheric values within a 2-sigma error and because most samples fall on the predicted excess air-line (cf. Figure 3.3), most of the observed  $^{20}\text{Ne}$  excesses in these groundwaters are expected to result from incorporation of excess air (EA) due to rapid fluctuations of the water table level [Heaton and Vogel, 1981]. Some previous studies have associated the presence of  $^{20}\text{Ne}$  to an exogenous source, possibly due to natural brine migration. This was the case, for example, of groundwaters within the Marcellus Shale footprint and groundwaters of the Michigan Basin [Castro *et al.*, 2009; Ma *et al.*, 2009a; Darrah *et al.*, 2014; 2015]. However, as indicated below, this does not seem to be the case in this study. Significant levels of EA are commonly present in modern Texas groundwaters [e.g., Castro *et al.*, 2007]. Predicted  $^{20}\text{Ne}$  and  $^{36}\text{Ar}$  ASW values in water with addition of increasing EA amounts are shown for temperatures of 18°C and 25°C, which correspond to the average mean annual air temperature (MAAT) for Springtown (1962-1978), Weatherford (1946-2014) and Mineral Wells (1948-2014) in north-central Texas (<http://www.ncdc.noaa.gov/cdo-web/search>) and to the highest measured water temperature of Trinity Aquifer groundwater samples [Nicot *et al.*, 2015], respectively (green solid lines, Figure 3.3a). In contrast to most samples and as also previously documented by Darrah *et al.* [2014] in a few water wells, four groundwater samples, all from the south cluster (samples 355, 358, 369 and 555; Figure 3.3a) display  $^{20}\text{Ne}$  and  $^{36}\text{Ar}$  concentrations below the ASW composition and point thus to significant

depletion of atmospheric-derived  $^{20}\text{Ne}$  and  $^{36}\text{Ar}$ , i.e., stripping of atmospheric noble gases. All four of these groundwater samples have high measured methane concentrations, between  $\sim 12$  mg/L and  $\sim 23$  mg/L. In particular, during sampling collection, a sustained natural gas flow of  $\sim 3$  L/min was measured at well 555 (drilled as a water well but not used and left unplugged). The presence of a gas phase (mostly  $\text{CH}_4$ ) within the aquifer in these four groundwater samples leads to exsolution of noble gases. This exsolution will be more severe for the light noble gases and that of  $^{20}\text{Ne}$  in particular, as opposed to the heavier ones ( $^{84}\text{Kr}$  and  $^{132}\text{Xe}$ ) as the lighter noble gases will go preferentially into the gas phase [Zartman *et al.*, 1961; Bosch and Mazor, 1988]. Expected noble gas concentrations in a residual water phase in contact with a gas phase for an initial ASW composition at  $18^\circ\text{C}$  and  $25^\circ\text{C}$  assuming a closed-system [Ballentine *et al.*, 2002] are shown in Figure 3.3a (red dashed lines). It is apparent that all these four samples are consistent with predicted stripped water values, sample 555 displaying the most severe depletion with values down to 0.18 and 0.22 times that of ASW at  $18^\circ\text{C}$  for  $^{20}\text{Ne}$  and  $^{36}\text{Ar}$ , respectively (Table A2). Similar depletion trends, also consistent with stripping due to the presence of a gas phase, are observed for  $^{84}\text{Kr}$  and  $^{132}\text{Xe}$  (Figures 3.3b, c) with values down to 0.28 and 0.36 times that of ASW at  $18^\circ\text{C}$  for sample 555, respectively. As expected, the heavier noble gases  $^{84}\text{Kr}$  and  $^{132}\text{Xe}$  point to a lower level of stripping with respect to the lighter noble gases (Figures 3.3a, b, c). This is clearly observed in sample 533, also with a high methane concentration, where stripping is observed for  $^{20}\text{Ne}$  but not for  $^{36}\text{Ar}$ ,  $^{84}\text{Kr}$  and  $^{132}\text{Xe}$ . These observations likely suggest not only the presence of localized gas sources but also a short contact time between the gas and liquid phases precluding equilibration between these two phases for the heavier noble gases in well 533. From Figure 3.3b, c, it is also apparent that sample 533 displays relative enrichment in water-phase atmospheric  $^{132}\text{Xe}$  as opposed to  $^{36}\text{Ar}$  and  $^{84}\text{Kr}$ , which points to an equilibration

temperature lower than the MAAT, at around 14°C [e.g., *Castro et al.*, 2007]. This, however, is unrelated to water-gas phase interaction processes.

If a gas phase (gaseous methane) were present throughout the Trinity Aquifer, fractionation of atmospheric noble gas components in the water would be widely observed [*Pinti and Marty*, 2000; *Ballentine et al.*, 2002]. Because, as pointed out earlier, EA has a greater impact on the light noble gas composition compared to the heavy noble gases (Figures 3.3a, b, c) in groundwater, we now focus solely on the heavy  $^{84}\text{Kr}$  and  $^{132}\text{Xe}$  noble gases fractionation in an attempt to reduce the impact of EA as much as possible and thus, any potential bias that might result. Unlike  $^{20}\text{Ne}$ , most samples display  $^{84}\text{Kr}$  and  $^{132}\text{Xe}$  corresponding to that of ASW composition as the heavier noble gases are not significantly affected by the EA component.

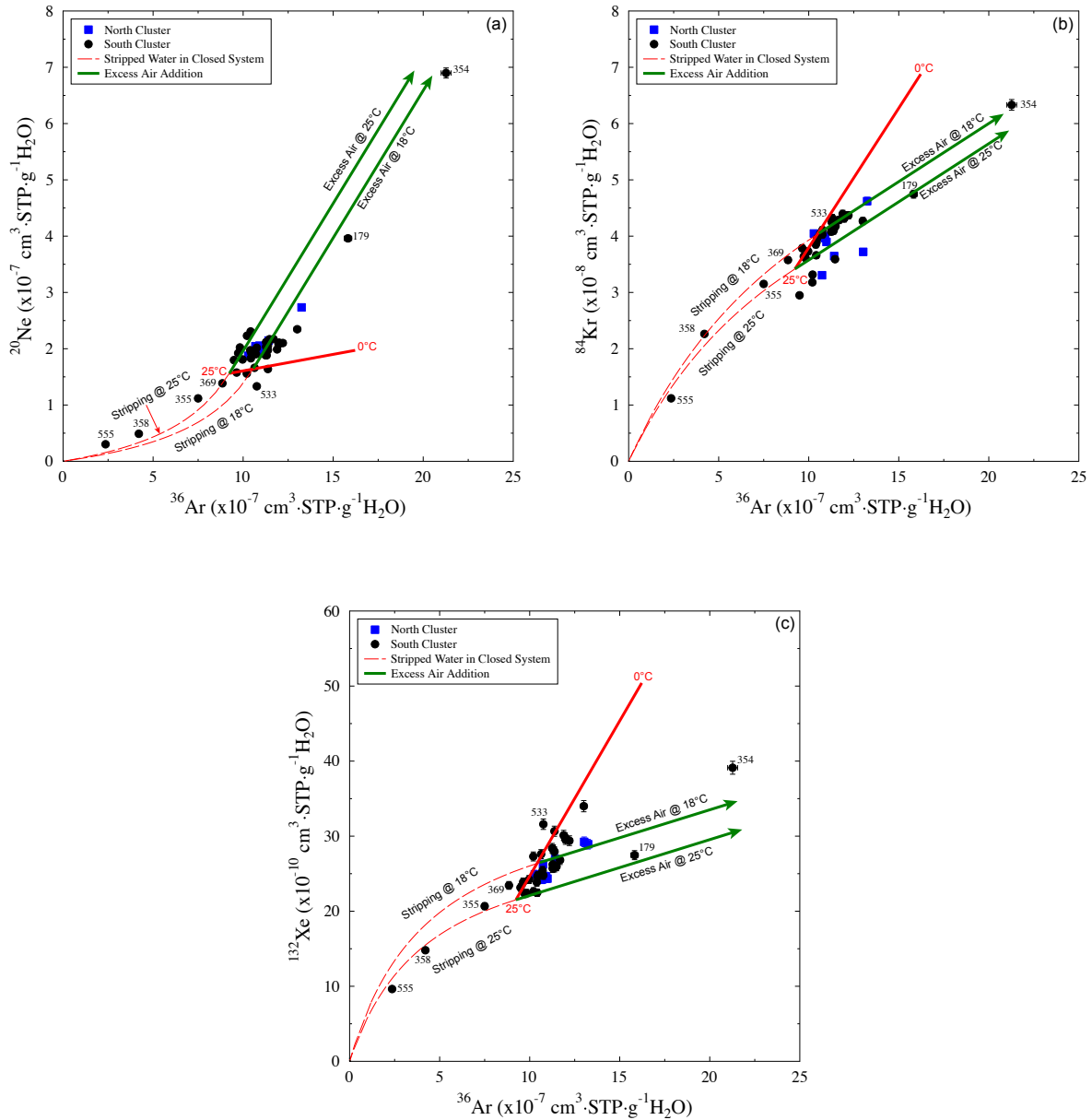


**Figure 3.3** (a)  $^{20}\text{Ne}$ , (b)  $^{84}\text{Kr}$  and (c)  $^{132}\text{Xe}$  concentrations as a function of  $^{36}\text{Ar}$  concentrations for all collected Trinity groundwater samples. Predicted  $^{20}\text{Ne}$ ,  $^{36}\text{Ar}$ ,  $^{84}\text{Kr}$  and  $^{132}\text{Xe}$  concentrations in air saturated water (ASW) are shown for temperatures varying from 0 °C to 25 °C (red solid line). Predicted  $^{20}\text{Ne}$ ,  $^{36}\text{Ar}$ ,  $^{84}\text{Kr}$  and  $^{132}\text{Xe}$  concentrations in the water phase are also calculated for two scenarios: 1) addition of excess air (EA) (green solid lines) and; 2) residual water phase following water-gas interaction in a closed-system (red dashed lines) at 18 °C and 25 °C.

Figure 3.4 shows  $F(^{132}\text{Xe}/^{36}\text{Ar})$  versus  $F(^{84}\text{Kr}/^{36}\text{Ar})$  for all collected water samples.  $F(^{132}\text{Xe}/^{36}\text{Ar})$  and  $F(^{84}\text{Kr}/^{36}\text{Ar})$  are measured ratios normalized to corresponding ASW values at 18°C (MAAT) of  $2.51 \times 10^{-3}$  and  $3.83 \times 10^{-2}$  for  $^{132}\text{Xe}/^{36}\text{Ar}$  and  $^{84}\text{Kr}/^{36}\text{Ar}$ , respectively (Table A5 and Figure A7; cf. Appendix A). The air value (red diamond) as well as the calculated closed system fractionation curve [red dashed line; cf. *Ballentine et al.*, 2002] for a residual water phase that has an initial ASW composition at 18°C are also shown. From Figure 3.4, it is apparent that most water samples display minimal fractionation in  $^{132}\text{Xe}/^{36}\text{Ar}$  and  $^{84}\text{Kr}/^{36}\text{Ar}$  ratios. In contrast, those samples with the highest methane contents do show significant fractionation. Samples 555 and 358 with the highest methane concentrations show, by far, the greatest fractionation, with  $F(^{132}\text{Xe}/^{36}\text{Ar})$  and  $F(^{84}\text{Kr}/^{36}\text{Ar})$  of 1.629 and 1.403, respectively (see also Figure A7). In contrast, samples 355 and 369, which also have elevated methane concentrations show only minor fractionation. The observed fractionation in these four samples which, as discussed above, underwent stripping of all atmospheric noble gases (Figures 3.3a, b, c) is consistent with water-gas phase interactions in a closed-system model. It should be noted that large quantities of EA in samples 179 and 354 drive their  $F(^{132}\text{Xe}/^{36}\text{Ar})$  and  $F(^{84}\text{Kr}/^{36}\text{Ar})$  values closer to that of air. The fact that only four samples (i.e., 355, 358, 369 and 555) show visible fractionation for all noble gases points, as suggested earlier, to localized gas-phase methane sources in the vicinity of these four wells, indicating that other water samples have likely never been in contact with a gas phase. If that were the case, significant stripping and fractionation of noble gases should be visible in dissolved noble gases in the Trinity Aquifer groundwater with F values following either a closed or open system fractionation curves (that is, in the upper right quadrant). Thanks to a downhole camera, we observed a continuous source of natural gas actively migrating into well 555 since well completion in 2012, a confirmation that water exposed to a natural gas

pocket will show heavy noble gas depletion. Additional information on natural gas accumulations in the Strawn is provided in Appendix A Text A4. Several hydrocarbon fields hosted in the Strawn Group are present in Parker and Hood counties [*Ehlmann and Ehlmann*, 1985].

A close analysis of driller log data available for these wells shows that all four of these wells are drilled through the unconformity into the Strawn Group as opposed to being only in the Trinity Group. It is likely that shallow non-commercial small gas accumulations, as are known to exist in the Strawn, were reached by these water wells (e.g., well 555) or that the wellbores are located close to one (e.g., well 358). Heavy depletion of atmospheric noble gases and, in particular, of the heavier  $^{84}\text{Kr}$  and  $^{132}\text{Xe}$  in only these four wells is consistent with continuously sustained gas-phase methane migration from a nearby source. Comparison of noble gas analyses from this stray gas and that from the Barnett Shale and Strawn Group further reinforce the finding that the source of the gas is in the Strawn Group [see also *Nicot et al.*, 2015]. *Darrah et al.* [2014] and *Kornacki and McCaffrey* [2014] have also concluded that the source of stray gas in these groundwater samples is likely the Strawn Group as opposed to the Barnett Shale.

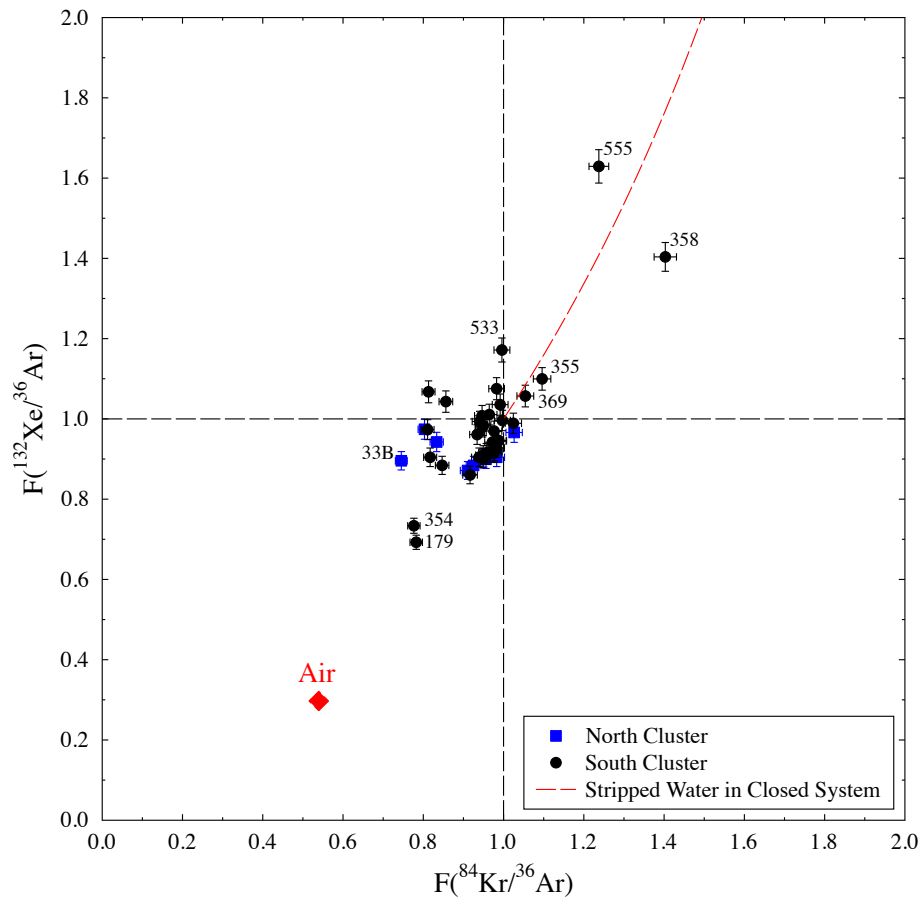


**Figure 3.4** Comparison of fractionation  $F$  levels of atmospheric noble gas isotopic ratios  $^{132}\text{Xe}/^{36}\text{Ar}$  versus  $^{84}\text{Kr}/^{36}\text{Ar}$  for all Trinity Aquifer groundwater samples.  $^{132}\text{Xe}/^{36}\text{Ar}$  and  $^{84}\text{Kr}/^{36}\text{Ar}$  ratios are normalized to the ASW value at  $18^\circ\text{C}$  (Table A5; cf. Appendix A). The air value is indicated by a red diamond. Calculated closed-system fractionation curve [red dashed line; cf. Ballentine *et al.* 2002] for a residual water phase that has an initial ASW composition at  $18^\circ\text{C}$  is also indicated.

In contrast to these four water wells with high dissolved methane concentrations showing depleted  $^{20}\text{Ne}$ ,  $^{36}\text{Ar}$ ,  $^{84}\text{Kr}$  and  $^{132}\text{Xe}$ , other water wells with significantly lower methane concentrations that display expected or higher than ASW  $^{20}\text{Ne}$ ,  $^{36}\text{Ar}$ ,  $^{84}\text{Kr}$  and  $^{132}\text{Xe}$  concentrations have also penetrated the Strawn Group and do not show stripping of heavy noble gases. The discrete distribution of small shallow natural gas accumulations in the Strawn explains both the scattered distribution of water wells with high methane concentrations and noble gas stripping as well as the presence of water wells penetrating into the Strawn Group but displaying significantly lower methane concentrations.

Figures A8a, c, e show  $F(^{132}\text{Xe}/^{36}\text{Ar})$  as a function of distance to the nearest production well (Barnett and/or non-Barnett well) for all collected water samples. From Figures A8a, c, e, it is apparent that  $F(^{132}\text{Xe}/^{36}\text{Ar})$  in water samples is not correlated with distance to nearest Barnett gas well ( $r = 0.19$ ;  $P = 0.20$ ), distance to nearest non-Barnett gas well ( $r = 0.01$ ;  $P = 0.95$ ) and distance to nearest gas production well ( $r = 0.02$ ;  $P = 0.91$ ; including both Barnett and non-Barnett). This lack of correlation further reinforces the hypothesis that dissolved gas in wells with high methane content has a natural origin and likely migrates into the Trinity Aquifer from the Strawn Group through natural pathways such as Strawn sandstone lenses in hydrological contact with Trinity Sands as opposed to faulty production wells as previously suggested [Darrah *et al.*, 2014].

By comparing  $^4\text{He}/^{20}\text{Ne}$  ratios of dissolved gas in groundwater samples and of natural gases from the Strawn Group, the impact of gas production wells can be evaluated [Darrah *et al.*, 2014]. With Strawn gas migrating away from production wells (Barnett and/or non-Barnett wells),  $^4\text{He}/^{20}\text{Ne}$  values in groundwater should display a gradual decrease from the  $^4\text{He}/^{20}\text{Ne}$  values observed in Strawn natural gases [Darrah *et al.*, 2014] (4800-29000; gray domain in

Figures A8b, d, f) to the ASW value at MAAT (0.265; dashed line in Figures A8b, d, f). However,  $^4\text{He}/^{20}\text{Ne}$  values show a complete absence of correlation with distance to nearest Barnett gas well ( $r = 0.20$ ;  $P = 0.19$ ), distance to nearest non-Barnett gas well ( $r = 0.09$ ;  $P = 0.55$ ) and distance to nearest gas production well ( $r = 0.07$ ;  $P = 0.66$ ; including both Barnett and non-Barnett), and thus do not support the notion that stray gas present in these water wells migrated from some nearby production wells from leaks along faulty surface casing as suggested by previous research [Darrah *et al.*, 2014].

Furthermore, positive correlation between  $\text{CH}_4/^{36}\text{Ar}$  ratios and  $\text{Cl}^-$  concentrations in water would indicate natural or anthropogenic deep brine migration [Darrah *et al.*, 2014]. However, no correlation between  $\text{CH}_4/^{36}\text{Ar}$  with  $\text{Cl}^-$  is observed for samples either above or below the  $\text{CH}_4$  saturation line ( $r = 0.12$ ;  $P = 0.48$ ; Figure A9; cf. Appendix A). Therefore, based on  $\text{CH}_4/^{36}\text{Ar}$  ratio versus  $\text{Cl}^-$  concentrations in water and/or on calculated  $^4\text{He}/^{20}\text{Ne}$  values, there is no basis at this stage to infer an influx of deep brine along with stray gas either from leaks of production wells or from natural flow along minor faults. Rather, our findings suggest that stray gas in the Trinity Aquifer is likely related to non-commercial small gas accumulations in the Strawn Group. At this stage, none of our observations and measurements points to migration of stray gas from nearby Strawn or Barnett production wells.

### 3.6 Acknowledgements

Funding for this project was provided by RPSEA award 11122-56 through the “Ultra-Deepwater and Unconventional Natural Gas and Other Petroleum Resources” program authorized by the U.S. Energy Policy Act of 2005. NSF grant EAR #1049822 provided additional financial support. We thank the editor as well as two reviewers for their insightful and

thorough reviews. We also thank all well owners for access to their water wells as well as Laura Bouvier for her assistance in the field and IHS for free access to their Enerdeq database.

### 3.7 References

- Ballentine, C. J., M. Mazurek, and A. Gautschi (1994), Thermal constraints on crustal rare gas release and migration: Evidence from Alpine fluid inclusions, *Geochimica et Cosmochimica Acta*, 58(20), 4333–4348.
- Ballentine, C. J., R. Burgess, and B. Marty (2002), Tracing Fluid Origin, Transport and Interaction in the Crust, *Reviews in Mineralogy and Geochemistry*, 47(1), 539–614, doi:10.2138/rmg.2002.47.13.
- Ballentine, C. J., R. K. O'niions, E. R. Oxburgh, F. Horvath, and J. Deak (1991), Rare gas constraints on hydrocarbon accumulation, crustal degassing and groundwater flow in the Pannonian Basin, *Earth and Planetary Science Letters*, 105(1–3), 229–246, doi:10.1016/0012-821X(91)90133-3.
- Bosch, A., and E. Mazor (1988), Natural gas association with water and oil as depicted by atmospheric noble gases: case studies from the southeastern Mediterranean Coastal Plain, *Earth and Planetary Science Letters*, 87(3), 338–346, doi:10.1016/0012-821X(88)90021-0.
- Bruner, K. R., and R. Smosna (2011), *A comparative study of the Mississippian Barnett Shale, Fort Worth Basin, and Devonian Marcellus Shale*, DOE/NETL.
- Castro, M. C. (2004), Helium sources in passive margin aquifers—new evidence for a significant mantle  $^3\text{He}$  source in aquifers with unexpectedly low in situ  $^3\text{He}/^4\text{He}$  production, *Earth and Planetary Science Letters*, 222(3), 897–913, doi:10.1016/j.epsl.2004.03.031.
- Castro, M. C., A. Jambon, G. de Marsily, and P. Schlosser (1998a), Noble gases as natural tracers of water circulation in the Paris Basin: 1. Measurements and discussion of their origin and mechanisms of vertical transport in the basin, *Water Resources Research*, 34(10), 2443–2466, doi:10.1029/98WR01956.
- Castro, M. C., C. M. Hall, D. Patriarche, P. Goblet, and B. R. Ellis (2007), A new noble gas paleoclimate record in Texas — Basic assumptions revisited, *Earth and Planetary Science Letters*, 257(1–2), 170–187, doi:10.1016/j.epsl.2007.02.030.
- Castro, M. C., L. Ma, and C. M. Hall (2009), A primordial, solar He–Ne signature in crustal fluids of a stable continental region, *Earth and Planetary Science Letters*, 279(3–4), 174–184, doi:10.1016/j.epsl.2008.12.042.
- Castro, M. C., M. Stute, and P. Schlosser (2000), Comparison of  $^4\text{He}$  ages and  $^{14}\text{C}$  ages in simple aquifer systems: implications for groundwater flow and chronologies, *Applied Geochemistry*, 15(8), 1137–1167, doi:10.1016/S0883-2927(99)00113-4.
- Castro, M. C., P. Goblet, E. Ledoux, S. Violette, and G. de Marsily (1998b), Noble gases as natural tracers of water circulation in the Paris Basin: 2. Calibration of a groundwater flow model using noble gas isotope data, *Water Resources Research*, 34(10), 2467–2483, doi:10.1029/98WR01957.

- Clarke, W. B., W. J. Jenkins, and Z. Top (1976), Determination of tritium by mass spectrometric measurement of  $^3\text{He}$ , *The International Journal of Applied Radiation and Isotopes*, 27(9), 515–522, doi:10.1016/0020-708X(76)90082-X.
- Darrah, T. H., A. Vengosh, R. B. Jackson, N. R. Warner, and R. J. Poreda (2014), Noble gases identify the mechanisms of fugitive gas contamination in drinking-water wells overlying the Marcellus and Barnett Shales, *Proceedings of the National Academy of Sciences*, 111(39), 14076–14081, doi:10.1073/pnas.1322107111.
- Darrah, T. H., R. B. Jackson, A. Vengosh, N. R. Warner, C. J. Whyte, T. B. Walsh, A. J. Kondash, and R. J. Poreda (2015), The evolution of Devonian hydrocarbon gases in shallow aquifers of the northern Appalachian Basin: Insights from integrating noble gas and hydrocarbon geochemistry, *Geochimica et Cosmochimica Acta*, 170 IS -, 321–355, doi:10.1016/j.gca.2015.09.006.
- Ehlmann, A. J., and R. J. Ehlmann (1985), THE ALEDO SOUTHEAST (1200'STRAWN) GAS FIELD AND ASSOCIATED DEEPER PRODUCTION, SOUTHEAST PARKER AND SOUTHWEST TARRANT COUNTIES, TEXAS, *AAPG Southwest Section*.
- Eikenberg, J., P. Signer, and R. Wieler (1993), U-Xe, U-Kr, and U-Pb systematics for dating uranium minerals and investigations of the production of nucleogenic neon and argon, *Geochimica et Cosmochimica Acta*, 57(5), 1053–1069.
- Eltschlager, K. K., J. W. Hawkins, W. C. Ehler, and F. Baldassare (2001), *Technical measures for the investigation and mitigation of fugitive methane hazards in areas of coal mining*, Department of the Interior Office of Surface Mining.
- Ewing, T. E. (1991), *The tectonic framework of Texas: Text accompanying the tectonic map of Texas*, Texas Bureau of Economic Geology.
- Hackley, P. C., E. H. Guevara, T. F. Hentz, and R. W. Hook (2009), Thermal maturity and organic composition of Pennsylvanian coals and carbonaceous shales, north-central Texas: Implications for coalbed gas potential, *International Journal of Coal Geology*, 77(3–4), 294–309, doi:10.1016/j.coal.2008.05.006.
- Heaton, T. H. E., and J. C. Vogel (1981), “Excess air” in groundwater, *Journal of Hydrology*, 50(0), 201–216, doi:10.1016/0022-1694(81)90070-6.
- Henry, J. D. (1982), Stratigraphy of the Barnett Shale (Mississippian) and Associated Reefs in the Northern Fort Worth Basin, *Petroleum Geology of the Fort Worth Basin and Bend Arch Area*, 157–177.
- Herkommer, M. A., and G. W. Denke (1982), Stratigraphy and hydrocarbons, Parker County, Texas, *Dallas Geological Society*.
- Hill, R. J., D. M. Jarvie, J. Zumberge, M. Henry, and R. M. Pollastro (2007), Oil and gas geochemistry and petroleum systems of the Fort Worth Basin, *AAPG Bulletin*, 91(4), 445–473, doi:10.1306/11030606014.

- Hilton, D. R., and D. Porcelli (2003), 2.06 - Noble Gases as Mantle Tracers, in *Treatise on Geochemistry*, edited by H. D. H. K. Turekian, pp. 277–318, Pergamon, Oxford.
- Holland, G., and S. Gilfillan (2013), Application of noble gases to the viability of CO<sub>2</sub> storage, in *The Noble Gases as Geochemical Tracers*, edited by P. Burnard, pp. 177–223, Springer, Berlin.
- Jackson, R. B., A. Vengosh, T. H. Darrah, N. R. Warner, A. Down, R. J. Poreda, S. G. Osborn, K. Zhao, and J. D. Karr (2013), Increased stray gas abundance in a subset of drinking water wells near Marcellus shale gas extraction, *Proceedings of the National Academy of Sciences of the USA*, 110(28), 11250–11255, doi:10.1073/pnas.1221635110/-/DCSupplemental/pnas.201221635SI.pdf.
- Kampbell, D. H., and S. A. Vandegrift (1998), Analysis of dissolved methane, ethane, and ethylene in ground water by a standard gas chromatographic technique, *J Chromatogr Sci*, 36(5), 253–256.
- Kornacki, A. S., and M. McCaffrey (2014), Monitoring the Active Migration and Biodegradation of Natural Gas in the Trinity Group Aquifer at the Silverado Development in Southern Parker County, Texas, *2014 AAPG Annual Convention and Exhibition*. Available from: <http://www.searchanddiscovery.com/abstracts/html/2014/90189ace/abstracts/1830218.html> (Accessed 11 November 2015)
- Kreitler, C. W. (2014), *Lessons Learned from the Barnett Shale Range Resources Litigation, Hydraulic Fracturing and Environmental Implications*, Austin.
- Kulongoski, J. T., D. R. Hilton, and J. A. Izbicki (2005), Source and movement of helium in the eastern Morongo groundwater Basin: The influence of regional tectonics on crustal and mantle helium fluxes, *Geochimica et Cosmochimica Acta*, 69(15), 3857–3872, doi:10.1016/j.gca.2005.03.001.
- Li, H., and K. H. Carlson (2014), Distribution and Origin of Groundwater Methane in the Wattenberg Oil and Gas Field of Northern Colorado, *Environ. Sci. Technol.*, 48(3), 1484–1491, doi:10.1021/es404668b.
- Lollar, B. S., and C. J. Ballentine (2009), Insights into deep carbon derived from noble gases., 2(8), 543–547, doi:10.1038/ngeo588.
- Ma, L., M. C. Castro, and C. M. Hall (2009a), Atmospheric noble gas signatures in deep Michigan Basin brines as indicators of a past thermal event, *Earth and Planetary Science Letters*, 277(1–2), 137–147, doi:10.1016/j.epsl.2008.10.015.
- Ma, L., M. C. Castro, and C. M. Hall (2009b), Crustal noble gases in deep brines as natural tracers of vertical transport processes in the Michigan Basin, *Geochemistry Geophysics Geosystems*, 10(6), Q06001, doi:10.1029/2009GC002475.
- Molofsky, L. J., J. A. Connor, A. S. Wylie, T. Wagner, and S. K. Farhat (2013), Evaluation of Methane Sources in Groundwater in Northeastern Pennsylvania, *Ground Water*, 51(3),

333–349.

- Montgomery, S. L., D. M. Jarvie, K. A. Bowker, and R. M. Pollastro (2005), Mississippian Barnett Shale, Fort Worth basin, north-central Texas: Gas-shale play with multi-trillion cubic foot potential, *AAPG Bulletin*, 89(2), 155–175, doi:10.1306/09170404042.
- Moritz, A., J.-F. Helie, D. L. Pinti, M. Larocque, D. Barnetche, S. Retailleau, R. Lefebvre, and Y. Gelinat (2015), Methane Baseline Concentrations and Sources in Shallow Aquifers from the Shale Gas-Prone Region of the St. Lawrence Lowlands (Quebec, Canada), *Environ. Sci. Technol.*, 49(7), 4765–4771, doi:10.1021/acs.est.5b00443.
- Nicot, J. P., Y. Huang, B. D. Wolaver, and R. A. Costley (2013), Flow and salinity patterns in the low-transmissivity Upper Paleozoic aquifers of North-Central Texas, *GCAGS Journal*, 2, 53–67.
- Nicot, J.-P., and B. R. Scanlon (2012), Water Use for Shale-Gas Production in Texas, U.S, *Environ. Sci. Technol.*, 46(6), 3580–3586, doi:10.1021/es204602t.
- Nicot, J.-P., B. R. Scanlon, R. C. Reedy, and R. A. Costley (2014), Source and Fate of Hydraulic Fracturing Water in the Barnett Shale: A Historical Perspective, *Environ. Sci. Technol.*, 48(4), 2464–2471, doi:10.1021/es404050r.
- Nicot, J.-P., P. Mickler, T. Larson, M. C. Castro, R. Darvari, R. Smyth, K. Uhlman, and C. Omelon (2015), *Understanding and Managing Environmental Roadblocks to Shale Gas Development: An Analysis of Shallow Gas, NORM, and Trace Metals*, Research Partnership to Secure Energy for America, Austin, <http://www.rpsea.org/projects/11122-56/>.
- Osborn, S. G., A. Vengosh, N. R. Warner, and R. B. Jackson (2011), Methane contamination of drinking water accompanying gas-well drilling and hydraulic fracturing, *Proceedings of the National Academy of Sciences*, 108(20), 8172–8176, doi:10.1073/pnas.1100682108.
- Oxburgh, E. R., R. K. O'Nions, and R. I. Hill (1986), Helium isotopes in sedimentary basins, *Nature*, 324(6098), 632–635, doi:10.1038/324632a0.
- Ozima, M., and F. A. Podosek (2002), *Noble Gas Geochemistry*, Cambridge University Press, New York.
- Pinti, D. L., and B. Marty (1995), Noble gases in crude oils from the Paris Basin, France: Implications for the origin of fluids and constraints on oil-water-gas interactions, *Geochimica et Cosmochimica Acta*, 59(16), 3389–3404, doi:10.1016/0016-7037(95)00213-J.
- Pinti, D. L., and B. Marty (2000), Chapter 7. NOBLE GASES IN OIL AND GAS FIELDS: ORIGINS AND PROCESSES, vol. 28, pp. 160–196, Fluids and Basin Evolution. Mineral Soc Can Short Course.
- Pinti, D. L., M. C. Castro, O. Shouakar-Stash, A. Tremblay, V. H. Garduño, C. M. Hall, J. F.

- Hélie, and B. Ghaleb (2012), Evolution of the geothermal fluids at Los Azufres, Mexico, as traced by noble gas isotopes,  $\delta^{18}\text{O}$ ,  $\delta\text{D}$ ,  $\delta^{13}\text{C}$  and  $^{87}\text{Sr}/^{86}\text{Sr}$ , *Journal of Volcanology and Geothermal Research*, 249(0), 1–11, doi:10.1016/j.jvolgeores.2012.09.006.
- Podosek, F. A., M. Honda, and M. Ozima (1980), Sedimentary noble gases, *Geochimica et Cosmochimica Acta*, 44(11), 1875–1884, doi:10.1016/0016-7037(80)90236-7.
- Pollastro, R. M., D. M. Jarvie, R. J. Hill, and C. W. Adams (2007), Geologic framework of the Mississippian Barnett Shale, Barnett-Paleozoic total petroleum system, Bend arch–Fort Worth Basin, Texas, *AAPG Bulletin*, 91(4), 405–436, doi:10.1306/10300606008.
- Porcelli, D., C. J. Ballentine, and R. Wieler (2002), An Overview of Noble Gas Geochemistry and Cosmochemistry, *Reviews in Mineralogy and Geochemistry*, 47(1), 1–19, doi:10.2138/rmg.2002.47.1.
- Siegel, D. I., N. A. Azzolina, B. J. Smith, A. E. Perry, and R. L. Bothun (2015), Methane Concentrations in Water Wells Unrelated to Proximity to Existing Oil and Gas Wells in Northeastern Pennsylvania, *Environ. Sci. Technol.*, 49(7), 4106–4112, doi:10.1021/es505775c.
- Siegel, D., B. Smith, E. Perry, R. Bothun, and M. Hollingsworth (2016), Dissolved methane in shallow groundwater of the Appalachian Basin: Results from the Chesapeake Energy predrilling geochemical database, *Environ. Geosci.*, 23(1), 1–47, doi:10.1306/eg.01051615015.
- Thompson, H. (2012), Fracking boom spurs environmental audit, *Nature*, 485(7400), 556–557, doi:10.1038/485556a.
- Torgersen, T., and B. M. Kennedy (1999), Air-Xe enrichments in Elk Hills oil field gases: role of water in migration and storage, *Earth and Planetary Science Letters*, 167(3–4), 239–253, doi:10.1016/S0012-821X(99)00021-7.
- US EIA (2015), *Annual Energy Outlook 2015*, US Energy Information Administration, Washington, DC.
- Kelley, V. A., J. Ewing, T. L. Jones, S. C. Young, N. Deeds, and S. Hamlin (2014), *Updated Groundwater Availability Model of the Northern Trinity and Woodbine Aquifers*, Texas Water Development Board.
- Warrier, R. B., M. C. Castro, C. M. Hall, and K. C. Lohmann (2013), Large atmospheric noble gas excesses in a shallow aquifer in the Michigan Basin as indicators of a past mantle thermal event, *Earth and Planetary Science Letters*, 375(0), 372–382, doi:10.1016/j.epsl.2013.06.001.
- Weiss, R. F. (1968), Piggyback sampler for dissolved gas studies on sealed water samples, *Deep Sea Research and Oceanographic Abstracts*, 15(6), 695–699.
- Wen, T., M. C. Castro, B. R. Ellis, C. M. Hall, and K. C. Lohmann (2015a), Assessing

- compositional variability and migration of natural gas in the Antrim Shale in the Michigan Basin using noble gas geochemistry, *Chemical Geology*, 417, 356–370, doi:10.1016/j.chemgeo.2015.10.029.
- Wen, T., M. C. Castro, C. M. Hall, D. L. Pinti, and K. C. Lohmann (2015b), Constraining groundwater flow in the glacial drift and saginaw aquifers in the Michigan Basin through helium concentrations and isotopic ratios, *Geofluids*, 16, 3–25, doi:10.1111/gfl.12133.
- Wetherill, G. (1954), Variations in the Isotopic Abundances of Neon and Argon Extracted from Radioactive Minerals, *Physical Review*, 96(3), 679–683, doi:10.1103/PhysRev.96.679.
- Zartman, R. E., G. J. Wasserburg, and J. H. Reynolds (1961), Helium, argon, and carbon in some natural gases, *J. Geophys. Res.*, 66(1), 277–306, doi:10.1029/JZ066i001p00277.
- Zhou, Z., C. J. Ballentine, R. Kipfer, M. Schoell, and S. Thibodeaux (2005), Noble gas tracing of groundwater/coalbed methane interaction in the San Juan Basin, USA, *Geochimica et Cosmochimica Acta*, 69(23), 5413–5428, doi:10.1016/j.gca.2005.06.027.

**CHAPTER 4**

**CHARACTERIZING THE NOBLE GAS ISOTOPIC  
COMPOSITION OF THE BARNETT SHALE AND STRAWN  
GROUP AND CONSTRAINING THE SOURCE OF STRAY GAS  
IN THE TRINITY AQUIFER, NORTH-CENTRAL TEXAS<sup>3</sup>**

**4.1 Abstract**

This study presents the complete set of stable noble gases for Barnett Shale and Strawn Group production gas together with stray flowing gas in the Trinity Aquifer, Texas. It places new constraints on the source of this stray gas and further shows that Barnett and Strawn gas have distinct crustal and atmospheric noble gas signatures, allowing clear identification of these two sources. Like stray gas, Strawn gas is significantly more enriched in crustal  $^4\text{He}^*$ ,  $^{21}\text{Ne}^*$  and  $^{40}\text{Ar}^*$  than Barnett gas. The similarity of Strawn and stray gas crustal noble gas signatures suggests that the Strawn is the source of stray gas in the Trinity Aquifer. Atmospheric  $^{22}\text{Ne}/^{36}\text{Ar}$  stray gas ratios mimic also that of Strawn, further reinforcing the notion that the source of stray gas in this aquifer is the Strawn. While noble gas signatures of Strawn and stray gas are consistent with a single-stage water degassing model, a two-stage oil modified groundwater

---

<sup>3</sup> Wen, T., M. C. Castro, J.-P. Nicot, C. M. Hall, D. L. Pinti, P. Mickler, R. Darvari, and T. Larson, Characterizing the Noble Gas Isotopic Composition of the Barnett Shale and Strawn Group and Constraining the Source of Stray Gas in the Trinity Aquifer, North-Central Texas, submitted to *Environ. Sci. Technol.*

exsolution fractionation model is required to explain the light atmospheric noble gas signature of Barnett Shale production gas. These distinct Strawn and Barnett noble gas signatures are likely the reflection of distinct evolution histories with Strawn gas being possibly older than that of Barnett Shale.

## 4.2 Introduction

Despite low or moderately rising natural gas prices, projected production of natural gas from unconventional shale gas and tight oil plays are forecasted to increase from 13.6 Tcf (trillion cubic feet) in 2015 to 29.0 Tcf in 2040 due to abundant domestic resources and technology improvements (e.g., hydraulic fracturing (HF) and horizontal drilling) [US EIA, 2016]. As a result, their share of total U.S. dry natural gas production will grow from 50% in 2015 to 69% in 2040 [US EIA, 2016]. Such a dramatic expansion of unconventional natural gas production has ignited public concern that production activities such as HF may allow migration of natural gas from targeted formations such as the Marcellus or Barnett Shales (depth of 1800 m to >2000 m) into shallow aquifers (<500 m), thereby threatening drinking water supplies.

The presence of stray gas in shallow groundwaters has been reported both within the Marcellus and Barnett Shale footprints [Osborn *et al.*, 2011; Thompson, 2012; Molofsky *et al.*, 2013; Jackson *et al.*, 2013a; Darrah *et al.*, 2014; Wen *et al.*, 2016]. Stray gas in groundwaters may originate from shallow or deep thermogenic gas accumulations [Osborn *et al.*, 2011; Jackson *et al.*, 2013a; Darrah *et al.*, 2014; 2015; Siegel *et al.*, 2015; Wen *et al.*, 2016] of natural or anthropogenic origin, from shallow microbial sources [Martini *et al.*, 1996; Warner *et al.*, 2013; Li and Carlson, 2014] or from a combination of both [Jackson *et al.*, 2013b; Li and Carlson, 2014; Nicot *et al.*, in review; Stolper *et al.*, 2015; Wen *et al.*, 2015a]. Here, “stray gas”

refers to natural gas present in shallow aquifers of an undetermined origin. In particular, within the Barnett Shale footprint in the Fort Worth Basin, a few groups have investigated the presence of elevated levels of methane in the shallow Trinity Aquifer with respect to its source and migration mechanisms [Darrah *et al.*, 2014; Kornacki and McCaffrey, 2014; Wen *et al.*, 2016]. While these studies agree that the shallow Strawn Group is likely the source of the stray gas in the Trinity Aquifer, they diverge with respect to an anthropogenic versus natural origin. Earlier studies using a combination of carbon isotopes and light noble gases [Darrah *et al.*, 2014] concluded that the presence of stray gas in the Trinity Aquifer has likely an anthropogenic origin due to faulty production wells [Darrah *et al.*, 2014]. In contrast, a more recent study of Trinity groundwaters using the entire set of stable noble gases supports a natural origin for this stray gas and argues that some of the drinking water wells reached non-commercially exploited natural gas accumulations in the Strawn Group [Wen *et al.*, 2016].

*Kornacki and McCaffrey* [2014] tentatively concluded that stray gas in the Trinity Aquifer in Parker County is of thermogenic origin migrating from the Strawn Group as opposed to the Barnett Shale. Their conclusions were based on nitrogen and carbon dioxide contents of groundwater and hydrocarbon samples. However, microbial activity and oxidation can alter the original geochemical signature and thus, obscure the original sources and/or mechanisms of fluid migration [Lollar and Ballentine, 2009; Molofsky *et al.*, 2013]. In contrast, stable noble gases (Helium – He, Neon – Ne, Argon – Ar, Krypton – Kr, Xenon - Xe) are chemically inert and are thus transported without being affected by chemical reactions [Ozima and Podosek, 2002; Hilton and Porcelli, 2003]. Noble gases in subsurface fluids (*e.g.*, freshwater, natural gas) are derived from the atmosphere, crust and mantle, all of which show distinct isotopic and elemental signatures [Ozima and Podosek, 2002; Porcelli *et al.*, 2002; Hilton and Porcelli, 2003; Castro *et*

*al.*, 2009; *Pinti et al.*, 2012]. This makes noble gases ideal natural tracers for studying the origin and evolution of crustal fluids in sedimentary basins [*Oxburgh et al.*, 1986; *Ballentine et al.*, 1991; *Pinti and Marty*, 1995; *Castro et al.*, 1998a; 1998b; *Hilton and Porcelli*, 2003; *Kulongoski et al.*, 2005; *Holland and Gilfillan*, 2013; *Warrier et al.*, 2013; *Wen et al.*, 2015a; 2015b]. In most subsurface fluids in sedimentary systems, noble gases are dominated by an atmospheric origin (Air Saturated Water or ASW) and/or a crustal component deriving primarily from radioactive decay of U, Th and  $^{40}\text{K}$  [*Ozima and Podosek*, 2002]. Here, the crustal component is identified with the “\*” notation.

In this study, analyses of the complete set of stable noble gases are presented (He, Ne, Ar, Kr, Xe) for Barnett Shale and Strawn Group production gas together with stray gas, i.e., a gas phase present in the Trinity Aquifer in Parker and Hood counties, Texas. Both atmospheric and crustal noble gas volume fractions and isotopic ratios are provided. This new production gas and stray gas dataset, together with recently published groundwater noble gas data from the Trinity Aquifer [*Wen et al.*, 2016], places new constraints on the source of stray gas in the shallow Trinity Aquifer and further shows that Barnett Shale and Strawn Group production gas have distinct crustal and atmospheric noble gas signatures allowing clear identification of these two sources. This new comprehensive noble gas data set reinforces the notion that the source of stray gas in the Trinity Aquifer is indeed the Strawn Group as opposed to the Barnett Shale.

### **4.3 Geologic Setting**

The Fort Worth Basin, where the Barnett Shale and Strawn Group are located, is a north-south elongated trough covering roughly 38,100 km<sup>2</sup> in north-central Texas in the southern United States (Figure B1; Appendix B) [*Pollastro et al.*, 2007; *Nicot et al.*, 2014]. It is floored by

a Precambrian basement. The Barnett Shale of Late Mississippian age (~331-323 Ma) is the primary petroleum source rock in the Fort Worth Basin and found at a depth of ~1800 m in the study area (Figure B2; Appendix B) [Montgomery *et al.*, 2005; Pollastro *et al.*, 2007; Bruner and Smosna, 2011; Nicot *et al.*, 2013; 2014]. Overlying the Barnett Shale are, from oldest to youngest, the ~150-200 m thick Marble Falls (mostly carbonates) and ~600-700 m thick mostly siliciclastic Bend/Atoka Formations, of Late Mississippian and Lower Pennsylvanian age (~323-299 Ma) [Herkommer and Denke, 1982; Nicot *et al.*, 2015]. The 650-750 m thick Lower Strawn (Kickapoo Creek Formation) is unconformably overlain by Cretaceous rocks in the study area and consists of alternating sandstone and dominant shale layers with episodic carbonates [Herkommer and Denke, 1982]. The Strawn Group and the overlying Cretaceous formations also include minor coal seams [Hackley *et al.*, 2009; Kornacki and McCaffrey, 2014; Kreitler, 2014]. Montgomery *et al.* [2005] and Pollastro *et al.* [2007] suggested that significant migration of hydrocarbons, both oil and gas, occurred from the Barnett Shale into the Strawn Group over geological times, thereby charging commercially-produced reservoirs. In addition, the presence of many randomly distributed non-commercially exploited natural gas accumulations in the Strawn Group are known to exist [Nicot *et al.*, 2015]. The timing of migration, however, is poorly constrained. Large sections of the basin have also undergone conventional production for decades, including the study area where most of the produced gas originated from the Strawn Group.

The Trinity Group hosting the Trinity Aquifer is the main source of drinking water in Parker and Hood counties, where it crops out [Henry, 1982; Kornacki and McCaffrey, 2014]. The Trinity Aquifer locally consists of sandstones, silts and conglomerates overlain by the carbonate Glen Rose Formation that acts as a confining unit. In the study area, the Cretaceous

sedimentary cover is very thin [ $< 200\text{m}$ ; *Herkommer and Denke*, 1982]. Basal sands of the Trinity Group overlie the Strawn Group in an angular unconformity (Figure B2; cf. Appendix B) [*Kornacki and McCaffrey*, 2014; *Van A Kelley et al.*, 2014]. Predevelopment hydraulic heads in the Trinity Aquifer indicate that the general direction of flow in the study area is along dip from the outcrop to the east [*Kelley et al.*, 2014].

There are no mapped faults at the surface in Parker and Hood counties but several exist at depth, impacting at least some of the Paleozoic section. In addition to the Ouachita thrust belt on the eastern edge of the Barnett, a major fault, “the Mineral Wells fault”, trending SW-NE is present in southern Denton and northern Parker counties (Figure B1; Appendix B) [*Ewing*, 1991; *Pollastro et al.*, 2007]. This fault, which was active throughout the Paleozoic, appears to be rooted in the Precambrian basement [*Montgomery et al.*, 2005; *Pollastro et al.*, 2007]. Several minor normal faults parallel to it are present in the Fort Worth Basin, including in southern Parker county [*Pollastro et al.*, 2007].

#### **4.4 Sampling and Analytical Methods**

Eleven wells were sampled (Figure 4.1, Table B1) in Parker and Hood Counties, in North-Central Texas for collection of 15 natural gas samples for analysis of volume fractions and isotopic ratios of He, Ne, Ar, Kr, and Xe (Tables B2 and B3). These include four stray gas samples from two wells drilled as water wells but with flowing gas and abandoned due to gas lock of the water pumps, ten gas samples from eight Barnett Shale production wells and one gas sample from a Strawn Group production well (Tables B2 and B3). Samples for noble gas analyses were collected in copper tubes [*Weiss*, 1968; *Wen et al.*, 2015a]. Gas samples collected at water well 555G and 556G as well as production wells BG5 and BG9 carry the A and B

notation for first and second sample collected, respectively. An inflatable bladder was used as packer to isolate a short section of the wellbore above the water level. The natural-gas pressure buildup purged the air from the restricted section and allowed easy sampling at the surface. The air column in water well 556G was purged for approximately 30 minutes prior to collecting sample 556GA and for an additional 30 minutes prior to collecting sample 556GB. Because purging time is longer prior to collecting sample 556GB than sample 556GA, less air contamination is expected in 556GB compared to 556GA. For all other wells, atmospheric contamination during sampling was minimized by allowing the natural gas to flush through the system for approximately 10 min. Three copper tubes (555GB, BG2, SG3) were clamped and divided into 2 segments. Each segment of gas sample was measured individually for noble gas volume fractions and isotopic ratios. All replicated analyses from the same copper tube are listed with the suffix -1 or -2 (Tables B2 and B3).

Noble gas measurements were carried out in the Noble Gas Laboratory at the University of Michigan. He and Ne were analyzed in a Thermo Scientific Helix SFT mass spectrometer while Ar, Kr and Xe were sequentially inlet into an ARGUS VI mass spectrometer using a computer-controlled double-head cryo-separator. Extraction, purification, and analysis procedures are described in detail in the Appendix B Text B1.

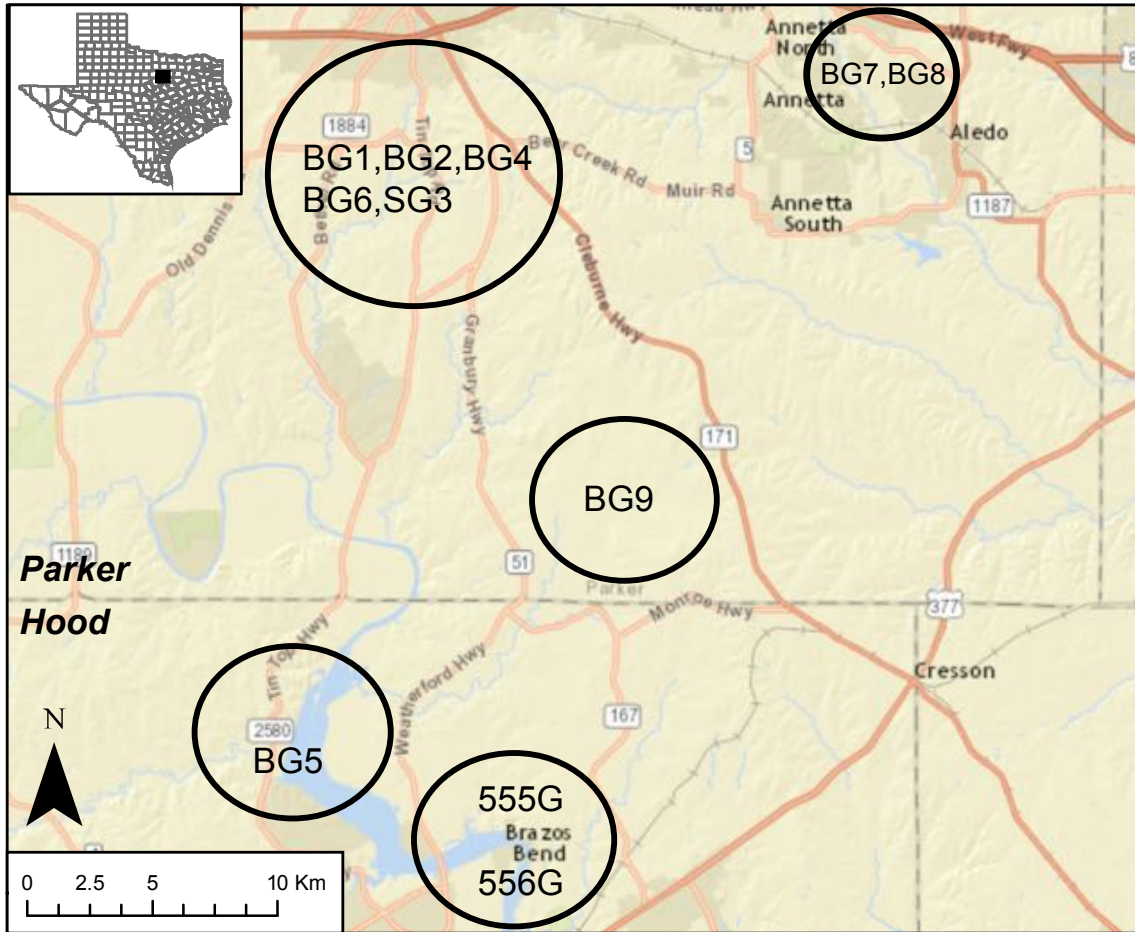


**Figure 4.1** Approximate location of all collected stray gases from water wells and production gases from Barnett and Strawn gas wells.

Stray gas and produced gas were collected using Isotech Isobag® and Isotube® technologies, respectively, for measurement of abundances of methane (CH<sub>4</sub>). Produced gas was analyzed by Isotech. Stray gas analyses for individual hydrocarbon and non-hydrocarbon gas components were carried out at the University of Texas at Austin using a two-channel Agilent 7890 Series Gas Chromatograph (GC). Detector responses have been calibrated using certified gas standards from Airgas, Inc. at a precision of ±1 mol% for each compound. No methane content is available for well 555G due to air contamination.

## **4.5 Results and Discussion**

### ***4.5.1 Noble Gas Signatures versus Methane Content***

Sample ID, sampling date, well depth and methane abundance are provided in Table B1. Total dissolved <sup>4</sup>He, <sup>22</sup>Ne, <sup>36</sup>Ar, <sup>84</sup>Kr and <sup>132</sup>Xe volume fractions and isotopic ratios are listed in Tables B2 and B3, respectively. <sup>3</sup>He/<sup>4</sup>He ratios (R) are normalized to the atmospheric ratio Ra, where Ra = (1.384±0.013) × 10<sup>-6</sup> [Clarke *et al.*, 1976].

Water wells 555G and 556G are 94 m and 91 m deep, respectively. These two water wells penetrate the Strawn Group according to drilling logs and are shallower than sampled Strawn gas well SG3 (544 m) which, in turn, is significantly shallower than all sampled Barnett gas wells with depths ranging from 1591 m to 1985 m (Table B1).

Water wells 555G and 556G have been venting natural gas since they were completed [Nicot *et al.*, 2015]. A gas flow of 2.5 and 3.3 L/min at these two wells, respectively, was measured at the time of collection, November 2014. CH<sub>4</sub> (C<sub>1</sub>) is largely dominant over all other components at well 556G with 73.6% by volume (Table B1). CH<sub>4</sub> is also the dominant component of Barnett and Strawn natural gas samples with values ranging from 75.1% to 82.1%.

The highest CH<sub>4</sub> volume fraction is found in Strawn gas well SG3 (Table B1). Barnett and Strawn gas molecular ratios C<sub>1</sub>/(C<sub>2+</sub>) are up to 6 and their δ<sup>13</sup>C<sub>CH4</sub> values are larger than -50‰, strongly suggesting that natural gases in both the Barnett and Strawn formations are of thermogenic origin.

Measured <sup>4</sup>He volume fractions in wells 555 and 556 vary from 2.33 × 10<sup>-3</sup> to 4.37 × 10<sup>-3</sup>. (Figure 4.2a; Table B2). Total <sup>4</sup>He volume fraction in the Strawn gas sample is 1.84 × 10<sup>-3</sup>, a value slightly lower than that in stray gas samples from water wells but significantly higher than that of collected Barnett gases in this study which range from 1.86 × 10<sup>-4</sup> to 6.71 × 10<sup>-4</sup> (Figure 4.2a; Table B2) [see also *Darrah et al.* 2014]. From Figure 4.2a, no obvious correlation is observed between total <sup>4</sup>He and methane content for either Barnett or Strawn gases. Crustal <sup>4</sup>He volume fractions (<sup>4</sup>He\*) for all gas samples (Appendix B Text B2; Table B2) vary between 1.82 × 10<sup>-4</sup> and 4.31 × 10<sup>-3</sup> and account for most of the measured He (97.6% to 100%). Similar to total He, crustal He volume fractions do not display an obvious correlation with methane content in these samples (Figure 4.2b). For all samples, R/Ra ratios vary between 0.0205 ± 0.0005 and 0.0426 ± 0.0004 (Figure 4.2c; Table B3), and correspond to typical crustal production values of 0.02-0.05 [*Oxburgh et al.*, 1986].

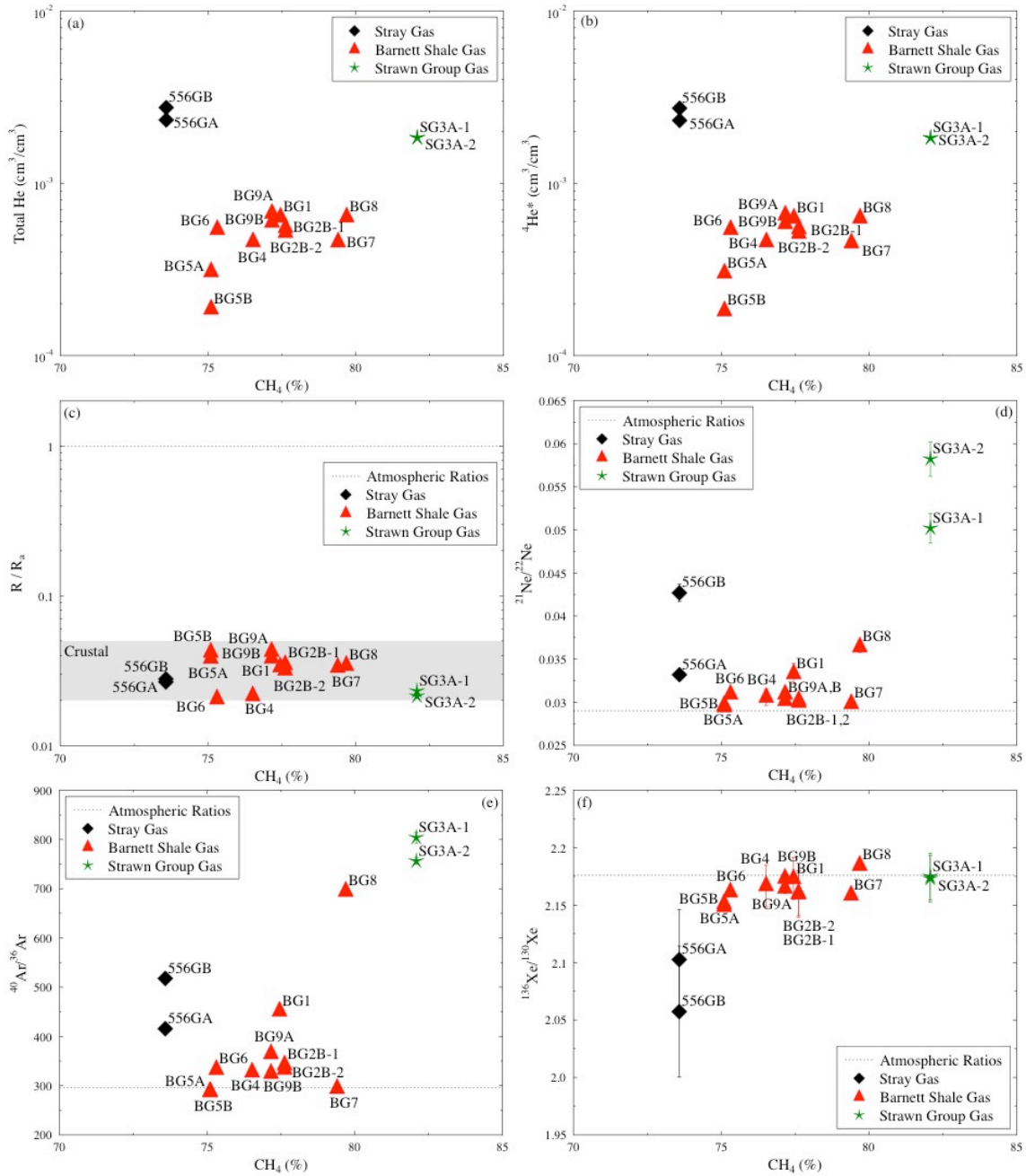


**Figure 4.2** (a) total  $^4\text{He}$  volume fractions, (b)  $^4\text{He}^*$  volume fractions, (c)  $R/R_a$  ratios, (d)  $^{21}\text{Ne}/^{22}\text{Ne}$  ratios, (e)  $^{40}\text{Ar}/^{36}\text{Ar}$  ratios and (f)  $^{136}\text{Xe}/^{130}\text{Xe}$  ratios as a function of methane volume fractions for all gas samples. Corresponding atmospheric and crustal noble gas values are indicated by dashed lines and shadow area, respectively.

All  $^{21}\text{Ne}/^{22}\text{Ne}$  ratios are above the atmospheric value of 0.029 [Ozima and Podosek, 2002] and reflect the addition of crustally produced  $^{21}\text{Ne}^*$  with values varying between  $0.0295 \pm 0.0001$  and  $0.0582 \pm 0.0020$  (Figure 4.2d; Table B3). Crustal  $^{21}\text{Ne}^*$  volume fractions for all gas samples are highly variable and range from  $1.00 \times 10^{-11}$  to  $2.44 \times 10^{-10}$ , representing contributions varying between 2.2% and 50.2% of total  $^{21}\text{Ne}$  (Table B2; Appendix B Text B2). The highest crustally produced  $^{21}\text{Ne}^*$  contribution by far is found in Strawn natural gas as opposed to the Barnett Shale, where the lowest  $^{21}\text{Ne}^*$  contributions are found. No crustally produced  $^{21}\text{Ne}^*$  was estimated for samples BG5A, BG5B and BG7 due to the observation of mass-dependent fractionation in these samples (Appendix B Text B3). Unlike  $^4\text{He}$ , atmospheric  $^{21}\text{Ne}$  contributions for all samples are much higher and vary between 49.8% and 97.8% of total  $^{21}\text{Ne}$ . Here too, no obvious correlation is observed between  $^{21}\text{Ne}/^{22}\text{Ne}$  ratios and methane content for Barnett and Strawn gases (Figure 4.2d). Measured  $^{20}\text{Ne}/^{22}\text{Ne}$  for stray gas sample 556GA is greater than the atmospheric value of 9.80 [Ozima and Podosek, 2002] suggesting the presence of a limited amount of mantle Ne [Moreira and Allègre, 1998; Castro et al., 2009]. Samples 555GA, 555GB (average of 555GB-1 and 555GB-2), and 556GB display  $^{20}\text{Ne}/^{22}\text{Ne}$  ratios indistinguishable from the atmospheric value within a 2-sigma error. Both Strawn gas measurements display  $^{20}\text{Ne}/^{22}\text{Ne}$  ratios below 9.80, and suggest the incorporation of crustal  $^{22}\text{Ne}^*$ . The presence of crustal  $^{22}\text{Ne}^*$  is not surprising as Strawn natural gas displays the highest  $^{21}\text{Ne}^*$  and both crustally produced  $^{21}\text{Ne}^*$  and  $^{22}\text{Ne}^*$  share one common parent isotope,  $^{25}\text{Mg}$ . Typical  $^{20}\text{Ne}/^{22}\text{Ne}$  crustal production ratio is  $\sim 0.3$  [Yatsevich and Honda, 1997] (Appendix B Text B4). In contrast, all Barnett Shale production gas samples, without exception, display significantly higher  $^{20}\text{Ne}/^{22}\text{Ne}$  ratios (Table B3), all above the atmospheric value, ranging from  $10.003 \pm 0.016$  to  $10.335 \pm 0.012$ . With the exception of samples BG5A, BG5B and BG7, which might display

high  $^{20}\text{Ne}/^{22}\text{Ne}$  ratios partly due to mass-dependent fractionation (e.g., molecular diffusion; Appendix B Text B3), high  $^{20}\text{Ne}/^{22}\text{Ne}$  ratios in all other Barnett samples are likely due to the presence of a mantle component.

Except for samples BG5A, BG5B and BG7, all other samples display  $^{40}\text{Ar}/^{36}\text{Ar}$  ratios above the atmospheric value of 295.5 (Figure 4.2e; Table B3), reflecting the addition of crustal  $^{40}\text{Ar}^*$ , with  $^{40}\text{Ar}/^{36}\text{Ar}$  values varying between  $325.12 \pm 0.12$  and  $803.66 \pm 11.03$ . As previously observed for  $^{21}\text{Ne}/^{22}\text{Ne}$ , Strawn natural gas displays the highest  $^{40}\text{Ar}/^{36}\text{Ar}$  values, indicating the presence of greater amounts of crustally produced  $^{40}\text{Ar}^*$  compared to Barnett Shale and stray gas (Figure 4.2e; Table B2). This contrasts to the lower  $^{40}\text{Ar}/^{36}\text{Ar}$  ratios in Barnett Shale production gas ( $287.50 \pm 0.04$  to  $695.06 \pm 2.04$ ) and is further discussed below. Crustal  $^{40}\text{Ar}^*$  volume fractions (cf., Appendix B Text B2) are significant and vary widely with respect to total  $^{40}\text{Ar}$  (9.1% to 63.2%), ranging from  $2.68 \times 10^{-6}$  to  $1.03 \times 10^{-4}$  for all samples (Table B2).

Kr isotopic ratios (e.g.,  $^{86}\text{Kr}/^{84}\text{Kr}$ , Table B3) are all indistinguishable from atmospheric values. Similar to Kr isotopic ratios, except for samples BG5A, BG5B, BG6 and BG7, all other samples display  $^{136}\text{Xe}/^{130}\text{Xe}$  values indistinguishable from that of the atmosphere [2.176; *Ozima and Podosek, 2002*], pointing to the absence of a crustally and/or mantle produced Xe component (Figure 4.2f; Table B3). Low  $^{136}\text{Xe}/^{130}\text{Xe}$  values in samples BG5A, BG5B, BG6, and BG7 might be due to mass-dependent fractionation (Appendix B Text B3).

Overall, noble gas measurements show that Strawn production gas is significantly more enriched in crustal  $^4\text{He}^*$ ,  $^{21}\text{Ne}^*$  and  $^{40}\text{Ar}^*$  than Barnett Shale production gas and thus, point to rather distinct noble gas signature between these two sources. These distinct noble gas signatures reflect either higher concentrations of parent elements in the Strawn Group or more likely, they reflect the presence of older natural gas in the Strawn Group than that currently in place in the

Barnett Shale. The presence of natural gas in the Strawn Group that may have been generated at an earlier time in the Barnett Shale and subsequently migrated to the Strawn Group is also consistent with findings by previous studies [Jarvie *et al.*, 2001; Montgomery *et al.*, 2005; Pollastro *et al.*, 2007].

#### ***4.5.2 Barnett Shale versus Strawn Group and Stray Natural Gas - Crustal and Atmospheric Noble Gas Signatures***

As shown above, crustal noble gas signatures of Barnett Shale and Strawn Group natural gas are significantly different (e.g.,  $^4\text{He}^*$ ,  $^{21}\text{Ne}^*$ ,  $^{40}\text{Ar}^*$ ; Figure 4.2) and allow discrimination between production natural gas from these two formations. Here, to identify the source of stray gas in these water wells and to further distinguish between Barnett and Strawn natural gas, we examine the evolution of  $^{21}\text{Ne}/^{22}\text{Ne}$  and  $^{40}\text{Ar}/^{36}\text{Ar}$  isotopic ratios with the inverse of their atmospheric dominant isotopes  $^{22}\text{Ne}$  and  $^{36}\text{Ar}$ , respectively.

Figure 4.3a shows a plot of  $^{40}\text{Ar}/^{36}\text{Ar}$  ratios versus  $1/^{36}\text{Ar}$  values for all our natural gas samples together with Barnett and Strawn production gas samples reported by Darrah *et al.* [2014]. The air value is also shown (blue square). Lower  $^{40}\text{Ar}/^{36}\text{Ar}$  and  $1/^{36}\text{Ar}$  values point to a greater atmospheric contribution while higher values reflect the addition of crustally produced  $^{40}\text{Ar}^*$  accompanied by corresponding decreasing amounts of an atmospheric contribution [Kennedy *et al.*, 1985]. Here, a linear correlation passing through the air value points to mixing between two end-members, one represented by air, the other represented by a crustal component enriched in  $^{40}\text{Ar}^*$  [see also Kennedy *et al.*, 1985 and Wen *et al.*, 2015a]. The volume fraction of  $^{40}\text{Ar}^*$  is defined by the slope of the observed linear regression line. From Figure 4.3a, it is apparent that Barnett Shale and Strawn Group natural gas display two distinct trends. Indeed,

$^{40}\text{Ar}^*$  volume fractions for Strawn natural gas are significantly higher than those of the Barnett Shale and vary between  $4.94 \times 10^{-5}$  and  $1.54 \times 10^{-4}$  (regression lines a and b). In contrast, significantly lower  $^{40}\text{Ar}^*$  volume fractions are observed in the Barnett Shale with values varying between  $3.30 \times 10^{-6}$  and  $1.14 \times 10^{-5}$  (regression lines c and d). Such variations could suggest a distinct geochemical composition for these two formations and, in particular, different concentrations of  $^{40}\text{K}$ , the  $^{40}\text{Ar}^*$  parent element. Alternatively, and maybe more likely, it points to the presence of an older Strawn natural gas compared to Barnett Shale gas. Of relevance is the fact that all stray gas samples fall on or between the regression lines defined by the  $^{40}\text{Ar}^*$  volume fraction signature of the Strawn Group. This observation strongly supports the origin of the stray gas in the Trinity Aquifer as being the Strawn Group. In contrast, the observed mismatch between our stray gas samples and the  $^{40}\text{Ar}^*$  signature of Barnett Shale natural gas argues against this formation as the source of the stray gas. These results support previous findings by *Kornacki and McCaffrey* [2014] and *Darrah et al.* [2014] who also tentatively concluded that the Strawn Group was the likely source of stray gas in the Trinity Aquifer.

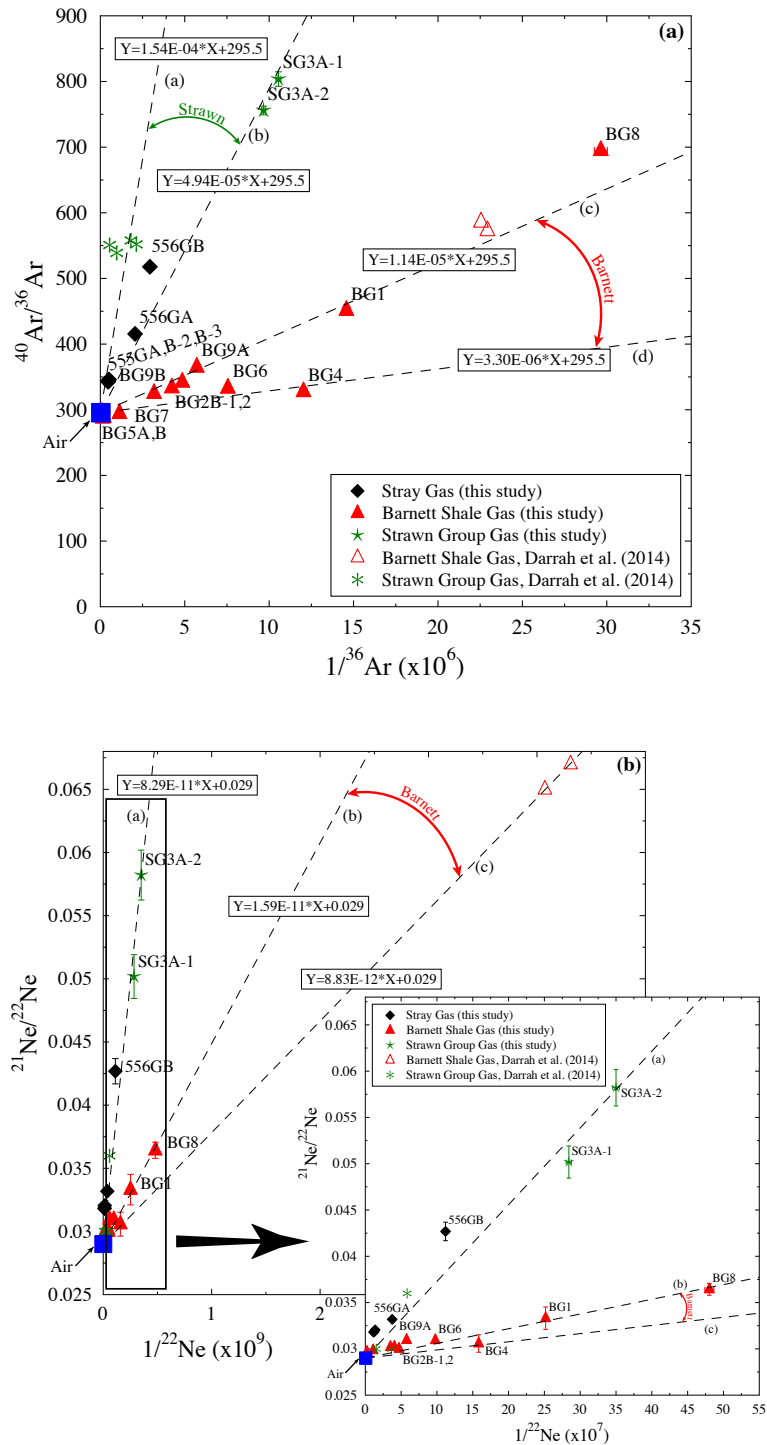


**Figure 4.3** (a)  $^{40}\text{Ar}/^{36}\text{Ar}$  versus  $1/^{36}\text{Ar}$  and (b)  $^{21}\text{Ne}/^{22}\text{Ne}$  versus  $1/^{22}\text{Ne}$  for all gas samples in this study as well as Barnett and Strawn gas samples from *Darrah et al.* [2014]. Linear regression lines are also shown for certain groups of gas samples (see text). Air values are shown for comparison.

A similar conclusion to that of  $^{40}\text{Ar}^*$  volume fractions can be drawn by analyzing the crustally produced  $^{21}\text{Ne}^*$ . This is clearly seen in Figure 4.3b where  $^{21}\text{Ne}/^{22}\text{Ne}$  ratios are plotted as a function of  $1/^{22}\text{Ne}$  values for all our natural gas samples and those reported by *Darrah et al.* [2014] for Barnett and Strawn production gas. Here too, the crustally produced  $^{21}\text{Ne}^*$  volume fractions in the Strawn natural gas have a value of  $8.29 \times 10^{-11}$ , which is significantly higher than that of Barnett Shale natural gas. From Figure 4.3b it can be clearly seen that stray gas samples fall on or very close to the mixing line defined by mixing between air and crustally produced Strawn natural gas. Barnett natural gas samples have a clearly distinct crustally produced  $^{21}\text{Ne}$  signature with  $^{21}\text{Ne}^*$  volume fraction contributions significantly lower than the Strawn and varying between  $8.83 \times 10^{-12}$  to  $1.59 \times 10^{-11}$ . The combined set of crustal  $^{21}\text{Ne}^*$  and  $^{40}\text{Ar}^*$  signatures of Strawn natural gas reinforces the notion that stray gas in the Trinity Aquifer does indeed originate in the Strawn Group. Another aspect of this analysis that strengthens our conclusions is the fact that both  $^{21}\text{Ne}^*$  and  $^{40}\text{Ar}^*$  volume fractions from this study and that of *Darrah et al.* [2014] for both the Strawn Group and Barnett Shale gas are rather consistent.

Analysis of the atmospheric component of noble gases further strengthens our findings by showing somewhat distinct noble gas signatures for both Barnett Shale and Strawn Group production gas and by pointing to a Strawn-like signature for stray gas in the Trinity Aquifer. This is particularly apparent when analyzing the noble gas signature of the lighter noble gases  $^{22}\text{Ne}$  and  $^{36}\text{Ar}$ . Indeed, unlike Kr and Xe, these are not subject to an additional atmospheric contribution from organic matter [e.g., *Frick and Chang*, 1977; *Podosek et al.*, 1980; *Torgersen and Kennedy*, 1999; *Ma et al.*, 2009; *Pitre and Pinti*, 2010]. In the discussion that follows,  $^{22}\text{Ne}$ ,  $^{36}\text{Ar}$ ,  $^{84}\text{Kr}$ , and  $^{132}\text{Xe}$  contents of all gases in this study are assumed to originate from recharge water in equilibrium with the atmosphere (ASW) at  $18^\circ\text{C}$  at an elevation of 274 m, i.e.,

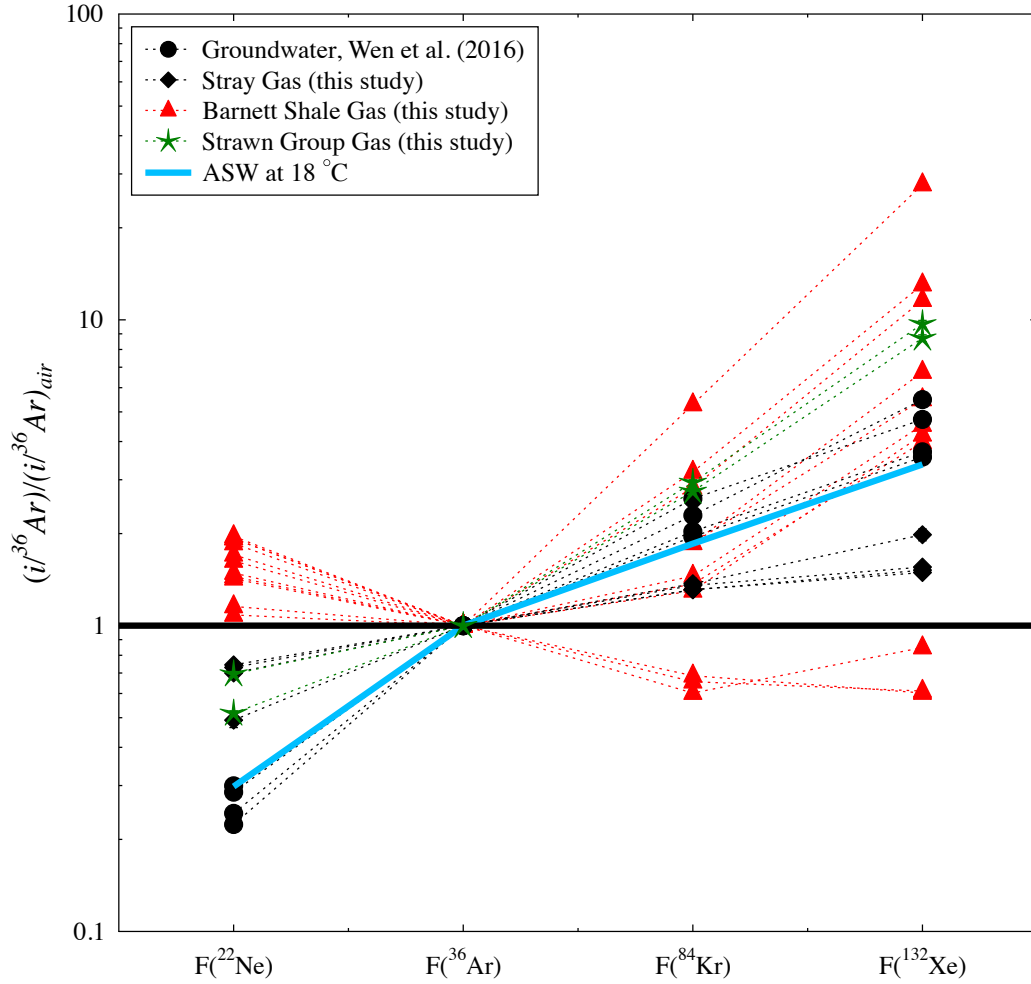
conditions corresponding to modern mean annual air temperature (MAAT) and average elevation of all sampled wells in this study. It should be noted that temperature differences of  $\pm 5^{\circ}\text{C}$  will have a negligible impact on our findings. Data from *Darrah et al.* [2014] are not discussed below due to the lack of heavy noble gas data in their study.

Figure 4.4 and Table B4 show  $F(^{22}\text{Ne})$ ,  $F(^{84}\text{Kr})$ , and  $F(^{132}\text{Xe})$  ratios for all gas samples in addition to Trinity groundwater samples with high methane content (samples 355, 358, 369, 555) reported by *Wen et al.* [2016].  $F(^{22}\text{Ne})$ ,  $F(^{84}\text{Kr})$ , and  $F(^{132}\text{Xe})$  represent measured  $^{22}\text{Ne}/^{36}\text{Ar}$ ,  $^{84}\text{Kr}/^{36}\text{Ar}$ , and  $^{132}\text{Xe}/^{36}\text{Ar}$  ratios normalized to corresponding air values (thick black line, Figure 4.4). ASW values for a temperature of  $18^{\circ}\text{C}$  are also shown (light blue line, Figure 4.4; see also Table B4).  $F(^{22}\text{Ne})$ ,  $F(^{84}\text{Kr})$ , and  $F(^{132}\text{Xe})$  values for all stray gas samples are located between ASW and air values (Figure 4.4). Because the solubility of light noble gases (e.g.,  $^{22}\text{Ne}$ ) in water is lower than that of heavy noble gases (e.g.,  $^{132}\text{Xe}$ ), light noble gases in the Trinity groundwater will go preferentially into the gas phase when groundwater is undergoing gas stripping. This results in elevated  $F(^{22}\text{Ne})$  but lower  $F(^{84}\text{Kr})$  and  $F(^{132}\text{Xe})$  values in the gas phase compared to the initial ASW values. As expected, Trinity groundwater samples with high methane content (black circles) display relative depletion in the light  $^{22}\text{Ne}$  isotope and relative enrichment of heavy ones compared to ASW (Figure 4.4). Thus a simple single-stage groundwater degassing model in a closed or open system at  $18^{\circ}\text{C}$  can adequately explain both, observed atmospheric noble gas ratios in stray gases as well as in Trinity groundwater samples (Figure 4.4; cf., Appendix B Text B5), an observation that is consistent with previous findings [*Wen et al.*, 2016]. Of relevance is the fact that  $F(^{22}\text{Ne})$  values of stray gas mimic those of Strawn natural gas, an observation which can also be explained by the single-stage groundwater degassing model. This observation further supports the source of stray gas in the Trinity Aquifer as being the Strawn Group. Unlike Strawn

production gas, however, all Barnett production gas displays distinctly high  $F(^{22}\text{Ne})$  values (Figure 4.4), all above that of air and suggests that a simple single-stage water degassing model for the Barnett Shale gas is not consistent with the light noble gas signature. On the other hand, a two-stage oil modified groundwater exsolution (OMGE) fractionation model [Battani *et al.*, 2000] can explain the light atmospheric noble gas signature observed in Barnett Shale production gas (Figure 4.5; Appendix B Text B5). This can be clearly seen in Figure 4.5 where  $^{84}\text{Kr}/^{36}\text{Ar}$  and  $^{132}\text{Xe}/^{36}\text{Ar}$  values are plotted as a function of  $^{22}\text{Ne}/^{36}\text{Ar}$  for all gas samples. Air and ASW at 18°C values are also shown for comparison, with  $^{22}\text{Ne}/^{36}\text{Ar}$  values of 0.053 and 0.016, respectively. Calculated closed- and open-system fractionation curves for an escaped gas phase that is in equilibrium with ASW at 18°C are also indicated (curved and dashed black lines, respectively). From Figure 4.5, it is apparent that although Strawn and stray gas display  $^{22}\text{Ne}/^{36}\text{Ar}$  values that are consistent with predicted values following the groundwater degassing model,  $^{22}\text{Ne}/^{36}\text{Ar}$  values in Barnett production gas are higher than the maximum predicted  $^{22}\text{Ne}/^{36}\text{Ar}$  value of 0.053 in the gas phase assuming a simple groundwater degassing model. On the other hand, it is apparent that all measured Barnett gas  $^{22}\text{Ne}/^{36}\text{Ar}$  ratios fall within the range predicted by the OMGE model for varying enrichment levels of  $^{84}\text{Kr}$  and  $^{132}\text{Xe}$ . Both Strawn and Barnett production gas display enrichment of the heavy atmospheric noble gases to varying degrees. This could be explained by sedimentary  $^{84}\text{Kr}$  and  $^{132}\text{Xe}$  excess noble gases of atmospheric origin adsorbed by organic matter (Figure B4) [e.g., Frick and Chang, 1977; Podosek *et al.*, 1980; Torgersen and Kennedy, 1999; Ma *et al.*, 2009; Pitre and Pinti, 2010], possibly sourced from the organic rich material in the Barnett Shale. It should be noted that the OMGE model is also in agreement with current knowledge of the Barnett Shale as the primary source rock for both oil and gas in the Fort Worth Basin [Herkommer and Denke, 1982; Jarvie *et al.*, 2001; Montgomery

*et al.*, 2005; *Hill et al.*, 2007; *Rodriguez and Philp*, 2010]. These results support distinct evolution histories for Strawn and Barnett Shale production gas.

Overall, this study shows that noble gases can be used to distinguish between different sources of shale gas, either due to their distinct evolution histories, different parent elements' amount and/or distinct ages. More specifically, this study shows that Barnett Shale production gas has a distinct noble gas signature from that of Strawn Group production gas and that this noble gas signature can be used to identify the source of methane present in the shallow Trinity Aquifer in Central Texas. It further shows that the source of methane in the Trinity is likely the Strawn Group, further reinforcing previous findings by *Darrah et al.* [2014], *Kornacki and McCaffrey* [2014] and *Wen et al.* [2016].



**Figure 4.4**  $F(^{22}\text{Ne})$ ,  $F(^{84}\text{Kr})$ , and  $F(^{132}\text{Xe})$  are plotted for gas samples.  $F(^{22}\text{Ne})$ ,  $F(^{84}\text{Kr})$ , and  $F(^{132}\text{Xe})$  are measured  $^{22}\text{Ne}/^{36}\text{Ar}$ ,  $^{84}\text{Kr}/^{36}\text{Ar}$ ,  $^{132}\text{Xe}/^{36}\text{Ar}$  ratios normalized to corresponding air values. F values of ASW at the temperature of 18 °C (light blue line) and air (black line) are shown. F values for groundwater samples with high methane content in the study area [Wen *et al.*, 2016] are also shown.

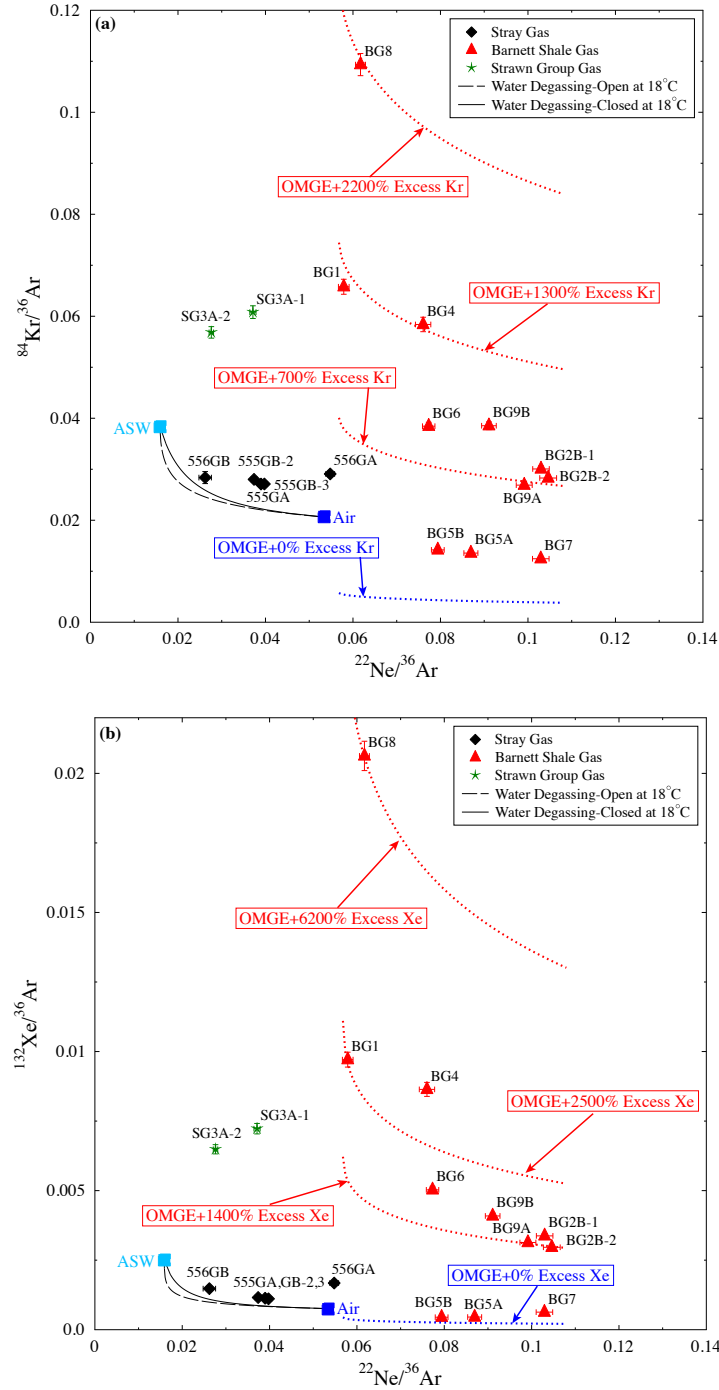


**Figure 4.5** (a)  $^{84}\text{Kr}/^{36}\text{Ar}$  versus  $^{22}\text{Ne}/^{36}\text{Ar}$  and (b)  $^{132}\text{Xe}/^{36}\text{Ar}$  versus  $^{22}\text{Ne}/^{36}\text{Ar}$  are shown for gas samples. Predicted values in the gas phase following a single-stage groundwater degassing model for closed-system (black curve) and open-system (black dashed curve) are shown in (a) and (b). Calculated values in the gas phase following oil-modified groundwater exsolution (OMGE) model with varying amount of sedimentary noble gas are also shown (blue and red dotted curves; see also Appendix B Text B5).

## **4.6 Acknowledgements**

Funding for this project was provided by RPSEA award 11122-56 through the “Ultra-Deepwater and Unconventional Natural Gas and Other Petroleum Resources” program authorized by the U.S. Energy Policy Act of 2005. NSF grant EAR #1049822 provided additional financial support. We also thank all well owners for access to their water wells as well as Laura Bouvier for her assistance in the field, Tongwei Zhang for the gas analyses, and IHS for free access to their Enerdeq database.

## 4.7 References

- Ballentine, C. J., R. K. O'Nions, E. R. Oxburgh, F. Horvath, and J. Deak (1991), Rare gas constraints on hydrocarbon accumulation, crustal degassing and groundwater flow in the Pannonian Basin, *Earth and Planetary Science Letters*, 105(1–3), 229–246, doi:10.1016/0012-821X(91)90133-3.
- Battani, A., P. Sarda, and A. Prinzhofer (2000), Basin scale natural gas source, migration and trapping traced by noble gases and major elements: the Pakistan Indus basin, *Earth and Planetary Science Letters*, 181(1–2), 229–249.
- Bruner, K. R., and R. Smosna (2011), *A comparative study of the Mississippian Barnett Shale, Fort Worth Basin, and Devonian Marcellus Shale*, DOE/NETL.
- Castro, M. C., A. Jambon, G. de Marsily, and P. Schlosser (1998a), Noble gases as natural tracers of water circulation in the Paris Basin: 1. Measurements and discussion of their origin and mechanisms of vertical transport in the basin, *Water Resources Research*, 34(10), 2443–2466, doi:10.1029/98WR01956.
- Castro, M. C., L. Ma, and C. M. Hall (2009), A primordial, solar He–Ne signature in crustal fluids of a stable continental region, *Earth and Planetary Science Letters*, 279(3–4), 174–184, doi:10.1016/j.epsl.2008.12.042.
- Castro, M. C., P. Goblet, E. Ledoux, S. Violette, and G. de Marsily (1998b), Noble gases as natural tracers of water circulation in the Paris Basin: 2. Calibration of a groundwater flow model using noble gas isotope data, *Water Resources Research*, 34(10), 2467–2483, doi:10.1029/98WR01957.
- Clarke, W. B., W. J. Jenkins, and Z. Top (1976), Determination of tritium by mass spectrometric measurement of  $^3\text{He}$ , *The International Journal of Applied Radiation and Isotopes*, 27(9), 515–522, doi:10.1016/0020-708X(76)90082-X.
- Darrah, T. H., A. Vengosh, R. B. Jackson, N. R. Warner, and R. J. Poreda (2014), Noble gases identify the mechanisms of fugitive gas contamination in drinking-water wells overlying the Marcellus and Barnett Shales, *Proceedings of the National Academy of Sciences*, 111(39), 14076–14081, doi:10.1073/pnas.1322107111.
- Darrah, T. H., R. B. Jackson, A. Vengosh, N. R. Warner, C. J. Whyte, T. B. Walsh, A. J. Kondash, and R. J. Poreda (2015), The evolution of Devonian hydrocarbon gases in shallow aquifers of the northern Appalachian Basin: Insights from integrating noble gas and hydrocarbon geochemistry, *Geochimica et Cosmochimica Acta*, 170 IS -, 321–355, doi:10.1016/j.gca.2015.09.006.
- Ewing, T. E. (1991), *The tectonic framework of Texas: Text accompanying the tectonic map of Texas*, Texas Bureau of Economic Geology.
- Frick, U., and S. Chang (1977), Ancient carbon and noble gas fractionation, *Lunar and Planetary Science Conference ....*

- Hackley, P. C., E. H. Guevara, T. F. Hentz, and R. W. Hook (2009), Thermal maturity and organic composition of Pennsylvanian coals and carbonaceous shales, north-central Texas: Implications for coalbed gas potential, *International Journal of Coal Geology*, 77(3–4), 294–309, doi:10.1016/j.coal.2008.05.006.
- Henry, J. D. (1982), Stratigraphy of the Barnett Shale (Mississippian) and Associated Reefs in the Northern Fort Worth Basin, *Petroleum Geology of the Fort Worth Basin and Bend Arch Area*, 157–177.
- Herkommer, M. A., and G. W. Denke (1982), Stratigraphy and hydrocarbons, Parker County, Texas, *Dallas Geological Society*.
- Hill, R. J., E. Zhang, B. J. Katz, and Y. Tang (2007), Modeling of gas generation from the Barnett Shale, Fort Worth Basin, Texas, *AAPG Bulletin*, 91(4), 501–521, doi:10.1306/12060606063.
- Hilton, D. R., and D. Porcelli (2003), 2.06 - Noble Gases as Mantle Tracers, in *Treatise on Geochemistry*, edited by H. D. H. K. Turekian, pp. 277–318, Pergamon, Oxford.
- Holland, G., and S. Gilfillan (2013), Application of noble gases to the viability of CO<sub>2</sub> storage, in *The Noble Gases as Geochemical Tracers*, edited by P. Burnard, pp. 177–223, Springer, Berlin.
- Jackson, R. B., A. Vengosh, T. H. Darrah, N. R. Warner, A. Down, R. J. Poreda, S. G. Osborn, K. Zhao, and J. D. Karr (2013a), Increased stray gas abundance in a subset of drinking water wells near Marcellus shale gas extraction, *Proceedings of the National Academy of Sciences of the USA*, 110(28), 11250–11255, doi:10.1073/pnas.1221635110/-/DCSupplemental/pnas.201221635SI.pdf.
- Jackson, R. E., A. W. Gorody, B. Mayer, J. W. Roy, M. C. Ryan, and D. R. Van Stempvoort (2013b), Groundwater Protection and Unconventional Gas Extraction: The Critical Need for Field-Based Hydrogeological Research, *Ground Water*, 51(4), 488–510, doi:10.1111/gwat.12074.
- Jarvie, D. M., B. L. Claxton, F. Henk, and J. T. Breyer (2001), *Oil and shale gas from the Barnett Shale, Ft. Worth Basin, Texas*, AAPG ACE Meeting.
- Kennedy, B. M., M. A. Lynch, J. H. Reynolds, and S. P. Smith (1985), Intensive sampling of noble gases in fluids at Yellowstone: I. Early overview of the data; regional patterns, *Geochimica et Cosmochimica Acta*, 49(5), 1251–1261, doi:10.1016/0016-7037(85)90014-6.
- Kornacki, A. S., and M. McCaffrey (2014), Monitoring the Active Migration and Biodegradation of Natural Gas in the Trinity Group Aquifer at the Silverado Development in Southern Parker County, Texas, *2014 AAPG Annual Convention and Exhibition*. Available from: <http://www.searchanddiscovery.com/abstracts/html/2014/90189ace/abstracts/1830218.html> (Accessed 11 November 2015)

- Kreitler, C. W. (2014), *Lessons Learned from the Barnett Shale Range Resources Litigation, Hydraulic Fracturing and Environmental Implications*, Austin.
- Kulongoski, J. T., D. R. Hilton, and J. A. Izbicki (2005), Source and movement of helium in the eastern Morongo groundwater Basin: The influence of regional tectonics on crustal and mantle helium fluxes, *Geochimica et Cosmochimica Acta*, 69(15), 3857–3872, doi:10.1016/j.gca.2005.03.001.
- Li, H., and K. H. Carlson (2014), Distribution and Origin of Groundwater Methane in the Wattenberg Oil and Gas Field of Northern Colorado, *Environ. Sci. Technol.*, 48(3), 1484–1491, doi:10.1021/es404668b.
- Lollar, B. S., and C. J. Ballentine (2009), Insights into deep carbon derived from noble gases., 2(8), 543–547, doi:10.1038/ngeo588.
- Ma, L., M. C. Castro, and C. M. Hall (2009), Atmospheric noble gas signatures in deep Michigan Basin brines as indicators of a past thermal event, *Earth and Planetary Science Letters*, 277(1–2), 137–147, doi:10.1016/j.epsl.2008.10.015.
- Martini, A. M., J. M. Budai, L. M. Walter, and M. Schoell (1996), Microbial generation of economic accumulations of methane within a shallow organic-rich shale, *Nature*, 383(6596), 155–158, doi:10.1038/383155a0.
- Molofsky, L. J., J. A. Connor, A. S. Wylie, T. Wagner, and S. K. Farhat (2013), Evaluation of Methane Sources in Groundwater in Northeastern Pennsylvania, *Ground Water*, 51(3), 333–349.
- Montgomery, S. L., D. M. Jarvie, K. A. Bowker, and R. M. Pollastro (2005), Mississippian Barnett Shale, Fort Worth basin, north-central Texas: Gas-shale play with multi-trillion cubic foot potential, *AAPG Bulletin*, 89(2), 155–175, doi:10.1306/09170404042.
- Moreira, M., and C. J. Allègre (1998), Helium–neon systematics and the structure of the mantle, *Chemical Geology*, 147(1-2), 53–59, doi:10.1016/S0009-2541(97)00171-X.
- Nicot, J. P., Y. Huang, B. D. Wolaver, and R. A. Costley (2013), Flow and salinity patterns in the low-transmissivity Upper Paleozoic aquifers of North-Central Texas, *GCAGS Journal*, 2, 53–67.
- Nicot, J.-P., B. R. Scanlon, R. C. Reedy, and R. A. Costley (2014), Source and Fate of Hydraulic Fracturing Water in the Barnett Shale: A Historical Perspective, *Environ. Sci. Technol.*, 48(4), 2464–2471, doi:10.1021/es404050r.
- Nicot, J.-P., P. Mickler, T. Larson, M. C. Castro, R. Darvari, R. Smyth, K. Uhlman, and C. Omelon (2015), *Understanding and Managing Environmental Roadblocks to Shale Gas Development: An Analysis of Shallow Gas, NORM, and Trace Metals*, Research Partnership to Secure Energy for America, Austin, <http://www.rpsea.org/projects/11122-56/>.

- Nicot, J.-P., P. Mickler, T. Larson, M. C. Castro, R. Darvari, K. Uhlman, and R. Costley, Methane occurrences in aquifers overlying the Barnett Shale play with a focus on Parker County, Texas, *Groundwater*, in review.
- Osborn, S. G., A. Vengosh, N. R. Warner, and R. B. Jackson (2011), Methane contamination of drinking water accompanying gas-well drilling and hydraulic fracturing, *Proceedings of the National Academy of Sciences*, 108(20), 8172–8176, doi:10.1073/pnas.1100682108.
- Oxburgh, E. R., R. K. O'Nions, and R. I. Hill (1986), Helium isotopes in sedimentary basins, *Nature*, 324(6098), 632–635, doi:10.1038/324632a0.
- Ozima, M., and F. A. Podosek (2002), *Noble Gas Geochemistry*, Cambridge University Press, New York.
- Pinti, D. L., and B. Marty (1995), Noble gases in crude oils from the Paris Basin, France: Implications for the origin of fluids and constraints on oil-water-gas interactions, *Geochimica et Cosmochimica Acta*, 59(16), 3389–3404, doi:10.1016/0016-7037(95)00213-J.
- Pinti, D. L., M. C. Castro, O. Shouakar-Stash, A. Tremblay, V. H. Garduño, C. M. Hall, J. F. Hélie, and B. Ghaleb (2012), Evolution of the geothermal fluids at Los Azufres, Mexico, as traced by noble gas isotopes,  $\delta^{18}\text{O}$ ,  $\delta\text{D}$ ,  $\delta^{13}\text{C}$  and  $87\text{Sr}/86\text{Sr}$ , *Journal of Volcanology and Geothermal Research*, 249(0), 1–11, doi:10.1016/j.jvolgeores.2012.09.006.
- Pitre, F., and D. L. Pinti (2010), Noble gas enrichments in porewater of estuarine sediments and their effect on the estimation of net denitrification rates, *Geochimica et Cosmochimica Acta*, 74(2), 531–539, doi:10.1016/j.gca.2009.10.004.
- Podosek, F. A., M. Honda, and M. Ozima (1980), Sedimentary noble gases, *Geochimica et Cosmochimica Acta*, 44(11), 1875–1884, doi:10.1016/0016-7037(80)90236-7.
- Pollastro, R. M., D. M. Jarvie, R. J. Hill, and C. W. Adams (2007), Geologic framework of the Mississippian Barnett Shale, Barnett-Paleozoic total petroleum system, Bend arch–Fort Worth Basin, Texas, *AAPG Bulletin*, 91(4), 405–436, doi:10.1306/103006060008.
- Porcelli, D., C. J. Ballentine, and R. Wieler (2002), An Overview of Noble Gas Geochemistry and Cosmochemistry, *Reviews in Mineralogy and Geochemistry*, 47(1), 1–19, doi:10.2138/rmg.2002.47.1.
- Rodriguez, N. D., and R. P. Philp (2010), Geochemical characterization of gases from the Mississippian Barnett Shale, Fort Worth Basin, Texas, *AAPG Bulletin*, 94(11), 1641–1656, doi:10.1306/04061009119.
- Siegel, D. I., N. A. Azzolina, B. J. Smith, A. E. Perry, and R. L. Bothun (2015), Methane Concentrations in Water Wells Unrelated to Proximity to Existing Oil and Gas Wells in Northeastern Pennsylvania, *Environ. Sci. Technol.*, 49(7), 4106–4112, doi:10.1021/es505775c.

- Stolper, D. A., A. M. Martini, M. Clog, P. M. Douglas, S. S. Shusta, D. L. Valentine, A. L. Sessions, and J. M. Eiler (2015), Distinguishing and understanding thermogenic and biogenic sources of methane using multiply substituted isotopologues, *Geochimica et Cosmochimica Acta*, doi:10.1016/j.gca.2015.04.015.
- Thompson, H. (2012), Fracking boom spurs environmental audit, *Nature*, 485(7400), 556–557, doi:10.1038/485556a.
- Torgersen, T., and B. M. Kennedy (1999), Air-Xe enrichments in Elk Hills oil field gases: role of water in migration and storage, *Earth and Planetary Science Letters*, 167(3–4), 239–253, doi:10.1016/S0012-821X(99)00021-7.
- US EIA (2015), *Annual Energy Outlook 2015*, US Energy Information Administration, Washington, DC.
- US EIA (2016), *Annual Energy outlook 2016*, US Energy Information Administration.
- Van A Kelley, J. Ewing, T. L. Jones, S. C. Young, N. Deeds, and S. Hamlin (2014), *Updated Groundwater Availability Model of the Northern Trinity and Woodbine Aquifers*, Texas Water Development Board.
- Warner, N. R., T. M. Kresse, P. D. Hays, A. Down, J. D. Karr, R. B. Jackson, and A. Vengosh (2013), Geochemical and isotopic variations in shallow groundwater in areas of the Fayetteville Shale development, north-central Arkansas, *Applied Geochemistry*, 35, 207–220.
- Warrier, R. B., M. C. Castro, C. M. Hall, and K. C. Lohmann (2013), Large atmospheric noble gas excesses in a shallow aquifer in the Michigan Basin as indicators of a past mantle thermal event, *Earth and Planetary Science Letters*, 375(0), 372–382, doi:10.1016/j.epsl.2013.06.001.
- Weiss, R. F. (1968), Piggyback sampler for dissolved gas studies on sealed water samples, *Deep Sea Research and Oceanographic Abstracts*, 15(6), 695–699.
- Wen, T., M. C. Castro, B. R. Ellis, C. M. Hall, and K. C. Lohmann (2015a), Assessing compositional variability and migration of natural gas in the Antrim Shale in the Michigan Basin using noble gas geochemistry, *Chemical Geology*, 417, 356–370, doi:10.1016/j.chemgeo.2015.10.029.
- Wen, T., M. C. Castro, C. M. Hall, D. L. Pinti, and K. C. Lohmann (2015b), Constraining groundwater flow in the glacial drift and saginaw aquifers in the Michigan Basin through helium concentrations and isotopic ratios, *Geofluids*, 16, 3–25, doi:10.1111/gfl.12133.
- Wen, T., M. C. Castro, J.-P. Nicot, C. M. Hall, T. Larson, P. Mickler, and R. Darvari (2016), Methane Sources and Migration Mechanisms in Shallow Groundwaters in Parker and Hood Counties, Texas—A Heavy Noble Gas Analysis, *Environ. Sci. Technol.*, doi:10.1021/acs.est.6b01494.

Yatsevich, I., and M. Honda (1997), Production of nucleogenic neon in the Earth from natural radioactive decay, *Journal of Geophysical Research*.

## CHAPTER 5

### SUMMARY AND CONCLUSIONS

This final chapter summarizes the major findings from each chapter and highlights the overall conclusion of the work presented in this dissertation.

#### 5.1 Summary of Major Results

**Chapter 2:** This chapter presents volume fractions and isotopic ratios of stable noble gases in Antrim Shale gas samples to clarify vertical fluid migration, to confirm the occurrence of a past thermal event in the Michigan Basin, to estimate ages of formation water associated with natural gas, and to distinguish between thermogenic and biogenic methane in the Antrim Shale. High horizontal and vertical variability in crustal noble gas signatures in the Antrim Shale are observed, which are due to variable noble gas input with brine migration from deeper formations and, to a smaller extent, are also due to variable in-situ production, in particular, the Lachine and Norwood Members. Estimated  $^4\text{He}$  ages (0.9 to 238.2 ka) considering external  $^4\text{He}$  input for Antrim Shale water match well for most samples with the timing of the major Wisconsin glaciation (10 to 79 ka) [*Dorr and Eschman, 1970; Schaetzl et al., 2008; Bergquist, 2009*] in the Michigan Basin, suggesting that Antrim Shale water was influenced by glaciation-induced recharge. Given measured atmospheric-derived  $^{36}\text{Ar}$  volume fractions and the

atmospheric  $^{40}\text{Ar}/^{36}\text{Ar}$  ratio of 295.5 [Ozima and Podosek, 2002], predicted  $^{40}\text{Ar}/^{36}\text{Ar}$  ratios can be calculated assuming that Ar is fully released from the source formation ( $T > 250\text{ }^{\circ}\text{C}$ ) [Elliot *et al.*, 1993]. The consistency between measured and predicted  $^{40}\text{Ar}/^{36}\text{Ar}$  ratios for most Antrim Shale gas samples indicates that paleo subsurface temperatures in the source rock should be higher than the Ar release temperature ( $250\text{ }^{\circ}\text{C}$ ) and thus high enough for thermogenic methane formation ( $157$  and  $221^{\circ}\text{C}$ ) [Stolper *et al.*, 2015]. Thermal maturity of the Antrim Shale in the study area is relatively low and does not support in-situ production of thermogenic methane [Rullkötter *et al.*, 1992], although the TOC content of the Antrim Shale is up to 24% [Martini *et al.*, 1998]. Therefore, thermogenic methane, which contributes most of the total produced methane in the Antrim within the study area, must originate from an external source. That might be either the deeper portion of the Antrim Shale located in the central Michigan Basin or more deeply buried Silurian and older strata underlying the Antrim Shale [Stolper *et al.*, 2015]. These findings confirm that noble gases are indeed excellent tracers capable of fingerprinting shale gas and tracing its migration in groundwater reservoir.

**Chapter 3:** Noble gas concentrations and isotopic ratios in groundwater from the shallow Trinity Aquifer within the Barnett Shale footprint are shown with a particular emphasis on atmospheric heavy noble gas isotopes (i.e.,  $^{84}\text{Kr}$  and  $^{132}\text{Xe}$ ). Four groundwater wells with high methane contents ( $> 10\text{ mg/L}$ ) display significant depletion in atmospheric noble gases compared to fresh recharge water, which is due to the loss of atmospheric noble gases from ASW into the present gas phase (stray gas). A simple groundwater degassing model can well explain the observed depletion in atmospheric noble gases, especially heavy noble gas isotopes,  $^{84}\text{Kr}$  and  $^{132}\text{Xe}$ . Combined with water well logs, the study of atmospheric noble gas signatures in these groundwater samples suggests that stray gas in the shallow Trinity Aquifer is likely related to

noncommercial small gas accumulations in the Strawn Group as these four groundwater wells have penetrated through the Trinity Aquifer and reached the underlying Strawn Group (Figure 5.1). Lack of correlation between noble gas signatures (i.e.,  $^{132}\text{Xe}/^{36}\text{Ar}$  and  $^4\text{He}/^{20}\text{Ne}$ ) and distance to the nearest production well do not support the notion that stray gas present in these water wells migrated from some nearby production wells from leaks along faulty surface casing. Furthermore, based on the absence of correlation between  $\text{CH}_4/^{36}\text{Ar}$  ratios and  $\text{Cl}^-$  concentrations in water, we conclude that there is no basis at this stage to infer an influx of deep brine along with stray gas either from leaks of production wells or from natural flow along minor faults. Rather, our findings suggest that stray gas in the Trinity Aquifer is likely from non-commercial small gas accumulations in the Strawn Group. At this stage, none of our observations and measurements points to migration of stray gas from nearby Strawn or Barnett production wells.

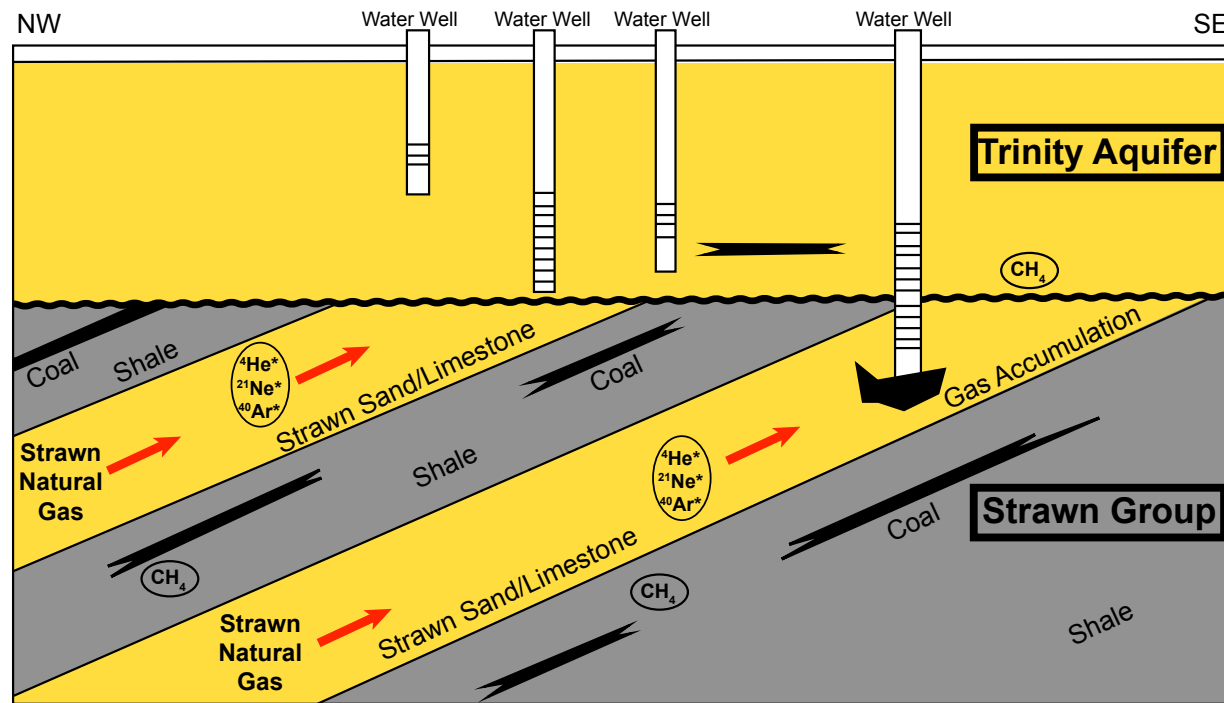


**Figure 5.1** Schematic cross-section of the Trinity Aquifer and Strawn Group in the study area [adapted from Kornacki and McCaffrey 2014]

**Chapter 4:** This study has focused on natural gas samples from production wells in the Barnett Shale and Strawn Group as well as from water wells in the Trinity Aquifer. Both crustal and atmospheric noble gas components are analyzed and compared for all samples. Strawn production gas is more enriched in crustal  $^4\text{He}^*$ ,  $^{21}\text{Ne}^*$  and  $^{40}\text{Ar}^*$  than Barnett production gas. These distinct noble gas signatures reflect either higher concentrations of parent elements in the Strawn Group or more likely, they reflect the presence of older natural gas in the Strawn Group than that currently in place in the Barnett Shale. The presence of natural gas in the Strawn Group that may have formed at an earlier time in the Barnett Shale and subsequently migrated to the Strawn Group is also consistent with findings by previous studies [Jarvie *et al.*, 2001; Montgomery *et al.*, 2005; Pollastro *et al.*, 2007]. The comparison of  $^{21}\text{Ne}/^{22}\text{Ne}$  and  $^{40}\text{Ar}/^{36}\text{Ar}$  isotopic ratios versus the inverse of their atmospheric dominant isotopes  $^{22}\text{Ne}$  and  $^{36}\text{Ar}$  for stray gas, Barnett and Strawn production gas suggests that stray gas in the Trinity represents a mixing of two end-members: (1) the air and (2) the crustal component defined by pristine Strawn gas. Noble gas composition of Barnett gas samples cannot explain observed noble gas signatures in stray gas samples. This reinforces the hypothesis that the Strawn Group is likely the source of stray gas in the Trinity Aquifer. Furthermore, an in-depth comparison of atmospheric noble gas components (i.e.,  $^{22}\text{Ne}$ ,  $^{36}\text{Ar}$ ,  $^{84}\text{Kr}$ , and  $^{132}\text{Xe}$ ) of Barnett and Strawn gas samples point to elevated  $^{22}\text{Ne}/^{36}\text{Ar}$  ratios in Barnett gas as well as elevated  $^{84}\text{Kr}/^{36}\text{Ar}$  and  $^{132}\text{Xe}/^{36}\text{Ar}$  ratios in both Barnett and Strawn gas, compared to ASW and air values. These elevated elemental ratios are investigated and compared to predicted values in the gas phase assuming two noble gas fractionation models. A two-stage Rayleigh-type fractionation model considering the oil phase is suggested to be the most viable option to explain such high  $^{22}\text{Ne}/^{36}\text{Ar}$  ratios in Barnett gases, while sedimentary Kr and Xe input is required to account for relative enrichment in  $^{84}\text{Kr}$  and

$^{132}\text{Xe}$  in Barnett and Strawn gases. These results support distinct evolution histories for Barnett Shale and Strawn Group production gas. This study highlights the use of both atmospheric and crustal noble gases to distinguish between natural gas from various formations, to identify the source of dissolved hydrocarbon in groundwater, and to trace its subsurface migration.

## **5.2 Overall Conclusions**

This dissertation focuses on noble gases in groundwater and natural gas within two shale plays: the Antrim Shale in the Michigan Basin, MI and the Barnett Shale in the Fort Worth Basin, TX, combined with a diversity of other natural tracers including major elements in water, radiocarbon ( $^{14}\text{C}$ ), major gas components ( $\text{CH}_4$ ,  $\text{CO}_2$ ) and stable isotopes ( $\delta^{13}\text{C}-\text{CH}_4$ ). This dissertation has investigated 17 shale gas samples from the Antrim Shale, 45 shallow groundwater samples and 4 stray gas (flowing gas) samples from 2 water wells within the Barnett Shale footprint, and 10 production gas samples from 8 Barnett Shale and 1 Strawn Group gas wells. The study of noble gas content in groundwater and natural gas in hydrocarbon systems provides a powerful tool to characterize natural gas generation, to trace the source of crustal fluids (i.e., natural gas and associated groundwater), to provide insights into migration pattern and mechanism of crustal fluids, and to delineate the degree of mixing between various crustal fluids enhancing our understanding of crustal fluid dynamics.

This dissertation is of great societal relevance with respect to conventional and unconventional oil and gas as well as environmental impact assessment. Indeed, there is concern by local communities, the industry and scientists that unconventional gas production in particular might negatively affect groundwater quality in production areas. This dissertation shows that noble gas-based environmental studies can greatly contribute to the identification of natural gas

sources in groundwater as well as the migration mechanisms of dissolved methane in drinking groundwater. These findings will positively impact future groundwater management plans in these regions.

### 5.3 References

- Bergquist, S. G. (2009), The glacial history and development of Michigan, *Michigan State University*, 1–12.
- Dorr, J. A. J., and D. F. Eschman (1970), *Geology of Michigan*, University of Michigan, Ann Arbor.
- Elliot, T., C. J. Ballentine, R. K. O'niions, and T. Ricchiuto (1993), Carbon, helium, neon and argon isotopes in a Po basin (northern Italy) natural gas field, *Chemical Geology*, 106(3-4), 429–440, doi:10.1016/0009-2541(93)90042-H.
- Jarvie, D. M., B. L. Claxton, F. Henk, and J. T. Breyer (2001), *Oil and shale gas from the Barnett Shale, Ft. Worth Basin, Texas*, AAPG ACE Meeting.
- Kornacki, A. S., and M. McCaffrey (2014), Monitoring the Active Migration and Biodegradation of Natural Gas in the Trinity Group Aquifer at the Silverado Development in Southern Parker County, Texas, *2014 AAPG Annual Convention and Exhibition*. Available from: <http://www.searchanddiscovery.com/abstracts/html/2014/90189ace/abstracts/1830218.html> (Accessed 11 November 2015)
- Martini, A. M., L. M. Walter, J. M. Budai, T. C. W. Ku, C. J. Kaiser, and M. Schoell (1998), Genetic and temporal relations between formation waters and biogenic methane: Upper Devonian Antrim Shale, Michigan Basin, USA, *Geochimica et Cosmochimica Acta*, 62(10), 1699–1720, doi:10.1016/S0016-7037(98)00090-8.
- Montgomery, S. L., D. M. Jarvie, K. A. Bowker, and R. M. Pollastro (2005), Mississippian Barnett Shale, Fort Worth basin, north-central Texas: Gas-shale play with multi-trillion cubic foot potential, *AAPG Bulletin*, 89(2), 155–175, doi:10.1306/09170404042.
- Ozima, M., and F. A. Podosek (2002), *Noble Gas Geochemistry*, Cambridge University Press, New York.
- Pollastro, R. M., D. M. Jarvie, R. J. Hill, and C. W. Adams (2007), Geologic framework of the Mississippian Barnett Shale, Barnett-Paleozoic total petroleum system, Bend arch–Fort Worth Basin, Texas, *AAPG Bulletin*, 91(4), 405–436, doi:10.1306/10300606008.
- Rullkötter, J., R. Marzi, and P. Meyers (1992), Biological Markers in Paleozoic Sedimentary Rocks and Crude Oils from the Michigan Basin: Reassessment of Sources and Thermal History of Organic Matter, in *Early Organic Evolution*, edited by M. Schidlowski, S. Golubic, M. Kimberley, D. McKirdy Sr, and P. Trudinger, pp. 324–335–335, Springer Berlin Heidelberg, Berlin, Heidelberg.
- Schaetzl, R. J., J. T. Darden, and D. S. Brandt (2008), *Michigan geography and geology*, Pearson Custom Pub.
- Stolper, D. A., A. M. Martini, M. Clog, P. M. Douglas, S. S. Shusta, D. L. Valentine, A. L. Sessions, and J. M. Eiler (2015), Distinguishing and understanding thermogenic and

biogenic sources of methane using multiply substituted isotopologues, *Geochimica et Cosmochimica Acta*, doi:10.1016/j.gca.2015.04.015.

## **APPENDICES**

Additional text, tables and figures that support the main results presented in Chapter 3-4 are provided in Appendices A and B, respectively. Supporting material presented in each appendix are briefly enumerated here and discussed in detail in each corresponding appendix.

Appendix A includes additional text, 5 tables (Tables A1-A5) and 9 figures (Figures A1-A9) that support main results presented in Chapter 3.

Appendix B consists of additional text, 5 tables (Tables B1-B5) and 4 figures (Figures B1-B4) that support main results presented in Chapter 4.

## **APPENDIX A**

### **SUPPLEMENTARY MATERIAL FOR CHAPTER 3**

#### **A1 Local Geology and Hydrostratigraphy**

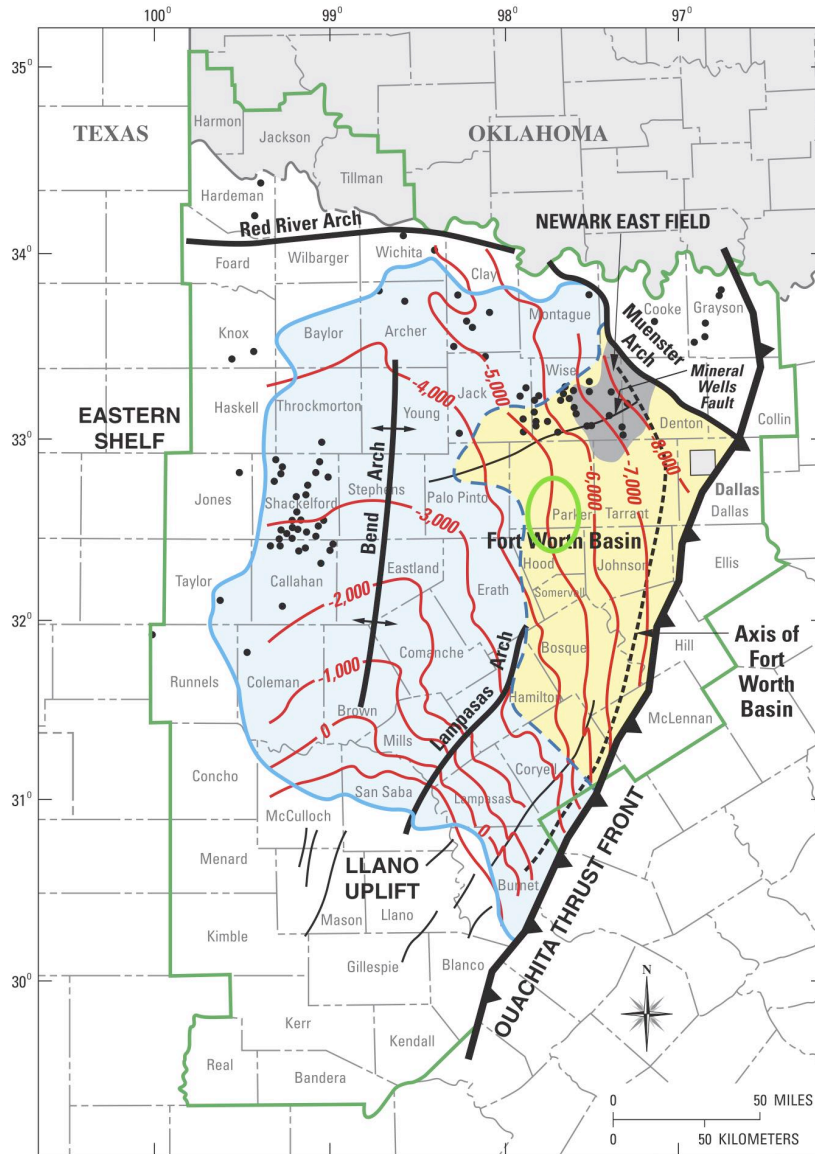
The study area is located at the edge of the commercially-viable Barnett Shale to the southwest of the more intensely developed so-called core area (Figure A1). The Barnett Shale in the core area is relatively deep (2.5-3 km) and becomes shallower in all directions moving away from the core to reach a depth of ~1.8 km in the study area. The Barnett Shale crops out to the south of the study area in the Llano Uplift. The sedimentary cover in the study and core areas is comprised of late Paleozoic sediments overlain unconformably by Cretaceous formations. In the study area, the Cretaceous sedimentary cover is very thin and < 200m-thick. Paleozoic formations crop out a few kilometers to the west. The Strawn Group (the Lower Strawn; Paleozoic age) directly underlies the base of the Trinity Group containing the freshwater Trinity Aquifer. In contrast, in the core area, the Cretaceous sedimentary cover is > 600m-thick. There it includes, besides the Trinity Group at its base, more recent overlying formations such as the Edwards Formation and Woodbine Formation, both hosting regional aquifers. It also unconformably covers a much thicker Strawn whose thickness increases considerably approaching the Ouachita thrust front that marks the structural limit of the Barnett to the East (Figure A1). The underlying Atoka, also of Pennsylvanian age, displays large increased thickness as well close to the thrust front (Figure A2).

The Barnett Shale has been known as the major source rock in the Fort Worth Basin. However, many of the known oil and gas reservoirs are away from the mature core area. Reservoirs are present in formations of various ages from Ordovician (Ellenburger Formation) to Mississippian (Marble Falls Formation) to Pennsylvanian Atoka and Strawn formations. The massive gas fields of the Bend Conglomerate of Atokan age (e.g., Boonsville field) are located mostly in Wise County, just north of Parker County. Closer to the study area, the Lower Strawn contains commercial deposits at various depths including the Center Mill Field at a depth of ~130m just east of the study area. The Lower Strawn and Upper Strawn (to the north of the study area) contains additional deeper deposits at relatively shallow depth < 1000m. The vast majority of these conventional reservoirs produce or produced from relatively shallow vertical wells that did not undergo sophisticated stimulation techniques such as hydraulic fracturing.

Although the Trinity Aquifer is classically described as an aquifer system with various sand layers separated by carbonate or shaly aquitards, in the study area, only the basal Hosston Sands (of the Twin Mountain Formation; other names of current usage also include Antlers Formation and Travis Peak Formation) are present and are overlain by the Glenrose Formation (carbonate) which is, in the study area, mostly included in the vadose zone. Cretaceous formations slightly dip to the east whereas Paleozoic formations dip to the northwest while increasing considerably in thickness toward the east (Figure A3).

Figure A4 shows the location of the study area (south cluster location) that depicts the Cretaceous veneer on top of the thick Pennsylvanian sedimentary package that crops out further to the west. Some of the easternmost outcrops in the region are exposed on the left-hand side of Figure A4 (Plb, Pkf, Pdb, and Pu, representing the base of the Upper Strawn, i.e., Lazy Bend and other formations). Then starting from the left-hand side and from the oldest Cretaceous

formation in the area: Twin Mountains Formation (Ktm), Glenrose limestone (Kgr), Paluxy Formation (Kpa), together forming the Trinity Group partially covered by Quaternary alluvium (Qal) and terrace deposits (Qt), especially in the Brazos River floodplain, and other Quaternary sediments (Qu) and then to the east the base of the Fredericksburg Group (Kgl, Ked, Kdc) comprised mostly of platform carbonates.



- EXPLANATION**
- USGS PROVINCE 45 BOUNDARY—BEND ARCH-FORT WORTH BASIN
  - GEOGRAPHIC EXTENT OF BARNETT SHALE IN THE FORT WORTH BASIN
  - AREA OF MAIN BARNETT SHALE GAS PRODUCTION (NEWARK EAST FIELD)
  - AREA OF POTENTIAL BARNETT SHALE GAS PRODUCTION
  - AXIS OF FORT WORTH BASIN
  - THRUST FRONT
  - STRUCTURAL CONTOUR, TOP OF ELLENBURGER GROUP (INTERVAL 1,000 FEET)
  - LOCATION OF WELLS SAMPLED FOR OIL AND GAS
  - FAULT

**Figure A1** Map showing extent of the Fort Worth Basin, its major structural features, extent of Mississippian Barnett Shale, and relation to early historical production (so-called “core area”). Contours are drawn on top of the Ordovician Ellenburger Group; contour intervals equal 1,000 feet [adapted from Bruner and Smosna, 2011]. Green circle shows the area of study.

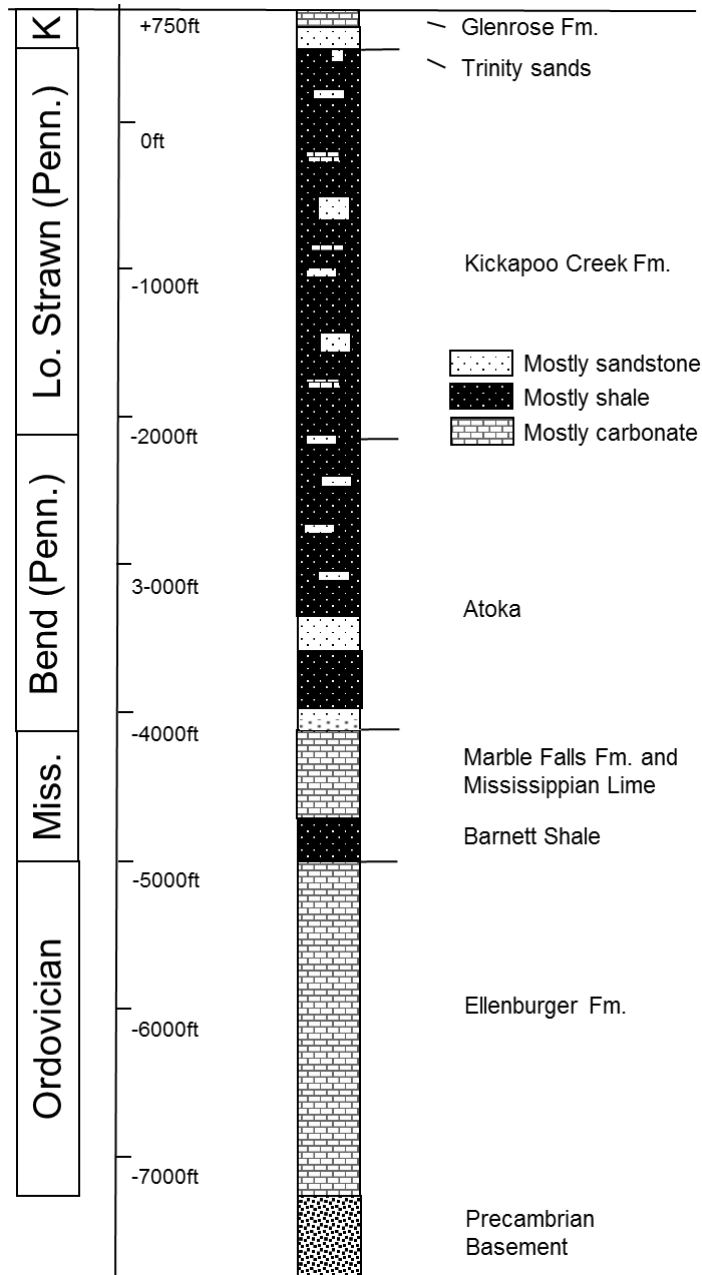


**Figure A2** Generalized local stratigraphic column within the study area in the vicinity of the Parker-Hood county line [data from *Herkommer and Denke*, 1982 and *CLI (Core Laboratories Inc.)*, 1972]

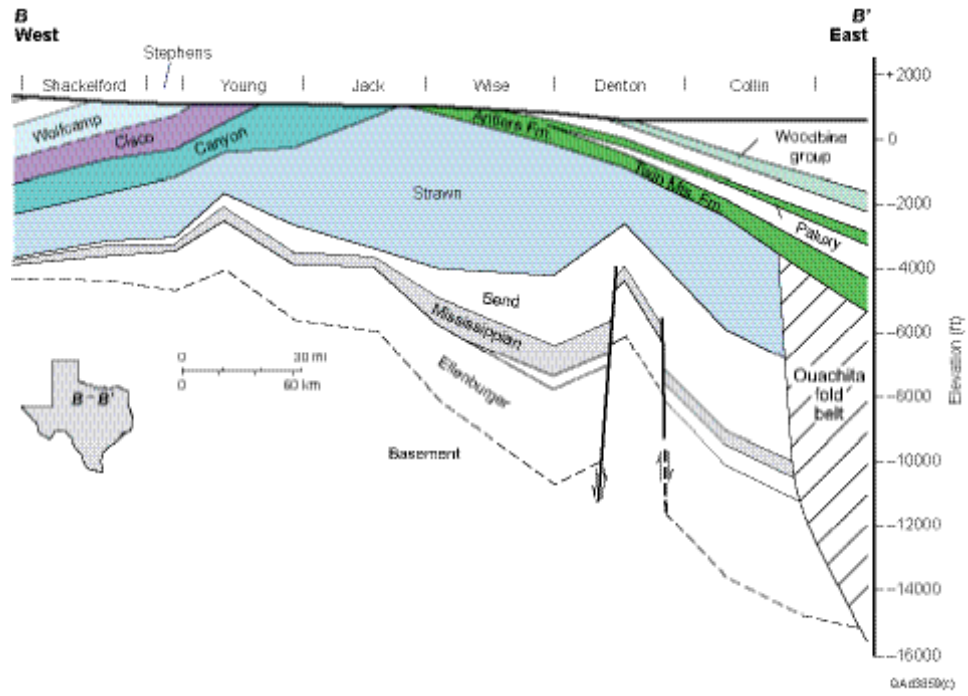


**Figure A3** EW generalized cross-sections through the Fort Worth Basin from *Nicot et al.* [2013].



## A2 Noble Gas Measurement Procedures

The complete measurement procedure for groundwater samples was carried out in the Noble Gas Laboratory at the University of Michigan. Additional sampling, extraction and purification procedures can be found in the literature [Castro *et al.*, 2009; Nicot *et al.*, 2015; Wen *et al.*, 2015a]. Analysis procedures are described briefly below.

After the extraction and purification phases, He and Ne are sequentially allowed to enter a Thermo Scientific® Helix SFT mass spectrometer while Ar, Kr and Xe are sequentially allowed into an ARGUS VI mass spectrometer using a computer-controlled double-head cryo-separator. He and Ne are pumped at ~10K into the low temperature (low-T) chamber of the cryo-separator while Ar, Kr and Xe are pumped at 104K into the high temperature (high-T) chamber of the cryo-separator. The cryo-temperature of both chambers is subsequently increased sequentially to release He, Ne, Ar, Kr, and Xe, at temperatures of 49K, 84K, 210K, 245K, and 290K, respectively. Specifically, at the He release temperature, He is introduced into the SFT mass spectrometer and the signal intensity of  $^4\text{He}$  is determined for the He concentration estimate. This estimate is then used by the automated system to optimize the amount of He that should be introduced for measurement of the  $^3\text{He}/^4\text{He}$  ratio.

Complete measurement procedures involve estimating the concentration of each noble gas component as well measuring He, Ne, Ar, Kr, and Xe isotopic ratios. Standard errors for concentrations are 1.5, 1.3, 1.3, 1.5 and 2.2%, respectively. First, a portion of a known volume of air is introduced into the molecular sieve section of the extraction system, and all noble gases are measured in turn with the Helix SFT and ARGUS VI mass spectrometers. This calibrates the mass spectrometer signal size for each noble gas. Subsequent to the air calibration run, the same measurement procedure is performed on a portion of the unknown sample. All noble gas isotopes

are measured using a Faraday detector, except for  $^3\text{He}$ , which is measured using an electron multiplier in ion counting mode.

**Table A1** Well location and methane concentrations for Trinity Aquifer groundwater samples.

| Sample ID        | Cluster | Depth (m)       | CH <sub>4</sub> (mg/L) |
|------------------|---------|-----------------|------------------------|
| 16               | South   | 46              | 0.60                   |
| 17               | South   | 53              | 0.18                   |
| 30 <sup>a</sup>  | North   | 67              | 0.001 <sup>c</sup>     |
| 31               | North   | 52              | 2.08                   |
| 33 <sup>a</sup>  | North   | 49              | 0.001 <sup>c</sup>     |
| 112              | South   | 91 <sup>b</sup> | 0.74                   |
| 178 <sup>a</sup> | South   | 34              | 0.07                   |
| 179              | South   | 24              | 0.001 <sup>c</sup>     |
| 180              | South   | 98              | 0.01                   |
| 207              | South   | 98              | 0.07                   |
| 211 <sup>a</sup> | South   | 107             | 3.44                   |
| 253              | North   | 107             | 0.001 <sup>c</sup>     |
| 254              | North   | 55              | 0.001 <sup>c</sup>     |
| 255 <sup>a</sup> | North   | 110             | 0.001 <sup>c</sup>     |
| 338 <sup>a</sup> | South   | 134             | 0.12                   |
| 340              | South   | >122            | 0.73                   |
| 347              | South   | 73              | 2.74                   |
| 348 <sup>a</sup> | South   | 55 <sup>b</sup> | 1.76                   |
| 351              | South   | 105             | 0.05                   |
| 354              | South   | 116             | 0.17                   |
| 355              | South   | 61-76           | 12.66                  |
| 356              | South   | 67 <sup>b</sup> | 1.39                   |
| 357 <sup>a</sup> | South   | 73              | 2.06                   |
| 358              | South   | 110             | 18.37                  |
| 364              | South   | 99              | 0.02                   |
| 365              | South   | 107-122         | 0.001 <sup>c</sup>     |
| 367              | South   | >122            | 0.03                   |
| 369              | South   | 91              | 11.90                  |
| 434 <sup>a</sup> | South   | 55 <sup>b</sup> | 4.83                   |
| 446              | South   | 30              | 0.02                   |
| 447              | South   | 30 <sup>b</sup> | 0.67                   |
| 533              | South   | 152             | 18.12                  |
| 534 <sup>a</sup> | South   | 76-85           | 0.03                   |
| 544              | South   | 128             | 0.96                   |
| 555              | South   | 94              | 22.71                  |

<sup>a</sup> Duplicates were collected from these 10 water well sites.

<sup>b</sup> Estimated from water temperature.

<sup>c</sup> Methane concentrations for these samples are below detection limit (0.001 mg/L) but are assumed to be 0.001 mg/L for plotting purposes.

**Table A2** Total and crustal (\*) noble gas isotopic concentrations (cm<sup>3</sup>STP/g<sub>H2O</sub>) for Trinity Aquifer groundwater samples. <sup>a</sup>

| Sample ID | Total <sup>4</sup> He<br>(x10 <sup>-7</sup> ) | Total <sup>20</sup> Ne<br>(x10 <sup>-7</sup> ) | Total <sup>36</sup> Ar<br>(x10 <sup>-6</sup> ) | Total <sup>84</sup> Kr<br>(x10 <sup>-8</sup> ) | Total <sup>132</sup> Xe<br>(x10 <sup>-9</sup> ) | <sup>4</sup> He*<br>(x10 <sup>-7</sup> ) | <sup>21</sup> Ne*<br>(x10 <sup>-12</sup> ) | <sup>40</sup> Ar*<br>(x10 <sup>-7</sup> ) |
|-----------|---|--|--|--|---|--|--|---|
| 16        | 113.460                                       | 2.171  | 1.169  | 4.287  | 2.681   | 112.226±1.693                            | -  | -   |
| 17        | 22.192  | 2.307  | 1.042  | 3.660  | 2.246   | 21.452±0.332                             | -  | -   |
| 30A       | 0.847   | -  | 1.074  | 3.306  | 2.622   | -  | -  | -   |
| 30B       | 0.844   | 1.922  | 1.099  | 3.897  | 2.435   | 0.306±0.021                              | -  | -   |
| 31        | 2.450   | 1.875  | 1.029  | 4.047  | 2.491   | 1.905±0.040                              | 1.567±1.195                                | -   |
| 33A       | 0.780   | 2.734  | 1.324  | 4.622  | 2.893   | -  | -  | -   |
| 33B       | 0.749   | -  | 1.303  | 3.721  | 2.924   | -  | -  | -   |
| 112       | 51.563  | 2.022  | 0.982  | 3.612  | 2.242   | 50.880±0.772                             | -  | -   |
| 178A      | 46.839  | 2.108  | 1.199  | 4.363  | 2.956   | 46.203±0.702                             | 13.135±4.099                               | -   |
| 178B      | 40.890  | 2.118  | 1.128  | 4.249  | 2.622   | 40.256±0.613                             | -  | -   |
| 179       | 6.688   | 3.961  | 1.582  | 4.746  | 2.747   | 5.441±0.100                              | -  | -   |
| 180       | 5.131   | 1.798  | 0.949  | 2.949  | 2.315   | 4.603±0.095                              | 2.849±0.288                                | -   |
| 207       | 68.923  | 2.159  | 1.149  | 4.177  | 2.596   | 68.017±1.029                             | -  | -   |
| 211A      | 161.578                                       | 1.884  | 1.125  | 4.081  | 2.841   | 160.880±2.421                            | 9.594±3.902                                | -   |
| 211B      | 144.314                                       | 1.830  | 1.043  | 3.887  | 2.462   | 143.609±2.162                            | 1.228±0.497                                | -   |
| 253       | 17.662  | 2.007  | 1.089  | 3.968  | 2.465   | 16.771±0.260                             | 1.170±0.607                                | -   |
| 254       | 2.097   | 2.054  | 1.091  | 3.999  | 2.459   | 1.521±0.033                              | -  | -   |
| 255A      | 0.797   | 2.145  | 1.141  | 3.646  | 2.696   | 0.187±0.050                              | -  | -   |
| 255B      | 0.721   | 2.045  | 1.068  | 4.024  | 2.421   | 0.147±0.017                              | -  | -   |
| 338A      | 20.742  | 1.921  | 0.973  | 3.640  | 2.231   | 20.157±0.311                             | -  | -   |
| 338B      | 17.244  | 2.230  | 1.021  | 3.316  | 2.264   | 16.543±0.260                             | -  | -   |
| 340       | 175.756                                       | 2.346  | 1.300  | 4.268  | 3.400   | 174.764±2.632                            | -  | -   |
| 347       | 158.057                                       | 1.809  | 0.997  | 3.731  | 2.423   | 157.245±2.366                            | 2.304±0.606                                | -   |
| 348A      | 84.840  | 2.080  | 1.197  | 4.315  | 2.980   | 84.107±1.270                             | 6.759±5.329                                | -   |
| 348B      | 75.991  | 2.055  | 1.138  | 4.096  | 2.579   | 75.255±1.137                             | 1.320±0.559                                | -   |
| 351       | 27.749  | 1.989  | 1.189  | 4.394  | 3.011   | 27.055±0.414                             | -  | -   |
| 354       | 50.274  | 6.898  | 2.127  | 6.332  | 3.912   | 47.890±0.752                             | -  | -   |

| Sample ID                | Total <sup>4</sup> He<br>(x10 <sup>-7</sup> ) | Total <sup>20</sup> Ne<br>(x10 <sup>-7</sup> ) | Total <sup>36</sup> Ar<br>(x10 <sup>-6</sup> ) | Total <sup>84</sup> Kr<br>(x10 <sup>-8</sup> ) | Total <sup>132</sup> Xe<br>(x10 <sup>-9</sup> ) | <sup>4</sup> He*<br>(x10 <sup>-7</sup> ) | <sup>21</sup> Ne*<br>(x10 <sup>-12</sup> ) | <sup>40</sup> Ar*<br>(x10 <sup>-7</sup> ) |
|--------------------------|---|--|--|--|---|--|--|---|
| 355                      | 221.951                                       | 1.118  | 0.750  | 3.151  | 2.067   | 221.284±3.326                            | -  | 24.031±0.733                              |
| 356                      | 129.050                                       | 1.973  | 1.039  | 3.850  | 2.386   | 128.233±1.933                            | -  | -   |
| 357A                     | 86.351  | 1.639  | 1.138  | 4.285  | 3.066   | 85.763±1.293                             | 14.036±4.471                               | -   |
| 357B                     | 77.394  | 1.559  | 1.020  | 3.180  | 2.729   | 76.841±1.159                             | -  | -   |
| 358                      | 338.724                                       | 0.489  | 0.421  | 2.263  | 1.480   | 337.918±5.075                            | 1.697±0.585                                | 32.916±0.536                              |
| 364                      | 26.067  | 1.883  | 1.131  | 4.322  | 2.822   | 25.163±0.385                             | -  | -   |
| 365                      | 8.334   | 1.904  | 1.072  | 4.059  | 2.541   | 7.778±0.125                              | -  | -   |
| 367                      | 13.838  | 2.169  | 1.146  | 3.590  | 2.598   | 13.149±0.213                             | -  | -   |
| 369                      | 242.641                                       | 1.385  | 0.885  | 3.576  | 2.344   | 241.953±3.636                            | 1.026±0.253                                | 17.856±0.689                              |
| 434A                     | 162.737                                       | 1.976  | 1.138  | 4.135  | 2.795   | 161.962±2.438                            | -  | -   |
| 434B                     | 151.179                                       | 1.917  | 1.046  | 3.956  | 2.476   | 150.395±2.264                            | -  | -   |
| 446                      | 12.532  | 2.037  | 1.128  | 4.104  | 2.572   | 11.903±0.187                             | -  | -   |
| 447                      | 155.929                                       | 2.017  | 1.076  | 4.028  | 2.478   | 154.932±2.333                            | 1.529±0.464                                | -   |
| 533                      | 1400.567                                      | 1.333  | 1.076  | 4.107  | 3.159   | 1398.345±20.982                          | 6.233±0.339                                | 42.064±1.609                              |
| 534A                     | 8.410   | 1.661  | 1.063  | 4.042  | 2.760   | 7.935±0.126                              | 9.019±3.378                                | -   |
| 534B                     | 8.420   | 1.577  | 0.964  | 3.785  | 2.389   | 7.952±0.126                              | -  | -   |
| 544                      | 340.365                                       | 2.101  | 1.220  | 4.370  | 2.940   | 339.208±5.097                            | 14.880±5.673                               | -   |
| 555                      | 235.251                                       | 0.303  | 0.236  | 1.119  | 0.963   | 234.485±3.523                            | 4.341±0.835                                | 33.477±1.226                              |
| ASW (0 °C) <sup>b</sup>  | 0.47  | 1.97   | 1.62   | 6.88   | 5.04  | -  | -  | -   |
| ASW (18 °C) <sup>b</sup> | 0.44  | 1.65   | 1.06   | 4.05   | 2.65  | -  | -  | -   |
| ASW (25 °C) <sup>b</sup> | 0.43  | 1.56   | 0.92   | 3.42   | 2.15  | -  | -  | -   |

<sup>a</sup> Measurement errors of noble gas concentrations are ±1.5%, ±1.3%, ±1.3%, ±1.5%, ±2.2% for <sup>4</sup>He, <sup>20</sup>Ne, <sup>36</sup>Ar, <sup>84</sup>Kr and <sup>132</sup>Xe respectively. All uncertainties are at ±1σ level of confidence.

<sup>b</sup> After Ozima and Podosek [2002].

**Table A3** Noble gas isotopic ratios in the Trinity Aquifer.

| Sample ID | R/Ra        | $^{20}\text{Ne}/^{22}\text{Ne}$ | $^{21}\text{Ne}/^{22}\text{Ne}$ | $^{40}\text{Ar}/^{36}\text{Ar}$ | $^{38}\text{Ar}/^{36}\text{Ar}$ | $^{86}\text{Kr}/^{84}\text{Kr}$ | $^{136}\text{Xe}/^{130}\text{Xe}$ |
|-----------|-------------|---------------------------------|---------------------------------|---------------------------------|---------------------------------|---------------------------------|-----------------------------------|
| 16        | 0.069±0.001 | 9.813±0.006                     | 0.0290±0.0001                   | 295.4±0.1                       | 0.1879±0.0001                   | 0.3032±0.0012                   | 2.194±0.005                       |
| 17        | 0.076±0.002 | 9.806±0.005                     | 0.0290±0.0001                   | 295.4±0.1                       | 0.1878±0.0001                   | 0.3046±0.0012                   | 2.192±0.003                       |
| 30A       | 0.597±0.005 | -                               | -                               | 295.8±0.1                       | 0.1881±0.0002                   | 0.3046±0.0005                   | 2.174±0.009                       |
| 30B       | 0.658±0.007 | 9.859±0.003                     | 0.0290±0.0001                   | 295.5±0.1                       | 0.1880±0.0002                   | 0.3045±0.0009                   | 2.146±0.043                       |
| 31        | 0.329±0.004 | 9.826±0.020                     | 0.0291±0.0001                   | 295.7±0.1                       | 0.1881±0.0001                   | 0.3037±0.0008                   | 2.194±0.005                       |
| 33A       | 0.882±0.007 | 9.805±0.006                     | 0.0290±0.0001                   | 295.9±0.1                       | 0.1880±0.0001                   | 0.3046±0.0004                   | 2.164±0.010                       |
| 33B       | 0.889±0.008 | -                               | -                               | 296.2±0.1                       | 0.1883±0.0002                   | 0.3041±0.0005                   | 2.169±0.009                       |
| 112       | 0.048±0.001 | 9.806±0.006                     | 0.0290±0.0001                   | 295.5±0.1                       | 0.1879±0.0001                   | 0.3048±0.0013                   | 2.194±0.003                       |
| 178A      | 0.042±0.003 | 9.805±0.016                     | 0.0296±0.0002                   | 296.3±0.7                       | 0.1885±0.0009                   | 0.3043±0.0017                   | 2.188±0.012                       |
| 178B      | 0.043±0.001 | 9.833±0.027                     | 0.0291±0.0001                   | 295.6±0.1                       | 0.1879±0.0001                   | 0.3034±0.0007                   | 2.195±0.005                       |
| 179       | 0.245±0.004 | 9.826±0.003                     | 0.0290±0.0001                   | 295.4±0.1                       | 0.1879±0.0001                   | 0.3047±0.0012                   | 2.203±0.003                       |
| 180       | 0.140±0.001 | 9.920±0.003                     | 0.0292±0.0001                   | 296.2±0.1                       | 0.1880±0.0002                   | 0.3043±0.0011                   | 2.174±0.009                       |
| 207       | 0.063±0.001 | 9.812±0.006                     | 0.0290±0.0001                   | 295.1±0.1                       | 0.1877±0.0001                   | 0.3043±0.0013                   | 2.204±0.005                       |
| 211A      | 0.032±0.001 | 9.825±0.024                     | 0.0295±0.0002                   | 296.4±0.6                       | 0.1862±0.0011                   | 0.3061±0.0019                   | 2.192±0.016                       |
| 211B      | 0.035±0.001 | 9.806±0.007                     | 0.0291±0.0001                   | 295.7±0.1                       | 0.1878±0.0001                   | 0.3035±0.0016                   | 2.206±0.004                       |
| 253       | 0.200±0.004 | 9.814±0.009                     | 0.0291±0.0001                   | 295.1±0.1                       | 0.1878±0.0001                   | 0.3040±0.0015                   | 2.199±0.005                       |
| 254       | 0.290±0.002 | 9.787±0.002                     | 0.0290±0.0001                   | 295.1±0.1                       | 0.1879±0.0001                   | 0.3028±0.0009                   | 2.196±0.004                       |
| 255A      | 0.774±0.007 | 9.793±0.013                     | 0.0290±0.0001                   | 295.5±0.1                       | 0.1879±0.0002                   | 0.3043±0.0006                   | 2.173±0.009                       |
| 255B      | 0.823±0.009 | 9.827±0.025                     | 0.0291±0.0001                   | 295.5±0.1                       | 0.1881±0.0001                   | 0.3036±0.0008                   | 2.191±0.005                       |
| 338A      | 0.063±0.002 | 9.769±0.019                     | 0.0289±0.0001                   | 294.9±0.1                       | 0.1877±0.0001                   | 0.3034±0.0007                   | 2.195±0.004                       |
| 338B      | 0.082±0.001 | 9.808±0.010                     | 0.0290±0.0001                   | 294.6±0.1                       | 0.1878±0.0002                   | 0.3043±0.0002                   | 2.166±0.010                       |
| 340       | 0.039±0.001 | 9.789±0.010                     | 0.0290±0.0001                   | 295.2±0.1                       | 0.1882±0.0002                   | 0.3043±0.0003                   | 2.167±0.011                       |
| 347       | 0.039±0.001 | 9.845±0.010                     | 0.0291±0.0001                   | 295.6±0.1                       | 0.1879±0.0001                   | 0.3049±0.0004                   | 2.170±0.009                       |
| 348A      | 0.042±0.002 | 9.813±0.014                     | 0.0293±0.0003                   | 295.1±0.4                       | 0.1875±0.0008                   | 0.3055±0.0015                   | 2.192±0.012                       |
| 348B      | 0.045±0.001 | 9.810±0.007                     | 0.0291±0.0001                   | 295.4±0.1                       | 0.1878±0.0001                   | 0.3035±0.0015                   | 2.202±0.005                       |
| 351       | 0.084±0.003 | 9.827±0.022                     | 0.0291±0.0002                   | 295.2±0.4                       | 0.1859±0.0014                   | 0.3035±0.0012                   | 2.137±0.017                       |
| 354       | 0.108±0.003 | 9.825±0.009                     | 0.0290±0.0002                   | 295.9±0.5                       | 0.1888±0.0010                   | 0.3042±0.0017                   | 2.204±0.013                       |
| 355       | 0.031±0.001 | 9.777±0.002                     | 0.0290±0.0001                   | 298.7±0.1                       | 0.1884±0.0001                   | 0.3030±0.0010                   | 2.194±0.003                       |

| Sample ID        | R/Ra        | $^{20}\text{Ne}/^{22}\text{Ne}$ | $^{21}\text{Ne}/^{22}\text{Ne}$ | $^{40}\text{Ar}/^{36}\text{Ar}$ | $^{38}\text{Ar}/^{36}\text{Ar}$ | $^{86}\text{Kr}/^{84}\text{Kr}$ | $^{136}\text{Xe}/^{130}\text{Xe}$ |
|------------------|-------------|---------------------------------|---------------------------------|---------------------------------|---------------------------------|---------------------------------|-----------------------------------|
| 356              | 0.038±0.001 | 9.799±0.004                     | 0.0290±0.0001                   | 295.0±0.1                       | 0.1876±0.0001                   | 0.3036±0.0007                   | 2.195±0.005                       |
| 357A             | 0.038±0.002 | 9.871±0.043                     | 0.0298±0.0003                   | 295.7±0.8                       | 0.1897±0.0013                   | 0.3050±0.0018                   | 2.191±0.011                       |
| 357B             | 0.038±0.001 | 9.829±0.002                     | 0.0290±0.0001                   | 296.0±0.1                       | 0.1882±0.0002                   | 0.3040±0.0012                   | 2.166±0.009                       |
| 358              | 0.031±0.001 | 9.725±0.030                     | 0.0293±0.0001                   | 303.3±0.1                       | 0.1883±0.0001                   | 0.3039±0.0011                   | 2.183±0.004                       |
| 364              | 0.160±0.003 | 9.791±0.002                     | 0.0290±0.0001                   | 295.4±0.1                       | 0.1881±0.0001                   | 0.3028±0.0009                   | 2.182±0.005                       |
| 365              | 0.113±0.001 | 9.805±0.006                     | 0.0290±0.0001                   | 294.7±0.1                       | 0.1877±0.0001                   | 0.3041±0.0013                   | 2.194±0.004                       |
| 367              | 0.103±0.002 | 9.831±0.002                     | 0.0290±0.0001                   | 294.8±0.1                       | 0.1876±0.0002                   | 0.3042±0.0006                   | 2.166±0.009                       |
| 369              | 0.030±0.001 | 9.787±0.002                     | 0.0291±0.0001                   | 297.5±0.1                       | 0.1881±0.0001                   | 0.3028±0.0011                   | 2.191±0.004                       |
| 434A             | 0.035±0.001 | 9.848±0.026                     | 0.0291±0.0002                   | 295.4±0.5                       | 0.1906±0.0016                   | 0.3032±0.0016                   | 2.202±0.010                       |
| 434B             | 0.037±0.001 | 9.820±0.002                     | 0.0290±0.0001                   | 296.0±0.1                       | 0.1880±0.0001                   | 0.3030±0.0010                   | 2.187±0.004                       |
| 446              | 0.104±0.003 | 9.810±0.006                     | 0.0290±0.0001                   | 295.2±0.1                       | 0.1878±0.0001                   | 0.3043±0.0013                   | 2.194±0.004                       |
| 447              | 0.046±0.001 | 9.822±0.006                     | 0.0291±0.0001                   | 295.4±0.1                       | 0.1877±0.0001                   | 0.3043±0.0013                   | 2.195±0.004                       |
| 533              | 0.030±0.001 | 9.819±0.002                     | 0.0295±0.0001                   | 299.4±0.1                       | 0.1879±0.0002                   | 0.3042±0.0009                   | 2.166±0.011                       |
| 534A             | 0.105±0.003 | 9.831±0.018                     | 0.0295±0.0002                   | 295.7±0.8                       | 0.1883±0.0008                   | 0.3028±0.0017                   | 2.189±0.011                       |
| 534B             | 0.103±0.001 | 9.797±0.002                     | 0.0290±0.0001                   | 295.4±0.1                       | 0.1882±0.0001                   | 0.3027±0.0010                   | 2.196±0.004                       |
| 544              | 0.035±0.002 | 9.810±0.022                     | 0.0297±0.0003                   | 295.4±0.7                       | 0.1888±0.0013                   | 0.3048±0.0017                   | 2.183±0.009                       |
| 555              | 0.035±0.002 | 9.875±0.049                     | 0.0304±0.0003                   | 309.7±0.5                       | 0.1928±0.0014                   | 0.3042±0.0018                   | 2.178±0.011                       |
| Air <sup>a</sup> | 1           | 9.80                            | 0.029                           | 295.5                           | 0.188                           | 0.305                           | 2.176                             |

<sup>a</sup> After *Ozima and Podosek* [2002].

## A3 He Systematics and Individual Helium Component Separation

### A3.1 Helium Systematics

Concentrations of He isotopes ( $^3\text{He}$ ,  $^4\text{He}$ ) in groundwater frequently exceed those expected for water in solubility equilibrium with the atmosphere (air-saturated water: ASW). This excess He can result from different sources: 1) an excess air component resulting from dissolution of small air bubbles caused by fluctuations of the groundwater table [Heaton and Vogel, 1981]; 2) the  $\beta$ -decay of natural background and bomb tritium (tritogenic  $^3\text{He}$ ); 3) the  $^6\text{Li}(n, \alpha)^3\text{H}$  ( $^3\text{He}$ ) reaction (i.e., nucleogenic  $^3\text{He}$ ) [Morrison and Pine, 1955]; 4) the  $\alpha$ -decay of the natural U and Th decay series elements (i.e., radiogenic  $^4\text{He}$ ), and; 5) mantle contributions to both  $^3\text{He}$  and  $^4\text{He}$  [Castro *et al.*, 2009]. Excess He ( $\text{He}_{\text{exc}}$ ) is calculated by removing the ASW ( $\text{He}_{\text{eq}}$ ) and excess air ( $\text{He}_{\text{ea}}$ ) components [Kipfer *et al.*, 2002] from total measured He concentrations ( $\text{He}_{\text{meas}}$ ) in groundwater samples [Stute *et al.*, 1992; Castro *et al.*, 2000].  $\text{He}_{\text{eq}}$  and  $\text{He}_{\text{ea}}$  are estimated following Ballentine and Hall [1999] based on measured dissolved Ne, Ar, Kr and Xe concentrations.

$\text{He}_{\text{exc}}$  comprises both the mantle ( $\text{He}_{\text{m}}$ ) and crustal ( $\text{He}_{\text{c}} = \text{He}_{\text{cin}} + \text{He}_{\text{cext}}$ ) components, where  $\text{He}_{\text{cin}}$  and  $\text{He}_{\text{cext}}$  are produced in-situ within the aquifer and externally at greater depths, respectively [Castro *et al.*, 2000; Ma *et al.*, 2005; Wen *et al.*, 2015b].  $^3\text{He}_{\text{t}}$  is the tritogenic  $^3\text{He}$ .  $^3\text{He}_{\text{exc}}$  is thus given by:

$$\begin{aligned} ^3\text{He}_{\text{exc}} &= ^3\text{He}_{\text{meas}} - ^3\text{He}_{\text{eq}} - ^3\text{He}_{\text{ea}} \\ &= (^4\text{He}_{\text{meas}} \times R_{\text{meas}}) - (^4\text{He}_{\text{eq}} \times R_{\text{eq}}) - (^4\text{He}_{\text{ea}} \times R_{\text{ea}}) \\ &= ^3\text{He}_{\text{cin}} + ^3\text{He}_{\text{cext}} + ^3\text{He}_{\text{m}} + ^3\text{He}_{\text{t}} \end{aligned} \quad (\text{A1})$$

and

$$\begin{aligned} ^4\text{He}_{\text{exc}} &= ^4\text{He}_{\text{meas}} - ^4\text{He}_{\text{eq}} - ^4\text{He}_{\text{ea}} \\ &= ^4\text{He}_{\text{cin}} + ^4\text{He}_{\text{cext}} + ^4\text{He}_{\text{m}} \end{aligned} \quad (\text{A2})$$

$R_{\text{meas}}$  is measured  $^3\text{He}/^4\text{He}$  ratio.  $R_{\text{eq}}$  is the  $^3\text{He}/^4\text{He}$  ratio of water in solubility equilibrium with the atmosphere, i.e.,  $R_{\text{eq}} = 0.983 \times R_a = (1.360 \pm 0.006) \times 10^{-6}$  [Benson and Krause, 1980] and  $R_{\text{ea}}$  is the  $^3\text{He}/^4\text{He}$  ratio of the excess air component [Wen *et al.*, 2015b]. Finally,

$$(R/R_a)_{\text{exc}} = (^3\text{He}_{\text{exc}} / ^4\text{He}_{\text{exc}}) / (^3\text{He}_a / ^4\text{He}_a) \quad (\text{A3})$$

where  $^3\text{He}_a$  and  $^4\text{He}_a$  represent the atmospheric  $^3\text{He}$  and  $^4\text{He}$  abundances, respectively.

The major fraction of the total  $^4\text{He}$  excess is typically of radiogenic (crustal) origin, resulting both from in-situ production and from an external flux. These two contributions are quantified below. Typically, He produced in the crust ( $R_c$ ) results in  $0.02 \leq R_c/R_a \leq 0.05$  [O'Nions and Oxburgh, 1983; Castro, 2004] while mantle-derived He ( $R_m$ ) is typically characterized by  $8 \leq R_m/R_a \leq 50$  [Graham, 2002; Ozima and Podosek, 2002; Starkey *et al.*, 2009]. It should be noted that crustal noble gases are produced both at depth and near the surface and near-surface production can be more significant than crustal production at depth. The amount of crustal production at depth versus near-surface is dependent on the type of formation in question and the amount of parent elements (U, Th) in that particular formation as well as the age of the formation. Thus, a shallow formation that has high concentrations of U and Th might produce more He than a formation that is deeper but that contains lower concentrations of parent elements even though it is older.

A typical way to separate the helium components of a groundwater sample is to plot [Weise and Moser, 1987]:

$$\frac{^3\text{He}_{\text{meas}} - ^3\text{He}_{\text{ea}}}{^4\text{He}_{\text{meas}} - ^4\text{He}_{\text{ea}}} \text{ vs. } \frac{^4\text{He}_{\text{eq}}}{^4\text{He}_{\text{meas}} - ^4\text{He}_{\text{ea}}}$$

Transforming the helium balance equation according to Stute *et al.* [1992], results in a linear equation of the form  $Y = aX + b$ :

$$\underbrace{\frac{{}^3\text{He}_{meas} - {}^3\text{He}_{ea}}{{}^4\text{He}_{meas} - {}^4\text{He}_{ea}}}_Y = \left[ R_{eq} - R_{ter} + \frac{{}^3\text{He}_t}{{}^4\text{He}_{eq}} \right] \underbrace{\frac{{}^4\text{He}_{eq}}{{}^4\text{He}_{meas} - {}^4\text{He}_{ea}}}_X + R_{ter} \quad (\text{A4})$$

where  $R_{ter}$  represents the  ${}^3\text{He}/{}^4\text{He}$  ratio originating from terrigenous sources (crustal and mantle helium). X values vary from 0 to 1 and larger X values indicate that the ASW component is more dominant in the total He concentration, and vice versa. Larger Y values mean more mantle helium or tritiogenic  ${}^3\text{He}$  incorporated into the water. In addition, we define  ${}^3\text{He}_{noea} = {}^3\text{He}_{meas} - {}^3\text{He}_{ea}$ ,  ${}^4\text{He}_{noea} = {}^4\text{He}_{meas} - {}^4\text{He}_{ea}$ , and  $R_{noea} = {}^3\text{He}_{noea}/{}^4\text{He}_{noea}$  for the sake of simplicity in the following analysis. Here  ${}^3\text{He}_{noea}$  and  ${}^4\text{He}_{noea}$  represent measured  ${}^3\text{He}$  and  ${}^4\text{He}$  concentrations for which the excess air component has been subtracted [Castro, 2004].

If the He isotopic data from a specific aquifer represents a two-component mixture, samples plotted in the above fashion will fall along a line. However, plot results using helium data from different aquifers from around the world, including the Great Hungarian Plain [Stute *et al.*, 1992] and the Carrizo aquifer [Castro *et al.*, 2000; Castro, 2004], clearly show that isotope data for most of the samples do not plot on a line. They appear scattered and cannot record a mixture between two components. Rather, these data must reflect a mixture of three or more components, be it from in-situ production, an external crustal origin, a mantle component or a component of tritiogenic origin in very young groundwater.

### ***A3.2 Individual Helium Component Separation***

Following the above descriptions, excess He components ( ${}^3\text{He}_{exc}$  and  ${}^4\text{He}_{exc}$ ) are calculated for all collected shallow groundwater samples (Table A4). While  ${}^3\text{He}$  and  ${}^4\text{He}$  present in most groundwater in sedimentary systems have a dominant crustal origin [Castro *et al.*, 1998a; 1998b; 2000; Kipfer *et al.*, 2002], the presence of a smaller mantle component is not uncommon.

In addition,  ${}^3\text{He}_{\text{exc}}$  can result from background  ${}^3\text{H}$  decay [ $\sim 5$  TU in Texas; *Castro et al.*, 2000] or the decay of bomb  ${}^3\text{H}$  since the nuclear bomb tests took place in the 50's and 60's with the peak of precipitation  ${}^3\text{H}$  ( $\sim 2000$  TU) observed in 1963 within the study area [*IAEA*, 1998]. Here the decay of 1 TU  ${}^3\text{H}$  yields  $2.5 \times 10^{-15}$   $\text{cm}^3\text{STP g}_{\text{H}_2\text{O}}$  of tritiogenic  ${}^3\text{He}$ . These three different He components can be identified based on  $R_{\text{exc}}/\text{Ra}$  values,  ${}^3\text{He}$  and  ${}^4\text{He}$  excesses [*Stute et al.*, 1992; *Castro et al.*, 2000; *Ma et al.*, 2005; *Warrier et al.*, 2012; *Wen et al.*, 2015a; 2015b].

In the analysis that follows we adopt  $0.02 \leq R_c/\text{Ra} \leq 0.05$  as our “reference” crustal value (Figures A5 and A6). Thus,  $R_{\text{exc}}/\text{Ra}$  values greater than the latter strongly suggest the presence of a significant mantle or tritiogenic He contribution. The observed decrease in  $R_{\text{exc}}/\text{Ra}$  values in sampled groundwater is accompanied by an increase in  ${}^3\text{He}_{\text{exc}}$  and  ${}^4\text{He}_{\text{exc}}$  (Table A4; Figure A5). For the north cluster, all groundwater samples except sample 253 (Table A4) display relatively small He excesses ( $<10$  times that of ASW values) with  $0.03 \leq R_{\text{exc}}/\text{Ra} \leq 0.2$  (Table A4). Specifically, sample 33 is entirely of atmospheric origin.  $R_{\text{exc}}/\text{Ra}$  values of north cluster samples 30, 31, 253 and 255 are much greater than typical crustal He values (Figure A6). Thus, these high  $R_{\text{exc}}/\text{Ra}$  values result either from natural or bomb  ${}^3\text{H}$  decay or the addition of a mantle He component. As to groundwater samples in the south cluster, He excesses increase significantly, up to two and three orders of magnitude over ASW concentrations for  ${}^3\text{He}$  and  ${}^4\text{He}$ , respectively, with  $R_{\text{exc}}/\text{Ra}$  values approaching typical crustal values. For all shallow groundwater samples, a clear negative correlation is observed between  $R_{\text{exc}}/\text{Ra}$  values and  ${}^3\text{He}_{\text{exc}}$  (not shown) and  ${}^4\text{He}_{\text{exc}}$  (Table A4; Figure A5). This observed inverse correlation between  $R_{\text{exc}}/\text{Ra}$  and  ${}^3\text{He}_{\text{exc}}$  and  ${}^4\text{He}_{\text{exc}}$  (Figure A5) was also previously observed in multiple aquifers in the Michigan Basin and in the Carrizo Aquifer in southwest Texas [*Castro*, 2004; *Ma et al.*, 2005; *Wen et al.*, 2015b]. This suggests that significant He excesses and, in particular, high crustal He values are found in the

shallow aquifers (e.g, Trinity Aquifer). Below, following Equation (4) and using He systematics, we estimate the contribution of crustal, mantle and atmospheric He components by adopting end-member values of 0.02 for  $R_c/R_a$  and 8 for  $R_m/R_a$ , respectively.

It is apparent from Figure A6 that except for samples 255 and 30B, the bulk of the He excess in most groundwater samples is due to the addition of both nucleogenic (crustal)  $^3\text{He}$  and radiogenic (crustal)  $^4\text{He}$ , with  $^4\text{He}_{\text{eq}}/^4\text{He}_{\text{noea}}$  ratios varying from 0.001 to 0.22 which represent the contribution of ASW  $^4\text{He}$  with respect to total  $^4\text{He}$ . Assuming the complete decay of 5 TU  $^3\text{H}$ , which is likely the maximum limit of background tritium in southwest Texas [*Castro et al.*, 2000],  $1.25 \times 10^{-14}$  cm<sup>3</sup>STP/g<sub>H<sub>2</sub>O</sub> of tritiogenic  $^3\text{He}$  would have been added to these water samples (magenta dashed line, Figure A6). It is apparent that most groundwater samples lie above the line corresponding to 5 TU tritiogenic  $^3\text{He}$  with 0% mantle helium contribution, pointing either to the presence of mantle He or the addition of post-bomb tritiogenic  $^3\text{He}$ . Thus tritiogenic  $^3\text{He}$  in those groundwater samples likely results from both background and post-bomb tritium decay. Samples 30B, 254 and 255 are located between lines corresponding to 0% mantle helium contribution with 0 TU and 5 TU tritiogenic  $^3\text{He}$ , respectively, suggesting that the actual naturally occurring  $^3\text{H}$  background might be lower than 5 TU within the study area.

$R_{\text{noea}}/R_a$  values of samples 253 and 364 are 0.19 and 0.16, higher than those of samples with  $^4\text{He}_{\text{eq}}/^4\text{He}_{\text{noea}}$  ratios less than 0.1. Except for samples 253 and 364, all other samples are located between lines corresponding to 5 TU tritiogenic  $^3\text{He}$  with 0% and 1% mantle He, respectively (Figure A6). If we assume that mantle He is absent in samples 253 and 364, complete decay of  $\sim 200$  TU tritiogenic  $^3\text{H}$  is required to account for the high  $R_{\text{noea}}/R_a$  values in these two samples (black line in Figure A6). Between 1963 (time of the bomb  $^3\text{H}$  peak) and 2014 (year of sampling), about four  $^3\text{H}$  half-lives have elapsed. A rough estimation was performed for

the amount of  $^3\text{H}$  that would be present in the recharge waters of this aquifer when the bomb tests reached their maximum. This simple calculation yields a value of  $\sim 213$  TU, which is much less than the observed  $^3\text{H}$  peak of  $\sim 2000$  TU in Waco, Texas [IAEA, 1998]. An alternative explanation for He signatures in samples 253 and 364 is that only 5 TU tritiogenic  $^3\text{He}$  is present in these two samples with up to 2% mantle derived He (Figure A6). Based on the above discussion, although we cannot exclude the possibility for the presence of a large amount of tritiogenic  $^3\text{He}$  in samples 253 and 364, high amounts of excess He (Figure A5) and the dominance of crustal  $^4\text{He}$  in these two samples strongly suggest that water ages of these two samples are much older than nearby groundwater samples (e.g., samples 30, 255 and 365) leading to the presence of larger amounts of mantle He (up to 2%). This greater mantle He component in samples 253 and 364 suggests the presence of a strong upward leakage of groundwater associated with the subsurface fault system, which is not well understood within the study area. Overall, most helium in the shallow groundwater samples is of crustal origin, with small but non-negligible amounts of tritiogenic and mantle He components in some samples.

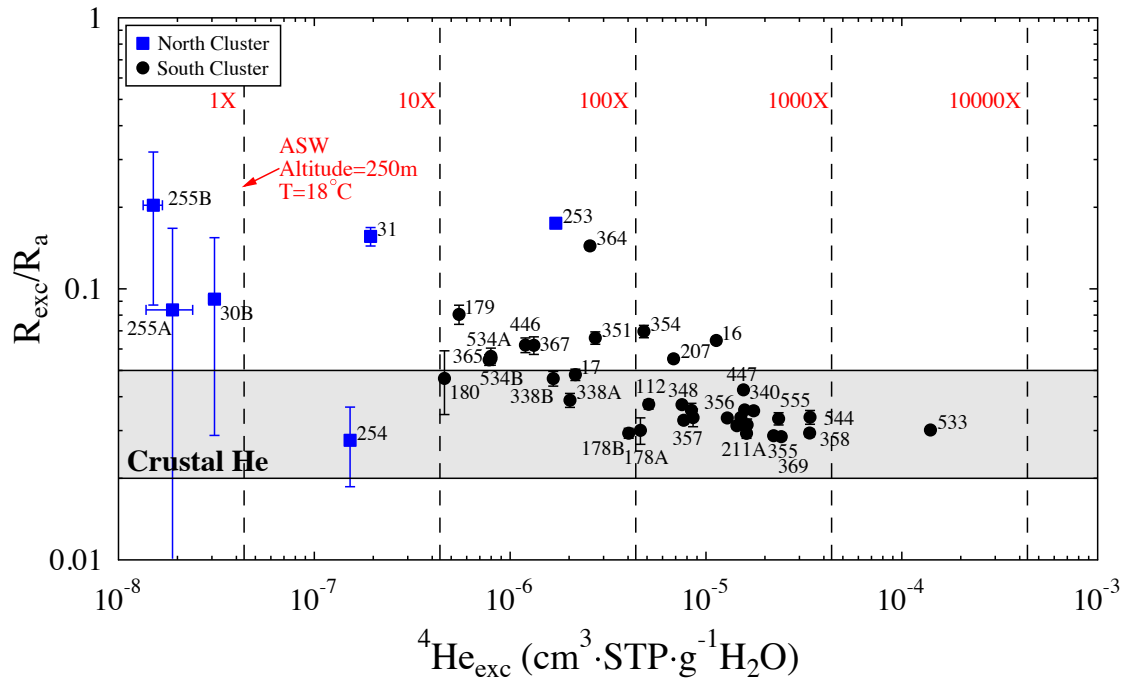


**Figure A5**  $R_{exc}/R_a$  values versus  ${}^4\text{He}_{exc}$  concentrations for the Trinity groundwater samples within the Barnett Shale footprint. Shaded areas indicate typical crustal  $R/R_a$  values (0.02–0.05).

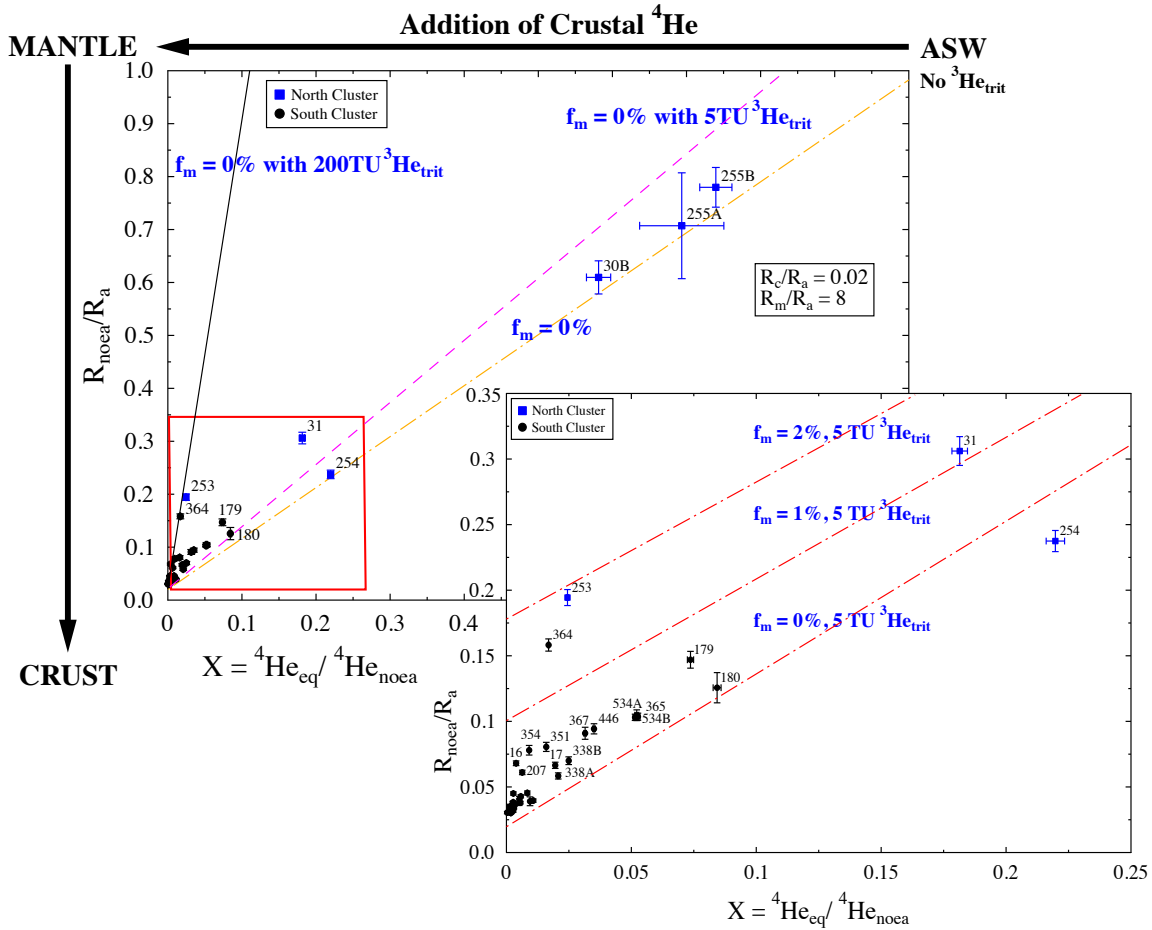


**Figure A6**  $R_{noea}/R_a$  versus  ${}^4\text{He}_{eq}/{}^4\text{He}_{noea}$  for Trinity groundwater samples within the Barnett Shale footprint.  $R/R_a$  values for the crust and the mantle are assumed to be 0.02 and 8, respectively [O'niions and Oxburgh, 1983; Oxburgh et al., 1986; Castro et al., 2000; Graham, 2002; Starkey et al., 2009]. The pre-bomb background tritium concentration in this area of 5 TU is also indicated [Castro et al., 2000]. Lines corresponding to 0%, 1% and 2% mantle helium and 0 TU, 5 TU, and 200 TU tritiogenic He are shown.

**Table A4** He component separation results for Trinity groundwater samples.

| Sample ID | $^3\text{He}_{\text{exc}}$ ( $\times 10^{-13}$ )   | $^4\text{He}_{\text{exc}}$ ( $\times 10^{-6}$ )    | $R_{\text{exc}}/R_a$ |
|-----------|--|--|----------------------|
|           | ( $\text{cm}^3\text{STP/g}_{\text{H}_2\text{O}}$ ) | ( $\text{cm}^3\text{STP/g}_{\text{H}_2\text{O}}$ ) |                      |
| 16        | 10.074±0.231                                       | 11.286±0.170                                       | 0.064±0.002          |
| 17        | 1.437±0.065  | 2.153±0.033  | 0.048±0.002          |
| 30A       | -  | 0.031±0.006  | -                    |
| 30B       | 0.039±0.027  | 0.031±0.002  | 0.092±0.063          |
| 31        | 0.419±0.032  | 0.194±0.004  | 0.156±0.012          |
| 33A       | -  | -  | -                    |
| 33B       | -  | -  | -                    |
| 112       | 2.646±0.097  | 5.099±0.077  | 0.037±0.001          |
| 178A      | 1.924±0.213  | 4.626±0.070  | 0.030±0.003          |
| 178B      | 1.636±0.064  | 4.030±0.061  | 0.029±0.001          |
| 179       | 0.611±0.048  | 0.548±0.010  | 0.080±0.007          |
| 180       | 0.299±0.079  | 0.462±0.009  | 0.047±0.012          |
| 207       | 5.219±0.136  | 6.832±0.103  | 0.055±0.002          |
| 211A      | 6.532±0.251  | 16.107±0.242                                       | 0.029±0.001          |
| 211B      | 6.224±0.149  | 14.381±0.216                                       | 0.031±0.001          |
| 253       | 4.134±0.13   | 1.710±0.027  | 0.175±0.006          |
| 254       | 0.058±0.019  | 0.152±0.003  | 0.028±0.009          |
| 255A      | 0.022±0.069  | 0.019±0.005  | 0.084±0.267          |
| 255B      | 0.042±0.024  | 0.015±0.002  | 0.203±0.116          |
| 338A      | 1.086±0.062  | 2.020±0.031  | 0.039±0.002          |
| 338B      | 1.072±0.065  | 1.660±0.026  | 0.047±0.003          |
| 340       | 8.602±0.235  | 17.510±0.264                                       | 0.035±0.001          |
| 347       | 7.796±0.139  | 15.756±0.237                                       | 0.036±0.001          |
| 348A      | 4.155±0.247  | 8.427±0.127  | 0.036±0.002          |
| 348B      | 3.903±0.103  | 7.542±0.114  | 0.037±0.001          |
| 351       | 2.483±0.125  | 2.721±0.042  | 0.066±0.003          |
| 354       | 4.647±0.233  | 4.819±0.076  | 0.070±0.004          |
| 355       | 8.805±0.201  | 22.153±0.333                                       | 0.029±0.001          |
| 356       | 5.937±0.152  | 12.845±0.194                                       | 0.033±0.001          |
| 357A      | 3.984±0.291  | 8.591±0.130  | 0.034±0.003          |
| 357B      | 3.489±0.092  | 7.696±0.116  | 0.033±0.001          |
| 358       | 13.759±0.405                                       | 33.832±0.508                                       | 0.029±0.001          |
| 364       | 5.096±0.144  | 2.556±0.039  | 0.144±0.005          |
| 365       | 0.591±0.025  | 0.781±0.013  | 0.055±0.002          |
| 367       | 1.133±0.082  | 1.322±0.021  | 0.062±0.005          |
| 369       | 9.550±0.244  | 24.221±0.364                                       | 0.028±0.001          |
| 434A      | 7.074±0.339  | 16.220±0.244                                       | 0.032±0.002          |
| 434B      | 6.989±0.174  | 15.065±0.227                                       | 0.034±0.001          |
| 446       | 1.028±0.062  | 1.197±0.019  | 0.062±0.004          |

| Sample ID | ${}^3\text{He}_{\text{exc}}$ ( $\times 10^{-13}$ ) | ${}^4\text{He}_{\text{exc}}$ ( $\times 10^{-6}$ )  | $R_{\text{exc}}/R_a$ |
|-----------|--|--|----------------------|
|           | ( $\text{cm}^3\text{STP/g}_{\text{H}_2\text{O}}$ ) | ( $\text{cm}^3\text{STP/g}_{\text{H}_2\text{O}}$ ) |                      |
| 447       | 9.118 $\pm$ 0.226                                  | 15.537 $\pm$ 0.234                                 | 0.042 $\pm$ 0.001    |
| 533       | 58.420 $\pm$ 1.402                                 | 140.013 $\pm$ 2.101                                | 0.030 $\pm$ 0.001    |
| 534A      | 0.622 $\pm$ 0.044                                  | 0.797 $\pm$ 0.013                                  | 0.056 $\pm$ 0.004    |
| 534B      | 0.612 $\pm$ 0.021                                  | 0.799 $\pm$ 0.013                                  | 0.055 $\pm$ 0.002    |
| 544       | 15.809 $\pm$ 0.895                                 | 33.979 $\pm$ 0.511                                 | 0.034 $\pm$ 0.002    |
| 555       | 10.788 $\pm$ 0.536                                 | 23.487 $\pm$ 0.353                                 | 0.033 $\pm$ 0.002    |

**Table A5** Isotopic ratios of atmospheric noble gases and chloride concentrations in groundwater samples.

| Sample ID | Cl <sup>-</sup> (mg/L) | <sup>4</sup> He/ <sup>20</sup> Ne | <sup>84</sup> Kr/ <sup>36</sup> Ar | <sup>132</sup> Xe/ <sup>36</sup> Ar | CH <sub>4</sub> / <sup>36</sup> Ar | F( <sup>84</sup> Kr/ <sup>36</sup> Ar) | F( <sup>132</sup> Xe/ <sup>36</sup> Ar) |
|-----------|------------------------|-----------------------------------|------------------------------------|-------------------------------------|------------------------------------|--|---|
|           |                        |                                   | (x10 <sup>-2</sup> )               | (x10 <sup>-3</sup> )                |                                    |  |   |
| 16        | 91.7                   | 52.26±1.04                        | 3.668±0.073                        | 2.294±0.059                         | 724.5±9.4                          | 0.957±0.019                            | 0.915±0.023                             |
| 17        | 662.2                  | 9.62±0.19                         | 3.514±0.070                        | 2.156±0.055                         | 247.0±3.2                          | 0.917±0.018                            | 0.860±0.022                             |
| 30A       | 34.4                   | -                                 | 3.078±0.061                        | 2.442±0.062                         | -                                  | 0.803±0.016                            | 0.974±0.025                             |
| 30B       | 34.4                   | 0.44±0.01                         | 3.547±0.070                        | 2.216±0.057                         | -                                  | 0.925±0.018                            | 0.884±0.023                             |
| 31        | 27.7                   | 1.31±0.03                         | 3.935±0.078                        | 2.422±0.062                         | 2825.1±36.7                        | 1.026±0.020                            | 0.966±0.025                             |
| 33A       | 242.6                  | 0.29±0.01                         | 3.490±0.069                        | 2.184±0.056                         | -                                  | 0.910±0.018                            | 0.871±0.022                             |
| 33B       | 242.6                  | -                                 | 2.857±0.057                        | 2.245±0.057                         | -                                  | 0.745±0.015                            | 0.896±0.023                             |
| 112       | 579.3                  | 25.50±0.51                        | 3.677±0.073                        | 2.282±0.058                         | 1060.5±13.8                        | 0.959±0.019                            | 0.911±0.023                             |
| 178A      | 191.1                  | 22.22±0.44                        | 3.640±0.072                        | 2.466±0.063                         | 82.0±1.1                           | 0.949±0.019                            | 0.984±0.025                             |
| 178B      | 191.1                  | 19.31±0.38                        | 3.767±0.075                        | 2.325±0.059                         | 87.2±1.1                           | 0.983±0.020                            | 0.928±0.024                             |
| 179       | 501.8                  | 1.69±0.03                         | 2.999±0.060                        | 1.736±0.044                         | -                                  | 0.782±0.016                            | 0.693±0.018                             |
| 180       | 425.8                  | 2.85±0.06                         | 3.108±0.062                        | 2.439±0.062                         | 16.9±0.2                           | 0.811±0.016                            | 0.973±0.025                             |
| 207       | 24.8                   | 31.93±0.63                        | 3.636±0.072                        | 2.260±0.058                         | 84.5±1.1                           | 0.948±0.019                            | 0.902±0.023                             |
| 211A      | 32.6                   | 85.75±1.70                        | 3.628±0.072                        | 2.526±0.065                         | 4276.1±55.6                        | 0.946±0.019                            | 1.008±0.026                             |
| 211B      | 32.6                   | 78.84±1.56                        | 3.727±0.074                        | 2.361±0.060                         | 4611.9±60.0                        | 0.972±0.019                            | 0.942±0.024                             |
| 253       | 33.1                   | 8.80±0.17                         | 3.644±0.072                        | 2.264±0.058                         | -                                  | 0.951±0.019                            | 0.903±0.023                             |
| 254       | 54.4                   | 1.02±0.02                         | 3.665±0.073                        | 2.254±0.058                         | -                                  | 0.956±0.019                            | 0.899±0.023                             |
| 255A      | 32.4                   | 0.37±0.01                         | 3.195±0.063                        | 2.362±0.060                         | -                                  | 0.833±0.017                            | 0.942±0.024                             |
| 255B      | 32.4                   | 0.35±0.01                         | 3.768±0.075                        | 2.267±0.058                         | -                                  | 0.983±0.020                            | 0.904±0.023                             |
| 338A      | 15.3                   | 10.80±0.21                        | 3.742±0.074                        | 2.293±0.059                         | 174.6±2.3                          | 0.976±0.019                            | 0.915±0.023                             |
| 338B      | 15.3                   | 7.73±0.15                         | 3.247±0.064                        | 2.216±0.057                         | 166.3±2.2                          | 0.847±0.017                            | 0.884±0.023                             |
| 340       | 16.8                   | 74.91±1.49                        | 3.283±0.065                        | 2.614±0.067                         | 787.2±10.2                         | 0.856±0.017                            | 1.043±0.027                             |
| 347       | 370.7                  | 87.36±1.73                        | 3.743±0.074                        | 2.430±0.062                         | 3847.4±50.0                        | 0.976±0.019                            | 0.970±0.025                             |
| 348A      | 26.8                   | 40.80±0.81                        | 3.605±0.072                        | 2.490±0.064                         | 2059.9±26.8                        | 0.940±0.019                            | 0.994±0.025                             |
| 348B      | 26.8                   | 36.98±0.73                        | 3.600±0.071                        | 2.267±0.058                         | 2166.5±28.2                        | 0.939±0.019                            | 0.904±0.023                             |
| 351       | 22.1                   | 13.95±0.28                        | 3.697±0.073                        | 2.533±0.065                         | 62.6±0.8                           | 0.964±0.019                            | 1.011±0.026                             |
| 354       | 26.8                   | 7.29±0.14                         | 2.977±0.059                        | 1.839±0.047                         | 109.2±1.4                          | 0.777±0.015                            | 0.734±0.019                             |

| Sample ID                | Cl <sup>-</sup> (mg/L) | <sup>4</sup> He/ <sup>20</sup> Ne | <sup>84</sup> Kr/ <sup>36</sup> Ar | <sup>132</sup> Xe/ <sup>36</sup> Ar | CH <sub>4</sub> / <sup>36</sup> Ar | F( <sup>84</sup> Kr/ <sup>36</sup> Ar) | F( <sup>132</sup> Xe/ <sup>36</sup> Ar) |
|--------------------------|------------------------|-----------------------------------|------------------------------------|-------------------------------------|------------------------------------|--|---|
|                          |                        |                                   | (x10 <sup>-2</sup> )               | (x10 <sup>-3</sup> )                |                                    |  |   |
| 355                      | 22.3                   | 198.52±3.94                       | 4.202±0.083                        | 2.756±0.070                         | 23639.5±307.3                      | 1.096±0.022                            | 1.100±0.028                             |
| 356                      | 280.9                  | 65.42±1.30                        | 3.704±0.074                        | 2.296±0.059                         | 1867.2±24.3                        | 0.966±0.019                            | 0.916±0.023                             |
| 357A                     | 25.1                   | 52.67±1.05                        | 3.767±0.075                        | 2.695±0.069                         | 2539.9±33.0                        | 0.983±0.020                            | 1.075±0.027                             |
| 357B                     | 25.1                   | 49.65±0.99                        | 3.117±0.062                        | 2.676±0.068                         | 2832.1±36.8                        | 0.813±0.016                            | 1.067±0.027                             |
| 358                      | 18.5                   | 692.38±13.74                      | 5.379±0.107                        | 3.518±0.090                         | 61111.8±794.5                      | 1.403±0.028                            | 1.404±0.036                             |
| 364                      | 23.5                   | 13.84±0.27                        | 3.823±0.076                        | 2.497±0.064                         | 21.0±0.3                           | 0.997±0.020                            | 0.996±0.025                             |
| 365                      | 25.0                   | 4.38±0.09                         | 3.788±0.075                        | 2.372±0.061                         | -                                  | 0.988±0.020                            | 0.946±0.024                             |
| 367                      | 36.3                   | 6.38±0.13                         | 3.132±0.062                        | 2.267±0.058                         | 38.5±0.5                           | 0.817±0.016                            | 0.904±0.023                             |
| 369                      | 29.5                   | 175.14±3.48                       | 4.041±0.080                        | 2.649±0.068                         | 18832.6±244.8                      | 1.054±0.021                            | 1.057±0.027                             |
| 434A                     | 29.2                   | 82.35±1.63                        | 3.634±0.072                        | 2.456±0.063                         | 5945.2±77.3                        | 0.948±0.019                            | 0.980±0.025                             |
| 434B                     | 29.2                   | 78.85±1.57                        | 3.782±0.075                        | 2.367±0.060                         | 6466.2±84.1                        | 0.987±0.020                            | 0.944±0.024                             |
| 446                      | 30.3                   | 6.15±0.12                         | 3.639±0.072                        | 2.281±0.058                         | 23.8±0.3                           | 0.949±0.019                            | 0.910±0.023                             |
| 447                      | 27.1                   | 77.31±1.53                        | 3.745±0.074                        | 2.304±0.059                         | 876.9±11.4                         | 0.977±0.019                            | 0.919±0.023                             |
| 533                      | 15.6                   | 1051.03±20.86                     | 3.818±0.076                        | 2.937±0.075                         | 23580.5±306.5                      | 0.996±0.020                            | 1.172±0.030                             |
| 534A                     | 24.4                   | 5.06±0.10                         | 3.801±0.075                        | 2.596±0.066                         | 36.1±0.5                           | 0.992±0.020                            | 1.036±0.026                             |
| 534B                     | 24.4                   | 5.34±0.11                         | 3.927±0.078                        | 2.479±0.063                         | 39.8±0.5                           | 1.024±0.020                            | 0.989±0.025                             |
| 544                      | 30.1                   | 161.97±3.22                       | 3.581±0.071                        | 2.409±0.062                         | 1101.8±14.3                        | 0.934±0.019                            | 0.961±0.025                             |
| 555                      | 52.5                   | 776.73±15.42                      | 4.744±0.094                        | 4.084±0.104                         | 134793.5±1752.3                    | 1.237±0.025                            | 1.629±0.042                             |
| ASW (18 °C) <sup>a</sup> | -                      | 0.265                             | 3.834                              | 2.506                               | 32172.6                            | 1                                      | 1                                       |

<sup>a</sup> After *Ozima and Podosek* [2002].

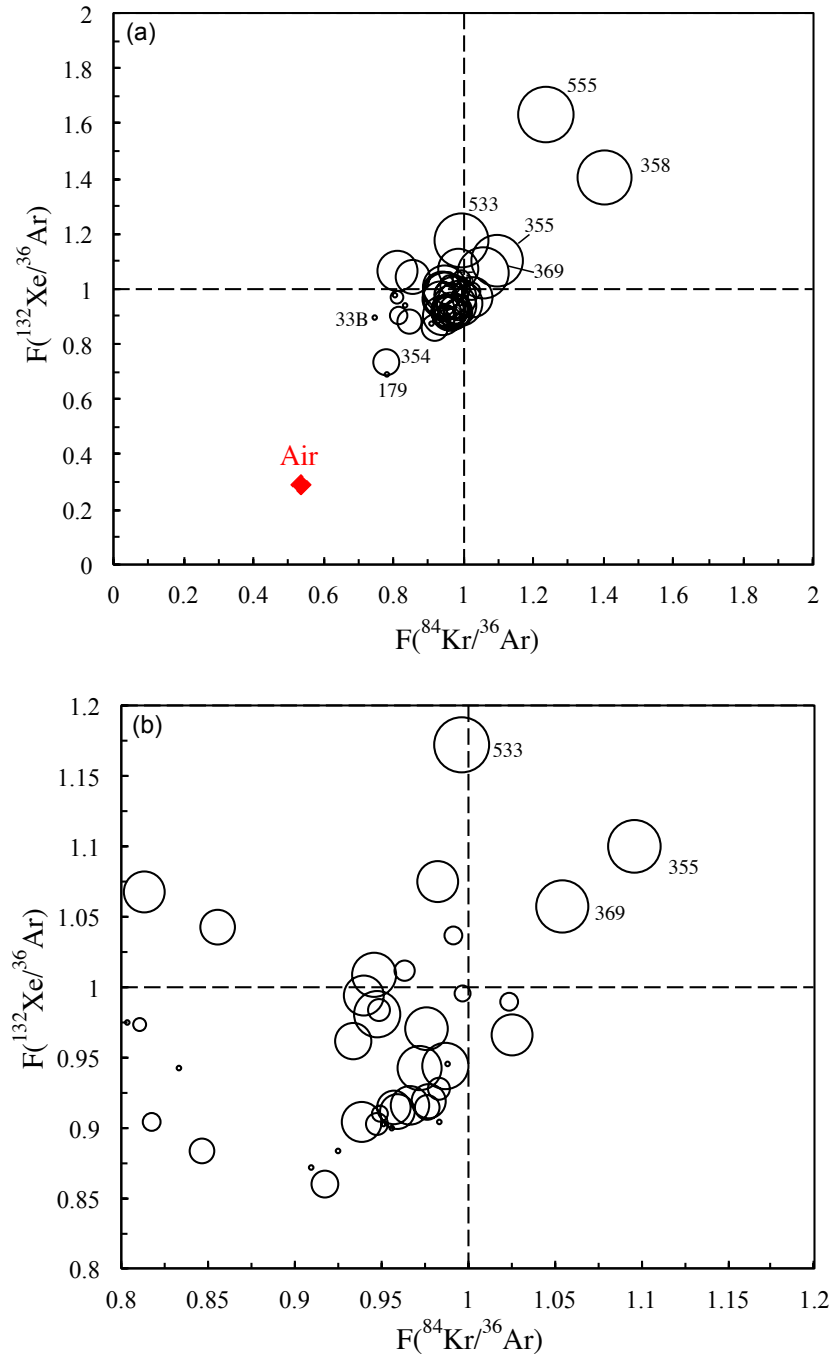


**Figure A7 (a)** Comparison of fractionation  $F$  levels of atmospheric noble gas isotopic ratios  $^{132}\text{Xe}/^{36}\text{Ar}$  versus  $^{84}\text{Kr}/^{36}\text{Ar}$  for all Trinity Aquifer groundwater samples, and **(b)** a close-up of (a).  $^{132}\text{Xe}/^{36}\text{Ar}$  and  $^{84}\text{Kr}/^{36}\text{Ar}$  ratios are normalized to the air saturated water value at 18°C (Table A5). The air value is indicated by a red diamond in (a). Circle sizes are proportional to methane concentrations in water.

#### **A4 Natural Gas Accumulations in the Strawn**

Additional details can be found elsewhere [Nicot *et al.*, 2015]. The presence of many natural gas accumulations in the Strawn in Parker and Hood counties is known although most are not commercially exploited<sup>6</sup>. These natural gas accumulations are able to sustain continuous gas flow in water wells for years if reached as observed with a downhole camera in well 555 during sampling [Nicot *et al.*, 2015]. Although localized gas pockets are limited in volume, it will take years for these pockets to deplete at the observed flow rates. For example, in well 555, during sample collection, a flow rate of 3 L/min (~5MCF/month) was measured. The well, as stated in the main text, was drilled in 2012 and had thus been in operation for 2 years at the time of sampling (2014). During these 2 years, assuming a constant flow rate of 3 L/min (it was left open by the well owner on purpose), ~120 MCF of gas were released. For comparison, the very shallow nearby Center Mill field (~<400 ft) which was exploited for 1 year (1985-1986) through three vertical gas wells produced a total of ~1600 MCF of methane. Assuming our well 555 would have the same amount of gas, ~26 years would be required to deplete or significantly lower the amount of methane present at this rate. Even considering that well 555 would have reached a gas accumulation pocket half the size of Center Mills, ~13 years would still be required to have this gas accumulation significantly depleted. It is also important to note that ~5MCF/month is actually equivalent to the end of life of the Center Mill Strawn wells. Some groundwater well owners made the comment that keeping these bubbling wells open as opposed to plugging them is beneficial to other water wells as the small natural gas accumulation is blown down. They also noted that a bubbling water well and a water well with no or little methane can be very close (<300 ft) even if drilled at the same depth. All these calculations and observations are pointing to localized and shallow sources able to sustain continuous gas flow.

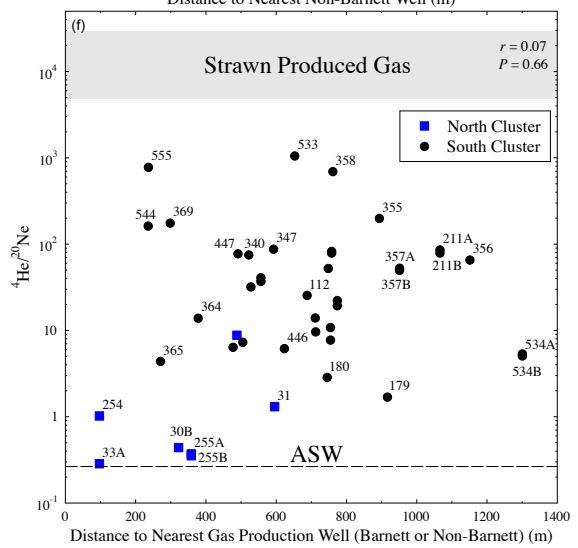
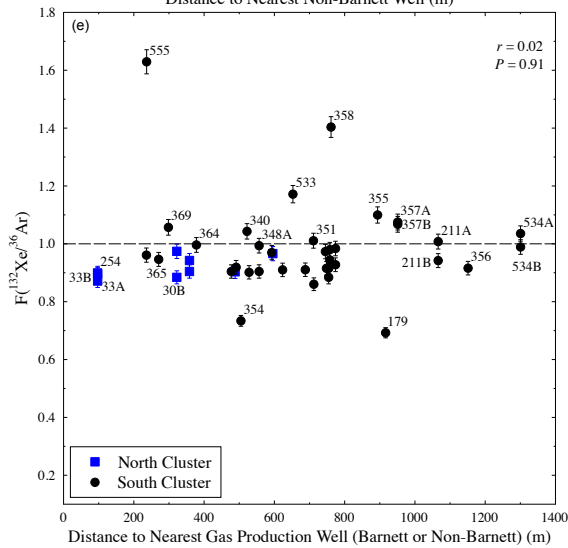
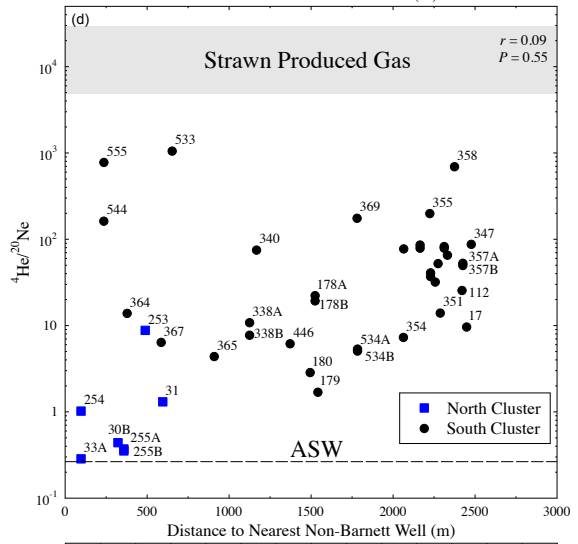
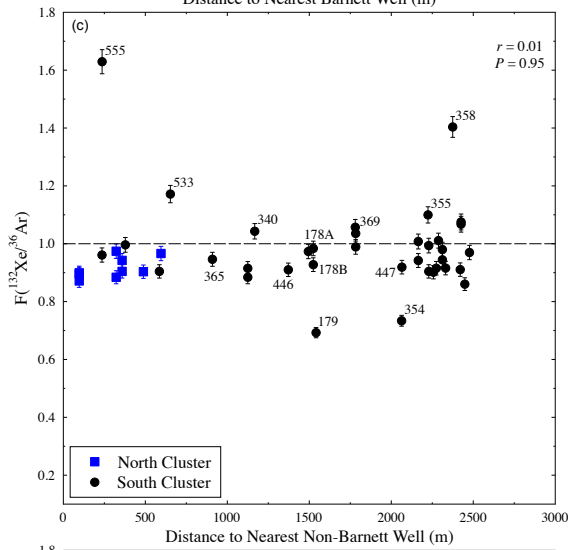
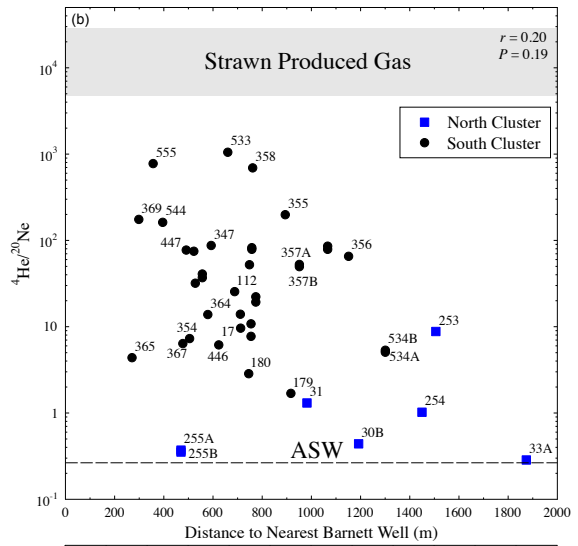
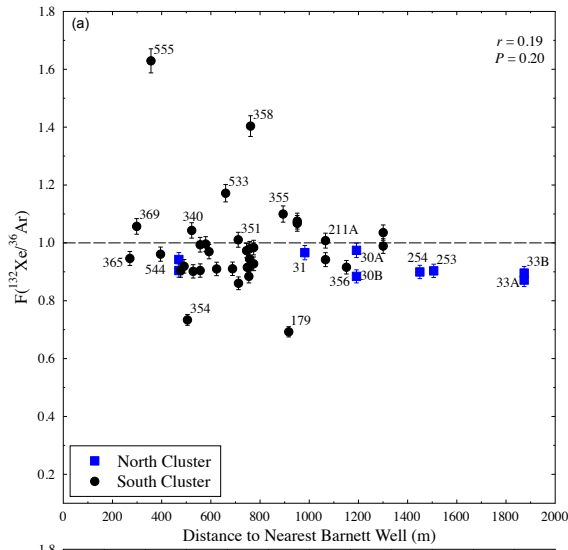


**Figure A8** (a)  $F(^{132}\text{Xe}/^{36}\text{Ar})$  and (b)  $^4\text{He}/^{20}\text{Ne}$  ratios versus distances to nearest Barnett gas well, (c)  $F(^{132}\text{Xe}/^{36}\text{Ar})$  and (d)  $^4\text{He}/^{20}\text{Ne}$  ratios versus distances to nearest non-Barnett gas well, and (e)  $F(^{132}\text{Xe}/^{36}\text{Ar})$  and (f)  $^4\text{He}/^{20}\text{Ne}$  ratios versus distances to nearest production gas well which can be either Barnett or non-Barnett gas wells.  $^4\text{He}/^{20}\text{Ne}$  values for typical Strawn gas [Darrah *et al.*, 2014] and ASW at 18°C are also indicated (gray domain and dashed line).

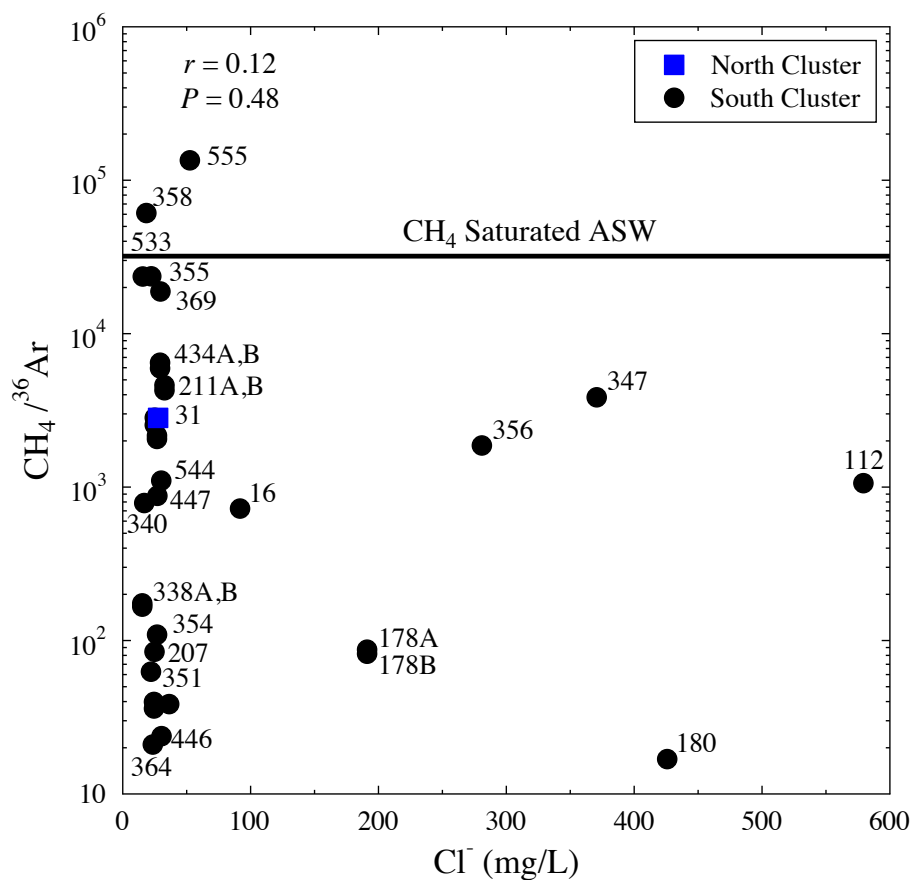


**Figure A9**  $\text{CH}_4 / ^{36}\text{Ar}$  ratios versus  $\text{Cl}^-$  concentrations are plotted for all collected water samples with methane concentrations above 0.001 mg/L in this study.  $\text{CH}_4 / ^{36}\text{Ar}$  value in  $\text{CH}_4$  saturated ASW at 18 °C is also indicated (black solid line).

## A5 References

- Ballentine, C. J., and C. M. Hall (1999), Determining paleotemperature and other variables by using an error-weighted, nonlinear inversion of noble gas concentrations in water, *Geochimica et Cosmochimica Acta*, 63(16), 2315–2336, doi:10.1016/S0016-7037(99)00131-3.
- Benson, B., and D. Krause Jr (1980), Isotopic fractionation of helium during solution: A probe for the liquid state, *J Solution Chem*, 9(12), 895–909–909, doi:10.1007/BF00646402.
- Bruner, K. R., and R. Smosna (2011), *A comparative study of the Mississippian Barnett Shale, Fort Worth Basin, and Devonian Marcellus Shale*, DOE/NETL.
- Castro, M. C. (2004), Helium sources in passive margin aquifers—new evidence for a significant mantle  $^3\text{He}$  source in aquifers with unexpectedly low in situ  $^3\text{He}/^4\text{He}$  production, *Earth and Planetary Science Letters*, 222(3), 897–913, doi:10.1016/j.epsl.2004.03.031.
- Castro, M. C., A. Jambon, G. de Marsily, and P. Schlosser (1998a), Noble gases as natural tracers of water circulation in the Paris Basin: 1. Measurements and discussion of their origin and mechanisms of vertical transport in the basin, *Water Resources Research*, 34(10), 2443–2466, doi:10.1029/98WR01956.
- Castro, M. C., L. Ma, and C. M. Hall (2009), A primordial, solar He–Ne signature in crustal fluids of a stable continental region, *Earth and Planetary Science Letters*, 279(3–4), 174–184, doi:10.1016/j.epsl.2008.12.042.
- Castro, M. C., M. Stute, and P. Schlosser (2000), Comparison of  $^4\text{He}$  ages and  $^{14}\text{C}$  ages in simple aquifer systems: implications for groundwater flow and chronologies, *Applied Geochemistry*, 15(8), 1137–1167, doi:10.1016/S0883-2927(99)00113-4.
- Castro, M. C., P. Goblet, E. Ledoux, S. Violette, and G. de Marsily (1998b), Noble gases as natural tracers of water circulation in the Paris Basin: 2. Calibration of a groundwater flow model using noble gas isotope data, *Water Resources Research*, 34(10), 2467–2483, doi:10.1029/98WR01957.
- CLI (Core Laboratories Inc.) (1972), *A survey of the subsurface saline water of Texas: Texas Water Development Board Report 157*, Austin.
- Darrah, T. H., A. Vengosh, R. B. Jackson, N. R. Warner, and R. J. Poreda (2014), Noble gases identify the mechanisms of fugitive gas contamination in drinking-water wells overlying the Marcellus and Barnett Shales, *Proceedings of the National Academy of Sciences*, 111(39), 14076–14081, doi:10.1073/pnas.1322107111.
- Graham, D. W. (2002), Noble Gas Isotope Geochemistry of Mid-Ocean Ridge and Ocean Island Basalts: Characterization of Mantle Source Reservoirs, *Reviews in Mineralogy and Geochemistry*, 47(1), 247–317, doi:10.2138/rmg.2002.47.8.
- Heaton, T. H. E., and J. C. Vogel (1981), “Excess air” in groundwater, *Journal of Hydrology*,

50(0), 201–216, doi:10.1016/0022-1694(81)90070-6.

Herkommer, M. A., and G. W. Denke (1982), Stratigraphy and hydrocarbons, Parker County, Texas, *Dallas Geological Society*.

IAEA (1998), Global Network for Isotopes in Precipitation, *www.univie.ac.at*. Available from: <http://www.univie.ac.at/cartography/project/wiser/> (Accessed 28 November 1998)

Kipfer, R., W. Aeschbach-Hertig, F. Peeters, and M. Stute (2002), Noble Gases in Lakes and Ground Waters, *Reviews in Mineralogy and Geochemistry*, 47(1), 615–700.

Ma, L., M. C. Castro, C. M. Hall, and L. M. Walter (2005), Cross-formational flow and salinity sources inferred from a combined study of helium concentrations, isotopic ratios, and major elements in the Marshall aquifer, southern Michigan, *Geochemistry Geophysics Geosystems*, 6(10), Q10004, doi:10.1029/2005GC001010.

Morrison, P., and J. Pine (1955), RADIOGENIC ORIGIN OF THE HELIUM ISOTOPES IN ROCK, *Ann NY Acad Sci*, 62(3 Radiogenic Or), 71–92, doi:10.1111/j.1749-6632.1955.tb35366.x.

Nicot, J. P., Y. Huang, B. D. Wolaver, and R. A. Costley (2013), Flow and salinity patterns in the low-transmissivity Upper Paleozoic aquifers of North-Central Texas, *GCAGS Journal*, 2, 53–67.

Nicot, J.-P., P. Mickler, T. Larson, M. C. Castro, R. Darvari, R. Smyth, K. Uhlman, and C. Omelon (2015), *Understanding and Managing Environmental Roadblocks to Shale Gas Development: An Analysis of Shallow Gas, NORM, and Trace Metals*, Research Partnership to Secure Energy for America, Austin, <http://www.rpsea.org/projects/11122-56/>.

O'Nions, R. K., and E. R. Oxburgh (1983), Heat and helium in the Earth, *Nature*, 306(5942), 429–431, doi:10.1038/306429a0.

Oxburgh, E. R., R. K. O'Nions, and R. I. Hill (1986), Helium isotopes in sedimentary basins, *Nature*, 324(6098), 632–635, doi:10.1038/324632a0.

Ozima, M., and F. A. Podosek (2002), *Noble Gas Geochemistry*, Cambridge University Press, New York.

Starkey, N. A., F. M. Stuart, R. M. Ellam, J. G. Fitton, S. Basu, and L. M. Larsen (2009), Helium isotopes in early Iceland plume picrites: Constraints on the composition of high  $^3\text{He}/^4\text{He}$  mantle, *Earth and Planetary Science Letters*, 277(1–2), 91–100.

Stute, M., C. Sonntag, J. Deak, and P. Schlosser (1992), Helium in deep circulating groundwater in the Great Hungarian Plain: Flow dynamics and crustal and mantle helium fluxes, *Geochimica et Cosmochimica Acta*, 56(5), 2051–2067, doi:10.1016/0016-7037(92)90329-H.

- Warrier, R. B., M. C. Castro, and C. M. Hall (2012), Recharge and source-water insights from the Galapagos Islands using noble gases and stable isotopes, *Water Resources Research*, 48(3), W03508–n/a, doi:10.1029/2011WR010954.
- Weise, S., and H. Moser (1987), Groundwater dating with helium isotopes, *Isotope techniques in water resources development. Proc. IAEA symposium, Vienna, 1987, (IAEA; Proceedings Series, STI/PUB/757)*, 105–126.
- Wen, T., M. C. Castro, B. R. Ellis, C. M. Hall, and K. C. Lohmann (2015a), Assessing compositional variability and migration of natural gas in the Antrim Shale in the Michigan Basin using noble gas geochemistry, *Chemical Geology*, 417, 356–370, doi:10.1016/j.chemgeo.2015.10.029.
- Wen, T., M. C. Castro, C. M. Hall, D. L. Pinti, and K. C. Lohmann (2015b), Constraining groundwater flow in the glacial drift and saginaw aquifers in the Michigan Basin through helium concentrations and isotopic ratios, *Geofluids*, 16, 3–25, doi:10.1111/gfl.12133.

## APPENDIX B

### SUPPLEMENTARY MATERIAL FOR CHAPTER 4

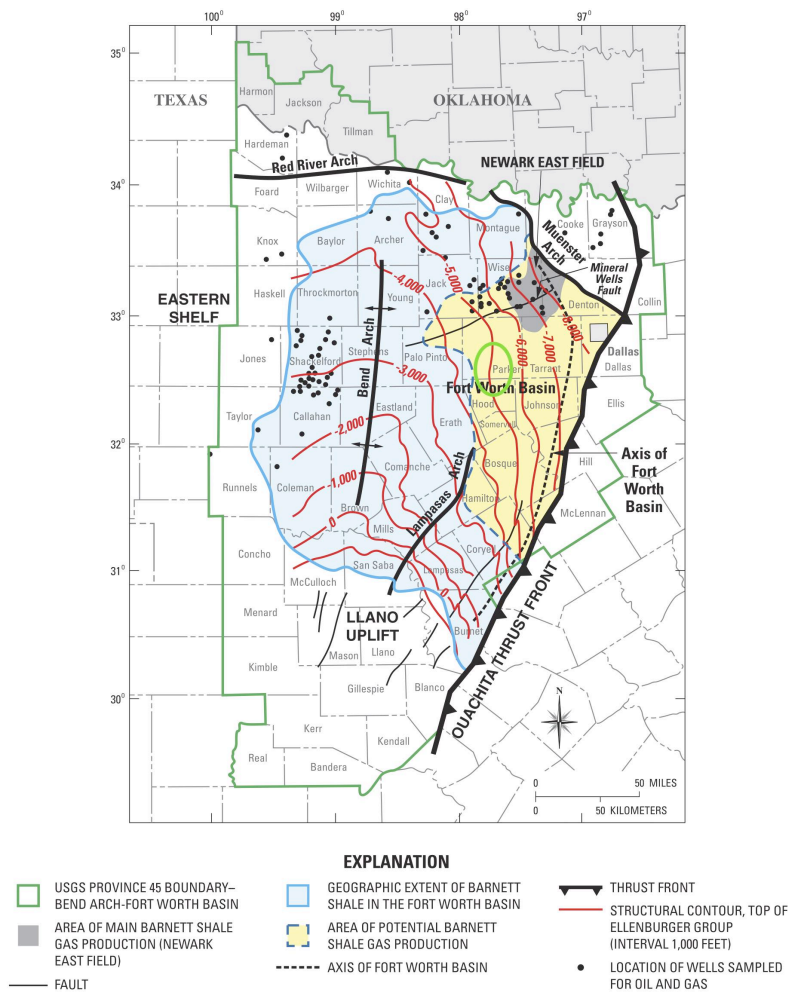


**Figure B1** Map showing extent of the Fort Worth Basin, its major structural features, extent of Mississippian Barnett Shale, and relation to early historical production (so-called “core area”). Contours are drawn on top of the Ordovician Ellenburger Group; contour intervals equal 1,000 feet [adapted from *Bruner and Smosna, 2011*]. Green circle shows the area of study.

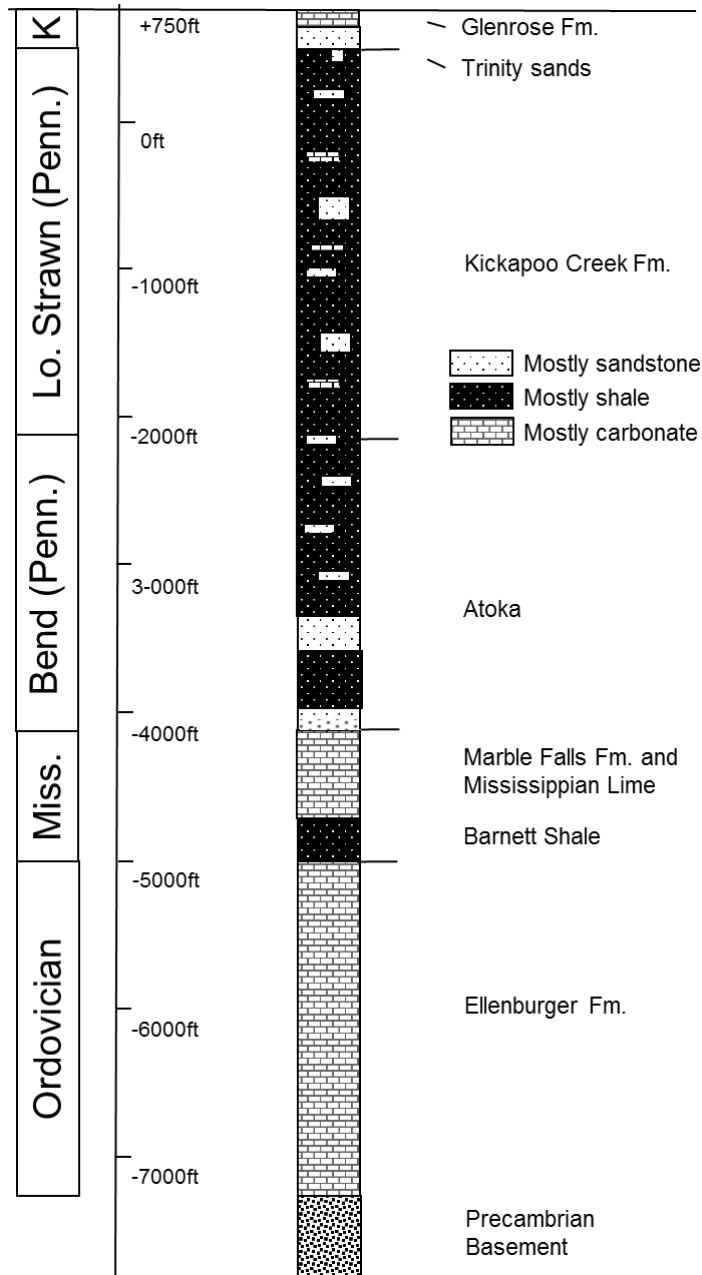


**Figure B2** Generalized local stratigraphic column within the study area in the vicinity of the Parker-Hood county line [data from *Herkommer and Denke*, 1982 and *CLI (Core Laboratories Inc.)*, 1972].

## B1 Noble Gas Measurement Procedures

The complete measurement procedure for gas samples was carried out in the Noble Gas Laboratory at the University of Michigan. Sampling procedures can be found in the literature [Wen *et al.*, 2015]. Extraction, purification, and analysis procedures are described briefly below.

Gas samples in Cu tubes are attached to a vacuum extraction and purification system. The copper tube is connected to a vacuum system at a pressure of  $\sim 2 \times 10^{-5}$  Torr. Once this pressure is achieved and the system isolated from its turbo-molecular vacuum pump, the lower clamp is opened to release the water/natural gas into a low He diffusion glass flask. Gas samples can be inlet into the molecular sieve and the first getter for the removal of water and active gases. Gases from the natural gas sample are subsequently admitted into a cleanup section of the line equipped with the second getter pump to remove the remaining active gases.

After the extraction and purification phases, He and Ne are sequentially allowed to enter a Thermo Scientific® Helix SFT mass spectrometer while Ar, Kr and Xe are sequentially allowed into an ARGUS VI mass spectrometer using a computer-controlled double-head cryo-separator. He and Ne are pumped at  $\sim 10$ K into the low temperature (low-T) chamber of the cryo-separator while Ar, Kr and Xe are pumped at 104K into the high temperature (high-T) chamber of the cryo-separator. The cryo-temperature of both chambers is subsequently increased sequentially to release He, Ne, Ar, Kr, and Xe, at temperatures of 49K, 84K, 210K, 245K, and 290K, respectively. Specifically, at the He release temperature, He is introduced into the SFT mass spectrometer and the signal intensity of  $^4\text{He}$  is determined for the He concentration estimate. This estimate is then used by the automated system to optimize the amount of He that should be introduced for measurement of the  $^3\text{He}/^4\text{He}$  ratio.

Complete measurement procedures involve estimating the volume fraction of each noble gas component as well measuring He, Ne, Ar, Kr, and Xe isotopic ratios. Standard errors for volume fractions are 1.5, 1.3, 1.3, 1.5 and 2.2%, respectively. First, a portion of a known volume of air is introduced into the molecular sieve section of the extraction system, and all noble gases are measured in turn with the Helix SFT and ARGUS VI mass spectrometers. This calibrates the mass spectrometer signal size for each noble gas. Subsequent to the air calibration run, the same measurement procedure is performed on a portion of the unknown sample. All noble gas isotopes are measured using a Faraday detector, except for  $^3\text{He}$ , which is measured using an electron multiplier in ion counting mode.

**Table B1** Sampling date, methane content and depth for groundwater stray gas samples and production gas samples from the Strawn Group and Barnett Shale.

| Sample ID                                     | Sampling Date | Depth (m) | CH <sub>4</sub> (%) |
|---|---------------|-----------|---------------------|
| <i>Stray Gas Samples from Groundwater</i>     |               |           |                     |
| 555G  | 11/03/2014    | 94        | -                   |
| 556G  | 11/03/2014    | 91        | 73.6                |
| <i>Natural Gas Samples from Strawn Group</i>  |               |           |                     |
| SG3   | 01/14/2015    | 544       | 82.1                |
| <i>Natural Gas Samples from Barnett Shale</i> |               |           |                     |
| BG1   | 01/14/2015    | 1908      | 77.5                |
| BG2   | 01/14/2015    | 1899      | 77.6                |
| BG4   | 01/14/2015    | 1858      | 76.5                |
| BG5   | 04/22/2015    | 1591      | 75.1                |
| BG6   | 04/22/2015    | 1807      | 75.3                |
| BG7   | 04/22/2015    | 1985      | 79.4                |
| BG8   | 04/22/2015    | 1980      | 79.7                |
| BG9   | 04/22/2015    | 1910      | 77.2                |

## B2 Calculation of Crustal Noble Gas Components ( $^4\text{He}^*$ , $^{21}\text{Ne}^*$ , $^{40}\text{Ar}^*$ )

R/Ra ratios of all collected gas samples from groundwater wells and Barnett and Strawn gas production wells vary from  $0.0213 \pm 0.0005$  to  $0.0426 \pm 0.0004$  (Table B3), which are within the typical crustal R/Ra production values of 0.02-0.05 [Oxburgh *et al.*, 1986]. Low R/Ra values of all these gas samples suggest dominant crustally produced He, irrespective of the presence of a minor atmospheric or mantle component leading to slightly higher R/Ra values. If He is treated as a mixture between a crustal and an atmospheric component, using a crustal Rc/Ra value of 0.02 and an atmospheric value of 1, crustal He volume fractions can be derived as follows [Ballentine *et al.*, 2002]:

$$^4\text{He}^* = \frac{^4\text{He}_{\text{measured}} \times (\text{Ra} - \text{R}_{\text{measured}})}{\text{Ra} - \text{Rc}} \quad (\text{B1})$$

where subscripts a, c and measured refer to the atmosphere, crust and measured values. Atmospheric Ra equals to  $1.384 \times 10^{-6}$  [Clarke *et al.*, 1976] while crustal value Rc is  $2.768 \times 10^{-8}$ . Crustal He volume fractions of all gas samples in this study are listed in Table B2.

Similarly, Ne and Ar are treated as a two-component mixture, with an atmospheric and a crustal end-member. Crustal  $^{21}\text{Ne}$  and  $^{40}\text{Ar}$  contributions ( $^{21}\text{Ne}^*$ ,  $^{40}\text{Ar}^*$ ) are estimated as follow [Ballentine *et al.*, 2002]:

$$^{21}\text{Ne}^* = ^{21}\text{Ne}_{\text{measured}} \times \left( 1 - \left( \frac{^{21}\text{Ne}}{^{22}\text{Ne}} \right)_{\text{air}} / \left( \frac{^{21}\text{Ne}}{^{22}\text{Ne}} \right)_{\text{measured}} \right) \quad (\text{B2})$$

$$^{40}\text{Ar}^* = ^{40}\text{Ar}_{\text{measured}} \times \left( 1 - \left( \frac{^{40}\text{Ar}}{^{36}\text{Ar}} \right)_{\text{air}} / \left( \frac{^{40}\text{Ar}}{^{36}\text{Ar}} \right)_{\text{measured}} \right) \quad (\text{B3})$$

where  $(^{21}\text{Ne}/^{22}\text{Ne})_{\text{air}} = 0.029$  and  $(^{40}\text{Ar}/^{36}\text{Ar})_{\text{air}} = 295.5$  [Ozima and Podosek, 2002]. Calculated  $^{21}\text{Ne}^*$  and  $^{40}\text{Ar}^*$  are reported in Table B2.

**Table B2** Noble gas volume fractions ( $\text{cm}^3/\text{cm}^3$ ) and corresponding isotopic ratios for groundwater stray gas samples and production gas samples from the Strawn Group and Barnett Shale.

| Sample ID                                     | Total $^4\text{He}$<br>( $\times 10^{-3}$ ) | Total $^{22}\text{Ne}$<br>( $\times 10^{-8}$ ) | Total $^{36}\text{Ar}$<br>( $\times 10^{-7}$ ) | Total $^{84}\text{Kr}$<br>( $\times 10^{-8}$ ) | Total $^{132}\text{Xe}$<br>( $\times 10^{-9}$ ) | $^4\text{He}^*$<br>( $\times 10^{-4}$ ) | $^{21}\text{Ne}^*$<br>( $\times 10^{-11}$ ) | $^{40}\text{Ar}^*$<br>( $\times 10^{-5}$ ) |
|---|---|--|--|--|---|---|---|--|
| <i>Stray Gas Samples from Groundwater</i>     |   |  |  |  |   |   |   |  |
| 555GA   | 4.03  | 8.11   | 20.80  | 5.64   | 2.35  | 39.63±0.59                              | 23.05±0.71                                  | 9.95±0.14                                  |
| 555GB-1                                       | 4.03  | 7.27   | 19.44  | 5.45   | 2.25  | 39.77±0.6                               | 22.17±0.86                                  | 9.81±0.14                                  |
| 555GB-2                                       | 4.37  | 8.69   | 21.85  | 5.92   | 2.43  | 43.09±0.65                              | 24.37±0.68                                  | 10.30±0.14                                 |
| 556GA   | 2.33  | 2.66   | 4.86   | 1.41   | 0.82  | 23.16±0.35                              | 11.15±0.58                                  | 5.83±0.09                                  |
| 556GB   | 2.75  | 0.89   | 3.40   | 0.96   | 0.50  | 27.29±0.41                              | 12.22±1.01                                  | 7.57±0.34                                  |
| <i>Natural Gas Samples from Strawn Group</i>  |   |  |  |  |   |   |   |  |
| SG3-1   | 1.84  | 0.35   | 0.95   | 0.58   | 0.69  | 18.31±0.27                              | 7.45±0.62                                   | 4.82±0.12                                  |
| SG3-2   | 1.84  | 0.29   | 1.03   | 0.59   | 0.67  | 18.34±0.28                              | 8.35±0.57                                   | 4.76±0.09                                  |
| <i>Natural Gas Samples from Barnett Shale</i> |   |  |  |  |   |   |   |  |
| BG1   | 0.64  | 0.40   | 0.69   | 0.45   | 0.67  | 6.28±0.09                               | 1.71±0.48                                   | 1.07±0.05                                  |
| BG2-1   | 0.55  | 2.12   | 2.06   | 0.62   | 0.70  | 5.46±0.08                               | 2.11±0.51                                   | 0.96±0.04                                  |
| BG2-2   | 0.52  | 2.47   | 2.36   | 0.67   | 0.70  | 5.13±0.08                               | 3.03±0.51                                   | 0.90±0.04                                  |
| BG4   | 0.46  | 0.63   | 0.83   | 0.49   | 0.72  | 4.58±0.07                               | 1.00±0.60                                   | 0.27±0.05                                  |
| BG5A  | 0.31  | 41.58  | 47.82  | 6.48   | 2.18  | 3.02±0.05                               | -   | -  |
| BG5B  | 0.19  | 57.17  | 72.01  | 10.22  | 3.23  | 1.82±0.03                               | -   | -  |
| BG6   | 0.54  | 1.02   | 1.32   | 0.51   | 0.67  | 5.4±0.08                                | 1.98±0.12                                   | 0.50±0.01                                  |
| BG7   | 0.46  | 9.09   | 8.83   | 1.10   | 0.56  | 4.51±0.07                               | -   | -  |
| BG8   | 0.64  | 0.21   | 0.34   | 0.37   | 0.70  | 6.29±0.09                               | 1.55±0.13                                   | 1.35±0.02                                  |
| BG9A  | 0.67  | 1.73   | 1.75   | 0.47   | 0.55  | 6.55±0.1                                | 3.39±0.38                                   | 1.22±0.02                                  |
| BG9B  | 0.60  | 2.86   | 3.14   | 1.21   | 1.28  | 5.84±0.09                               | 3.40±0.17                                   | 0.93±0.01                                  |
| Air a   | 0.005                                       | 167.80   | 314.20   | 64.98  | 23.39   | -                                       | -   | -  |

<sup>a</sup> Ozima and Podosek [2002]

**Table B3** Noble gas isotopic ratios for groundwater stray gas samples and production gas samples from the Strawn Group and Barnett Shale.

| Sample ID                                     | R/Ra          | <sup>20</sup> Ne/ <sup>22</sup> Ne | <sup>21</sup> Ne/ <sup>22</sup> Ne | <sup>38</sup> Ar/ <sup>36</sup> Ar | <sup>40</sup> Ar/ <sup>36</sup> Ar | <sup>86</sup> Kr/ <sup>84</sup> Kr | <sup>136</sup> Xe/ <sup>130</sup> Xe |
|---|---------------|------------------------------------|------------------------------------|------------------------------------|------------------------------------|------------------------------------|--------------------------------------|
| <i>Stray Gas Samples from Groundwater</i>     |               |                                    |                                    |                                    |                                    |                                    |                                      |
| 555GA   | 0.0363±0.0007 | 9.806±0.012                        | 0.0318±0.0001                      | 0.1883±0.0004                      | 343.36±0.19                        | 0.3060±0.0004                      | 2.167±0.009                          |
| 555GB-1                                       | 0.0333±0.0006 | 9.795±0.018                        | 0.0321±0.0001                      | 0.1881±0.0007                      | 345.97±0.29                        | 0.3053±0.0005                      | 2.153±0.014                          |
| 555GB-2                                       | 0.0333±0.0006 | 9.837±0.014                        | 0.0318±0.0001                      | 0.1884±0.0005                      | 342.66±0.22                        | 0.3046±0.0010                      | 2.175±0.010                          |
| 556GA   | 0.0266±0.0004 | 10.021±0.012                       | 0.0332±0.0002                      | 0.1864±0.0021                      | 415.54±1.07                        | 0.3053±0.0003                      | 2.103±0.044                          |
| 556GB   | 0.0278±0.0010 | 9.880±0.381                        | 0.0427±0.0010                      | 0.1938±0.0030                      | 517.74±5.01                        | 0.3095±0.0022                      | 2.057±0.057                          |
| <i>Natural Gas Samples from Strawn Group</i>  |               |                                    |                                    |                                    |                                    |                                    |                                      |
| SG3-1   | 0.0231±0.0003 | 9.634±0.026                        | 0.0502±0.0017                      | 0.1826±0.0113                      | 803.66±11.03                       | 0.3062±0.0012                      | 2.175±0.020                          |
| SG3-2   | 0.0213±0.0005 | 9.550±0.020                        | 0.0582±0.0020                      | 0.1801±0.0068                      | 755.89±6.56                        | 0.3065±0.0011                      | 2.173±0.020                          |
| <i>Natural Gas Samples from Barnett Shale</i> |               |                                    |                                    |                                    |                                    |                                    |                                      |
| BG1   | 0.0337±0.0008 | 10.085±0.020                       | 0.0333±0.0012                      | 0.1794±0.0133                      | 451.59±7.42                        | 0.3067±0.0013                      | 2.173±0.018                          |
| BG2-1   | 0.0348±0.0004 | 10.280±0.015                       | 0.0300±0.0002                      | 0.1792±0.0040                      | 342.21±1.96                        | 0.3050±0.0011                      | 2.160±0.019                          |
| BG2-2   | 0.0320±0.0005 | 10.317±0.014                       | 0.0302±0.0002                      | 0.1829±0.0037                      | 333.54±1.64                        | 0.3041±0.0014                      | 2.160±0.020                          |
| BG4   | 0.0215±0.0004 | 10.003±0.016                       | 0.0306±0.0009                      | 0.1847±0.0128                      | 327.74±6.21                        | 0.3073±0.0012                      | 2.167±0.018                          |
| BG5A  | 0.0383±0.0007 | 10.205±0.016                       | 0.0297±0.0001                      | 0.1840±0.0001                      | 288.62±0.06                        | 0.3034±0.0014                      | 2.149±0.004                          |
| BG5B  | 0.0421±0.0008 | 10.123±0.008                       | 0.0295±0.0001                      | 0.1842±0.0001                      | 287.50±0.04                        | 0.3029±0.0008                      | 2.151±0.002                          |
| BG6   | 0.0205±0.0005 | 10.335±0.012                       | 0.0309±0.0001                      | 0.1848±0.0005                      | 333.09±0.23                        | 0.3043±0.0022                      | 2.161±0.004                          |
| BG7   | 0.0334±0.0005 | 10.289±0.009                       | 0.0298±0.0001                      | 0.1829±0.0001                      | 294.49±0.05                        | 0.3037±0.0009                      | 2.159±0.003                          |
| BG8   | 0.0344±0.0005 | 10.020±0.067                       | 0.0364±0.0006                      | 0.1904±0.0019                      | 695.06±2.04                        | 0.3016±0.0018                      | 2.185±0.004                          |
| BG9A  | 0.0426±0.0004 | 10.322±0.025                       | 0.0310±0.0002                      | 0.1877±0.0015                      | 365.04±0.57                        | 0.3025±0.0021                      | 2.165±0.005                          |
| BG9B  | 0.0385±0.0005 | 10.323±0.017                       | 0.0302±0.0001                      | 0.1838±0.0002                      | 325.12±0.12                        | 0.3029±0.0017                      | 2.173±0.004                          |
| Air <sup>a</sup>                              | 1             | 9.80                               | 0.029                              | 0.188                              | 295.5                              | 0.305                              | 2.176                                |

<sup>a</sup> Ozima and Podosek [2002]

### B3 Mass-Dependent Fractionation (MDF) in Barnett Gas Samples

In Figure B3a Barnett gas samples are divided into two groups: 1) BG1, BG2, BG4, BG6, BG8, and BG9 have higher  $^{20}\text{Ne}/^{22}\text{Ne}$  and  $^{21}\text{Ne}/^{22}\text{Ne}$  values than ASW reflecting a three-component mixing between the atmosphere, the crust, and the mantle and; 2) BG5A, BG5B, and BG7 fall on the mass dependent fractionation line (MFL; blue dashed line in Figure B3a) [see also *Matsumoto et al.*, 2004] suggesting that the original noble gas isotopic ratios of these three samples have been modified due to the severe air contamination followed by mass dependent fractionation (MDF).

Because molecular diffusion is the mechanism with the greatest potential to create fractionation between the different isotopes [*Marty et al.*, 1988; *Castro et al.*, 2009], when referring to mass fractionation above, we implicitly refer to fractionation due to molecular diffusion. Fractionated noble gas isotopic ratios or elemental ratios in escaped and retained phases after molecular diffusion can be estimated as follow [*Matsumoto et al.*, 2004]:

$$\left(\frac{i}{j}\right)_{retained} = \left(\frac{i}{j}\right)_{initial} \times f^{\sqrt{\frac{M_j}{M_i}} - 1} \quad (\text{B4})$$

$$\left(\frac{i}{j}\right)_{escaped} = \left(\frac{i}{j}\right)_{initial} \times \frac{1-f^{\sqrt{\frac{M_j}{M_i}}}}{1-f} \quad (\text{B5})$$

where subscripts retained, escaped and initial refer to the noble gas isotopic ratios (or elemental ratios) in the retained, escaped and initial phases.  $i$  and  $j$  represent noble gas isotopes (e.g.,  $^{20}\text{Ne}$ ,  $^{22}\text{Ne}$ ,  $^{36}\text{Ar}$ ,  $^{38}\text{Ar}$ ) while  $M_i$  and  $M_j$  represent the mass of isotope.  $f$  stands for the fraction of isotope  $j$  in the retained phase.

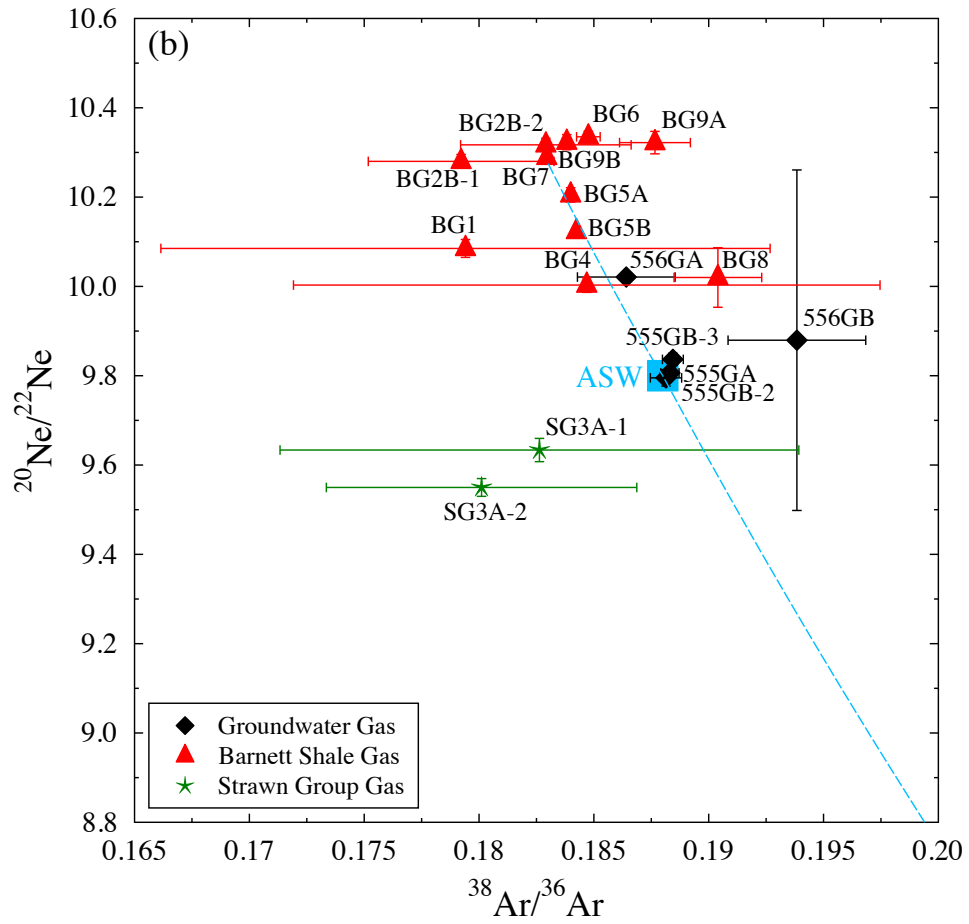
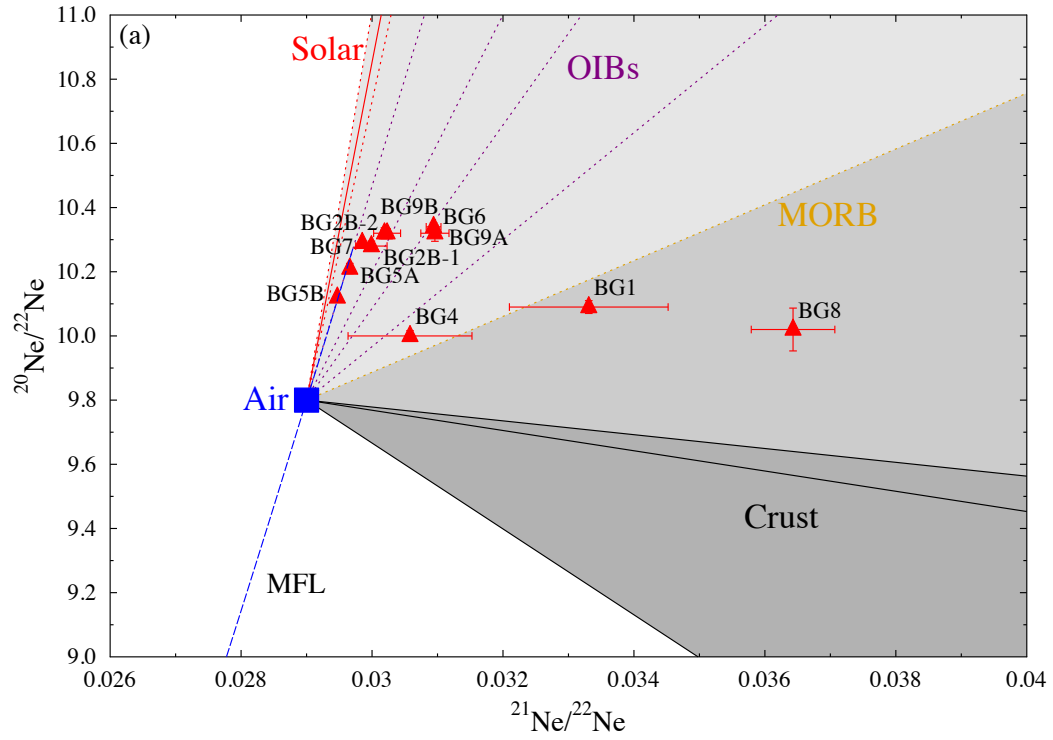
From Figure B3b, it can be seen that Barnett gas samples with highest  $^{20}\text{Ne}/^{22}\text{Ne}$  ratios (e.g., BG9A, BG6) have  $^{38}\text{Ar}/^{36}\text{Ar}$  ratios similar to the air value (0.188) and fall above the MDF

line (light blue dashed line) passing through the ASW value [Matsumoto *et al.*, 2004], ruling out the possibility of single or multiple stages of MDF. Furthermore,  $^{22}\text{Ne}$  and  $^{36}\text{Ar}$  volume fractions of most Barnett gas samples, except for samples BG5A, BG5B and BG7, are significantly lower than those in the air (Table B2), which suggests these Barnett gas samples have been well preserved during sample collection and storage prior to laboratory analysis. Samples BG5A, BG5B and BG7 fall on the MDF line calculated after Matsumoto *et al.* [2004] assuming noble gas isotopes diffuse from ASW into the gas phase (Figure B3b). This mass dependent fractionation generates higher  $^{20}\text{Ne}/^{22}\text{Ne}$  ratios in an escaped phase and complementary lower  $^{20}\text{Ne}/^{22}\text{Ne}$  ratios in the residual phase [Matsumoto *et al.*, 2004]. In contrast,  $^{38}\text{Ar}/^{36}\text{Ar}$  ratios increase in the residual phase but decrease in the escaped phase relative to the ASW value.

In addition to mass dependent fractionation, the addition of crustal noble gas isotopes (e.g.,  $^{40}\text{Ar}^*$ ) will also alter the original ASW noble gas signatures (e.g.,  $^{40}\text{Ar}/^{36}\text{Ar}$ ). To compare the impact of MDF and crustal component on noble gas isotopic ratios (e.g.,  $^{40}\text{Ar}/^{36}\text{Ar}$ ), we plot  $^{20}\text{Ne}/^{22}\text{Ne}$  versus  $^{40}\text{Ar}/^{36}\text{Ar}$  ratios for all collected gas samples (Figure B3c). As you can see, samples BG5A, BG5B and BG7 fall on the MDF line (light blue dashed line) passing through ASW values, which again indicates that these three samples have gone through severe air contamination followed by mass dependent fractionation. However, most Barnett gas samples display much higher  $^{40}\text{Ar}/^{36}\text{Ar}$  ratios compared to predicted  $^{40}\text{Ar}/^{36}\text{Ar}$  values following MDF (Figure B3c). Therefore, compared to the addition of  $^{40}\text{Ar}^*$ , the impact of MDF on  $^{40}\text{Ar}/^{36}\text{Ar}$  ratios of most Barnett gas samples is negligible (e.g., BG1, BG8) or minor (e.g., BG6).

Unlike noble gas isotopic ratios, noble gas elemental ratios (e.g.,  $^{22}\text{Ne}/^{36}\text{Ar}$ ) will be influenced not only by diffusion-controlled processes but also solubility-controlled processes in a two-phase or multi-phase system. The impact of diffusion-controlled processes on noble gas

elemental ratios can be evaluated through equations (4) and (5). Noble gas solubility in water increases with mass with  $\text{Ne} < \text{Ar} < \text{Kr} < \text{Xe}$ . For a two-phase (i.e., water and gas) system, assuming that all noble gases are initially in the water phase and equilibrated with air, solubility-controlled fractionation will lead  $^{22}\text{Ne}/^{36}\text{Ar}$  to increase in the escaped gas phase while decreasing in the retained water phase. Additional details about solubility-controlled noble gas fractionation can be found in Text B5. In Figure B3d, we compare  $^{20}\text{Ne}/^{22}\text{Ne}$  and  $^{22}\text{Ne}/^{36}\text{Ar}$  ratios of our gas samples with predicted values for two scenarios: (1) noble gases are fractionated from ASW without excess air (light blue dashed line) and (2) noble gases are fractionated from ASW with a large amount of excess air (assuming that the noble gas composition in ASW mimic that of air; blue dashed line in Figure B3d). It is clear that most Barnett gas samples display much higher  $^{22}\text{Ne}/^{36}\text{Ar}$  ratios than predicted ratios following MDF. If diffusion were the only fractionating mechanism, the fractionated  $^{20}\text{Ne}/^{22}\text{Ne}$  values of Barnett gas would be far larger than observed for the magnitude of fractionation that occurs in  $^{22}\text{Ne}/^{36}\text{Ar}$ . The dominant fractionation in elemental ratios (i.e.,  $^{22}\text{Ne}/^{36}\text{Ar}$ ) is therefore a solubility-controlled process. Expanded discussion about this solubility-controlled process can be found in Text B5.



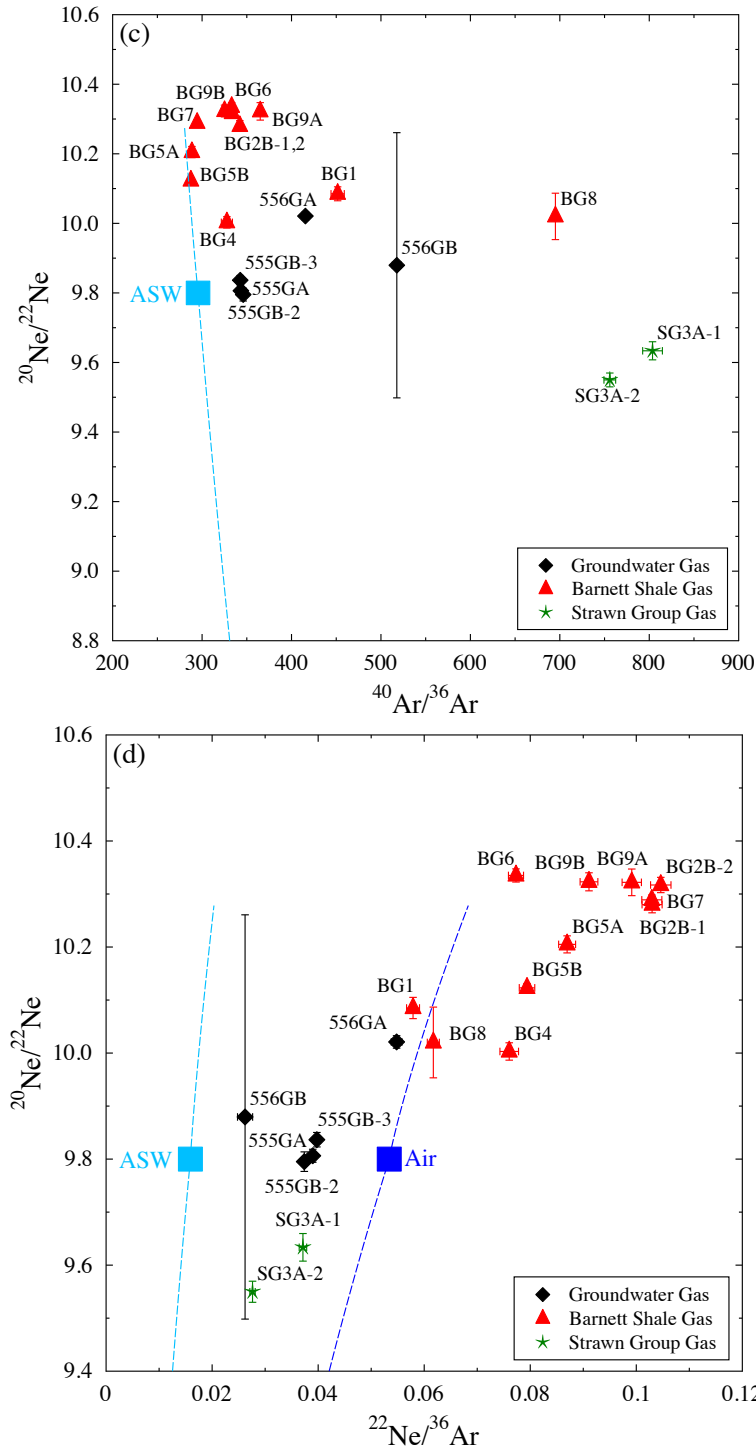


**Figure B3**  $^{20}\text{Ne}/^{22}\text{Ne}$  as a function of (a)  $^{21}\text{Ne}/^{22}\text{Ne}$ , (b)  $^{38}\text{Ar}/^{36}\text{Ar}$ , (c)  $^{40}\text{Ar}/^{36}\text{Ar}$ , and (d)  $^{22}\text{Ne}/^{36}\text{Ar}$  for all gas samples. Calculated ratios in the escaped gas phase following mass-dependent fractionation [Matsumoto *et al.*, 2004] are shown for two scenarios: (1) ASW at 18 °C (light blue dashed line) and (2) air (blue dashed line). In (a), mixing lines (Air-Solar, Air-MORB [mid-ocean ridge basalt], Air-OIBs [ocean island basalt], and Air-Crust) are indicated for previously reported values as summarized in Castro *et al.* [2009].

#### B4 Neon (Ne) Systematics

In subsurface fluids (e.g., natural gas and groundwater), crustal Ne is generally dominant due to production of nucleogenic  $^{21}\text{Ne}$ , which results mainly from reactions between  $\alpha$  particles from U-Th decay and O and Mg atoms in the crust [Wetherill, 1954; Hilton and Porcelli, 2003]. Production of nucleogenic  $^{20}\text{Ne}$  and  $^{22}\text{Ne}$  in the crust which occurs mostly through nuclear reactions  $^{17}\text{O}(\alpha,p)^{20}\text{Ne}$  and  $^{23}\text{Na}(n,\alpha)^{20}\text{Ne}$  for  $^{20}\text{Ne}$  and  $^{19}\text{F}(\alpha,n)^{22}\text{Ne}$ ,  $^{19}\text{F}(\alpha,p)^{22}\text{Ne}$ , and  $^{25}\text{Mg}(n,\alpha)^{22}\text{Ne}$  for  $^{22}\text{Ne}$  [Wetherill, 1954] is typically negligible. When in excess with respect to ASW (air saturated water) values,  $^{20}\text{Ne}$  typically has a mantle origin. Because the  $^{22}\text{Ne}$  nuclear production rate is far more pronounced in the crust than that of  $^{20}\text{Ne}$  [Wetherill, 1954; Ballentine and Burnard, 2002], when crustal production of these two isotopes takes place and dominates, it leads to an extremely small  $^{20}\text{Ne}/^{22}\text{Ne}$  ratio of  $\sim 0.3$  [Yatsevich and Honda, 1997], a value that is far smaller than that of air [9.8; Ozima and Podosek, 2002].

## B5 Solubility-Controlled Noble Gas Fractionation

As discussed in Text B3, diffusion-controlled fractionation alone is not enough to account for observed  $^{22}\text{Ne}/^{36}\text{Ar}$  ratios in Barnett gas samples. Here, we explore processes that might account for high  $^{22}\text{Ne}/^{36}\text{Ar}$  ratios in Barnett gas samples. We start by defining modeling conditions and solubility of noble gases in various phases (i.e., gas, water, oil). Two models which apply to our physical system are considered and briefly introduced, describing solubility-controlled processes in a multi-phase (water-gas and water-gas-oil) system.

$^{22}\text{Ne}$ ,  $^{36}\text{Ar}$ ,  $^{84}\text{Kr}$ , and  $^{132}\text{Xe}$  in sedimentary systems (e.g., the Barnett Shale) is almost entirely of atmospheric origin [Ozima and Podosek, 2002].  $^{22}\text{Ne}$ ,  $^{36}\text{Ar}$ ,  $^{84}\text{Kr}$ , and  $^{132}\text{Xe}$  contents of all gases in this study are assumed to originate from ASW at 18 °C at an elevation of 274 m, i.e., modern mean annual air temperature and average elevation of all sampled wells in this study. Under these conditions, atmospheric noble gas ratios (e.g.,  $^{22}\text{Ne}/^{36}\text{Ar}$ ) can be calculated. Table B4 lists  $^{22}\text{Ne}/^{36}\text{Ar}$ ,  $^{84}\text{Kr}/^{36}\text{Ar}$ ,  $^{132}\text{Xe}/^{36}\text{Ar}$  ratios in ASW at 18 °C for comparison.

The average depth of sampled Barnett gas wells is ~1900 m. Modern reservoir temperature in the Barnett Shale is about 90°C [Curtis, 2002]. However the maximum burial temperature in the Barnett Shale is about 150°C [Jarvie et al., 2001; Montgomery et al., 2005]. Henry's constants of stable noble gases in water are calculated based on empirical equations for temperatures of 18°C, 90°C, and 150°C, respectively (Table B5) [Crovetto et al., 1982; Smith and Kennedy, 1983; Smith, 1985]. The Barnett Shale is identified as the source and reservoir of both oil and gas in the Fort Worth Basin. So it is likely that oil might have interacted with the groundwater phase. Henry's constants for stable noble gases in oil [API=34; [Jarvie et al., 2001] are also calculated based on previously reported empirical equations [Kharaka and Specht, 1988; Ballentine et al., 2002] for a temperature of 150°C and are listed in Table B5.

### ***B5.1 Single-stage Groundwater Degassing Fractionation Model***

Due to the higher solubility of the heavier noble gases (e.g.,  $^{36}\text{Ar}$ ) compared to the lighter ones (e.g.,  $^{22}\text{Ne}$ ) in both water and oil, light noble gases will preferentially escape into the gas phase compared to the heavy noble gases when the groundwater is degassing. Therefore, light/heavy noble gas ratios (i.e.,  $^{22}\text{Ne}/^{36}\text{Ar}$ ,  $^{84}\text{Kr}/^{36}\text{Ar}$ ,  $^{132}\text{Xe}/^{36}\text{Ar}$ ) will be increasing in the escaped gas phase but decreasing in the retained water phase during the groundwater degassing process. In the discussion that follows, we take  $^{22}\text{Ne}/^{36}\text{Ar}$  as an example for the sake of succinctness.  $^{22}\text{Ne}/^{36}\text{Ar}$  ratios in the gas phase can be calculated as follow [Ballentine *et al.*, 2002]:

$$\left(\frac{i}{j}\right)_{gas} = \left(\frac{i}{j}\right)_{initial} \frac{1-f\alpha}{1-f} \quad (\text{B6})$$

where subscripts gas and initial refer to the noble gas isotopic ratios (or elemental ratios) in the escaped gas and initial water phases.  $i$  and  $j$  represent noble gas isotopes (e.g.,  $^{22}\text{Ne}$ ,  $^{36}\text{Ar}$ ) and  $\text{CH}_4$ .  $f$  stands for the fraction of isotope  $j$  in the retained water phase. The exponent coefficient  $\alpha$  is given by:

$$\alpha = \frac{K_i}{K_j} \quad (\text{B7})$$

where  $K_i$  and  $K_j$  represent Henry's constants of  $i$  and  $j$  (Table B5).

When the volume ratio of gas/water approaches zero, the maximum fractionation of noble gases and  $\text{CH}_4$  in the gas phase can be estimated:

$$\left(\frac{i}{j}\right)_{gas} = \left(\frac{i}{j}\right)_{initial} \times \alpha \quad (\text{B8})$$

For ASW at 18 °C, the  $^{22}\text{Ne}/^{36}\text{Ar}$  ratio in the initial water phase is 0.016, the predicted maximum  $^{22}\text{Ne}/^{36}\text{Ar}$  ratio in the escaped gas phase under current reservoir conditions (i.e., 90°C)

in the Barnett Shale is 0.030 according to equations (7) and (8), which is lower than  $^{22}\text{Ne}/^{36}\text{Ar}$  ratios of all Barnett gas samples. Alternatively, if we assume that groundwater degassing occurs at 18 °C, predicted maximum  $^{22}\text{Ne}/^{36}\text{Ar}$  ratio in the gas phase is 0.053, which is still lower than those of all Barnett gas samples (Figure 4.5a). The incorporation of excess air in groundwater samples is not uncommon [Heaton and Vogel, 1981], and results in elevated  $^{22}\text{Ne}/^{36}\text{Ar}$  ratio in the groundwater, with the upper limit to be the air value of 0.053. Even if we assign  $^{22}\text{Ne}/^{36}\text{Ar}$  ratio of 0.053 to the initial water phase, predicted maximum  $^{22}\text{Ne}/^{36}\text{Ar}$  ratio in the escaped phase is 0.102 at 90°C, which is still lower than  $^{22}\text{Ne}/^{36}\text{Ar}$  ratio of some Barnett gas samples (e.g., BG2-1). Therefore, a single-stage groundwater degassing model alone cannot account for the observed high  $^{22}\text{Ne}/^{36}\text{Ar}$  ratios in Barnett gas samples.

It is also important to note that multi-stage groundwater degassing process is not considered in this study although this multi-stage of degassing and re-dissolution can also lead to higher  $^{22}\text{Ne}/^{36}\text{Ar}$  ratios in both escaped gas and retained water phases. Two reasons for not considering this process are: (1) this multi-stage process requires an environment with fluctuating physical conditions that would cause gas exsolution followed by re-solution [Ballentine et al., 2002; Zhou et al., 2012], and (2) this process has extreme water mass balance limitations [Ballentine et al., 2002]. These conditions are not fulfilled in the Barnett Shale.

### ***B5.2 Two-stage Oil Modified Groundwater Exsolution (OMGE) Fractionation Model***

Since an oil phase exist in the Barnett Shale within our study area, a model that can potentially explain the observed high  $^{22}\text{Ne}/^{36}\text{Ar}$  ratios in Barnett gas samples, must take into account the existence of an oil phase during the noble gas fractionation. The solubility of  $^{36}\text{Ar}$  is larger than that of  $^{22}\text{Ne}$  in the oil phase, which will lead to elevated  $^{22}\text{Ne}/^{36}\text{Ar}$  ratio in the retained

groundwater phase when oil and water phases are in equilibrium. The retained groundwater phase becomes subsequently in contact with a free gas phase (e.g., CH<sub>4</sub>) and the following process is similar to that of groundwater degassing. This oil modified groundwater exsolution (OMGE) fractionation model was proposed by *Battani et al.* [2000] to explain high <sup>20</sup>Ne/<sup>36</sup>Ar ratios of natural gases in the Pakistan Indus basin. <sup>22</sup>Ne/<sup>36</sup>Ar ratio in the final escaped gas phase can be estimated as follows [*Battani et al.*, 2000]:

$$\left(\frac{i}{j}\right)_{gas} = \left(\frac{i}{j}\right)_{initial} f_1^{\alpha_1-1} \left(\frac{1-f_2^{\alpha_2}}{1-f_2}\right) \quad (B9)$$

where subscripts gas and initial stand for noble gas signatures in the final escaped gas phase and initial water phase (ASW).  $f_1$  refers to the fraction of isotope  $j$  in the retained water phase in equilibrium with the oil phase prior to getting in touch with the gas phase.  $f_2$  refers to the fraction of isotope  $j$  in the retained water phase in equilibrium with the gas phase. The exponent coefficient  $\alpha_1$  and  $\alpha_2$  are defined by *Battani et al.* [2000]:

$$\alpha_1 = \frac{K_i^{water}/K_j^{water}}{K_i^{oil}/K_j^{oil}} \quad (B10)$$

$$\alpha_2 = \frac{K_i^{water}}{K_j^{water}} \quad (B11)$$

where  $K_i$  and  $K_j$  represent corresponding Henry's constants of  $i$  and  $j$  in the water or oil phases.

### ***B5.3 Noble Gas Fractionation in Barnett Gas Samples***

Unlike Strawn gases, all Barnett gases display higher F(<sup>22</sup>Ne) values than that of air. This is discussed further below. Except for BG5A, BG5B, and BG7, all Strawn and Barnett gases show significantly higher F(<sup>132</sup>Xe) values than that of ASW (Figure 4.4). In addition, Strawn natural gases as well as some Barnett natural gas samples (i.e., BG1, BG4, BG8) display

significantly higher  $F(^{84}\text{Kr})$  with respect to ASW. Low  $F(^{84}\text{Kr})$  and  $F(^{132}\text{Xe})$  values in samples BG5A, BG5B, and BG7 are due partly to mass-dependent fractionation (Text B3). Below we attempt to answer two questions: (1) why are  $F(^{22}\text{Ne})$  values of all Barnett gases higher than that of the atmosphere; and (2) why are some Barnett and Strawn natural gas samples significantly enriched in the heavy noble gases  $^{84}\text{Kr}$  and  $^{132}\text{Xe}$  over  $^{36}\text{Ar}$  compared to ASW or air compositions.

Figures 4.5a and 4.5b show  $^{84}\text{Kr}/^{36}\text{Ar}$  and  $^{132}\text{Xe}/^{36}\text{Ar}$  values as a function of  $^{22}\text{Ne}/^{36}\text{Ar}$  for all gas samples. Air and ASW (18 °C) values are also shown for comparison, in particular, with  $^{22}\text{Ne}/^{36}\text{Ar}$  values equal to 0.053 and 0.016, respectively. Calculated closed- and open-system fractionation curves for an escaped gas phase which is in equilibrium with ASW at 18 °C are also indicated (black lines). From these figures, it is apparent that while all stray gases display noble gas ratios close to a two-mixing component between air and ASW, Strawn natural gas is highly enriched in  $^{84}\text{Kr}$  and  $^{132}\text{Xe}$  (its  $^{84}\text{Kr}/^{36}\text{Ar}$  and  $^{132}\text{Xe}/^{36}\text{Ar}$  values are 53% and 174% larger than corresponding ASW values at 18 °C) while displaying expected ASW-air values for the lighter noble gases, with expected  $^{22}\text{Ne}/^{36}\text{Ar}$  values. The observed offset between predicted and measured  $^{84}\text{Kr}/^{36}\text{Ar}$  and  $^{132}\text{Xe}/^{36}\text{Ar}$  ratios in stray gases is likely due to input from Strawn natural gas, leading to slightly higher  $^{84}\text{Kr}/^{36}\text{Ar}$  and  $^{132}\text{Xe}/^{36}\text{Ar}$  ratios in stray gases compared to predicted values. In contrast to Strawn natural gas and stray gas in the Trinity Aquifer,  $^{22}\text{Ne}/^{36}\text{Ar}$  ratios of all Barnett gases are higher than the maximum predicted  $^{22}\text{Ne}/^{36}\text{Ar}$  value of 0.053 in the gas phase assuming a simple groundwater degassing model, suggesting that a simple single-stage water degassing model is unable to explain such high  $^{22}\text{Ne}/^{36}\text{Ar}$  values. The possibility of multi-stage process of groundwater degassing and gas re-dissolution is excluded due to the fact that this multi-stage process requires an unusual environment (e.g., recurring changes in subsurface

temperature, pressure, and salinity) and has extreme water mass balance limitations (large mass of the fluid phase) which do not comply with conditions in our system [Ballentine *et al.*, 2002]. Therefore, an alternative model needs to be considered to explain the observed  $^{22}\text{Ne}/^{36}\text{Ar}$  in Barnett Shale gases. A two-stage groundwater gas stripping and re-dissolution (GGSR) fractionation model was proposed to explain elevated  $^{22}\text{Ne}/^{36}\text{Ar}$  ratios in subsurface  $\text{CO}_2$  gas samples [Gilfillan *et al.*, 2008; 2009; Zhou *et al.*, 2012]. This GGSR model was also applied to the Marcellus Shale [Darrah *et al.*, 2014; 2015]. However, because the GGSR model does not consider the presence of an oil phase, it is not applicable to the Barnett Shale. Indeed, the presence of an oil phase is an integral part of the Barnett Shale history, in particular, within our study area. According to previous studies, the Barnett Shale is the primary source rock for both oil and gas in the Fort Worth Basin [Herkommer and Denke, 1982; Jarvie *et al.*, 2001; Montgomery *et al.*, 2005; Hill *et al.*, 2007; Rodriguez and Philp, 2010]. An alternative viable model to explain high  $^{22}\text{Ne}/^{36}\text{Ar}$  ratios in Barnett gases is the two-stage oil modified groundwater exsolution (OMGE) fractionation model proposed by Battani *et al.* [2000] to explain high  $^{20}\text{Ne}/^{36}\text{Ar}$  ratios of natural gases in the Pakistan Indus basin. This OMGE model postulate that noble gas fractionation occurs in two steps assuming that noble gases are initially in ASW at  $18^\circ\text{C}$ : (1) step 1 corresponds to noble gas redistribution between oil and water phases under  $150^\circ\text{C}$  [maximum burial temperatures in the Barnett Shale; Jarvie *et al.*, 2001 and Montgomery *et al.*, 2005], resulting in loss of noble gases from water to oil, and; (2) step 2 corresponds to noble gas fractionation between this residual water and gas phase at  $90^\circ\text{C}$  [bottom hole temperature in Barnett production wells; Curtis, 2002]. The absence of an oil phase in step 2 can be explained by the migration of hydrocarbon (oil and/or gas) from the Barnett Shale into shallower formations within the Fort Worth Basin over geologic times [Jarvie *et al.*, 2001;

Montgomery *et al.*, 2005]. As the primary source of hydrocarbon in the Fort Worth Basin, the Barnett Shale has donated oil and gas to shallower formations and oil in the Barnett Shale could have been converted into gas under high temperature [Jarvie *et al.*, 2001; Montgomery *et al.*, 2005; Hill *et al.*, 2007]. Because heavy noble gases (e.g.,  $^{36}\text{Ar}$ ) are more soluble than  $^{22}\text{Ne}$  in both water and oil, loss of noble gases into the oil phase in step 1 will lead to lower  $^{22}\text{Ne}/^{36}\text{Ar}$  ratios in the oil phase and complementary elevated  $^{22}\text{Ne}/^{36}\text{Ar}$  values in the residual water phase. At step 2, the gas phase in equilibrium with this residual water phase will acquire much higher  $^{22}\text{Ne}/^{36}\text{Ar}$  ratios compared to the air value. Predicted  $^{22}\text{Ne}/^{36}\text{Ar}$  ratios in the gas phase based on trial and error estimates match best with measured values for all Barnett gas samples if 97.6% of  $^{36}\text{Ar}$  from the initial ASW are assumed to escape into the oil phase while 2.4% of initial ASW  $^{36}\text{Ar}$  remain in the residual water phase after step 1 (Figure 4.5; blue dotted line with a label “OMGE+0% Excess Kr/Xe”).

Predicted  $^{84}\text{Kr}/^{36}\text{Ar}$  and  $^{132}\text{Xe}/^{36}\text{Ar}$  values, however, are much lower than corresponding measured values and reflect enrichments of both  $^{84}\text{Kr}$  and  $^{132}\text{Xe}$  with respect to ASW. This could be explained by a sedimentary excess  $^{84}\text{Kr}$  and  $^{132}\text{Xe}$  [Frick and Chang, 1977; Podosek *et al.*, 1980; Torgersen and Kennedy, 1999; Ma *et al.*, 2009; Pitre and Pinti, 2010], possibly sourced from the organic rich material (e.g., black shale, kerogen) in the Barnett Shale. Building on the above OMGE model, we estimate 700%-2200% and 1400%-6200% for excess Kr and Xe, respectively, to account for observed elevated  $^{84}\text{Kr}/^{36}\text{Ar}$  and  $^{132}\text{Xe}/^{36}\text{Ar}$  values of Barnett gases (excluding BG5A, BG5B, and BG7 due to mass-dependent fractionation). The observed noble gas enrichment ( $F(^{132}\text{Xe}) > F(^{84}\text{Kr}) > F(^{36}\text{Ar})$ ; Figure 4.4) and the general pattern of required sedimentary noble gases (excess Xe > excess Kr) suggest physical adsorption on sediments or organic matter [Fanale and Cannon, 1971]. Following the single-stage water degassing model,

220%-270% of excess Kr and 600%-830% of excess Xe are needed to account for measured  $^{84}\text{Kr}/^{36}\text{Ar}$  and  $^{132}\text{Xe}/^{36}\text{Ar}$  values for our Strawn gases (not shown). It seems that the contribution of sedimentary noble gases in Barnett gases is much greater than in Strawn gases. However, due to the scarcity of noble gas data, in particular, heavy noble gas data for Strawn gases, more work is needed to test this hypothesis. Figure B4 shows  $^{132}\text{Xe}/^{36}\text{Ar}$  versus  $^{84}\text{Kr}/^{36}\text{Ar}$  for all gas samples.  $^{84}\text{Kr}/^{36}\text{Ar}$  and  $^{132}\text{Xe}/^{36}\text{Ar}$  values in kerogen [Frick and Chang, 1977], air, and ASW at 18 °C are also shown for reference. The shadow area represents calculated values in the mixture of air, ASW, and kerogen components. We find most gas samples are located within the shadow area suggesting that heavy noble gases in these samples are a mixture of atmospheric (ASW and/or air) and sedimentary (e.g., kerogen) components. Two groups of other gas samples are outside of this shadow area: (1) BG5A, BG5B, BG7 and (2) Strawn gases and Barnett gases BG1, BG4, and BG8. Significantly lower  $^{84}\text{Kr}/^{36}\text{Ar}$  and  $^{132}\text{Xe}/^{36}\text{Ar}$  values in BG5A, BG5B, and BG7 again are due to the mass-dependent fractionation (Text B3). Although BG1, BG4, and BG8 display  $^{84}\text{Kr}/^{36}\text{Ar}$  and  $^{132}\text{Xe}/^{36}\text{Ar}$  values distinct from predicted values following mixing model between atmospheric and kerogen components, their Kr and Xe enrichment mimics closely that previously observed in Elk Hills oil field gases [Torgersen and Kennedy, 1999] (black crosses in Figure B4), which suggest mixing between atmospheric noble gases and alternative sedimentary noble gas source other than the kerogen reported in Frick and Chang [1977]. Under this scenario, the original ASW-like signature for heavy noble gases would have been modified by OMGE process, prior to addition of sedimentary Kr and Xe possibly during hydrocarbon generation and/or hydrocarbon migration and accumulation in the oil and gas source rock.

**Table B4** Isotopic ratios of atmospheric noble gases in stray gas as well as production gas from the Strawn Group and Barnett Shale.

| Sample ID                                     | $^{22}\text{Ne}/^{36}\text{Ar}$ | $^{84}\text{Kr}/^{36}\text{Ar}$ | $^{132}\text{Xe}/^{36}\text{Ar}$ | F( $^{22}\text{Ne}/^{36}\text{Ar}$ ) | F( $^{84}\text{Kr}/^{36}\text{Ar}$ ) | F( $^{132}\text{Xe}/^{36}\text{Ar}$ ) |
|---|---------------------------------|---------------------------------|----------------------------------|--------------------------------------|--------------------------------------|---------------------------------------|
|   | ( $\times 10^{-2}$ )            | ( $\times 10^{-2}$ )            | ( $\times 10^{-3}$ )             |                                      |                                      |                                       |
| <i>Stray Gas Samples from Groundwater</i>     |                                 |                                 |                                  |                                      |                                      |                                       |
| 555GA   | 3.898±0.072                     | 2.709±0.054                     | 1.131±0.029                      | 0.730±0.013                          | 1.310±0.026                          | 1.519±0.039                           |
| 555GB-1                                       | 3.738±0.069                     | 2.801±0.056                     | 1.157±0.030                      | 0.700±0.013                          | 1.354±0.027                          | 1.555±0.040                           |
| 555GB-2                                       | 3.975±0.073                     | 2.711±0.054                     | 1.111±0.028                      | 0.744±0.014                          | 1.311±0.026                          | 1.492±0.038                           |
| 556GA   | 5.479±0.101                     | 2.908±0.058                     | 1.677±0.043                      | 1.026±0.019                          | 1.406±0.028                          | 2.252±0.058                           |
| 556GB   | 2.621±0.143                     | 2.837±0.118                     | 1.476±0.066                      | 0.491±0.027                          | 1.372±0.057                          | 1.983±0.088                           |
| <i>Natural Gas Samples from Strawn Group</i>  |                                 |                                 |                                  |                                      |                                      |                                       |
| SG3-1   | 3.713±0.071                     | 6.081±0.124                     | 7.227±0.188                      | 0.695±0.013                          | 2.940±0.060                          | 9.706±0.252                           |
| SG3-2   | 2.762±0.051                     | 5.684±0.113                     | 6.487±0.166                      | 0.517±0.010                          | 2.748±0.055                          | 8.712±0.223                           |
| <i>Natural Gas Samples from Barnett Shale</i> |                                 |                                 |                                  |                                      |                                      |                                       |
| BG1   | 5.790±0.122                     | 6.579±0.147                     | 9.709±0.267                      | 1.084±0.023                          | 3.181±0.071                          | 13.039±0.359                          |
| BG2-1   | 10.298±0.189                    | 3.006±0.060                     | 3.374±0.086                      | 1.928±0.035                          | 1.453±0.029                          | 4.531±0.116                           |
| BG2-2   | 10.462±0.192                    | 2.828±0.056                     | 2.963±0.076                      | 1.959±0.036                          | 1.368±0.027                          | 3.980±0.102                           |
| BG4   | 7.604±0.175                     | 5.839±0.142                     | 8.639±0.252                      | 1.424±0.033                          | 2.823±0.068                          | 11.603±0.338                          |
| BG5A  | 8.695±0.160                     | 1.356±0.027                     | 0.455±0.012                      | 1.628±0.030                          | 0.656±0.013                          | 0.611±0.016                           |
| BG5B  | 7.939±0.146                     | 1.419±0.028                     | 0.449±0.011                      | 1.487±0.027                          | 0.686±0.014                          | 0.602±0.015                           |
| BG6   | 7.731±0.142                     | 3.844±0.076                     | 5.028±0.128                      | 1.448±0.027                          | 1.859±0.037                          | 6.753±0.173                           |
| BG7   | 10.293±0.189                    | 1.245±0.025                     | 0.631±0.016                      | 1.927±0.035                          | 0.602±0.012                          | 0.848±0.022                           |
| BG8   | 6.172±0.113                     | 10.935±0.217                    | 20.628±0.527                     | 1.156±0.021                          | 5.287±0.105                          | 27.704±0.708                          |
| BG9A  | 9.915±0.182                     | 2.688±0.053                     | 3.134±0.080                      | 1.856±0.034                          | 1.300±0.026                          | 4.210±0.108                           |
| BG9B  | 9.108±0.167                     | 3.853±0.076                     | 4.089±0.105                      | 1.705±0.031                          | 1.863±0.037                          | 5.492±0.140                           |
| Air <sup>a</sup>                              | 5.341                           | 2.068                           | 0.745                            | 1.000                                | 1.000                                | 1.000                                 |
| ASW (18 °C) <sup>a</sup>                      | 1.590                           | 3.834                           | 2.506                            | 0.298                                | 1.854                                | 3.366                                 |
| ASW (25 °C) <sup>a</sup>                      | 1.726                           | 3.700                           | 2.331                            | 0.323                                | 1.789                                | 3.130                                 |

<sup>a</sup> Ozima and Podosek [2002]

**Table B5** Parameter used in single-stage and two-stage fractionation models <sup>a</sup>.

| Temperature<br>(°C) | Salinity<br>(M) | Henry's Constants for Water Phase (atm)           |        |       |       |       |
|---------------------|-----------------|---|--------|-------|-------|-------|
|                     |                 | He  | Ne     | Ar    | Kr    | Xe    |
| 18 °C               | 0               | 141451  | 118016 | 35161 | 18919 | 10624 |
| 90 °C               | 0               | 118960  | 122481 | 64440 | 42970 | 30453 |
| 150 °C              | 0               | 73115   | 85056  | 52966 | 40265 | 29684 |
| Temperature<br>(°C) | Salinity<br>(M) | Henry's Constants for Water Phase (dimensionless) |        |       |       |       |
|                     |                 | He  | Ne     | Ar    | Kr    | Xe    |
| 18 °C               | 0               | 106.98  | 89.26  | 26.59 | 14.31 | 8.04  |
| 90 °C               | 0               | 72.13   | 74.27  | 39.07 | 26.06 | 18.47 |
| 150 °C              | 0               | 38.05   | 44.26  | 27.56 | 20.95 | 15.45 |
| Temperature<br>(°C) | Salinity<br>(M) | Henry's Constants for Oil Phase (atm)             |        |       |       |       |
|                     |                 | He  | Ne     | Ar    | Kr    | Xe    |
| 90 °C               | 0               | 26286   | 23374  | 6078  | 2557  | 1150  |
| 150 °C              | 0               | 15766   | 15022  | 6162  | 3103  | 2359  |

<sup>a</sup> Calculated from *Crovetto et al.* [1982], *Smith* [1985], and *Kharaka and Specht* [1988]

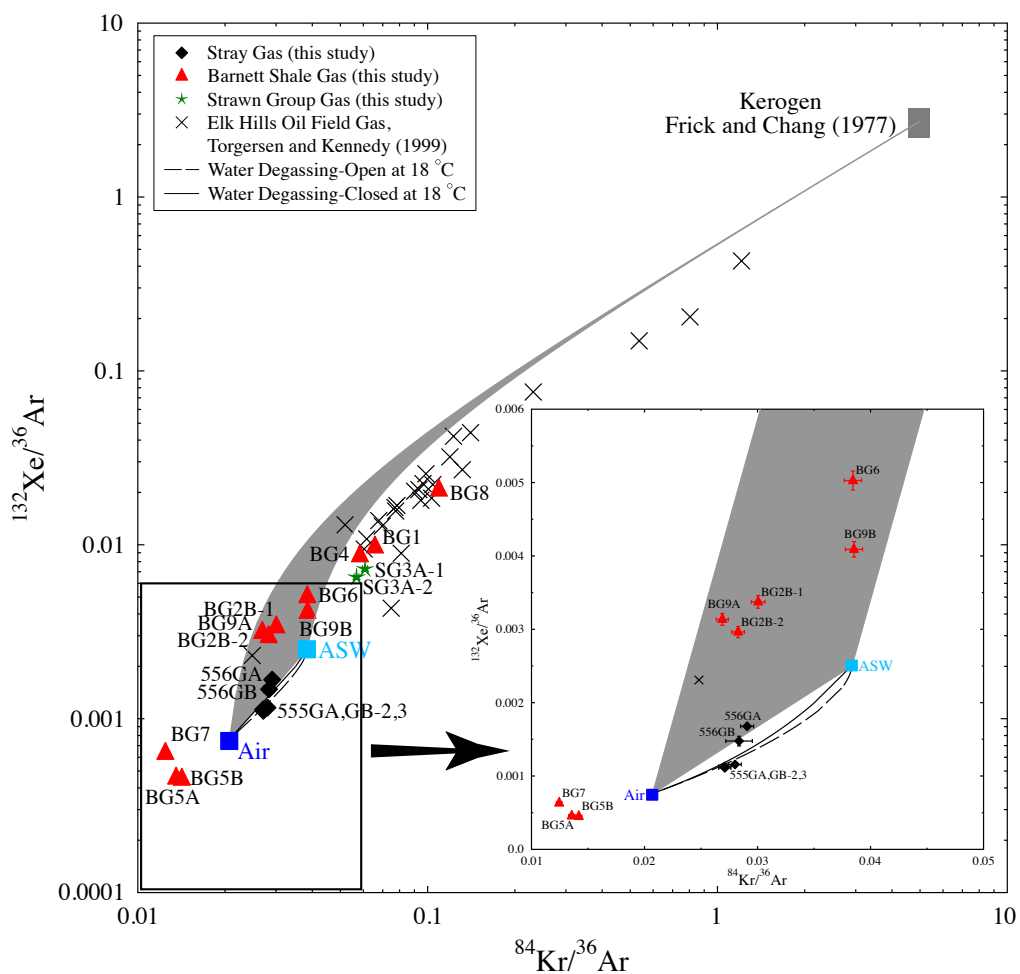


**Figure B4**  $^{132}\text{Xe}/^{36}\text{Ar}$  versus  $^{84}\text{Kr}/^{36}\text{Ar}$  are shown for gas samples. Predicted values in the gas phase following a single-stage groundwater degassing model for closed-system (black curve) and open-system (black dashed curve) are shown. Previously reported  $^{84}\text{Kr}/^{36}\text{Ar}$  and  $^{132}\text{Xe}/^{36}\text{Ar}$  values in kerogen [gray square in the upper-right corner; *Frick and Chang, 1977*] and oil field gases [black crosses; *Torgersen and Kennedy, 1999*] are also shown for reference.

## B6 References

- Ballentine, C. J., and P. G. Burnard (2002), Production, Release and Transport of Noble Gases in the Continental Crust, *Reviews in Mineralogy and Geochemistry*, 47(1), 481–538, doi:10.2138/rmg.2002.47.12.
- Ballentine, C. J., R. Burgess, and B. Marty (2002), Tracing Fluid Origin, Transport and Interaction in the Crust, *Reviews in Mineralogy and Geochemistry*, 47(1), 539–614, doi:10.2138/rmg.2002.47.13.
- Battani, A., P. Sarda, and A. Prinzhofer (2000), Basin scale natural gas source, migration and trapping traced by noble gases and major elements: the Pakistan Indus basin, *Earth and Planetary Science Letters*, 181(1–2), 229–249.
- Bruner, K. R., and R. Smosna (2011), *A comparative study of the Mississippian Barnett Shale, Fort Worth Basin, and Devonian Marcellus Shale*, DOE/NETL.
- Castro, M. C., L. Ma, and C. M. Hall (2009), A primordial, solar He–Ne signature in crustal fluids of a stable continental region, *Earth and Planetary Science Letters*, 279(3–4), 174–184, doi:10.1016/j.epsl.2008.12.042.
- Clarke, W. B., W. J. Jenkins, and Z. Top (1976), Determination of tritium by mass spectrometric measurement of  $^3\text{He}$ , *The International Journal of Applied Radiation and Isotopes*, 27(9), 515–522, doi:10.1016/0020-708X(76)90082-X.
- CLI (Core Laboratories Inc.) (1972), *A survey of the subsurface saline water of Texas: Texas Water Development Board Report 157*, Austin.
- Crovetto, R., R. Fernandez-Prini, and M. L. Japas (1982), Solubilities of inert gases and methane in  $\text{H}_2\text{O}$  and in  $\text{D}_2\text{O}$  in the temperature range of 300 to 600 K, *J. Chem. Phys.*, 76(2), 1077–1086, doi:10.1063/1.443074.
- Curtis, J. B. (2002), Fractured shale-gas systems, *AAPG Bulletin*, 86(11), 1921–1938.
- Darrah, T. H., A. Vengosh, R. B. Jackson, N. R. Warner, and R. J. Poreda (2014), Noble gases identify the mechanisms of fugitive gas contamination in drinking-water wells overlying the Marcellus and Barnett Shales, *Proceedings of the National Academy of Sciences*, 111(39), 14076–14081, doi:10.1073/pnas.1322107111.
- Darrah, T. H., R. B. Jackson, A. Vengosh, N. R. Warner, C. J. Whyte, T. B. Walsh, A. J. Kondash, and R. J. Poreda (2015), The evolution of Devonian hydrocarbon gases in shallow aquifers of the northern Appalachian Basin: Insights from integrating noble gas and hydrocarbon geochemistry, *Geochimica et Cosmochimica Acta*, 170 IS -, 321–355, doi:10.1016/j.gca.2015.09.006.
- Fanale, F. P., and W. A. Cannon (1971), Physical adsorption of rare gas on terrigenous sediments, *Earth and Planetary Science Letters*, 11(1-5), 362–368, doi:10.1016/0012-821X(71)90195-6.

- Frick, U., and S. Chang (1977), Ancient carbon and noble gas fractionation, *Lunar and Planetary Science Conference* ....
- Gilfillan, S. M. V. et al. (2009), Solubility trapping in formation water as dominant CO<sub>2</sub> sink in natural gas fields, *Nature*, 458(7238), 614–618, doi:10.1038/nature07852.
- Gilfillan, S. M. V., C. J. Ballentine, G. Holland, D. Blagburn, B. S. Lollar, S. Stevens, M. Schoell, and M. Cassidy (2008), The noble gas geochemistry of natural CO<sub>2</sub> gas reservoirs from the Colorado Plateau and Rocky Mountain provinces, USA, *Geochimica et Cosmochimica Acta*, 72(4), 1174–1198, doi:10.1016/j.gca.2007.10.009.
- Heaton, T. H. E., and J. C. Vogel (1981), “Excess air” in groundwater, *Journal of Hydrology*, 50(0), 201–216, doi:10.1016/0022-1694(81)90070-6.
- Herkommer, M. A., and G. W. Denke (1982), Stratigraphy and hydrocarbons, Parker County, Texas, *Dallas Geological Society*.
- Hill, R. J., E. Zhang, B. J. Katz, and Y. Tang (2007), Modeling of gas generation from the Barnett Shale, Fort Worth Basin, Texas, *AAPG Bulletin*, 91(4), 501–521, doi:10.1306/12060606063.
- Hilton, D. R., and D. Porcelli (2003), Noble gases as mantle tracers, in the Mantle and Core, in *Treatise on Geochemistry*, edited by H. D. Holland and K. K. Turekian, Elsevier, New York.
- Jarvie, D. M., B. L. Claxton, F. Henk, and J. T. Breyer (2001), *Oil and shale gas from the Barnett Shale, Ft. Worth Basin, Texas*, AAPG ACE Meeting.
- Kharaka, Y. K., and D. J. Specht (1988), The solubility of noble gases in crude oil at 25–100°C, *Applied Geochemistry*, 3(2), 137–144, doi:10.1016/0883-2927(88)90001-7.
- Ma, L., M. C. Castro, and C. M. Hall (2009), Atmospheric noble gas signatures in deep Michigan Basin brines as indicators of a past thermal event, *Earth and Planetary Science Letters*, 277(1–2), 137–147, doi:10.1016/j.epsl.2008.10.015.
- Marty, B., A. Criaud, and C. Fouillac (1988), Low enthalpy geothermal fluids from the Paris sedimentary basin—1. Characteristics and origin of gases, *Geothermics*, 17(4), 619–633.
- Matsumoto, T., M. Honda, I. McDougall, I. Yatsevich, and S. Y. O'Reilly (2004), Isotope fractionation of neon during stepheating extraction?: a comment on “Re-interpretation of the existence of a primitive plume under Australia based on neon isotope fractionation during step heating” by Gautheron and Moreira (2003), *Terra Nova*, 16(1), 23–26, doi:10.1046/j.1365-3121.2003.00522.x.
- Montgomery, S. L., D. M. Jarvie, K. A. Bowker, and R. M. Pollastro (2005), Mississippian Barnett Shale, Fort Worth basin, north-central Texas: Gas-shale play with multi-trillion cubic foot potential, *AAPG Bulletin*, 89(2), 155–175, doi:10.1306/09170404042.

- Oxburgh, E. R., R. K. O'Nions, and R. I. Hill (1986), Helium isotopes in sedimentary basins, *Nature*, 324(6098), 632–635, doi:10.1038/324632a0.
- Ozima, M., and F. A. Podosek (2002), *Noble Gas Geochemistry*, Cambridge University Press, New York.
- Pitre, F., and D. L. Pinti (2010), Noble gas enrichments in porewater of estuarine sediments and their effect on the estimation of net denitrification rates, *Geochimica et Cosmochimica Acta*, 74(2), 531–539, doi:10.1016/j.gca.2009.10.004.
- Podosek, F. A., M. Honda, and M. Ozima (1980), Sedimentary noble gases, *Geochimica et Cosmochimica Acta*, 44(11), 1875–1884, doi:10.1016/0016-7037(80)90236-7.
- Rodriguez, N. D., and R. P. Philp (2010), Geochemical characterization of gases from the Mississippian Barnett Shale, Fort Worth Basin, Texas, *AAPG Bulletin*, 94(11), 1641–1656, doi:10.1306/04061009119.
- Smith, S. P. (1985), *Noble gas solubility in water at high temperature*, Eos.
- Smith, S. P., and B. M. Kennedy (1983), The solubility of noble gases in water and in NaCl brine, *Geochimica et Cosmochimica Acta*, 47(3), 503–515, doi:10.1016/0016-7037(83)90273-9.
- Torgersen, T., and B. M. Kennedy (1999), Air-Xe enrichments in Elk Hills oil field gases: role of water in migration and storage, *Earth and Planetary Science Letters*, 167(3–4), 239–253, doi:10.1016/S0012-821X(99)00021-7.
- Wen, T., M. C. Castro, B. R. Ellis, C. M. Hall, and K. C. Lohmann (2015), Assessing compositional variability and migration of natural gas in the Antrim Shale in the Michigan Basin using noble gas geochemistry, *Chemical Geology*, 417, 356–370, doi:10.1016/j.chemgeo.2015.10.029.
- Wetherill, G. (1954), Variations in the Isotopic Abundances of Neon and Argon Extracted from Radioactive Minerals, *Physical Review*, 96(3), 679–683, doi:10.1103/PhysRev.96.679.
- Yatsevich, I., and M. Honda (1997), Production of nucleogenic neon in the Earth from natural radioactive decay, *Journal of Geophysical Research*.
- Zhou, Z., C. J. Ballentine, M. Schoell, and S. H. Stevens (2012), Identifying and quantifying natural CO<sub>2</sub> sequestration processes over geological timescales: The Jackson Dome CO<sub>2</sub> Deposit, USA, *Geochimica et Cosmochimica Acta*, 86, 257–275, doi:10.1016/j.gca.2012.02.028.